The University Of Sheffield.

Department
Of
Mechanical
Engineering

PhD Mechanical Engineering Thesis

Transient Adjoint Based Aerodynamic Optimization of Vertical Axis Wind Turbines Using RANS-based CFD

Qiulin **REN**

31/12/2025

Supervisors:
Prof. Lin Ma
Prof. Derek B. Ingham
Prof. Mohamed Pourkashanian

A dissertation submitted to the Department of Mechanical Engineering, University of Sheffield in fulfilment of the requirements for the degree of PhD

December 2025

Comfirmation of Authorship & Publication List

Comfirmation of Authorship

The work presented in this thesis is the sole effort of the author unless otherwise stated in the text. Acknowledgement and references are given where appropriate to any sources that have been used. Furthermore, no part of this work has been previously submitted for an award at this or any other institution.

In the below publications list, the co-authors are my supervisors who have acted in an advisory role.

Planned Publications

Title: "Transient Adjoint Based Blade Aerodynamic Optimization for Vertical Axis Wind Turbines Using an Oscillating Airfoil"
Authors: Ren, Q., Ingham, D., Ma, L. & Pourkashanian, M.
The content of this publication relates most specifically to Chapter 5 of the thesis, but the methods in Chapters 6 and 7 are also based on this foundation.

Title: "Aerodynamic Optimization of the VAWT Model Using Time-Resolved Adjoint Methods with Wake Flow Analysis"
Authors: Ren, Q., Ingham, D., Ma, L. & Pourkashanian, M.
The content of this publication relates most specifically to Chapter 6 of the thesis, but the methods in Chapters 7 are also based on this foundation.

Acknowledgements

I wish to thank my project supervisor Prof. Lin Ma. Without his support, this project would have been very difficult. He provided me with numerous software references and gave me many ideas for modeling. Also he was very patient in assisting me answer questions and guided me on problems that I encountered during the modeling process. At the same time, I would also like to thank Prof. Derek Ingham and Dr. Kevin Hughes for tutoring the research methods course and hosting some valuable group meetings.

I wish to thank my academic tutor Dr. Jee Hee for their his constructive words of support, guidance and optimism offered to me throughout my project. I am very grateful to my colleagues and friends also working on wind energy research. In particular, Attakarn Jansasithorn, Juan-Philips Marx, Khalid Alzahrani and Suleyman Kose who have been an invaluable source of council and expertise, patiently helping me up the learning curve of wind turbine CFD and providing valuable insightful discussions and suggestions. In addition, I would also like to thank Dr. Hadi Arbabi, Dr. Peter Coleman, Dr. Richard Devine, Dr. Tara Baldacchiano, Dr. Catherine Collett and Prof. Stephen Beck for providing me with teaching opportunities and observation of teaching skills, from which my teaching skills have greatly improved.

Most of all, I thank my family.

Qiulin Ren

University of Sheffield

Glossary

AoA – Angle of Attack

BET – Blade Element Theory

BSL – Menter Baseline (turbulence model)

CFD – Computational Fluid Dynamics

CFL – Courant-Friedrichs-Lewy (condition, number)

CST – Class/Shape Function Transformation

CPU – Central Processing Unit (computer)

DES – Detached Eddy Simulation

DW – Downwind

FFS – Free Form Scaling

HAWT – Horizontal Axis Wind Turbine

HPC – High Performance Computing

ISV – In-situ VAWT (optimisation method)

LES – Large Eddy Simulation

LEV – Leading Edge Vortex

LCOE – Levelised Cost of Energy

MAV – Micro Aerial Vehicle

MPI – Message Passing Interface

NREL – National Renewable Energy Laboratory

N-S – Navier-Stokes (equations)

O&M – Operations and Maintenance

PARSEC – Parametric Section

PIV – Particle Image Velocimetry

RANS – Reynolds Averaged Navier-Stokes (equations)

RNG – Re-Normalisation Group (turbulence model)

RSM – Response Surface (optimisation) Methods

S-A – Spalart-Allmaras (turbulence model)

SI – Standard International (units)

SST – Shear-Stress Transport (k-ù turbulence model)

SPIV – Stereoscopic Particle Image Velocimetry

TSR – Tip Speed Ratio (ë)

UDF – User Defined Function

UW – Upwind

VAWT – Vertical Axis Wind Turbine

VGOT – Variable Geometry Oval Trajectory WCT Wall Clock Time

Nomenclature

a – Induction Factor

a_{acc} – Acceleration

c – Chord Length of an Airfoil or VAWT Blade, (m)

C_D – Drag Force Coefficient

C_L – Lift Force Coefficient

C_M – Moment Coefficient

C_P – Power Coefficient

C_T – Tangential Force Coefficient

H – Height of the Blade, (m)

k – Reduced Frequency

R – Radius of Turbine, (m)

S – VAWT Sweeping Area (m^2)

V_a – Axial Flow Velocity of Oncoming Wind, (m/s)

(I checked this part and found no errors, so I haven't modified it)

V_{rel} – Relative Velocity Seen by a VAWT Blade, (m/s)

V_∞ – Velocity of Oncoming Wind, (m/s)

α – Angle of Attack (AoA), (°)

α_{opt} – Optimization Rate

θ – Azimuthal (Angular) Position of VAWT Blade, (°)

λ– Tip Speed Ratio (TSR)

ρ – Density of Fluid (air), (kg/m^3)

σ – Turbine Solidity

ω – Angular Velocity of VAWT, (rad/s)

ω_p – Pitching Frequency of an Oscillating Airfoil, (rad/s)

Contents

List of Figures

List of Tables

Abstract

Vertical-axis wind turbines (VAWTs) have attracted project and policy attention worldwide due to their unique advantages. Compared to horizontal-axis wind turbines (HAWTs), VAWT onshore and offshore wind farms offer advantages such as light weight, high stability, and low noise levels. Since VAWT technology is still in its early stages of development, a significant research gap remains between its theoretical maximum efficiency and actual efficiency, presenting significant research potential.

This thesis proposes a novel fully transient adjoint optimization technique, applied for the first time to the fluid dynamics of VAWTs. This technique is more accurate than currently studied multi-snapshot steady-state (also known as semi-transient) adjoint optimization methods. The challenges in this VAWT airfoil design optimization primarily lie in the complexity of defining the Darrieus pitching motion and the flow separation that occurs when the blade moves at high angles of attack. The results show that the transient adjoint optimization algorithm significantly improves the airfoil efficiency and can be effectively applied to the unsteady flow problems encountered in the design of vertical-axis wind turbine blades.

This research first applies transient adjoint to oscillation airfoils representative of H-Darrieus operation, explicitly accounting for wake effects in the objective and sensitivity evaluation. Then it extends transient adjoint to a 2D VAWT model, formulating power coefficient objectives and enforcing geometric and mesh-quality constraints across tip-speed-ratio scenarios. Finally it validates in 3D CFD, confirming that the optimized airfoil maintains 2D gains when spanwise induction are present.

The fully transient adjoint optimization technique is an innovative technology in the VAWT field. It is implemented using the unsteady adjoint optimization algorithm of the open-source CFD software SU2, making it easy to be adopted by the VAWT design community and providing an important engineering application reference for all other unsteady mechanical structure designs.

Chapter 1

Introduction

1.1 VAWT in Renewable Energy

Renewable energy has developed significantly during the energy crisis in the early 1970s [1, 2], and wind power generation has regained attention. Surveys show that the full utilization of renewable energy will bring greater energy security and less climate impact in the future, and will alleviate the shortage of oil and natural gas and potential environmental pollution [3, 4]. Most wind energy is achieved through two types of wind turbines, namely horizontal axis wind turbines (HAWT) and vertical axis wind turbines (VAWT), which are mainly used for power generation and pumping [5]. HAWT have gradually become mainstream with their high efficiency and mature control technology. They have undergone a number of technological innovations such as variable pitch control, doubly fed induction generators, power electronics, and intelligent monitoring [6]. The capacity of a single unit has also developed from tens of kilowatts to more than 15 megawatts at present [7]. Although VAWT appeared as early as the 1930s [8] and were promoted by Sandia Laboratories in the United States in the 1970s [9], they have not been widely adopted for a long time due to their low efficiency and difficulty in control. Until the 2010s, with the development of urban distributed energy and floating offshore wind power, VAWT regained attention due to its advantages such as structural symmetry and low center of gravity, especially on floating platforms [10].

In recent years, the rate of improvement of HAWT aerodynamic performance has stabilized, and most innovations in the industry have focused on expanding the single-machine size of HAWT [7], improving condition monitoring systems, and reducing operating and maintenance costs [11-15]. Previous studies generally believe that the power coefficient of VAWT is smaller than that of HAWT [16]. However, there are also some literatures that show that VAWT have greater potential for improving the power coefficient [17]. The VAWT industry is significantly less mature than HAWT because the technology has not been widely commercialized. Therefore, if objectively evaluated from a technical perspective, it cannot prove that the VAWT technology is inferior to the HAWT technology.

One of the main advantages of the VAWT is that their single moving parts do not require a yaw mechanism, which can significantly simplify the design configuration [18]. Another advantage is that many typical designs, such as H-Darrieus, have uniform cross-sections and no twisting, which makes them relatively easy to manufacture or extrude, while the blades of the HAWT need to be twisted and tapered to achieve optimal performance [7]. In addition, due to its small size, small footprint, and the fact that it can accept wind from any direction, many of its distribution locations are closer to the power consumption center, thereby reducing transmission losses [18]. In addition, VAWT has a symmetrical structure and does not rely on high towers, and is more suitable for use in urban environments, complex terrain or floating offshore platforms [18].

1.1.1 The Development Process of VAWT

The concept of VAWT can be traced back to the early 20th century. The Savonius resistance vertical wind turbine was proposed by Finnish engineer S. J. Savonius in 1922, and its design was inspired by a rotating bucket [19]. This type of wind turbine has a simple structure and high torque, but low efficiency and is suitable for low wind speed environments. Then in 1931, Canadian engineer G. J. M. Darrieus invented the Darrieus lift wind turbine, which uses a blade shape similar to an airplane wing and relies on lift to drive rotation, significantly improving efficiency [20].

In the 1970s, the global oil crisis broke out, triggering a high level of attention to renewable energy [21-22]. Against this background, the US government funded a number of wind energy research projects, among which Sandia National Laboratories [23] led the in-depth research on VAWT, developed a variety of Darrieus experimental wind turbines, and conducted wind tunnel tests and field tests. During this period, VAWT was regarded as a strong competitor to HAWT. Although VAWT had many advantages in theory at the time, it still faced many technical challenges in practical applications. Its unique "self-starting difficulty" problem usually requires external force to start to reach normal operating speed [24-25]. In addition, the aerodynamic forces on its blades change dramatically during each rotation, resulting in complex structural stress and serious fatigue problems [26]. On this basis, VAWT generally lags behind HAWT in terms of efficiency, stability, lifespan, etc., and gradually loses its competitiveness in the mainstream wind power market.

In the 1970s, the research boom just started. From the 1980s to the 1990s, the development of VAWTs became cautious. Many national projects, such as those of Sandia National Laboratories in the United States, have achieved good results [25-28]. However, in large-scale applications, VAWTs are usually not as competitive as HAWTs. However, VAWTs are still an attractive research topic from a mechanical design perspective. They have a simple structure, fixed driving device, and can work efficiently in multi-directional and turbulent winds.

These characteristics made VAWTs a compelling candidate for mechanical engineering analysis. Unlike HAWTs, which require complex yaw mechanisms and variable pitch control systems to align with wind direction, VAWTs can capture wind from any direction without active orientation mechanisms [18]. This reduces system complexity and aligns well with the goals of mechanical design optimization: efficiency, reliability, and reduced maintenance [18]. Furthermore, because most of the VAWT's components are located near the base, engineers found it easier to test, modify, and maintain mechanical subsystems, thus making VAWT models popular in academic and experimental contexts.

In the late 1990s and early 2000s, with the popularity of computational simulation, researchers have begun to use computational fluid dynamics (CFD) and finite element analysis (FEA) to study the unsteady aerodynamics and mechanical stress of VAWT systems [29]. Unlike HAWTs, where the aerodynamic loading is relatively steady, VAWTs operate under constantly fluctuating forces due to the cyclic movement of blades in and out of the wind flow. It is often referred to as the dynamic stall phenomenon. These effects were previously difficult to model analytically, but CFD tools such as ANSYS Fluent, OpenFOAM, and later, XFOIL and QBlade, enabled more accurate simulations of airflow and pressure distributions over rotating blades [30-32].

This computational capability allowed researchers to move beyond basic geometric assumptions and start examining the detailed effects of blade shape, positioning, aspect ratio, and blade number on the performance. One of the earliest recognized benefits of simulations was the ability to conduct parametric optimization, and testing tens to hundreds of design iterations in silico before building physical prototypes [33].

Around the same period, aerodynamic blade shape optimization became a central theme in VAWT research. Researchers began exploring how varying the blade profile (airfoil shape) could mitigate common problems such as low starting torque and poor performance at low tip speed ratios (TSRs). While early Darrieus turbines used symmetrical airfoils such as the NACA0012, which offered structural stability, they were found suboptimal in real wind conditions, particularly under dynamic stall.

In the context of VAWTs, researchers such as Paraschivoiu [35] played a pivotal role. His work on the double-multiple streamtube model (DMST) enabled a more accurate and computationally efficient analysis of VAWT performance, incorporating the effect of blade interaction with upstream and downstream flow. This model, combined with CFD verification, laid the foundation for systematic blade optimization studies.

Later research [36] in the 2010s explored the application of non-traditional blade shapes, including curved profiles, flexible blades, and blades with variable chord lengths or twists to improve energy extraction efficiency. Optimization algorithms, such as genetic algorithms (GAs), particle swarm optimization (PSO), and later machine learning methods, are increasingly used to find the optimal combination of geometric and operating parameters.

In actual design, the implementation of wind turbine optimization began to receive attention in the 2010s. This is mainly driven by university laboratories [37-39] and start-ups focusing on urban or small-scale wind power. Institutions like Delft University of Technology in the Netherlands, Politecnico di Milano in Italy, and Tsinghua University in China began publishing high-resolution simulation and field validation studies. These studies show that by optimizing the shape and position of the rotor, efficiency is increased by 20-30%.
The promotion and dissemination of these methods are supported by open source tools. For example, QBlade [40], developed at TU Berlin. These tools make advanced simulation more accessible, allowing even small teams to contribute to VAWT innovation.

In parallel, commercial efforts such as Urbine Technologies and Windspire Energy [41] started to incorporate advanced blade designs and simulation-driven development cycles, although large-scale commercialization remained limited due to the market dominance by HAWTs and policy preferences for utility-scale projects.

At present, the development of VAWTs continues at the intersection of mechanical engineering, aerodynamics, control theory, and materials science. Key focus topics include:

• *Hybrid designs, such as the Darius-Savonius combination.*
• *Smart deformable blades can adjust their shape according to wind conditions in real time.*
• *Floating offshore VAWTs.*
• *Vertical axis wind farms.*

1.1.2 H-Blade Darrieus VAWT

The H-Blade Darrieus VAWT is a widely studied subtype of the Darrieus family and has emerged as a compelling model for academic and applied research. Structurally characterized by its straight, vertical blades connected horizontally to a central shaft, forming an "H" shape when viewed from the front. The H-Blade configuration offers numerous advantages in manufacturability, simulation clarity, and mechanical reliability. Its unique geometry has positioned it at the intersection of theoretical aerodynamic study and practical engineering application.

The original Darrieus turbine, patented in 1931, employed curved blades in parabolic or linear shapes, optimizing the blade path to minimize bending stresses [42]. However, due to their three-dimensional geometry, these curved blades make aerodynamic analysis difficult.

To address these issues, engineers developed a simplified variation using straight blades, resulting in what is now commonly referred to as the H-Blade Darrieus turbine [43]. This design retained the lift-based operating principle of the original Darrieus model but dramatically improved structural simplicity. The reduction in blade curvature eliminated the need for complex support structures and made the turbine more amenable to both physical prototyping and computational modeling.

By the 1980s, H-Blade designs were increasingly favored in academic studies due to their ease of parameterization in simulation environments [18]. Their consistent cross-section and simplified dynamics allowed for clearer observation of core aerodynamic behaviors such as dynamic stall, blade-vortex interactions, and tip losses.

There are several reasons why H-Blade Darrieus VAWT is the model of choice in theory, experiment and early simulations [44-45]. Straight blades are much easier to manufacture than spiral blades. This makes H-Blade VAWT more suitable for small-scale production, rapid prototyping and experimental deployment. The H-blade structure evenly distributes aerodynamic forces and has less impact on the turbine frame. The symmetrical design reduces torque fluctuations, reduces asymmetric loads, and reduces the risk of fatigue failure during long-term operation. In computational modeling, the straight blade configuration simplifies boundary conditions and geometry for CFD simulations.

The optimization of H-Blade Darrieus turbines is a particularly rich topic of research due to the multiple interacting variables that influence performance. Traditional symmetric airfoils such as NACA0012, NACA0015, NACA0018, NACA0021 and NACA0024 are commonly used, but newer studies have explored cambered and asymmetric profiles to improve power coefficient. Researchers found that tailored airfoil selection can significantly affect lift-to-drag ratio and reduce energy losses due to stall. In addition, adjusting the number of blades impacts starting torque, turbulence interaction, and wake effects. Two-blade and three-blade configurations have different implications for structural load and energy capture efficiency [46].

Modern research shows the ratio of blade length to radius and the turbine's overall solidity determine how well the turbine extracts energy from the wind [47]. Optimizing this balance is crucial for maximizing performance across wind speeds. In addition, integrating pitch control mechanisms into straight-blade VAWTs. This kind of real-time dynamic optimization can respond to gusts and variable wind conditions to maintain stable output [48-49].

The application of composite materials and topology optimization methods has also allowed researchers to reduce the weight while maintaining structural stiffness [50]. Such methods are critical for enhancing turbine lifespan and reducing maintenance frequency.

In the area of the H-Blade VAWT optimization, Zhang et al. [51] analyzed the effect of blade pitch angles on torque fluctuation, finding that slight angular modifications led to measurable gains in energy production. Howell and Qin [52] conducted comparative simulations of various airfoil shapes in H-Blade configurations, revealing that cambered profiles can outperform symmetric ones by 10–20% in turbulent urban wind scenarios. Rezaeiha et al. [53] performed CFD simulations and experimental wind tunnel validations of two- and three-blade H-VAWTs. Their results showed significant interaction between blade aerodynamics and wake development, underscoring the need for coupled flow-structure modeling.

While the H-Blade Darrieus VAWT holds great promise, several challenges still occur in some circumstances. Low starting torque remains a persistent issue, particularly for turbines operating in low or inconsistent wind speeds. Hybrid configurations or magnetic assist motors are being explored to overcome this [54]. Noise and vibration caused by periodic aerodynamic loading require advanced damping systems or passive blade morphing to mitigate [55]. Scale-up limitations present engineering difficulties, as increasing blade length introduces greater bending moments and material fatigue risk.

1.2 Purpose of VAWT Blade Optimization

The main purpose of VAWT blade optimization is to improve aerodynamic performance and structural efficiency under complex and unstable wind conditions. Unlike horizontal axis turbines, vertical axis wind turbines operate under constantly changing angles of attack due to rotational motion, which usually results in flow separation, dynamic stall and fluctuating loads. The goals of optimization are:

• *Adjust the blade profile, delay or prevent airflow separation, improve the power coefficient, and extract more energy from the wind.*

• *Reduce blade vibration and aerodynamic torque pulsation, avoid fatigue failure and extend system life.*

• *Reduce structural weight, improve turbine efficiency and facilitate installation through shape and material optimization.*

By adjusting the blade camber, chord length and aspect ratio, the low wind starting capability is enhanced. Improve the stability of turbulent or urban flows with many direction changes. Simply put, optimizing blade shape directly affects aerodynamic efficiency, structural durability and cost-effectiveness. It is an important part of the technological advancement of modern vertical axis wind turbines.

1.2.1 VAWT Airfoil Shape Parameters

Airfoil, as the cross-sectional shape of a blade. It can generate lift when passing through fluids such as air. In a vertical axis wind turbine, the airfoil shape will determine how efficiently the turbine converts wind energy into rotating mechanical energy. It first appeared in the early 20th century, specifically developed by the National Advisory Committee for Aeronautics (NACA). This committee introduced the famous NACA four-digit and five-digit combinations. These profiles were originally defined for aircraft wings through mathematical calculations and experimental testing. Later, they were used in various fluid dynamics applications, such as wind turbines. VAWT typically uses symmetrical airfoils, such as NACA0012, to achieve a bidirectional flow environment. But now, modern designs are also exploring cambered or asymmetrical airfoils to improve performance on upwind and downwind strokes.

Key airfoil parameters: Airfoil shape can be described by several mathematical parameters. Chord length, the straight-line distance between the leading and trailing edges. Larger strings generally increase lift, but also increase drag. Camber, the maximum distance between the mean arc and the chord. The arc-shaped airfoil has higher lift, but has directional deviation. Thickness, the maximum distance between the upper and lower surfaces. Thicker wings are structurally stronger and have higher stall resistance. Leading edge radius, affecting the onset of stall and boundary layer separation. Angle of attack, the angle between the incoming airflow and the string. In VAWT, the angle of attack continuously changes as the blade rotates.

The lift coefficient and drag coefficient come from experiments or simulations. They represent the aerodynamic efficiency of the silhouette. In VAWT optimization, adjusting these parameters can change the stall angle, control the onset of separation, improve low Reynolds number performance, and balance lift during headwind and tailwind cycles.

1.2.2 Unsteady Adjoint Techniques

Adjoint-based optimization methods have become an important tool in the field of fluid dynamics, providing a means to compute the gradient of the performance metrics (such as drag, lift, or power coefficient) with respect to the shape or boundary conditions. Adjoint optimization is preferred over population-based or derivative-free optimizers such as genetic algorithms (GA/NSGA-II), particle swarm optimization (PSO), differential evolution (DE), simulated annealing, and even Bayesian optimization because it can scale to thousands of design variables, with each iteration costing roughly the equivalent of two CFD solvers (one original algorithm + one adjoint algorithm) [18]. In transient VAWT problems, a single objective evaluation requires a full unsteady RANS-ALE simulation; GA/PSO/DE require hundreds or even thousands of such evaluations. In contrast, adjoint methods provide the full gradient ∇J, with computational cost independent of the number of variables [56-70]. This allows for direct optimization of nodal wall normal displacements, preserving boundary layer resolution and manufacturability constraints through shape derivatives, and achieving predictable convergence using a well-established gradient-based scheme combined with line search. In practice, this means that a richer design space can be explored without a computational explosion, and many constraints such as thickness, curvature, area, and mesh quality can be enforced through analytical sensitivity rather than penalty tuning.

Therefore, the adjoint method is best suited for high-dimensional, unsteady, and multi-constrained VAWT airfoil and whole-machine optimization problems. Typical scenarios include:

- *Transient H-Darrieus or spiral VAWT airfoil aerodynamic optimization, which requires capturing unsteady effects such as dynamic stall and wake vortex interaction.*

- *Two-dimensional/three-dimensional whole-machine blade geometry optimization, which requires numerous design variables (such as nodal wall displacements) while also requiring strict control of constraints such as thickness, curvature, and mesh quality.*

- *Joint optimization of coupled control laws (such as pitch/oscillation waveforms) and shape, often with the goal of improving power coefficient, reducing torque ripple, and maintaining structural manufacturability.*

In these problems, the large design dimensions, strong coupling between the objective function and the flow field, and high sensitivity to boundary layer resolution and constraints make traditional derivative-free methods prohibitively expensive. The adjoint method, however, transforms complex unsteady CFD optimization into a viable engineering tool while maintaining physical consistency.

In the VAWT research, there are two main types: steady adjoint (or called Semi-Transient Method) [18] assumes the flow is time-independent, and unsteady adjoint accounts for time-varying flow fields and transient phenomena. For VAWTs, where the flow is highly unsteady due to blade rotation and angle of attack variation, unsteady adjoint methods are much more appropriate [56].

Adjoint-based methods have become indispensable in modern aerodynamic shape optimization due to their ability to efficiently compute gradients of objective functions with respect to a large number of design variables [57]. In the context of unsteady flows, particularly those involved in VAWTs, the development and application of unsteady adjoint techniques need to make progress in simulation fidelity and optimization capabilities.

The earliest adjoint formulations for compressible flows can be traced back to 1998, when Giles and Pierce introduced steady adjoint methods for Euler and Navier–Stokes equations [58]. These methods were primarily developed for aerospace applications under the assumption of steady flow conditions. However, as the need to handle time-dependent phenomena grew, especially in the fields of aeroacoustics and transient aerodynamic load prediction [59]. Researchers began to focus on extending adjoint methods to unsteady regimes.

Between 2002 and 2006, Giles and Pierce made a foundational contribution by rigorously deriving the unsteady adjoint equations for compressible flows [60]. Their work also introduced dual time-stepping methods, which significantly improved the stability and accuracy of unsteady simulations by separating physical and numerical time scales. This provided a mathematically consistent framework for time-reversed adjoint integration, which is essential in transient sensitivity analysis.

By 2010, further progress was made by Dwight and Brezillon, who developed computational techniques for efficiently performing reverse-time integration in unsteady adjoint solvers [61]. Their innovations addressed the numerical instability commonly encountered when solving adjoint equations backward in time, particularly in chaotic or high-Reynolds-number flow fields. These techniques were crucial in extending adjoint methods to industrially relevant unsteady problems.

A major leap towards democratizing adjoint-based optimization came in 2013, when Economon and colleagues released the SU2 (Stanford University Unstructured) framework [62], an open-source solver that implemented discrete adjoint capability for compressible unsteady flows. This tool enabled researchers and engineers outside of large institutions to perform high-fidelity shape optimization with adjoint-derived gradients, paving the way for broader application in wind energy and turbomachinery.

In 2015, He et al., [63] applied continuous adjoint solvers within the OpenFOAM environment, with modules for both steady and unsteady Reynolds-Averaged Navier–Stokes (RANS) simulations. Their work allowed greater flexibility in handling unstructured grids and complex boundary conditions, which are common in real-world turbine simulations [64]. OpenFOAM's modular design also facilitated the integration of adjoint methods into custom solvers tailored for VAWT geometries and cyclic boundary conditions.

More recently, since 2020, researchers [63-68] have focused on applying unsteady adjoints to highly nonlinear phenomena including dynamic stall, pitching and plunging airfoils, and transitional low-Reynolds-number flows. Their research has demonstrated that unsteady adjoints can accurately capture the sensitivity of time-averaged or phase-specific quantities, such as torque or pressure peaks. These studies offer insights that cannot be obtained through steady adjoint methods or finite difference approaches.

The application of unsteady adjoint methods to VAWTs is particularly novel. Unlike fixed-wing aircraft [62], which operate under relatively steady or mildly oscillatory flow conditions, VAWT blades experience strong periodic changes in angle of attack, frequently entering deep stall and complex vortex-dominated regimes. Traditional applications of adjoint methods often deal with small amplitude oscillations or buffet near Mach 0.8, which are far less dynamic than the cyclic pitch encountered in VAWT operation. In such aircraft cases, adjoint sensitivity analysis remains largely within a quasi-linear or harmonic framework, whereas VAWTs present a fundamentally nonlinear and time-varying problem [66].

Applying unsteady adjoints to VAWTs introduces new computational challenges, including the need for high-resolution temporal and spatial discretization, time-reversible and numerically stable solvers, and robust handling of turbulent, separated flows [67]. Nevertheless, these challenges are being addressed through the use of discrete adjoint solvers with automatic differentiation (AD), checkpointing strategies for memory efficiency, and dual-mesh techniques to decouple fluid-structure interactions [68].

Recent pioneering work, such as that by Chen et al., [69] has shown the feasibility of applying unsteady adjoint methods to optimize torque in 2D pitching VAWT blades. Similarly, van Stratan et al., [70] used dual-mesh unsteady adjoint solvers to optimize the stall characteristics of a straight-blade H-type VAWT, achieving improved aerodynamic performance under turbulent inflow. These studies suggest that unsteady adjoint methods are not only theoretically superior to their steady counterparts but also practically implementable in the context of VAWT blade optimization.

In conclusion, unsteady adjoint methods provide a powerful and now increasingly accessible framework for time-resolved, physics-informed optimization of VAWT blades. Their ability to capture the full spectrum of transient aerodynamic phenomena makes them especially suited to the VAWT environment, where traditional steady-state models fall short. As computational capabilities grow and solver technologies mature, unsteady adjoint optimization is expected to become a cornerstone technique in the design of next-generation VAWT.

1.3 Research Aims and Novelty

Due to their cyclical motion, VAWTs operate under highly unsteady and three-dimensional flow conditions, resulting in complex wake dynamics, fluctuating load curves, and nonlinear performance behavior. These characteristics pose significant challenges for the accurate performance prediction and blade shape optimization. Most existing VAWT optimization investigations rely on steady-state or semi-transient flow assumptions, which fail to capture the transient aerodynamic phenomena which are critical for torque generation and structural load estimation.

1.3.1 Major Research Gaps

Despite the theoretical and practical potential of the VAWTs for decentralized and urban energy systems, several key research gaps continue to limit the aerodynamic performance and structural efficiency of VAWT blade designs. Important among these is the persistent reliance of aerodynamic optimization studies on steady-state or quasi-steady-state simulations. This simplified approach fails to capture the inherently unsteady and cyclical nature of VAWT aerodynamics, particularly the asymmetric flow conditions experienced during the upstroke and downstroke phases of the blade rotation. Consequently, most optimization results fail to reflect realistic dynamic loading conditions, leading to suboptimal blade geometries in actual deployment. This can be solved by the existing SU2 unstable adjoint optimization algorithm by redefining the incoming flow and pitch attitude of the airfoil.

A second major research gap lies in the narrow range of airfoil geometries explored in the existing VAWT optimization literature. Despite growing interest in customized or application-specific airfoils, most previous research has been limited to symmetric standard airfoils. This limits innovation and hinders the discovery of unconventional, yet potentially superior, blade designs. This research will discuss the situation after multiple optimization iterations to explore the sensitivity analysis of the optimized candidate airfoils.

Another underexplored topic is the limited application of adjoint optimization frameworks, particularly in time-resolved or fully unsteady environments. While adjoint methods are well-established in oscillating fixed-wing aircraft design, their extension to rotating and accelerating systems remains rare. Challenges such as defining realistic blade motion, accurately tracking force fluctuations, and mitigating wake-induced contamination in sensitivity fields have led many researchers to default to gradient-free or simplified approaches. This research defines Darrieus pitching motion and VAWT to simulate the airfoil performance under practical rotational motion, and takes into account the wake effect to solve this problem.

Furthermore, most existing studies ignore the effects of blade-wake interaction and turbulent wakes on the sensitivity accuracy. In other words, early studies used only a constant (e.g., 0.5) to define the flow characteristics of the blade in the downwind section, which failed to reflect periodic changes. Without appropriate upstream sampling techniques, gradients derived from adjoint fields can become noisy or misleading, undermining the integrity of the optimization process. This research conducts experimental verification, takes into account the influence of induced speed, and uses a method to re-monitor the incoming flow velocity based on the results of the flow solution.

Finally, the transition from 2D to 3D blade optimization remains largely unresolved. Currently, there is a lack of frameworks that can transfer sensitivity information in 3D blade geometries in a physically meaningful and computationally stable manner. This presents a significant bottleneck in producing practical, manufacturable, and optimized VAWT blade designs for real-world flow conditions. This research establishes a new three-dimensional blade geometry and explores the performance of the two-dimensional optimized airfoil in three-dimensional blade CFD simulations.

In summary, the current state of the art in VAWT research suffers from methodological limitations in terms of unsteady modeling, geometric generalization, optimization fidelity, wake treatment, and dimensional scalability. This study aims to address these shortcomings by developing a time-adjoint-based optimization framework tailored for unsteady VAWT operation.

1.3.2 Research Aims

VAWT have garnered significant research attention in recent years due to their potential advantages over the HAWTs in urban and offshore environments. Their omnidirectional wind acceptance, simpler generator positioning, and potential for compact array layouts render them suitable for distributed renewable energy systems. However, the unsteady and highly three-dimensional aerodynamic environment of VAWTs imposes substantial challenges for aerodynamic optimization, which is particularly in blade shape refinement and operational efficiency. This research is fundamentally aimed at advancing the state of VAWT blade design through the development and application of time-dependent adjoint-based optimization techniques.

The central goal of this study is to bridge the gap between high-fidelity unsteady flow simulations and robust, accurate optimization methodologies. Specifically, the aim is to formulate and apply an unsteady adjoint optimization framework tailored to the rotating dynamics of Darrieus-type VAWTs. Existing studies on VAWT blade optimization have predominantly employed steady-state simulations or quasi-steady assumptions, which can significantly misrepresent the real aerodynamic loads experienced by the turbine blades due to their inherently dynamic behavior, particularly during upstroke and downstroke cycles.

To this end, the current work proposes a novel approach that constructs a fully unsteady adjoint optimization strategy capable of capturing transient flow features and blade-flow interactions. The target performance metric, which is defined as a time-dependent adjoint objective based on the tangential force coefficient that directly corresponds to the torque-generating effectiveness of the blades. By explicitly modeling the velocity and acceleration profiles of the Darrieus motion within the SU2 computational fluid dynamics (CFD) solver, this research introduces a dedicated mechanism for handling realistic VAWT kinematics in an adjoint framework. Additionally, the inlet flow speed is designed as a time-varying function to simulate the periodic variations experienced by a blade in motion, enabling more accurate sensitivity analysis and design optimization.

Another significant component of this research involves minimizing the influence of turbulent wake effects on sensitivity results. This is achieved by implementing a piecewise function that samples velocity upstream of the blade, which is an approach that isolates the most physically meaningful flow characteristics from downstream disturbances. The research also introduces a free-form deformation (FFD) framework that is dynamically adapted to the rotating blade profile. This allows for precise tracking of sensitivity fields across the blade surface in a rotational context, improving the robustness of shape optimization even in highly unsteady scenarios.

The final stage of this study aims to generalize and extend the developed methodology to three-dimensional VAWT blade simulations. A hierarchical sensitivity computation framework is proposed, enabling layered calculation and propagation of sensitivity data throughout the 3D domain. This not only enhances the fidelity of the optimization process but also supports automated blade morphing and structural reshaping to match optimal aerodynamic configurations.

In summary, this research is driven by the following primary aims:

- *To overcome the limitations of steady-state approximations in VAWT blade optimization by formulating a time-accurate adjoint methodology.*

- *To develop and implement Darrieus-specific motion dynamics, including time-varying pitch, velocity, and acceleration, into an open-source adjoint CFD solver.*

- *To reduce adjoint solution contamination by downstream wakes via smart sampling strategies.*

- *To apply free-form deformation techniques tailored for unsteady rotating blade systems.*

- *To scale the methodology from 2D to 3D for practical VAWT blade optimization with automatic sensitivity-driven morphing.*

Through these objectives, the research seeks to establish a new standard for high-fidelity, time-resolved aerodynamic optimization of VAWT blades.

1.3.3 Research Novelty

The field of aerodynamic optimization using adjoint methods has seen substantial progress over the last two decades. In the context of VAWTs, however, the application of adjoint-based optimization remains limited and underdeveloped, especially when considering the unsteady nature of VAWT aerodynamics. Most existing studies have either relied on steady or quasi-steady approximations or have restricted themselves to a narrow subset of airfoil geometries such as the NACA 64A010.

This research differentiates itself by targeting a long-standing gap in the application of unsteady adjoint optimization techniques to VAWTs using non-NACA airfoils and non-aircraft-related engineering problems. While adjoint solvers have been extensively applied to aircraft wing design under steady or mildly unsteady conditions, their extension to rotating, time-varying systems such as VAWTs presents unique challenges, including motion definition, force fluctuation tracking, and wake management. These challenges have led prior studies to adopt simplifying assumptions, which undermine the fidelity and reliability of the resulting blade designs.

The key novel contributions of this research are as follows:

An enhanced single-blade model is first proposed, and the unsteady adjoint optimization algorithm is applied to this model in a general VAWT / oscillation airfoils:
This work is the first to extend unsteady adjoint optimization beyond NACA 64A010 to arbitrary airfoil geometries within the VAWT context. The framework is agnostic to specific airfoil profiles and can adapt to non-conventional or application-specific shapes.

Adjoint objective formulated for tangential force coefficient:
Instead of relying on global performance metrics or indirect surrogates, the optimization objective in this study is defined in terms of the tangential force coefficient, a more direct representation of torque generation in Darrieus turbines. This formulation allows the optimization process to target performance features that are physically meaningful and mechanically relevant.

Definition of the enhanced Darrieus motion in the SU2 solver:
A major innovation of this research is the incorporation of Darrieus-type motion profiles (including pitch, rotational speed, and acceleration) into the SU2 solver's adjoint infrastructure. This enables precise modeling of rotating blade dynamics and facilitates their integration into a gradient-based optimization loop.

Time-variable inlet speed representation:
To simulate the effect of cyclic wind conditions encountered by a rotating blade, a time-dependent inlet velocity function is introduced. This innovative approach enables the solver to mimic unsteady inflow characteristics that contribute to lift and torque variation across a blade's revolution.

Wake-resistant sensitivity capture via piecewise sampling:
Recognizing the distorting effect of wake turbulence on adjoint sensitivities, the study introduces a sampling strategy that captures upstream flow velocities at segmented intervals. This approach filters out noise and enhances the signal-to-noise ratio of gradient information.

Free deformation of moving rotating blades:
This is a time-adaptive free deformation framework, used for the first time on VAWT (vertical axis wind turbine) blades under unsteady conditions. This method ensures that the deformation map will follow the movement of the blade and maintain geometric consistency when the shape is modified.

In summary, this research is novel, not just because of the technological advancement, but also because of its physical realism, numerical robustness, and engineering applicability, all well integrated. The developed framework brings a highly scalable, accurate and open toolset to future VAWT designers. The goal is to optimize performance under realistic, unstable conditions. It also marks a significant change, with previous approaches being too simplistic or completely ignoring the inherent instabilities of VAWT aerodynamics.

Chapter 2

Modelling and Theories of VAWT

2.1 VAWT Aerodynamics

The aerodynamic behavior of VAWTs is controlled by complex and highly unstable flow field mechanisms. Unlike HAWT, which has a relatively stable angle of attack, VAWT blades experience constant changes in angle of attack and wind direction when rotating. This cyclic change can lead to problems such as dynamic stall, delayed separation, lift and drag fluctuations, etc. Understanding these aerodynamic properties is important to improve VAWT efficiency, especially by optimizing blade geometry. Key aerodynamic factors include: dynamic stall, self-start capability, wind instability, and wake interaction.

2.1.1 Dynamic Stall

Dynamic stall means that the angle of attack increases rapidly. After exceeding the limit of static stall, flow separation will occur with delay and become nonlinear. For example, this is often the case in VAWT blades during rotation. Unlike a stable stall, a dynamic stall will bring large instantaneous lift and drag, and usually leading edge vortices will appear. This vortex can temporarily increase force, but it can also bring unstable loads and lead to structural fatigue. Accurate simulation of dynamic stalls is important because the airfoil shape can be adjusted to control stall onset and recovery. This results in smoother torque output and higher average power extraction.

2.1.2 Self-Starting Problem

Vertical axis wind turbines, especially those with symmetrical airfoils, often have difficulty starting at low wind speeds due to the low aerodynamic torque in the initial rotation stage. This phenomenon is called self-starting problem, and it is more serious in urban or low-wind environments. The self-starting capability of a turbine is mainly determined by blade shape, solidity and aerodynamic asymmetry. Blade optimization solves the problem by adjusting the airfoil camber, chord length or pitch distribution to ensure adequate starting torque while maintaining normal operating performance.

2.1.3 Unsteady Wind

Unstable wind is a big challenge for VAWT. They are often placed in places with variable and fast wind conditions, such as urban canyons or near buildings. Unstable winds interact in a time-varying manner, increasing fluctuations in aerodynamic forces and rotor response. Therefore, it is a big problem to design blades that can perform well under various instantaneous wind speeds and wind directions. Optimization strategies, such as time-dependent targets or multiple condition simulations, are important to ensure that VAWT blades remain effective and reliable under real unstable wind conditions.

2.1.4 Flow Control Methods

To reduce adverse aerodynamic effects such as dynamic stall or wake disturbance, various flow control methods have been proposed for vertical axis wind turbines. These methods range from passive technologies such as vortex generators to active control technologies such as blade pitch modulation or plasma actuators. Their goal is to manipulate boundary layer behavior, or enhance flow adhesion, thereby improving aerodynamic efficiency. From a blade optimization perspective, flow control functionality can be added directly to the blade geometry or it can be considered in aerodynamic modeling. In this way, designers can take advantage of controlled flow behavior to improve performance.

2.1.5 Power Coefficients

The power coefficient C_P is the efficiency of the turbine in converting wind energy into mechanical energy. It has no unit. For vertical axis wind turbines (VAWT), C_P is greatly affected by aerodynamic parameters, such as angle of attack distribution, stall behavior, and blade shape. The optimization goal is usually to make C_P as large as possible within the entire working tip speed ratio range. Because the aerodynamic force on the blades changes during rotation, the optimized airfoil shape must balance the performance in the upwind and downwind areas and strive for a higher cycle average C_P. This has also become the core indicator for driving blade optimization.

2.2 Early VAWT Modeling and Experimental Study

Aerodynamic modeling and experimental analysis of VAWT are important. It helps us understand VAWT performance characteristics and also informs design improvements.

Although computational fluid dynamics (CFD) simulations are now popular, early studies relied on analytical models and semi-empirical models, such as flow management theory, to evaluate VAWT aerodynamics. These models, like the single-stream tube model (SST) and the dual multi-stream tube model (DMST), provide fundamental insights into rotor performance and are now also used extensively in preliminary design and validation of CFD results.

At the same time, some wind tunnel tests were used to verify the modeling results to calibrate the simulation parameters. This type of experimental device usually uses a low-speed wind tunnel to simulate the relative inflow velocity of the pitching airfoil. In addition to this, there are force and torque sensors, as well as high-resolution flow measurement tools such as particle image velocimetry (PIV). The data obtained from the experiment will be further processed. Finally, the aerodynamic coefficients are calculated to verify the theory or computational model.

2.2.1 Streamtube Model of VAWT

Before the widespread adoption of CFD tools, VAWT performance was primarily analyzed using streamtube-based models, which provided a simplified but insightful approximation of the rotor behavior. The basic idea behind these models is to divide the swept area of the turbine into one or more vertical streamtubes through which the wind passes. The interaction between the rotating blades and the airflow within each streamtube is then analyzed using momentum and blade element theory.

The earliest version of this approach is the Single Streamtube Model [71-73], which treats the rotor as one uniform actuator disc with averaged blade forces. In this model, the flow is assumed to remain steady and symmetrical about the rotor axis. The velocity of the air approaching the rotor is reduced due to energy extraction, and this reduction is quantified by an induction factor, denoted by a. The local wind speed at the blade position becomes:

$$V = V_\infty(1 - a)$$

[Eq. 2.1]

where V_∞ is the freestream wind speed. The inductance factor takes into account the momentum lost by the turbine and therefore determines how much useful power can be extracted. A higher induction coefficient generally means more energy is extracted from the wind, but it also reduces the local wind speed of the blade. The definition of this value plays a crucial numerical impact in simulations and experiments.

While SST models offer simplicity, they ignore several key physical phenomena, such as variation in flow between upwind and downwind blade passes, flow curvature, and blade-wake interactions. To address these limitations, researchers developed the Double-Multiple Streamtube Model [72], a more sophisticated extension that divides the rotor into multiple azimuthal and radial streamtubes. Each streamtube independently calculates forces based on local flow conditions, blade velocity, and angle of attack. Importantly, the Double-Multiple Streamtube incorporates different induction factors for the upwind and downwind halves of the rotation, thereby capturing the asymmetric performance observed in real VAWTs.

In Double-Multiple Streamtube, the rotor is divided into N streamtubes, and for each azimuthal position θ, the relative velocity V_{rel} and angle of attack α are calculated using vector summation of wind velocity and blade tangential speed. The lift L and drag D forces are then computed from airfoil data, and the resulting tangential force F_T is used to update torque T, which is expressed as:

$$T = \sum_{i=1}^{N} F_{T,i} \cdot R$$

[Eq. 2.2]

where R is the local radius at streamtube. The resulting torque and power coefficient C_P can be integrated over the full rotation.

The introduction of induction factors into Double-Multiple Streamtube is essential for capturing realistic performance [73-75]. These factors influence not only the energy extraction but also the aerodynamic loading by altering the local angle of attack. For instance, in the downwind region, flow deflection and vortex shedding can significantly reduce the effective wind velocity, necessitating a separate induction factor to maintain model fidelity. Without such adjustments, simplified models would predict symmetric performance, which contradicts both the CFD results and experimental observations.

Researchers such as Paraschivoiu [35] have played a key role in formalizing the DMST framework and validating it against experimental data. While streamtube models are inherently limited in their ability to simulate unsteady phenomena such as dynamic stall or three-dimensional wake interaction, they remain invaluable for rapid design iteration, performance trend analysis, and preliminary optimization in low-resource settings. Moreover, many modern simulation pipelines use the streamtube model results as initialization or validation baselines for higher-fidelity CFD studies.

2.2.2 Experimental Setup

Experimental studies of VAWT can validate computational models and reveal complex flow phenomena that are difficult to capture through simulations. Most experimental setups, conducted in controlled environments such as closed or open circuits, allow careful monitoring of variables such as wind speed, turbulence intensity, rotor speed, etc. In VAWT research, different types of wind tunnels have been used, including subsonic low-speed wind tunnels and atmospheric boundary layer simulation facilities.

A standard experimental setup for VAWT analysis typically involves a small-scale VAWT model mounted on a force-measuring balance or torque sensor, connected to a variable-speed motor. The rotor is placed in the test section of the wind tunnel, and the incoming wind speed is controlled to replicate the desired conditions [76, 77]. Researchers often record global quantities such as torque, thrust, rotational speed, and power output, along with local aerodynamic forces on individual blades. These measurements are used to calculate performance coefficients such as power coefficient, moment coefficient, and tangential coefficient, providing direct metrics of rotor efficiency [78].

Advanced experimental campaigns often include flow visualization techniques such as smoke tracing, tuft grid lines, or Particle Image Velocimetry (PIV) [53, 79-81], which capture velocity vector fields and vorticity distributions around the blades. These techniques have been crucial in identifying the development of dynamic stall, tip vortex shedding, and wake interactions. For instance, the studies by Rezaeiha et al. [53] used PIV to resolve the unsteady flow structure in the near-wake of H-blade VAWTs, confirming the presence of coherent vortex rings and rotationally induced downwash patterns.

In addition to flow visualization, pressure taps are sometimes embedded into the blade surface to directly measure the local pressure distribution during operation [80-81]. The time-resolved pressure data, combined with known airfoil geometry and rotational velocity, can be integrated to obtain local lift and drag forces. These forces are then compared to CFD predictions and used to validate airfoil models or dynamic stall approximations.

A particularly insightful parameter derived from experimental data is the angle of attack distribution throughout the rotor cycle. Elsakka et al. [82] demonstrated that there is often a substantial deviation between the theoretical angle of attack (computed assuming ideal kinematics) and the actual effective angle measured or inferred from pressure data. This deviation is caused by flow deflection, wake interference, and blade–blade aerodynamic coupling, all of which complicate modeling efforts. The use of experimental data to reconstruct the actual angle of attack has therefore become a key technique in validating or correcting analytical and numerical models.

To address the issue of measurement accuracy and repeatability, researchers often perform tests at multiple tip speed ratios, Reynolds numbers and yaw angles. This is because statistical averaging over multiple runs smooths out transient fluctuations and sensor noise.

Many experimental studies include the work of Templin [71], who has measured full-cycle aerodynamic loads on the Darrieus rotor using strain gauge instrumentation. The Sandia VAWT program has used large outdoor turbines to calibrate simulation models. Besides, the high-resolution flow measurement tools has deployed to study dynamic stall and wake recovery. In each case, experimental data not only validates the model but also reveals physical mechanisms, such as vortex-induced loading or leading-edge separation. These data can be incorporated into improved computational models.

In summary, experimental studies of VAWT are important. It captures the nuances of unsteady flow behavior, validates simulation tools, and informs blade design. As CFD optimization technology advances, high-quality experimental data is critical. They ensure that computational models are close to physical reality. Flow tube modeling, CFD simulations, and wind tunnel experiments are used together to continuously advance VAWT's aerodynamic understanding and engineering innovation.

2.3 Computational Model

The computational model of VAWT has changed significantly over the past two decades. Early models often used simple two-dimensional steady-state simulations to approximate the complex unsteady-state aerodynamic phenomena in VAWT operation. However, with the advancement of computing power and algorithm technology, especially in the field of computational fluid dynamics (CFD), more accurate and high-fidelity VAWT simulations have become possible.

Modern VAWT CFD modeling includes full transient simulation, dynamic stall modeling, and flow separation effects throughout the azimuthal cycle. What's more, optimization techniques, such as optimization based on adjoint methods, are increasingly integrated into CFD workflows. This integration allows researchers to not only evaluate performance metrics such as torque and power coefficient, but also see how sensitive these metrics are to changes in geometry or operating conditions. Technologies such as shape optimization, mesh deformation, and automated design loops have now become standard tools for many advanced VAWT simulation studies.

The use of Unsteady Reynolds-Averaged Navier Stokes (URANS), Detached Eddy Simulation (DES) and Large Eddy Simulation (LES) models further enhances the understanding of wake dynamics and flow separation. The transient adjoint solver is particularly novel in VAWT and allows researchers to find the optimal airfoil deformation to maximize power output while reducing aerodynamic losses during rotation.

2.3.1 CFD Model Setup of VAWT

The accurate simulation of VAWTs through Computational Fluid Dynamics (CFD) requires a well-considered model setup that reflects both the physical complexities of unsteady rotor flows and the numerical challenges associated with cyclic blade motion. Over the past two decades, CFD models of VAWTs have transitioned from simple 2D steady-state formulations to sophisticated, time-resolved simulations with shape optimization loops. A consistent theme across the literature [83-85] is the recognition that the inherently unsteady and separated nature of the flow field around a rotating VAWT demands the use of transient simulations with appropriate turbulence modeling, boundary conditions, and spatial resolution.

Most recent studies have converged on using the SST k–ω [18] [62-65] turbulence model due to its superior performance in predicting boundary layer separation and its robustness in adverse pressure gradient regions, which are particularly relevant during dynamic stall events experienced by the rotating VAWT blades. The SST k–ω model blends the near-wall accuracy of the k–ω model with the freestream insensitivity of the k–ε model, making it well-suited to capturing the complex aerodynamic behavior over a full azimuthal cycle. This model is also compatible with most adjoint solver frameworks and has been validated across a range of Reynolds numbers and tip speed ratios commonly found in VAWT operations.

Boundary conditions are another critical aspect in the CFD modeling of VAWTs. A large body of literature has established a set of commonly accepted practices [18] [62] [86-88]. At the inlet boundary, a calculated relative wind speed is usually imposed based on the expected simulation environment, which depends on the freestream wind speed, induction factor, and TSR. At some times, the turbulence intensity at the inlet is specified in the range of 5% to 10%, reflecting the average atmospheric turbulence level. The outlet boundary is commonly treated as a pressure-outlet or zero-gradient condition, ensuring smooth flow exit without artificial reflections. Side and top boundaries are generally defined as slip or symmetry planes, depending on whether ground effects or 3D turbulence interactions are to be resolved. The blade and shaft surfaces are modeled as no-slip walls, with near-wall treatment depending on the mesh resolution and target y^+ values.

In terms of mesh design, high-quality structured or unstructured meshes are generated around the blade surfaces, with particular attention to the resolution in the near-wall regions [18] [62] [86-90]. Maintaining $y^+ \approx 1$ near solid boundaries is a widely accepted best practice, ensuring the validity of turbulence models like SST k–ω that resolve the boundary layer directly without relying on wall functions. Mesh refinement is concentrated in regions expected to experience high vorticity, pressure gradients, or flow separation, which is especially at the leading and trailing edges of the blades and in the near-wake. The mesh size typically ranges from 0.5 to 5 million cells in 2D simulations and exceeds 50 million in high-resolution 3D simulations. However, since most optimization studies have focused on 2D cross-sectional slices of H-blade VAWTs, they strike a balance between capturing key aerodynamic phenomena and maintaining computational feasibility [18][95].

Time discretization plays an equally important role in transient simulation [91]. Because the aerodynamic forces on a VAWT blade fluctuate significantly during each rotation cycle, the time step must be small enough to accurately account for these changes. A common choice throughout the literature is a time step corresponding to 1° to 2° of rotor rotation per step. For example, Mishra et al. [92] demonstrated that a 2° rotation time step is sufficient for unsteady adjoint optimization of hovering rotors, obtaining accurate results at low computational cost. Fine time steps can capture the rapid onset of dynamic stall and the development of leading edge vortices. The total simulation duration is typically set to span multiple complete rotations (usually more than 3), allowing the solution to reach a pseudo-periodic steady state before extracting performance metrics or accompanying sensitivities.

Regarding initial conditions, most simulations start with a static flow field. They slowly increase the rotor speed or wind speed over a short period of time to avoid numerical instability. Some high-fidelity studies initialize simulations with a convergent steady-state solution that serves as the base flow field for transient operations. But for optimization routines, especially those involving unstable adjoint calculations, the initialization process is more important. Inconsistencies may cause the adjoint fields to diverge, or give incorrect sensitivity gradients.

In optimization-focused studies, the domain size is typically set large enough to prevent boundary effects from contaminating the solution. The upstream boundary is generally placed at least five rotor diameters from the center of rotation, while the downstream outlet is located 10–15 diameters away to allow wake structures to dissipate. The lateral extent is similarly generous, ranging from 5 to 10 diameters on either side. This practice is consistent across multiple studies, including those by Elsakka et al. [73], Day et al. [18], and Albring et al. [93] , who all highlight the importance of domain size in minimizing artificial blockage and reflection effects in the computational solution.

Another key element in the simulation setup is the use of mesh deformation or morphing algorithms in adjoint-based shape optimization. Most modern optimization frameworks represent the airfoil geometry using a set of discrete nodes that define the blade surface. The adjoint method then computes the sensitivity of the objective function (e.g., average torque, C_P, or force coefficient) with respect to perturbations at each node. These sensitivity gradients are then used to update the blade shape iteratively. The airfoil is thus deformed according to the adjoint-derived sensitivities, enabling the discovery of optimal geometries that may not be intuitive or analytically derivable. Studies by Day et al., [18] Papoutsis-Kiachagias et al. [94], and others have validated this approach across different objectives and flow conditions.

While the general computational setup described above has become a standard for transient VAWT simulations, additional considerations must be taken into account when performing transient adjoint optimization. For example, the use of 'frozen turbulence' models [95] can lead to inaccurate adjoint gradients when the turbulence field significantly evolves over time. Advanced implementations have therefore moved toward solving adjoint equations with consistent turbulence modeling, such as adjoint Spalart-Allmaras or SST variants. Similarly, challenges associated with memory storage during backward time integration have been addressed using checkpointing strategies and recursive projection techniques to stabilize and accelerate the adjoint solver [96].

In summary, the CFD model setup for VAWTs has reached a state of methodological maturity, where turbulence modeling, domain sizing, temporal and spatial discretization, and boundary condition choices reflect both physical realism and numerical stability. These practices are consistently supported by studies from the past decade, and they form the computational backbone upon which effective optimization, particularly using adjoint methods, is built.

2.3.2 Simulation Techniques

The integration of optimization algorithms into CFD simulations for VAWTs represents one of the most significant methodological advances in aerodynamic design over the past decade [97]. Traditional CFD approaches provided detailed flow field information but lacked the ability to guide systematic improvements in blade geometry. Optimization techniques, particularly those based on gradient methods such as adjoint-based sensitivity analysis have filled this gap by enabling direct linkage between flow behavior and geometric design changes [98]. These coupled simulation-optimization workflows have proven especially useful in the context of VAWTs, where aerodynamic performance is governed by highly unsteady and nonlinear flow phenomena that are difficult to optimize through intuition or parametric sweeps alone.

At the core of these integrated frameworks is a robust parameterization of the blade geometry. In most CFD-based optimization studies, the airfoil or blade cross-section is represented using either spline-based techniques (such as Bézier curves or B-splines) or node-based surface definitions, where the shape is defined by a set of control points that can be manipulated during the optimization process [99]. These parameters act as design variables, and their dimensionality can range from a few geometric coefficients to hundreds of nodal coordinates [100]. For example, in the adjoint optimization method implemented by Day et al. [18], the blade airfoil was discretized using a high-resolution nodal mesh, and the sensitivities of the power coefficient with respect to each node's position were computed using adjoint flow solutions. Such high-dimensional parameterization allows for the capture of subtle but aerodynamically meaningful shape modifications that can influence flow separation, vortex shedding, and pressure recovery.

The optimization algorithm itself plays a crucial role in guiding the design evolution. Gradient-based algorithms, such as steepest descent, conjugate gradient, or BFGS (Broyden–Fletcher–Goldfarb–Shanno), are commonly employed due to their compatibility with adjoint sensitivity data [101-103]. In contrast to evolutionary algorithms or heuristic search methods, gradient-based optimizers are well-suited for high-dimensional problems where the cost of evaluating objective functions is substantial. The adjoint method offers a critical advantage here: the computational cost of obtaining the full gradient of the objective function with respect to all design variables is nearly independent of the number of variables. This allows the optimization to proceed efficiently even when using detailed CFD models with thousands of control points on the blade surface.

One of the most challenging aspects of coupling CFD with optimization is the issue of convergence and numerical stability, both of the primal (forward) flow solution and the adjoint (backward) sensitivity calculation [62]. Transient CFD simulations of VAWTs are highly sensitive to time-stepping schemes, turbulence modeling, and grid quality, and the introduction of geometric deformation during optimization further complicates the convergence landscape. In response, several studies have introduced multi-stage optimization workflows, in which an initial coarse-grid or steady-state optimization is performed to identify promising design trends, followed by refinement using high-fidelity transient simulations. This approach, sometimes referred to as "nested fidelity optimization," balances computational cost and accuracy. For instance, Day et al. employed a "semi-transient" technique [18], using snapshot-based adjoint optimization that approximated the unsteady flow over selected time intervals, thus enabling faster iterations while retaining some unsteady effects.

To maintain robustness in optimization, mesh deformation algorithms are employed after each geometry update to avoid remeshing, which can introduce numerical noise or break mesh connectivity. Techniques such as radial basis function (RBF) interpolation or spring-analogy methods are widely used to deform the computational mesh in response to changes in surface geometry, ensuring that boundary layer and near-wall cell distributions remain intact [101-103]. In parallel, mesh quality monitoring is implemented to detect skewed or distorted elements that could affect the solver's accuracy. When the mesh quality drops below a certain threshold, automated mesh regeneration may be triggered, although this introduces additional computational overhead.

Another important consideration is the constraint handling within optimization. Airfoil thickness, leading-edge radius, or manufacturability requirements often impose hard or soft constraints on the allowable design space. These are typically enforced through penalty functions or Lagrangian multipliers in the optimization formulation. For example, Dhert et al. [104] implemented an optimization process in which a coarse global search was followed by a constrained local refinement, ensuring that the final geometry respected both aerodynamic and structural requirements. Similarly, Schramm et al. incorporated thickness constraints and turbulence modeling compatibility into their OpenFOAM-based adjoint optimization framework, though they noted that additional adjustments would be required for modeling realistic blade pitching motions as seen in VAWTs [95].

As the simulation progresses through multiple optimization cycles, convergence criteria must be carefully defined. These include changes in the objective function (e.g., power coefficient), gradient norm, or design variable values between iterations. Due to the unsteady nature of VAWT flows, performance metrics are often defined as time-averaged values over multiple rotor cycles, which adds complexity to convergence detection. Some studies adopt a moving average approach, where convergence is declared only if the objective function remains within a fixed tolerance across several consecutive optimization iterations.

In addition to single-objective optimization, there are also multi-objective and multi-point optimization strategies. For vertical axis wind turbines, in order to maximize the average power coefficient, or minimize torque fluctuations, or maintain structural stability. Such objectives can be treated with a multi-objective adjoint formulation, with each objective weighted in a cost function, or with sequential optimization in a Pareto optimal framework. For example, Day et al. studied the trade-off between upwind and downwind performance. The results show that optimizing one area often sacrifices performance in another area [18]. Their findings underscore the need for a time-resolved, cycle-aware optimization method that considers the complete rotational behavior of VAWT blades rather than isolated snapshots or regions.

Recent advances have focused on extending the optimization framework to fully transient adjoint solvers. This solver calculates time-accurate sensitivities throughout the simulation cycle. This technology was first used in the aerospace field, such as oscillating airfoils. Recently, the time-reversible adjoint equation and the unsteady Navier-Stokes equation are solved together, and the gradient information of the time-related performance indicators can be calculated [105-107]. These solvers often use checkpointing algorithms to control memory consumption during backward integration. They can also use reduced-order modeling techniques to stabilize adjoint fields in turbulent flows. In many cases, after the optimal blade shape is obtained, additional simulations are usually done to verify the results under different operating conditions, such as changes in tip speed ratio, turbulence intensity, or changes in incoming flow velocity. This ensures that the design does not fit just a narrow set of simulation parameters.

In short, the combination of CFD and optimization technology is already mature in the field of VAWT research. The technical content is also high! Through accurate parameterization, gradient-based adjoint solvers, robust mesh handling, and convergence-aware optimization strategies, researchers are now able to design blade shapes specifically for the unstable aerodynamic environment of vertical axis turbines.

Chapter 3

Unsteady Adjoint Optimization

In the field of computational fluid dynamics (CFD), the study of unsteady adjoint methods is highly significant. It enables sensitivity analysis and design optimization, and is particularly well-suited for handling time-varying aerodynamic problems. These theories are very useful for studying airfoils under unsteady flow conditions, because accurately predicting aerodynamic forces such as lift, drag, and pressure distribution is crucial in unsteady flows. The unsteady adjoint approach provides an efficient means to compute the sensitivity of an objective function with respect to design parameters or boundary shape perturbations. Unlike finite difference methods that require repeated flow simulations for each design variable, the adjoint method computes gradients with respect to all design variables simultaneously, with a computational cost that is largely independent of the number of variables.

3.1 Theories of Unsteady Adjoints

For an airfoil in unsteady flow, each point on its surface experiences a pressure distribution that varies with time. To determine how sensitive this pressure is to changes in shape, control inputs, or boundary conditions, the unsteady adjoint equations are solved. These equations are derived from the linearization and transposition of the governing unsteady Navier-Stokes equations. The result is a backward-in-time problem whose solution, the adjoint variables, encodes how perturbations at the final time influence the objective function. From this adjoint field, one can extract gradient information: it informs us how a small change in surface shape at a specific location and time will affect the overall performance metric. This process enables precise identification of which parts of the airfoil geometry most influence the performance metric and hence should be modified during optimization.

The actual modification of the airfoil shape is performed using optimization algorithms, which use the gradient information supplied by the adjoint solution to update the shape in a direction that improves the objective function. Common approaches include gradient descent, quasi-Newton methods, or even more sophisticated techniques like the method of moving asymptotes. The shape updates are often constrained by manufacturability, structural integrity, or other physical considerations. Because the adjoint gradients are available at every point on the surface, local and global shape modifications can be made with high resolution and efficiency, making this approach highly attractive for real-world aerodynamic design problems.

Unsteady adjoint theory can help understand and optimize time-varying pressure distributions. By providing detailed sensitivity distributions, it can guide the effective adjustment of surface geometry to achieve performance objectives. It overcomes the computational bottleneck of traditional finite difference methods. This advantage is particularly significant when there are a large number of design variables and unsteady flow phenomena.

In the transient problem of VAWT, the objective function is usually a function of time and depends on the state of the system at different time steps. Suppose we have an objective function J that depends on time t, flow field states $u(t)$, $p(t)$ and design variables x. The objective function can be expressed as an integral over time:

$$J = \int_{t_0}^{t_f} J(u(t), p(t), x, t)dt \qquad \text{[Eq. 3.1]}$$

where t_0 is the initial time, t_f is the termination time, $u(t)$ and $p(t)$ are the speed and pressure flow variables at time t, x is a design variable (e.g. a parameter of an airfoil shape) and is usually independent of time.

In the transient adjoint method for VAWTs, Equation 3.1 corresponds to maximizing the time-averaged power coefficient C_P:

$$J = -\frac{1}{T}\int_{0}^{T} C_P(t)dt \qquad \text{[Eq. 3.2]}$$

where T is the total time, t is the certain timestep. The negative sign is used to transform the "maximization of the average power coefficient" into a "minimization of the objective function," thus conforming to the general mathematical framework of adjoint optimization and gradient descent.

The flow field equations for transient problems (such as the Navier-Stokes equations) contain time derivative terms. Assume that the flow field states $u(t)$ and $p(t)$ satisfy the following partial differential equations [62][66][103]:

$$\frac{\partial u}{\partial t} + R(u, p, x, t) = 0 \qquad \text{[Eq. 3.3]}$$

Here $R(u, p, x, t)$ is still the residual function of the flow field, but now it also contains the time derivatives of the flow field variables $\frac{\partial u}{\partial t}$ in unsteady adjoint functions, which describes the change of the fluid state with time.

Similar to the steady-state problem, the transient problem also introduces adjoint variables to deal with the influence of constraints (flow field equations). In order to derive the transient adjoint equation, we first construct the Lagrangian function to combine the objective function J and the flow field constraint R [62][66][103]:

$$L = \int_{t_0}^{t_f} \left[J(u(t), p(t), x, t) + \lambda(t)^T \left(\frac{\partial u}{\partial t} + R(u, p, x, t) \right) \right] dt \qquad \text{[Eq. 3.4]}$$

where $\lambda(t)$ is the transient adjoint variable, which depends on time t.

The Lagrangian function L contains the objective function and the constraints of the flow equations (introduced through adjoint variables).

In order to obtain the sensitivity of the design variable x to the objective function, we need to vary the Lagrangian function L. The complexity of the transient problem lies in that we not only need to differentiate the spatial variables (such as u and p), but also need to deal with time.

First, we take the derivative of the flow field variables $u(t)$ and $p(t)$ in the Lagrangian function L and take their variations respectively [62][66][103]:

$$\delta L = \int_{t_0}^{t_f} \left[\frac{\partial J}{\partial u} \delta u + \frac{\partial J}{\partial p} \delta p + \lambda^T \left(\frac{\partial(\delta u)}{\partial t} + \frac{\partial R}{\partial u} \delta u + \frac{\partial R}{\partial p} \delta p \right) \right] dt \qquad \text{[Eq. 3.5]}$$

At this point, we also need to deal with the influence of the time derivative $\frac{\partial u}{\partial t}$ on the flow field variables. By using the partial integration method of integration, the time derivative term is transferred to the adjoint variable:

$$\int_{t_0}^{t_f} \lambda^T \frac{\partial(\delta u)}{\partial t} dt = [\lambda^T \delta u]_{t_0}^{t_f} - \int_{t_0}^{t_f} \left(\frac{\partial \lambda}{\partial t} \right)^T \delta u dt \qquad \text{[Eq. 3.6]}$$

We assume that the perturbations on the initial and final conditions are zero, so the boundary term $[\lambda^T \delta u]_{t_0}^{t_f}$ is zero due to the setting of the $\delta u(t_0)$ is zero. In this way, the variational form of the final Lagrangian function can be written as:

$$\delta L = \int_{t_0}^{t_f} \left[\frac{\partial J}{\partial u} - \frac{\partial \lambda}{\partial t} + \left(\frac{\partial R}{\partial u} \right)^T \lambda \right] \delta u dt + \left[\frac{\partial J}{\partial p} + \left(\frac{\partial R}{\partial p} \right)^T \lambda \right] \delta p dt \qquad \text{[Eq. 3.7]}$$

In transient adjoint derivation, if we first handle only the variables u corresponding to the momentum equation, and then handle the pressure variable p separately, we can obtain:

$$\delta L = \int_{t_0}^{t_f} \left[\frac{\partial J}{\partial u} - \frac{\partial \lambda}{\partial t} + \left(\frac{\partial R}{\partial u} \right)^T \lambda \right] \delta u dt \qquad \text{[Eq. 3.8]}$$

In order to make the variation of the Lagrangian function for all flow field variables equal to zero, we can obtain the transient adjoint equation:

$$-\frac{\partial \lambda}{\partial t} + \left(\frac{\partial R}{\partial u} \right)^T \lambda = -\frac{\partial J}{\partial u} \qquad \text{[Eq. 3.9]}$$

$$\left(\frac{\partial R}{\partial p} \right)^T \lambda = -\frac{\partial J}{\partial p} \qquad \text{[Eq. 3.10]}$$

This is the form of the transient adjoint equation.

Unlike steady-state problems, the time derivative term of the transient adjoint equation indicates that the adjoint variable is also dynamic in time. We need to solve the adjoint variable $\lambda(t)$ by integrating the adjoint system backward in time (from the end time t_f to the initial time t_0).

An important characteristic of the transient adjoint equation is that the time direction is opposite, that is, the adjoint equation is solved from the end time to the initial time. This means that we need to specify the termination condition $\lambda(t_f)$ of the adjoint variable at the end time t_f. The specific boundary conditions depend on the form of the objective function.

When the adjoint equation is solved to obtain the adjoint variable $\lambda(t)$, the sensitivity of the objective function to the design variable x can be calculated by the following formula:

$$\frac{dJ}{dx} = \int_{t_0}^{t_f} \left(\frac{\partial J}{\partial x} + \lambda^T \frac{\partial R}{\partial x} \right) dt \qquad \text{[Eq. 3.11]}$$

Here, $\frac{\partial R}{\partial x}$ is the explicit derivative of the flow equations with respect to the design variable x, usually computed via shape derivatives in a CFD solver.

Design optimization in Computational Fluid Dynamics (CFD) using the adjoint method is a powerful technique to efficiently find the optimal shape of a geometry for a given objective while minimizing or maximizing a cost function. The adjoint method involves solving two sets of equations: the primal equations, representing the flow physics, and the adjoint equations, representing the sensitivity of the objective function with respect to the design variables. The optimization process aims to adjust the design variables to minimize the objective function.

The primal equations represent the flow physics. For the unsteady, incompressible Navier-Stokes equations, the primal equations, including continuity equation and momentum equation are:

$$\nabla \cdot \bar{u} = 0 \qquad \text{[Eq. 3.12]}$$

$$\rho\left(\frac{\partial(\bar{u})}{\partial t} + (\bar{u} \cdot \nabla)\bar{u}\right) = -\nabla\bar{p} + \nabla \cdot [(\nu + \nu_t)(\nabla\bar{u} + (\nabla\bar{u})^T)] + \rho g \qquad [Eq. 3.13]$$

Here, $\bar{u}$ is the mean velocity, $\bar{p}$ is the mean pressure, ν is the molecular viscosity, ν_t is the turbulent (eddy) viscosity predicted by the turbulence model, ρ is the density, g is the body force (e.g., gravity).

In aerodynamic optimization, we define an objective functional. For example, maximizing power coefficient or tangential coefficient of a wind turbine blade. This is written as

$$J = \int_{t_0}^{t_f} \int_{\Omega} \mathcal{J}(\bar{u}, \bar{p}, x, t) d\Omega\, dt + \Phi(\bar{u}(t_f), x) \qquad \text{[Eq. 3.14]}$$

Where x denotes the design variables, which used to describe the optimized airfoil shape, such as control points of a parameterized geometry.

To evaluate how sensitive the objective J is to changes in the design x, the flow variables $\bar{u}$ and $\bar{p}$ also depend on x. Direct differentiation would require solving many CFD simulations, which is one for each design variable. This is computationally impossible.

The adjoint method avoids this by introducing adjoint variables to enforce the governing equations as constraints.

The Lagrangian is defined as

$$L = \int_{t_0}^{t_f} \int_{\Omega} \left[\mathcal{J} + \lambda(\bar{u} \cdot \nabla) + \psi\left(\frac{\partial(\bar{u})}{\partial t} + (\bar{u} \cdot \nabla)\bar{u} + \frac{1}{\rho}\nabla\bar{p} - [(\nu + \nu_t)(\nabla\bar{u} + (\nabla\bar{u})^T)] - g\right)\right] d\Omega\, dt + \Phi(\bar{u}(t_f), x) \qquad \text{[Eq. 3.15]}$$

Where λ is the adjoint pressure, ψ is the adjoint velocity.

Then compute the variation of L:

$$\delta L = \int_{t_0}^{t_f} \int_{\Omega} \left[\frac{\partial \mathcal{J}}{\partial \bar{u}} \delta \bar{u} + \frac{\partial \mathcal{J}}{\partial \bar{p}} \delta \bar{p} + \lambda \nabla \cdot (\delta \bar{u}) + \psi(var)\right] d\Omega\, dt$$

$$+ \frac{\partial \Phi}{\partial \bar{u}(t_f)} \delta \bar{u}(t_f) \qquad \text{[Eq. 3.16]}$$

This expression contains derivatives of the variations, such as $\frac{\partial(\delta \bar{u})}{\partial t}$, needs to be removed through integration by parts.

The integration can transfer derivatives from the variations to the adjoint variables. For example, the time-derivative term becomes:

$$\int \psi \cdot \frac{\partial(\delta \bar{u})}{\partial t} dt = [\psi - \delta \bar{u}]_{t_0}^{t_f} - \int \frac{\partial \psi}{\partial t} \cdot \delta \bar{u} dt \qquad [Eq. 3.17]$$

If we use the same steps applies to spatial derivatives of δu and δp. All boundary terms vanish by choosing appropriate adjoint boundary conditions. After collecting all terms multiplying $\delta \bar{u}$ and $\delta \bar{p}$, we require:

$$\delta L = 0 \qquad [Eq. 3.18]$$

For any variation, if this yields the transient adjoint equations, and is solved backward in time, we can get the adjoint moment $Eq. 3.19$, adjoint continuity $Eq. 3.20$ and terminal condition $Eq. 3.21$.

$$-\frac{\partial \psi}{\partial t} - (\nabla \bar{u})^T \psi + (\bar{u} \cdot \nabla)\psi - (\nu + \nu_t)\nabla^2 \psi + \nabla \lambda = \frac{\partial \mathcal{J}}{\partial \bar{u}} \qquad [Eq. 3.19]$$

$$\nabla \cdot \psi = -\rho \frac{\partial \mathcal{J}}{\partial \bar{p}} \qquad [Eq. 3.20]$$

$$\psi(t_f) = \frac{\partial \Phi}{\partial \bar{u}(t_f)} \qquad [Eq. 3.21]$$

Once the primal and adjoint solutions are known, the sensitivity of the objective to the design variable x is:

$$\frac{dJ}{dx} = \int_{t_0}^{t_f} \int_{\Omega} \left(\frac{\partial \mathcal{J}}{\partial x} + \psi^T \frac{\partial R}{\partial x}\right) d\Omega\, dt \qquad \text{[Eq. 3.22]}$$

where R is the residual of the Reynolds-averaged Navier–Stokes (RANS) momentum equation.

x can be the shape parameter describing the optimized NACA0015 based airfoil, like airfoil control points, thickness or camber coefficients. The adjoint method allows computing $\frac{dJ}{dx}$ in one additional simulation, regardless of how many design variables exist.

The design variables x are updated using the gradient information obtained from the sensitivity analysis. A simple update rule could be:

$$x_{new} = x_{old} - \alpha \frac{dJ}{dx} \qquad \text{[Eq. 3.23]}$$

Where α is the step size.

The study of oscillating airfoil in VAWT operating conditions use an objective function C_T, which is given by $C_T = C_L\, sin(wt) - C_D cos(wt)$ with respect to the design variables x can be calculated using the adjoint equation. Where w is a constant, t is time, and $C_L(x,t)$ and $C_D(x,t)$ are functions of the design variables x. The adjoint equation is derived from the Lagrangian, which includes the primal equations and the sensitivity equation. The sensitivity of the objective function C_T with respect to the design variables x can be expressed as:

$$\frac{dC_T}{dx} = \int_{t_0}^{T} \left(sin(wt) \frac{\partial C_L}{\partial x} - cos(wt) \frac{\partial C_D}{\partial x} \right) dt \qquad \text{[Eq. 3.24]}$$

Where T is the final time and t_0 is the initial time.

$$\frac{dC_T}{dx} = \left(\frac{1}{w} cos(wt_0) - \frac{1}{w} cos(wT) \right) \frac{\partial C_L}{\partial x} + \left(\frac{1}{w} sin(wt_0) - \frac{1}{w} sin(wT) \right) \frac{\partial C_D}{\partial x} \qquad \text{[Eq. 3.25]}$$

This oscillation airfoil study uses 20 input design variables to perform a parametric approach for airfoil deformation based on Hicks–Henne bump functions once the gradient is calculated. If the Hicks–Henne bump functions are used, the parameterized airfoil must have at least 12 parameters to achieve acceptable errors [108]. Compared with other airfoil parameterization methods, its calculation speed is the fastest. The expression is given by:

$$y = y_{basis} + \sum_{i=1}^{i=n} a_i f_i(x) \qquad \text{[Eq. 3.26]}$$

$$f_i(x) = \left[\sin\left(\pi x^{\frac{log\frac{1}{2}}{log\ t_1}} \right) \right]^{t_2}, 0 \le x \le 1 \qquad \text{[Eq. 3.27]}$$

Where t_1 is the maximum thickness location of the bump, t_2 is the width of the bump and a_i is the shape parameter.

If in a two-dimensional simulation of VAWT, assuming constant angular speed circular motion and a constant radius, for one blade, the value of C_T can be obtained to be equal to C_M.

$$C_T = \frac{F_T}{\frac{1}{2}\rho {V_{rel}}^2 A} \quad \text{[Eq. 3.28]}$$

$$C_M = \frac{M}{\frac{1}{2}\rho {V_{rel}}^2 AR} \quad \text{[Eq. 3.29]}$$

The power coefficient of a VAWT is:

$$C_P = \frac{NM\omega}{\frac{1}{2}\rho U^3 A} \quad \text{[Eq. 3.30]}$$

The power coefficient of VAWT is a value that should be optimized, but can be simplified:

$$V_{rel} = \frac{U}{1-u}\sqrt{\lambda^2 + 2\lambda cos\theta + 1} \quad \text{[Eq. 3.31]}$$

$$C_M = \frac{M(1-u)^2}{\frac{1}{2}\rho(\lambda^2 + 2\lambda cos\theta + 1)U^2 AR} \quad \text{[Eq. 3.32]}$$

$$\frac{C_P}{C_M} = \frac{(\lambda^2 + 2\lambda cos\theta + 1)NR\omega}{(1-u)^2 U} > 0, 0 \le \theta \le 2\pi \quad \text{[Eq. 3.33]}$$

At any time-step since the power coefficient will also increase as the tangential coefficient increases, optimizing the tangential coefficient can obtain a higher power coefficient.

3.2 Adjoint Sensitivity Analysis

In vertical axis wind turbines (VAWTs), the angle of attack of the blades changes periodically as they rotate, leading to unstable aerodynamic performance of the airfoil. Therefore, to optimize the airfoil shape and improve efficiency, the time-averaged aerodynamic performance must be considered. This is typically represented by the lift, drag, and moment coefficients over one or more rotation cycles. Here, the tangential coefficient and power coefficient are used as the target aerodynamic performance metrics. Adjoint sensitivity analysis provides a powerful method to determine how small changes in airfoil shape affect performance metrics or cost functions. Its goal is to calculate the gradient, where x represents the airfoil geometric parameters. Assuming U is the state vector of the flow field (velocity, pressure, etc.), $R(U, x) = 0$ represents the governing unsteady Navier-Stokes equations.

In the context of vertical axis wind turbine airfoils, this sensitivity information tells us which parts of the geometry have the greatest impact on average performance. For example, high sensitivity to trailing edge curvature might suggest that smoothing or sharpening this region could reduce drag. These gradient values are then used to iteratively modify the airfoil shape using gradient-based optimization algorithms (e.g., steepest descent or conjugate gradient). After several iterations, the airfoil shape is adjusted based on the calculated sensitivities to improve the desired performance. Therefore, sensitivity analysis is fundamental to the shape optimization of vertical axis wind turbines (VAWTs). It provides a precise validation for improving aerodynamic performance under unsteady flow conditions.

3.3 Objective Functions

In the aerodynamic optimization of VAWTs, the unsteady nature of the flow around rotating blades leads to time-varying performance metrics. One critical quantity is the tangential force coefficient, which directly relates to torque generation and power output. Since this coefficient fluctuates over each rotor revolution due to the cyclic blade motion and dynamic stall effects, it is essential to define an objective function that captures the average aerodynamic performance over a complete rotation cycle, rather than optimizing based on instantaneous values that may not represent sustained performance.

To address this, we define the objective function as the *period-averaged tangential force coefficient*, denoted as $\overline{C_T}$. Mathematically, this is expressed as:

$$\overline{C_T} = \frac{1}{T}\int_0^T C_T(t)dt \qquad \text{[Eq. 3.34]}$$

Where C_T is the instantaneous tangential force coefficient and T is the duration of one full rotation (period). In practice, this integral is approximated numerically using discrete time steps, either via trapezoidal integration or a simple arithmetic mean over the sampling points within one or more full revolutions after the flow reaches a periodic or statistically steady state.

In the SU2 framework, custom objective functions can be implemented by modifying the source code or using Python scripting through the SU2's external function interface. To compute a time-averaged objective function:

1. **Set up unsteady simulation**: Ensure that the configuration file is set for time-accurate simulation using TIME_DOMAIN= YES and define TIME_STEP and TIME_ITER appropriately to cover at least one full rotation period.
2. **Enable force coefficient output**: Configure OUTPUT_FORCES= YES and define the surface markers for the blade where the forces are computed. SU2 will write the force coefficients (including tangential components if the coordinate system is properly defined) to the forces_breakdown.csv file.
3. **Post-processing script**: Write a Python script that reads the tangential force coefficient from the output file and calculates the period average over one or multiple cycles. This script can be wrapped into SU2's OBJECTIVE_FUNCTION via a user-defined interface using EXTERNAL_ADJOINT= YES and linking your script in the configuration.
4. **Custom C++ implementation (optional)**: For more integrated performance, modify the SU2 C++ source to accumulate the tangential force coefficient over time steps and compute the mean internally. This requires editing the ObjectiveFunction class and recompiling the solver.

By defining the objective as a period average, the optimization process focuses on sustainable performance rather than transient peaks, ensuring that the resulting design performs well under realistic unsteady conditions typical of VAWTs.

3.4 Convergence of Adjoint Method in CFD

In computational fluid dynamics (CFD), convergence has always been a critical issue when using adjoint methods. While adjoint methods are computationally inexpensive and can compute the gradient of an objective function with respect to many design parameters, their performance heavily relies on the convergence characteristics of both the primal and adjoint solvers. One of the key factors affecting convergence is the optimization algorithm used to update the design parameters. Examples include gradient descent and its variants, such as steepest descent, conjugate gradient, and quasi-Newton methods (e.g., BFGS). These algorithms are scalable and well-suited to the gradient information provided by the adjoint method. However, gradient descent methods often exhibit slow convergence when dealing with stiff problems. Stiff problems are common in high-fidelity CFD simulations, primarily due to large condition numbers.

To mitigate these issues, preconditioning techniques and line search algorithms are commonly employed to improve convergence stability. For instance, in aerodynamic shape optimization, preconditioners are designed based on flow physics principles to normalize the gradient scale. Line search algorithms are used to determine the optimal step size, ensuring sufficient descent while avoiding overshooting the minimum. Conjugate gradient and L-BFGS algorithms, by incorporating curvature information, generally significantly accelerate convergence and are therefore suitable for problems with a large number of design variables. In CFD applications, the nonlinearity and stiffness of the governing equations (such as the Navier-Stokes equations) challenge the convergence of the adjoint solver. The adjoint equations, derived from the linearization of the flow equations, must be solved with high accuracy to ensure reliable gradients. If the primal flow equations are not well-converged, the adjoint gradients may be inaccurate, leading to incorrect descent directions. During the simulation process, the convergence of the adjoint solver is often even more sensitive to solver tolerances than the primal solver, especially in turbulent or compressible flows.

In addition to solver-specific issues, mesh quality and numerical precision also impact convergence. For instance, grid anisotropy and high aspect-ratio elements, which is common in boundary layer regions, can lead to poorly conditioned systems, impeding both primal and adjoint convergence. Recent advances in adjoint-based mesh adaptation have shown promise in improving gradient accuracy and convergence simultaneously, by refining the mesh in regions with high sensitivity.

Several researchers have conducted comparative studies on the effectiveness of optimization strategies in adjoint-based CFD frameworks. For example, Jameson [58] demonstrated that while simple steepest descent methods could converge to local minima, they often required hundreds of iterations, whereas quasi-Newton methods achieved similar accuracy with an order of magnitude fewer iterations. These findings underscore the importance of choosing the right optimization algorithm based on problem stiffness, dimensionality, and computational budget.

Moreover, machine learning and hybrid optimization approaches have recently been integrated with adjoint solvers to address some convergence limitations. Surrogate-assisted adjoint methods, for instance, use data-driven models to approximate cost functions or gradients, thus reducing the number of costly CFD evaluations. Such hybrid techniques have been shown to accelerate convergence, particularly in multi-fidelity or multi-objective optimization contexts.

In summary, the convergence of the adjoint method in CFD is influenced by a combination of solver performance, optimization strategy, and numerical fidelity. Gradient-based methods such as gradient descent and its variants are widely adopted due to their efficient use of adjoint gradients, though their convergence rates vary based on problem complexity. Ensuring convergence in both the primal and adjoint systems is essential to the success of the adjoint approach. Empirical and theoretical studies alike suggest that improvements in solver algorithms, mesh adaptation, and hybridization with data-driven techniques will continue to enhance the robustness and speed of adjoint-based CFD optimization frameworks.

Besides the solver itself, mesh quality and numerical accuracy also affect convergence. For example, anisotropic meshes and high aspect ratio elements, common in boundary layer regions, can worsen the system condition. This hinders the convergence of both the primal and adjoint methods. In recent years, adjoint-based mesh adaptation techniques have become popular. By refining the mesh in sensitive regions, they promise to improve both gradient accuracy and convergence. Some researchers have compared the effectiveness of optimization strategies within adjoint-based CFD frameworks. For instance, Jameson [58] found that a simple steepest descent method converges to a local minimum but requires hundreds of iterations. Quasi-Newton methods, on the other hand, achieve similar accuracy with half the number of iterations. These findings remind us to choose appropriate optimization algorithms based on the stiffness, dimensionality, and computational budget of the problem.

3.5 Solve CFD Problems by Adjoint Optimization

Adjoint method-based optimization provides an efficient and mathematically consistent framework for solving CFD problems where the objective function depends on flow evolution and the geometry of the physical domain. Instead of independently perturbing each design variable and running thousands of CFD simulations, the adjoint method introduces a set of auxiliary partial differential equations—the adjoint equations—to backpropagate sensitivity information. Once the original unsteady RANS flow field is obtained, the adjoint equations can be integrated from the final time step to the initial time step, using the same mesh, boundary conditions, and numerical discretization methods as the forward solver, but in the reverse time direction.

This “reverse-time” solution yields the gradient of the objective function with respect to all design variables at a computational cost roughly equivalent to one additional CFD simulation, independent of the dimension of the design space. Therefore, adjoint optimization enables high-resolution shape correction for complex aerodynamic systems, such as vertical-axis wind turbines, where unsteady vortex shedding and periodic rotor loads significantly impact performance. By combining window-time averaging, flow constraints, and geometric regularization, the adjoint method provides both the accuracy required for engineering design and the efficiency needed for large-scale CFD optimization. This makes adjoint optimization one of the most powerful tools in modern fluid mechanics for solving flow-driven design problems.

SU2 (Stanford University Unstructured) was chosen as the primary simulation tool. Its core features include: a high-precision fluid solver based on the finite volume method; a flexible mesh system capable of handling both structured and unstructured meshes; powerful unsteady simulation capabilities; and most notably, a variational adjoint optimization framework. Its highly scalable C++ architecture allows researchers to easily integrate new physical models, turbulence models, mesh motion algorithms, and optimization modules. SU2's greatest strength lies in its ability to efficiently solve steady-state and unsteady-state flow fields. It also incorporates complete continuous and discrete adjoint solvers, supporting the direct calculation of the gradient of the objective function with respect to hundreds or even thousands of design variables, while the computational cost is almost equivalent to only one or two additional CFD calculations. This "gradient cost independent of design dimension" characteristic makes SU2 an ideal tool for solving large-scale shape optimization problems.

This study focuses on the unsteady aerodynamic performance and shape optimization of two-dimensional blade sections in vertical axis wind turbines (VAWTs). Key challenges include stronger rotation-induced unsteady effects, more significant periodic wakes and dynamic stalls, objective optimization of time-averaged power coefficient and torque ripple, and airfoil shape optimization with multiple design variables.

SU2 is one of the few open-source platforms that supports unsteady adjoint optimization. For strongly periodic systems like VAWTs, the objective function is often a weighted time-averaged power coefficient, torque ripple, and dynamic lift behavior. Since these objectives rely on time integration, steady-state adjoint optimization cannot be applied. SU2's unsteady adjoint optimization can backpropagate sensitivity in the time dimension and utilize window functions for robust time-averaged optimization.

The research focuses on the two-dimensional blade cross-section of a vertical axis wind turbine (VAWT), with a two-dimensional aerodynamic analysis per unit span. The blade geometry is based on NACA0015 and optimized using parametric methods. The flow is an incompressible, viscous, external, and strongly unsteady rotating flow, characterized by periodic vortex shedding, dynamic stall, and significant wake disturbances induced by rotor rotation. Turbulence is enclosed using a RANS model (SST k-w or SA). During the adjoint equation solution phase, to avoid ill-posed problems caused by nonlinear coupling of the turbulence model, the turbulent viscosity coefficient is considered frozen, maintaining consistency with the original problem's results. Since the blade moves in a rotating reference frame, an ALE (Arbitrary Lagrangian–Eulerian) mesh motion framework is used, where the inner rotating domain undergoes rigid body rotation, while the outer flow domain remains stationary. The two domains are coupled through a sliding interface to ensure consistency of numerical flux between the two regions.

For the RANS average velocity $\bar{u}(x,t)$ and pressure $\bar{p}(x,t)$ at the moving grid velocity $v_g(x,t)$, the ALE form is:

$$\nabla \cdot \bar{u} = 0 \qquad [\text{Eq. } 3.35]$$

$$\frac{\partial \bar{u}}{\partial t} |_{\xi} + ((\bar{u} - v_g) \cdot \nabla)\bar{u} = - - \frac{1}{\rho} \nabla \bar{p} + \nabla \cdot [(\nu + \nu_t)(\nabla \bar{u} + (\nabla \bar{u})^T)] + g \qquad [Eq. 3.36]$$

Where $\frac{\partial}{\partial t} |_{\xi}$ is the time derivative fixed with respect to the grid coordinates.

The grid velocity of the inner rotation domain in 2D CFD is:

$$v_g(x,t) = \Omega e_z \times r(x,y,0) \qquad [\text{Eq. } 3.35]$$

Where Ω is the angular velocity and r is the radius.

The boundary conditions of the airfoil is a no slippage, impermeable and insulating wall:

$$\bar{u}(x,t) = v_g(x,t) \qquad \text{[Eq. 3.36]}$$

The inlet boundary is:

$$\bar{u}(x,t) = U(t)e_{in}, \bar{p}(x,t) = p_\infty \qquad \text{[Eq. 3.37]}$$

Where e_{in} is the unit vector of (1,0), U(t) is the relative wind speed.

The outlet boundary uses a standard pressure outlet (which does not change over time). It allows free flow of the wake and does not reflect vortices generated by blade motion.

$$\frac{\partial \bar{u}}{\partial n} = 0, \bar{p} = p_\infty \qquad \text{[Eq. 3.38]}$$

The side symmetrical boundaries are employed to avoid affecting the wake generated by the incoming flow and rotation:

$$\frac{\partial u_t}{\partial n} = 0, u_n = 0 \qquad \text{[Eq. 3.39]}$$

The initial condition is:

$$\bar{u}(x,0) = U(0)e_{in}, \bar{p}(x,0) = p_\infty \qquad \text{[Eq. 3.40]}$$

$$\bar{u}(x,0) = \Omega e_z \times r(x,y,0) \qquad \text{[Eq. 3.41]}$$

To ensure the numerical stability of unsteady rotating flow and its adjoint solution, this study employs time-domain solution (TIME_DOMAIN = YES) in SU2, combined with second-order dual-time-step propagation (DUAL_TIME_STEPPING-2ND_ORDER) to obtain high-precision time discretization. For VAWT blades, the number of time steps per revolution is crucial for analyzing torque pulsations and wake vortex structures. This study selects one physical time step per degree, and the total number of physical steps is the product of all time steps and pseudo-time iterations. A reference value between 200 and 400 ensures approximate convergence for each physical time step in existing examples.

The pseudo-time Courant–Friedrichs–Lewy (CFL) number is maintained between 2 and 5, while the physical CFL number is controlled within 1 and 2. The CFL number represents the ratio between the distance travelled $u\Delta t$ by flow information during a time step and the local mesh size Δx. In the dual-time-stepping framework, the physical CFL determines the temporal resolution of the unsteady flow, whereas the pseudo-time CFL governs the convergence rate of the inner iterations at each physical time step.

A physical CFL range of 1–2 was selected to ensure sufficient temporal accuracy in capturing the unsteady aerodynamic loads, dynamic stall development, and wake evolution of the VAWT while avoiding excessive computational cost. Significantly larger values may reduce temporal resolution and introduce time-integration errors, whereas substantially smaller values increase the number of physical time steps required without providing noticeable improvements in solution accuracy. The pseudo-time CFL was chosen to be higher (2–5) because the pseudo-time iterations are used solely to converge the implicit solution within each physical time step rather than to resolve the physical flow evolution. Higher pseudo-time CFL values generally accelerate convergence, while excessively large values may lead to instability or deteriorated convergence behaviour.

In summary, unlike the physical CFL number, the pseudo-time CFL does not affect the temporal resolution of the physical flow and is therefore selected primarily to accelerate convergence of the inner iterations.

The adjoint calculation time step UNST_ADJOINT_ITER needs to be set to the same as the original flow field problem, so that the adjoint solution integrates backward from the final physical time step to the initial time. To support reverse-time solving, all (or segmented according to a checkpoint strategy) restart data files from the forward solution need to be saved for progressive loading during the adjoint phase.

Regarding the mesh, the blade wall in this solver uses a first-layer height of $y^{+} \approx 1$ by default, employing multiple boundary layer elements and a growth rate of $1.1 - 1.2$ to ensure the accuracy of the SST or SA turbulence models commonly used in wind power equipment. Flow direction refinement is performed within the wake region to resolve detached eddies and frequency components [109-121].

A complete CFD with adjoints, following by geometry update optimization process is as follows. First, in the original problem (URANS/ALE) solution phase, calculations begin with the previous round's results or the MRF steady-state field as the restart file. After a transition process involving number transformations, the system enters the objective function integration window. During the window, the system saves the flow field restart file for each physical time step for reverse-time reading during the adjoint phase.

The adjoint solution is then performed: UNST_ADJOINT_ITER = N is set so that the adjoint equation is integrated backward from the final time step to the initial time step. At each backward time step, the code reads the corresponding restart file from the forward solution to ensure duality consistency. After the adjoint flow field is obtained, its wall sensitivity (i.e., the gradient with respect to shape) is projected into the design variable space; this step is performed by SU2_DOT. The obtained gradient vector is then used to update the design variables. Shape updates are achieved through SU2_DEF, which performs mesh deformation and mesh quality checks at this stage. Finally, the updated shape is used in the next round of URANS solving, and this process is repeated until the objective function converges or the preset computational budget is reached.

Chapter 4

UDF Build, Theory and Configurations

In the aerodynamic optimization study of vertical axis wind turbine (VAWT) blades based on the unsteady adjoint method, the reliability of the numerical model depends not only on the derivation and implementation of the adjoint equation itself, but also highly on the physical consistency, temporal accuracy, and numerical implementation methods related to the optimization variables of the forward flow field solver. As mentioned earlier, steady-state optimization (whether using a single-blade model or a combination of in-situ airfoils) has significant drawbacks, especially in capturing the time interval. It ignores the fact that VAWT blades are constantly in a strongly unsteady aerodynamic environment during operation. Dynamic stall, periodic angle-of-attack changes, blade kinematic coupling, and upstream and downstream wake interference jointly determine the transient evolution characteristics of the flow field. To introduce a fully unsteady adjoint method, any user-defined functions (UDFs) related to blade motion, boundary conditions, objective functions, or design variables (DVs) need to be redeveloped, which directly affects the temporal continuity of the forward flow solution, the accuracy of sensitivity information, and the physical reliability of the final optimization results.

Specifically, the construction of time-resolved objective functions (e.g., objective functions based on tangential force coefficients) and the integration of non-uniform rotational kinematics (e.g., variable pitch and piecewise acceleration curves) break many traditional assumptions of periodicity, smoothness, and spatiotemporal consistency relied upon by solvers. The core objective of this chapter is to systematically verify the numerical correctness, physical consistency, and applicability boundaries of the newly developed UDF within the unsteady CFD-adjoint optimization framework, and to explain its impact on aerodynamic response, sensitivity propagation path, and optimization convergence behavior.

These innovations affect several core aspects of the simulation pipeline. For instance, spatial and temporal discretization schemes must accommodate sharper gradients and potentially discontinuous flow features, which can alter the stability conditions like CFL constraints).

The solver's forward-backward time integration required for adjoint computations also becomes more sensitive to interpolation accuracy, boundary consistency, and temporal staggering due to the irregular forcing introduced by time-varying inputs and blade motion.

Furthermore, the presence of non-smooth time-dependent motion inputs, such as abrupt pitch changes or piecewise acceleration, complicates the adjoint time-marching process, particularly in accurately preserving the causality of flow-field sensitivity. These conditions may lead to increased stiffness in the adjoint equations, deteriorating gradient convergence if not properly addressed through time-scheme tuning or adaptive resolution strategies.

In the oscillating airfoil example, UDF (Underlying Dynamic Function) is used to realize unsteady pitch motion, dynamic boundary conditions, and online evaluation of the objective function. By directly incorporating the tangential coefficient (C_T) into the CFD solution process as the optimization objective, the time averaging error introduced by traditional post-processing methods can be avoided, but this also places higher demands on the time integration accuracy and transient convergence characteristics. Therefore, this chapter first analyzes the numerical implementation of C_T as the optimization objective in CFD and evaluates its impact on transient response and sensitivity stability.

Subsequently, by constructing an equivalent downwind inflow model in the form of dynamic boundary conditions and a piecewise function, this chapter explores the feasibility of reproducing the periodic inflow asymmetry characteristics of VAWT blades within a finite computational domain. The relevant analysis focuses on whether this type of boundary modeling method introduces non-physical mutations in the time dimension and its potential impact on unsteady inverse integral stability.

In the rotating airfoil and real VAWT blade examples, the functionality is further extended to in-situ blade deformation and multi-blade synchronous deformation mechanisms. By designing a geometric update strategy based on the design variable distribution (DV distribution), this chapter verifies the effectiveness of the proposed deformation mechanism in maintaining geometric continuity and temporal consistency, and analyzes the impact of multi-blade synchronous deformation on flow field periodicity, load coherence, and associated sensitivity coupling characteristics.

Besides the UDF itself, this chapter systematically discusses key numerical settings such as near-wall mesh definition, time step and unit displacement scale, initial conditions, and residual convergence criteria. While these factors do not directly participate in the definition of optimization variables, they indirectly determine the accuracy and noise level of sensitivity information during the backpropagation of the adjoint equations by affecting the resolvability of the forward unsteady flow field. Especially under high Reynolds number and strongly separated flow conditions, the coupling relationship between near-wall resolution and time step is one of the prerequisites for ensuring the usability of the unsteady adjoint method.

Furthermore, this chapter compares and analyzes the applicability of continuous adjoint and discrete adjoint in the current problem, focusing on their application in complex UDFs. This study addresses the discrepancies in implementation and numerical consistency under various conditions. Furthermore, through scale analysis, it clarifies the impact of model boundary settings, 3D flow field extension, and surface definition methods on the accompanying optimization results, thus providing a reliable numerical foundation for the 3D blade optimization discussed in subsequent chapters.

Collectively, while these contributions represent a breakthrough in physical realism and design fidelity, they also necessitate a deeper academic discussion on solver design, numerical scheme compatibility, and best practices for adjoint stability in highly transient, rotational, and turbulent environments. The following sections analyze each of these dimensions in detail, providing a structured assessment of how the proposed innovations influence the broader numerical ecosystem within which the adjoint optimization is embedded.

This study utilizes the SU2 open-source multiphysics computing platform for both numerical implementation and engineering applications, and systematically configures and verifies several of its advanced functional modules. Specifically, SU2's Automatic Differentiation (AD) capability is the core of its efficient gradient calculation and optimization design. Backward differentiation, based on the adjoint method principle, obtains the gradient of the objective function with respect to a large number of design variables through a single backpropagation, with computational complexity almost independent of the number of variables, making it particularly suitable for high-dimensional problems such as aerodynamic shape optimization. In contrast, forward differentiation propagates derivatives variable by variable, offering a more intuitive structure and is often used in scenarios with lower variable dimensionality or for algorithm debugging and verification. SU2 also provides a Python interface wrapper (pywrapper), which exposes the core solver, mesh processing, and optimization process as a callable Python API through a binding mechanism between C/C++ and Python, significantly improving the efficiency of algorithm prototype development, automated parameter scanning, and coupling with machine learning frameworks. In terms of parallel computing, SU2 relies on MPI (Message Passing Interface) to achieve distributed memory parallelism, effectively improving the scalability and computational efficiency of large-scale 3D computing through domain decomposition and inter-process communication mechanisms. This paper mainly focuses on numerical experiments and functional verification based on SU2 version 7.3.0. Furthermore, it has been confirmed that, under the condition of building from source, the aforementioned advanced functions and custom extension functions such as automatic differentiation, parallel computing, and development interfaces in SU2 version 8.3.0 can be stably built and run normally in the MSYS2 MINGW64 environment on the Windows platform, thus providing reliable support for cross-platform high-performance computing and secondary development.

4.1 UDF Settings and its Effect on Oscillating Airfoil

In the unsteady adjoint optimization framework, the definition of the objective function directly determines the physical meaning of sensitivity information and its propagation mode in the time dimension. For vertical axis wind turbine (VAWT) blades, the traditional method of using lift coefficient, drag coefficient, or their ratio (also called lift-to-drag ratio) as optimization targets is essentially still based on steady or quasi-steady aerodynamic assumptions. Its optimization results tend to improve local airfoil performance rather than directly affecting the blade's energy extraction capability in the rotating system.

In general-purpose CFD-adjoint optimization platforms such as SU2, the default aerodynamic optimization targets are often defined in the form of controlling C_L and reducing C_D, with clear physical meaning and mature numerical implementation. However, for Darrieus-type VAWT blades, the actual driving torque comes from the tangential aerodynamic component, i.e., the tangential force coefficient C_T. As demonstrated in

Chapter 2, there is a strict one-to-one correspondence between the time-integrated tangential force coefficient of a single blade in the rotating coordinate system and the equivalent single-blade power coefficient. Therefore, using C_T as the optimization target is more in line with the energy conversion mechanism of VAWT at the physical level.

However, unlike C_L and C_D, C_T is not directly defined by the force components of the flow field in a fixed reference direction, but rather by the projections of lift and drag onto the time-varying tangential direction. This characteristic determines that C_T is an explicitly time-dependent quantity. In unsteady CFD calculations, each time step corresponds to an instantaneous $C_T(t)$. At the optimization level, the objective function is no longer a single scalar, but a time series or its time integral functional.

Therefore, this section systematically analyzes the UDF setting method required to introduce a time-dependent tangential force coefficient-based objective function in SU2 through an oscillating airfoil example, and evaluates the impact of this setting on forward CFD solutions and associated sensitivity calculations.

4.1.1 Optimization Objective on CFD

For blades undergoing periodic pitching or equivalent rotational motion, their instantaneous tangential force coefficient can typically be expressed as the projection of lift and drag components onto the tangential direction, i.e.:

$$C_T = C_L cos\alpha + C_D sin\alpha \qquad \text{[Eq. 4.1]}$$

This expression is theoretically rigorous and has been widely used in quasi-steady models and post-processing analyses. However, in the unsteady CFD-adjoint optimization framework, directly constructing the optimization objective function based on numerically calculated C_L and C_D introduces unnecessary complexity in terms of numerical consistency and adjoint sensitivity definition.

In SU2, C_L and C_D are essentially post-processing variables defined relative to a fixed reference direction. Their calculation relies on integrating the instantaneous aerodynamic force vector obtained from the blade surface pressure and shear stress, and then projecting it onto predefined lift and drag directions. For VAWT blades, the actual power contribution direction is not fixed but a tangential direction that varies with time. Therefore, if C_L and C_D are used as intermediate variables for tangential projection, it is equivalent to introducing two direction transformations at the numerical level, which may amplify projection errors and weaken temporal continuity in unsteady rotating systems.

Based on the above considerations, this study directly defines C_T in SU2 as the projection of the instantaneous aerodynamic force onto the tangential direction. Specifically, at each time step, the instantaneous aerodynamic vector is first calculated on the blade surface from the flow field solution:

$$F_n = \begin{bmatrix} F_{xn,} \\ F_{yn} \end{bmatrix} \quad \text{[Eq. 4.2]}$$

Subsequently, a tangential unit vector consistent with the instantaneous motion direction of the blade is defined:

$$e_{Tn} = \begin{bmatrix} -cos\phi n \\ sin\phi n \end{bmatrix} \quad \text{[Eq. 4.3]}$$

And based on this, the instantaneous tangential force coefficient is calculated:

$$C_T^n = \frac{F^n \cdot e_T^n}{\frac{1}{2}\rho U_{ref}^2 c} \quad \text{[Eq. 4.4]}$$

Where c is the chord length (m).

This definition avoids the secondary projection process of C_L and C_D, allowing C_T to directly connect with the flow field state variables, thus maintaining a clear and consistent sensitivity transfer path in unsteady optimization problems. Since C_T is explicitly time-dependent, it is no longer a single scalar in unsteady optimization, but a sequence that evolves over time.

In the SU2 implementation, the objective function is progressively accumulated over time using a user-defined function (UDF), ensuring that the instantaneous aerodynamic response at each time step is consistently incorporated into the optimization process.

The C_T objective function constructed in this way not only more closely approximates the energy extraction mechanism of VAWT in a physical sense, but also provides a more robust and consistent definition of the objective functional for unsteady adjoint solutions at the numerical implementation level. This approach lays a reliable foundation for subsequent unsteady adjoint optimizations involving rotating blades, multi-blade coupling, and three-dimensional flow conditions.

In SU2, changing the optimization objective from the traditional lift coefficient to the airfoil tangential force (i.e., a trigonometric function combination of lift and drag) requires source code extension, not just modification of the configuration file. The specific process is as follows: First, a custom objective function is added to the objective function module of SU2, and it is registered as a new objective type in the objective function enumeration and configuration parsing system. Then, in the objective function calculation routine, based on the lift coefficient and drag coefficient already calculated by the direct solver, and combined with the angle of attack given in the configuration file, the tangential force objective function is constructed. During implementation, the su2double type must be used throughout, and AD-compatible mathematical functions must be called to ensure that backward automatic differentiation (AD) can correctly record the computation graph and automatically generate the adjoint gradient. Under these conditions, no additional derivation or implementation of the adjoint equation is required; SU2's adjoint solver can directly differentiate the new objective function. After modifying and recompiling the source code, the tangential force objective can be called in the forward solution, adjoint solution, and shape optimization processes by specifying the new objective function name in the configuration file. This process does not introduce new parallel communication operations, thus maintaining the same scalability as the original lift-drag target in the MPI parallel computing environment. This has been stably verified in the MSYS2 MINGW64 environment on the Windows platform.

4.1.2 Influence of the Customized Optimization Objectives

From the perspective of the flow control equations, defining the optimization objective as C_T has no direct impact on the forward CFD solution. The Navier-Stokes equations, discretization scheme, time-progression algorithm, and stability conditions remain unchanged. The flow field evolution is entirely determined by geometry, boundary conditions, and time step, while C_T is only obtained as a post-processing variable projected from instantaneous surface forces. Therefore, it is unaffected in terms of numerical stability, convergence behavior, and time-progression accuracy.

When using C_T as the objective function, the structure of the adjoint equations remains unchanged, but their source terms and boundary contributions differ because they are now defined relative to C_T rather than C_L or C_D. Specifically, C_T depends on the force component in the direction of blade motion, which, in rotating systems like Darius-type vertical-axis wind turbines (VAWTs), is a time-dependent vector field.

This means that, while the flow solver is unaffected, the adjoint source term must now account for the projection of the surface force perturbation onto the motion's potentially nonuniform tangential direction, which varies with time as the blade rotates. If the motion includes variable angular velocity or pitch oscillations, the direction and magnitude of the C_T vector basis will vary continuously.

Furthermore, since C_T is inherently time-dependent, the objective is no longer a scalar quantity but rather a time-integrated functional, for example, the total torque over one revolution. This necessitates a time-accurate adjoint formulation, where the adjoint field is extended backward in time and influenced by the original flow at each time step. While this is standard practice in unsteady adjoint methods, it increases sensitivity to the accuracy of the time discretization and may require storage or recalculation strategies to reconstruct the original flow field during the adjoint integration.

In summary, using time-varied C_T as the optimization objective significantly increases the sensitivity of unsteady adjoint calculations to the following factors:

- *Time step accuracy: Time discretization errors directly contaminate the objective function gradient.*

- *Flow field reconstruction accuracy: Forward flow fields need to be stored or recalculated to ensure adjoint consistency.*

- *Transient load noise: High-frequency fluctuations caused by dynamic stall can amplify sensitivity noise.*

Therefore, in practical calculations, it is essential to use appropriate time steps, residual convergence criteria, and necessary time filtering strategies to ensure the stability and interpretability of the optimization process.

4.1.3 Airfoil Pitch Acceleration

In the unsteady oscillating airfoil example, the time description of the blade pitch motion not only determines the instantaneous angle of attack variation but also directly affects the additional unsteady inertial terms, dynamic stall development process, and aerodynamic phase characteristics in the flow field. For unsteady adjoint optimization, the definitions of pitch angular velocity and angular acceleration are particularly crucial because they not only affect the forward flow field solution but also influence the back propagation path of the adjoint variables through time-dependent boundary conditions and the objective function.

In SU2, the blade pitch motion is usually explicitly given by a time function, with the core state variable being the pitch angle $\theta(t)$. In this study, to ensure the continuity and differentiability of the kinematic description, the pitch angle is defined as a smooth periodic function.

The changes in angular velocity and angular acceleration per unit time are expressed as follows:

$$d\emptyset = -\left(tan^{-1}\frac{sin\omega t_2}{\frac{\lambda}{1-a}+cos\omega t_2} - tan^{-1}\frac{sin\omega t_1}{\frac{\lambda}{1-a}+cos\omega t_1}\right) \qquad [\text{Eq.} 4.5]$$

$$\dot{\alpha} = -\frac{\omega cos\omega t\left(\frac{\lambda}{1-a}+cos\omega t\right)+\omega sin^2\omega t}{sin^2\omega t+\left(\frac{\lambda}{1-a}+cos\omega t\right)^2} \qquad [\text{Eq.} 4.6]$$

It should be noted that in unsteady CFD solutions, although the Navier-Stokes equations themselves do not explicitly include pitch acceleration terms, when dynamic meshes or moving boundaries are used to describe blade motion, the pitch velocity and acceleration indirectly affect the flow field evolution through boundary velocities, mesh velocities, and non-inertial reference frame terms.

In the numerical implementation of SU2, pitch motion is not directly input through a discrete angle table, but is calculated in real time at each time step using a user-defined time function. Specifically, at the nth time step, the current physical time is input into the UDF, and the instantaneous pitch angle, angular velocity, and angular acceleration can be calculated.

Compared to the traditional approach of only specifying the pitch angle as a function of time, explicitly defining and using pitch angular velocity and angular acceleration has two advantages. First, from a physical modeling perspective, the triggering and development of dynamic stall is not only related to the instantaneous angle of attack, but also closely related to the rate of change of the angle of attack. By explicitly distinguishing instantaneous pitch angle, angular velocity, and angular acceleration in the numerical model, the unsteady added mass effect and vortex dynamics response during rapid pitch can be described more accurately. Secondly, from the perspective of numerical and adjoint consistency, the explicit definition of pitch angular velocity and angular acceleration avoids the time discretization error introduced by approximating derivatives through numerical difference, ensuring strict consistency between the forward flow field and the adjoint equations in the time dimension.

In this implementation, pitch angle, angular velocity, and angular acceleration are all given as explicit time functions, rather than as design variables in the optimization. This approach ensures that the kinematic description remains unchanged throughout the optimization process, thus strictly limiting the influence of design variables on the flow field to the geometry and aerodynamic response levels, which is beneficial for the subsequent physical interpretation of adjoint sensitivity. At the same time, this explicit time function form also provides a unified interface for introducing more complex kinematic models (such as variable angular velocity or non-sinusoidal pitch).

4.1.4 Influence of the Airfoil Pitch Acceleration

In unsteady aerodynamic simulations of the VAWTs, particularly those involving optimization, blade pitch motion is often introduced to improve performance or simulate realistic operational control strategies. While constant or sinusoidal pitch variations are relatively well understood in CFD frameworks, introducing non-uniform pitch acceleration presents a series of theoretical and numerical considerations, especially when computing transient adjoint sensitivities.

From the perspective of the flow solver, time-varying pitch acceleration is handled through prescribed boundary motion or dynamic mesh transformations. If the mesh deformation is smooth and the motion is continuous, the solver can generally accommodate non-linear pitch profiles without significant issues. The primary numerical concern arises when the pitch acceleration is discontinuous or piecewise-defined, which can introduce unusual changes (eg. Induced factors that change over time in the leeward region) in local velocity and pressure fields. These effects may produce stronger leading-edge vortices, flow separations, or sudden changed pressure gradients. Only if the mesh resolution is sufficient and time stepping is appropriately chosen, the primal solution remains more stable. Therefore, the models in each subsequent chapter were tested in this regard.

The more significant impact lies in the adjoint sensitivity solver, where the blade's pitch history directly affects how perturbations propagate backward in time. Since adjoint equations are linearizations of the governing equations around the unsteady primal solution, any abrupt change in pitch acceleration introduces a localized, time-sensitive perturbation in the flow field. This creates adjoint source terms that are sharply concentrated in time and space, potentially leading to:

- *High gradients in adjoint fields, especially near the blade surface.*
- *Non-smooth temporal sensitivity evolution, which may impair gradient convergence during optimization.*
- *Increased numerical stiffness during backward time integration.*

Moreover, the pitch angle and its time derivatives (velocity and acceleration) directly influence the velocity boundary conditions and grid motion Jacobians, which appear in both the primal and adjoint formulations. When pitch acceleration varies in a non-smooth manner, it may lead to discontinuities in mesh motion derivatives, affecting the accuracy of adjoint flux linearizations and their contribution to the total sensitivity.

From a theoretical standpoint, the main consideration is that the design perturbation interacts with a time-dependent motion field. Therefore, when computing shape derivatives, the total derivative of the objective function includes not only the local spatial sensitivity $\frac{\partial J}{\partial x}$ but also cross terms involving time and motion derivatives, such as:

$$\frac{dJ}{d\alpha} = \int_0^T \left(\frac{\partial J}{\partial x} \cdot \frac{dx}{d\alpha} + \frac{\partial J}{\partial u} \cdot \frac{du}{d\alpha}\right) dt \qquad \text{[Eq. 4.7]}$$

Where α is the time-varying pitch profile, and velocity $\frac{dx}{d\alpha}$ and acceleration $\frac{du}{d\alpha}$ are time derivatives. The adjoint solver must be aware of the kinematic context in which shape changes occur, particularly in rotational and moving boundaries.

Another consideration is the effect on adjoint boundary conditions. For rotating blades with variable pitch, the normal and tangential directions at the blade surface vary over time, which alters the projection of adjoint fluxes and may require redefinition of boundary adjoint terms for consistency. If neglected, this can lead to physically incorrect gradients, especially in cases where C_T is used as the objective function.

In summary, while non-uniform pitch acceleration does not destabilize the primal CFD solver under proper conditions, it introduces localized temporal and spatial stiffness into the adjoint problem. Accurate adjoint treatment requires:

- *Smooth temporal resolution of the pitch profile,*
- *Consistent time-stepping between primal and adjoint solvers,*
- *Careful handling of mesh motion derivatives,*
- *Reassessment of adjoint boundary conditions and source terms.*

In optimization contexts where pitch is a control variable or enters into the motion definition, it is therefore critical to represent pitch dynamics analytically or with high-order interpolation, ensuring that the adjoint gradients remain accurate and meaningful for shape or control optimization.

4.1.5 Dynamic Boundary Conditions on CFD

Method 1: Inlet velocity magnitude and direction change simultaneously with time:

In SU2 (especially the velocity inlet of INC_* which cannot be compressed), cfg usually cannot directly write time functions like U(t) and α (t) in MARKER_INLET. Therefore, the most stable and common implementation in engineering is to use an external script to drive the process in a loop according to physical time steps: at each step, the input velocity vector is changed to the current time step's $U(t) = U(t)(cosa(t), sina(t))$, and then SU2 is run for only one physical time step. A restart statement is written, and then restart is used to continue to the next step. The specific process is as follows: Prepare a "single-step template cfg" (fixing UNST_TIMESTEPS = 1 and OUTPUT_WRT_FREQ = 1, leaving the entry line MARKER_INLET = (INLET, T, $|V|$, dirx, diry, dirz) for script overriding), then write a Python script to calculate $U(t)$, $a(t)$ for each step, modifying $|V|$ and (dirx,diry) in MARKER_INLET, and changing RESTART_SOL from NO in the first step to YES in subsequent steps, looping through SU2_CFD (1 step at a time) until all physical steps are completed; this will allow users to obtain the time-varying values in history.csv. $C_L(t)$, $C_D(t)$, and the entire unsteady process is linked by restart_flow.dat. The biggest advantage of this method is that the airfoil geometry is completely static, requiring no moving mesh or rotor-stator interface. The angle of attack change is equivalently achieved through the change of the incoming flow direction, which is extremely convenient. However, the cost is equally clear: because the incoming flow direction changes, the far-field boundary will be strongly excited, and the far field must be made much larger to avoid artificial boundary reflection/coupling contamination of aerodynamics. In particular, the upper and lower symmetrical boundaries often exhibit violent fluctuations that lead to errors. Therefore, symmetrical boundaries with small domains are generally not recommended under such moving incoming flow conditions.

Method 2: Modify only the inlet velocity, and let the airfoil oscillate:

If the simulation needs a less large far field and more stable symmetrical boundaries, a more "numerically friendly" approach is to give the inlet boundary only U(t) (constant direction, e.g., always along the x direction), while the angle of attack variation/periodic load is generated by the rigid body motion of the airfoil itself (pitch oscillation or heave oscillation). Also considering that cfg generally does not directly support U(t), you can first use the script above to drive the "inlet only changes size" step by step: each step of the script only covers |V| of MARKER_INLET, and the direction (dirx,diry,direz) remains unchanged; at the same time, airfoil oscillation can be achieved through SU2's dynamic mesh/ALE motion module (e.g., enabling rigid body motion/mesh deformation in the configuration, and calculating the airfoil attitude or displacement at the current time in each step). The advantages of this approach are: the incoming flow direction remains unchanged, the boundary conditions are always "directly facing" the computational domain, and the far-field and symmetric boundaries are not strongly excited by the rotating incoming flow. Therefore, it is generally more stable and more suitable for long-term integration and frequency domain analysis under the same computational resources. The disadvantage is that it requires handling dynamic mesh quality, time consistency, and if modeling of relative motion of multiple parts. If you don't want to restart SU2 every step, another more efficient approach is to modify the SU2 source code: add the INLET_U_* option in CConfig and calculate U(t) at the inlet boundary conditions according to the current physical time. This way, the entire transient process can be completed in one run (the direction remains unchanged, only the amplitude is replaced), but you need to recompile and maintain the own branch.

Method 3: Python Fitting/Interpolation-Driven Time-Varying Entry Point:
Define the entry velocity (and its direction/angle when needed) as a time series curve fitted from experimental data or high-fidelity results. Use Python for interpolation/fitting, and continuously feed the current entry conditions to SU2 during the calculation process. The most common implementation is: Python first reads the t/U (or t/α) data table, performs spline/polynomial/piecewise linear fitting, then iterates through the physical time steps, writing the fitted U(t) (and optional α(t)) into the cfg function at each step (or directly passing it through a modified interface), and uses `restart` to chain the entire unsteady process. The biggest advantage of this method is its ease of defining complex operating conditions: such as gusts, non-sinusoidal, non-periodic, and noisy measured velocity curves. It can even quickly switch between different fitting strategies (smoothing, filtering, constrained slope, etc.), which is much more convenient than writing piecewise functions in cfg or modifying equations in C++.

However, its costs are also clear: First, the solution is slow because Python loops and frequent I/O (writing to cfg, reading and writing to restart, starting the solver) significantly reduce efficiency, especially when there are many physics steps, the overhead is considerable; second, the numerical risk is higher. If the fitted curve changes too quickly per unit time (e.g., U(t) jumps too much, the slope is too steep, the sampling interval does not match TIME_STEP), the entry condition is equivalent to applying a strong transient excitation to the system, which can easily lead to CFL runaway, internal iteration non-convergence, "divergence", residual jumps, or even symptoms of "equation non-closure/inconsistent solutions". In engineering, two things are usually done to reduce the risk: First, apply slope limiting/smoothing filtering to the fitted curve to ensure that the entry changes of adjacent time steps are small enough. Second, make the TIME_STEP, INNER_ITER, and CFL strategies more conservative, and locally encrypt the time steps during abrupt changes when necessary; otherwise, the convenience of this method can easily be offset by instability.

4.1.6 Influence of Dynamic Boundary Conditions on CFD

In this study, the inlet boundary condition is defined as a time-varying velocity profile whose periodic modulation is synchronized with the rotation period of the vertical-axis wind turbine (VAWT). This formulation simulates more realistic wind input conditions by introducing weak instabilities at the inlet, thereby emulating the time-varying wind environment encountered by actual rotating blades. As a result, the flow field is not driven by a constant inflow velocity, but rather by a low-amplitude sinusoidal or piecewise variation with a period matching one full rotor rotation.

From the perspective of the original (flow) solver, such dynamic boundary conditions can significantly impact the numerical stability or accuracy of the simulation. However, because the inflow velocity variations in this study are designed to be continuous, small, and smooth, and their amplitudes are typically small compared to the average inflow velocity, standard time discretization schemes do not require excessively small time steps to capture the fluctuations. The CFL condition is still primarily governed by the local flow velocity near the blade and the mesh resolution, rather than the inlet modulation itself.

However, even slight boundary variations have a significant impact on unsteady simulations and associated sensitivity analyses. Particularly noticeable is the emergence of periodic fluctuations in the flow field. This indicates that the governing equations and their solutions are no longer steady, or even pseudo-state. Instead, the unsteadiness at the boundary propagates throughout the computational domain. It also interacts with blade motion, wake development, and vortex shedding. Although the amplitude is small, the phase difference between the inflow modulation and the blade position alters the instantaneous forces on the blades. This affects time-resolved physical quantities such as the tangential force coefficient (Ct).

4.1.7 Piecewise Function Simulation of Equivalent Downwind Flow

In the operation of a real vertical axis wind turbine (VAWT), the flow environment experienced by the blades on the upwind and downwind sides differs significantly. On the upwind side, the blades are primarily controlled by the relative inflow formed by the superposition of the free flow and their own tangential velocity. On the downwind side, however, the flow is influenced by the upstream blade wake, induced velocity decay, and a strong unsteady vortex structure. This flow characteristic manifests as significant velocity deficit, enhanced turbulence, and inflow non-uniformity, with its spatial and temporal distribution highly dependent on the specific rotor structure and operating parameters.

If a symmetrical relative inflow description is still used in the oscillating airfoil equivalent model, it will fail to reflect the true flow degradation characteristics experienced by the downwind blades. Therefore, this study introduces an equivalent downwind inflow simulation method based on a piecewise function to approximately reproduce the asymmetric flow environment on the downwind side of the VAWT in a two-dimensional model.

It is important to emphasize that this piecewise function is not based on empirical assumptions or artificial adjustments, but rather on a reverse calibration using the flow field solution of the complete VAWT numerical model in Section 5.6. Specifically, in the real VAWT model, by statistically analyzing and averaging the local velocities at different azimuth angles along the blade trajectory, the characteristic distribution of the relative incoming velocity as a function of azimuth in the downwind region was obtained. This distribution reflects the combined result of wake interaction and induced effects, and is a direct product of the complete rotating flow field solution.

Based on this, to preserve this key asymmetric feature in the oscillating airfoil model, the inlet velocity amplitude is defined as a piecewise function of azimuth: the velocity expression based on relative motion is used in the upwind region, while in the downwind region, a calibrated velocity attenuation factor is introduced to ensure that the inlet velocity amplitude is consistent with the average velocity level on the downwind side of the real VAWT. In this way, the two-dimensional model introduces flow asymmetry consistent with the three-dimensional rotating model without significantly increasing computational complexity.

The primary objective of this piecewise function simulation method is not to precisely reconstruct the instantaneous wake structure, but rather to statistically reproduce the systematic reduction in the downwind inflow velocity level. This allows the oscillating airfoil model to more closely approximate the actual VAWT condition in terms of aerodynamic amplitude, load phase, and tangential force contribution. This equivalent treatment provides more physically representative flow input conditions for subsequent unsteady adjoint optimization based on oscillating airfoils.

4.1.8 Influence of Piecewise Function Simulation

Introducing a piecewise function-based equivalent downwind inflow description into the oscillating airfoil equivalent model systematically impacts the unsteady CFD flow field structure and aerodynamic response. Compared to inlet velocity models employing symmetric or continuous analytical forms, this piecewise function explicitly distinguishes the inflow characteristics on the upwind and downwind sides, allowing the two-dimensional model to statistically inherit the asymmetry of the real VAWT rotating flow field, thereby altering the aerodynamic loading of the blade in different azimuth intervals.

Firstly, at the flow field level, the piecewise function simulation significantly alters the velocity level and shear distribution in the downwind region. Because the inlet velocity amplitude is systematically reduced in the downwind region, the effective Reynolds number experienced by the blade in this interval decreases, leading to earlier boundary layer separation and changes in the scale and shear frequency of vortices. This effect manifests in the instantaneous flow field as an increase in downwind vortex intensity and aggravated velocity deficit in the wake region, with overall characteristics consistent with the downwind flow degradation trend observed in the full VAWT numerical model. Therefore, it is evident that the piecewise function does not simply introduce artificial perturbations, but rather reproduces the non-negligible wake effect in a rotating system in an average sense.

Secondly, regarding aerodynamic response, the piecewise function has a identifiable impact on both load amplitude and phase. Compared to the symmetrical inflow model, the reduction in downwind inlet velocity directly weakens the peak values of lift and tangential force in this interval, resulting in a significant asymmetry in the aerodynamic distribution within a single cycle. This asymmetry alters the integral result of the tangential force time history, thus affecting the distribution characteristics of the equivalent single-blade power contribution. It is noteworthy that this effect is not a simple overall scaling, but rather reshapes the temporal structure of unsteady aerodynamic forces by changing the azimuth interval and phase position of the load peak.

Furthermore, the piecewise function simulation also indirectly modulates dynamic stall behavior. Due to the reduced downwind inflow velocity amplitude, the effective angle of attack change rate and peak angle of attack of the blade in this interval both change, thereby affecting the triggering time and development intensity of dynamic stall. Under certain operating conditions, the piecewise function model exhibits a delayed or weakened dynamic stall process on the downwind side, while maintaining stall characteristics similar to the continuous inflow model on the upwind side. This difference results in the overall stall behavior exhibiting an asymmetric evolution process within a cycle that more closely resembles the actual VAWT operating state.

From a numerical perspective, the piecewise function places higher demands on the stability of unsteady CFD solutions. If the piecewise function exhibits non-smoothness at interval connections or near extreme points, it may introduce high-frequency excitations at the inlet boundary, thereby inducing non-physical oscillations in the flow field. By employing the continuity handling strategy described in the preceding section, the changes in the piecewise function over the time dimension remain smooth, allowing the forward unsteady calculation to proceed stably within a reasonable time step without residual amplification or convergence deterioration caused by abrupt changes in inlet conditions.

It should be noted that although a piecewise function is introduced into the oscillating airfoil equivalent model to simulate downwind inflow degradation, this treatment does not imply a significant or non-physical reduction in the downwind inlet velocity. Conversely, the velocity loss introduced by the piecewise function in this study remains relatively small in magnitude, its effect being more about introducing flow asymmetry than significantly reducing the overall incoming kinetic energy level.

From a physics perspective, the flow characteristics on the downwind side of a real vertical axis wind turbine (VAWT) are primarily determined by the upstream blade wake-induced effect and the overall rotor scale. For medium and large VAWTs, the blade spacing is relatively large, and the rotor diameter is significantly increased. The wake of a single blade undergoes significant diffusion and dissipation during propagation, resulting in a relatively limited direct velocity reduction effect on the downstream blades. Therefore, on an engineering scale, the downwind incoming flow exhibits more of a combined effect of mild velocity loss and enhanced turbulence than a strong average velocity decay.

Based on this understanding, this study did not attempt to "amplify" the wake effect by significantly reducing the downwind inlet velocity when constructing the piecewise function. Instead, it adopted a velocity correction with limited amplitude based on statistical analysis of the complete VAWT numerical flow field. This correction primarily aims to break the statistical symmetry between the upwind and downwind sides, enabling the oscillating airfoil model to reflect the uneven aerodynamic distribution in a real rotating system. Numerical results show that, within the considered operating range, the downwind velocity loss introduced by the piecewise function has a relatively small impact on the overall flow field energy level; its main effects are manifested in the modulation of load phase, tangential force distribution, and unsteady aerodynamic time structure.

The aforementioned scale effect is further verified in Chapter 5.6. Through comparative analysis of three different VAWT sizes, the influence of downwind velocity loss on aerodynamic distribution and equivalent power contribution is systematically evaluated. The results show that as the turbine size increases, the impact of downwind velocity loss on overall performance prediction and optimization results gradually weakens, while the piecewise function model maintains a consistent physical trend across different scales. This comparative result indirectly demonstrates that the piecewise function simulation method used in this study has good robustness in terms of scale scalability.

4.2 UDF Settings and its Effect on Rotational Airfoil

In the previous section, the oscillating airfoil model was used to equivalently describe the local unsteady aerodynamic behavior of a vertical axis wind turbine (VAWT) blade during rotation. This model reproduced key features such as blade angle of attack variation, relative velocity modulation, and downwind flow degradation within a two-dimensional fixed computational domain by using time-varying pitch angles, inlet velocity amplitudes, and piecewise functions. However, it is important to note that the oscillating airfoil model is essentially a kinematic equivalent model; the blade does not undergo actual spatial displacement, nor does it exhibit strictly defined rotational motion.

When the research object transitions from a single equivalent airfoil to a real rotating blade, both the description of the aerodynamic problem and the numerical implementation path undergo fundamental changes. The rotating airfoil not only experiences periodic changes in angle of attack and relative velocity, but its spatial position itself also changes over time, resulting in significant non-uniformity and path dependence of the flow field in the Eulerian reference frame. Furthermore, in the rotating model, any change in blade geometry is "transported" along the rotational trajectory to different spatial locations, thus having a more complex impact on the overall flow field structure and aerodynamic force distribution.

Therefore, this section focuses on how to implement numerical modeling of rotating airfoils using user-defined functions (UDFs) within the SU2 framework, and systematically analyzes the differences between this setting and the oscillating airfoil model. Specifically, this section focuses on the following aspects:

- *The essential differences between rotating and oscillating airfoils at the physical modeling level;*

- *The numerical generation method of rotational motion in SU2 and its impact on the flow field;*

- *Establishing a consistent kinematic basis for subsequent in-situ blade deformation and multi-blade synchronous deformation.*

4.2.1 DV Deformation Mechanism of In-Situ Blade Deformation

The fundamental difference between oscillating airfoil models and rotating airfoil models lies in whether the blades undergo actual spatial displacement. In a rotating airfoil model, the blades rotate rigidly around the rotor center at a constant or given angular velocity, and their instantaneous position is uniquely determined by the azimuth angle. Therefore, the blades are located at different spatial coordinates at each time step, and the flow they experience depends not only on the current angle of attack and relative velocity but also closely on the wake structure formed in previous time steps. This path dependence is one of the core characteristics distinguishing rotating airfoil models from oscillating airfoil models.

From an aerodynamic perspective, oscillating airfoil models are mainly used to study unsteady responses at the "local blade element" level, while rotating airfoil models can directly describe the aerodynamic behavior of the blades across the entire rotor scale, serving as a necessary step connecting local blade element models with overall aircraft performance analysis.

In SU2, oscillating airfoil models are typically implemented using a fixed mesh combined with time-varying boundary conditions or kinematic parameters; the computational domain itself does not change over time. Rotating airfoil models require explicitly incorporating the time-varying geometric position, primarily achieved through dynamic meshes or geometric update mechanisms based on rigid body motion.

In this study, the rotating airfoil is not implemented using a rotating reference frame, but rather employs an explicit time-progressing rigid body rotation description. Specifically, at each time step, the UDF calculates the instantaneous azimuth angle of the blade based on the current physical time and performs a rotational transformation on the blade surface node coordinates accordingly, thereby updating the blade's geometric position in the Eulerian reference frame. This approach allows the flow field to naturally accumulate the wake structure formed during blade motion without requiring additional modifications to the governing equations.

Compared to the "attitude-only update, position-only update" approach in oscillating airfoil models, the geometric updates in rotating airfoil models significantly alter the flow field topology, especially when the blade passes through the downwind region, where the flow environment is directly affected by the wake residue from the previous cycle. This characteristic makes the rotating airfoil model numerically closer to the actual VAWT operation, but it also places higher demands on mesh quality, time step size, and numerical stability.

Within the SU2 framework, the generation of the rotating airfoil is not accomplished through simple built-in parameter options, but rather relies on a user-defined geometry update mechanism. At each time step, a customized UDF will read the current physical time and calculates the corresponding rotation angle, then applies a rigid body rotation transformation to the blade surface nodes, and finally updates the boundary information related to the blade to ensure that the aerodynamic integral is consistent with the geometric position. This process is executed step-by-step in the forward unsteady CFD calculation, thus achieving a continuous description of the rotational motion. Since the rotation angle is an explicit time function, this kinematic description exhibits good controllability and consistency within the adjoint optimization framework, and also provides a clear interface for subsequently introducing design variables into blade geometry deformation.

The introduction of the rotating airfoil model transforms blade geometry from merely an "aerodynamic shape" into a physical entity that moves through space over time. This characteristic dictates that, in the rotating model, any geometric deformation based on design variables must be defined in the blade's in-situ coordinate system and remain consistent throughout the rotation. Therefore, the rotating airfoil model provides the necessary physical and numerical foundation for the in-situ blade deformation mechanism and multi-blade synchronous deformation strategy proposed in subsequent chapters.

4.2.2 Influence of In-Situ Blade DV Deformation Mechanism

Although the kinematic definition of a rotating airfoil is relatively straightforward at the numerical implementation level, the overall numerical model undergoes fundamental changes in scale setting and boundary conditions when the computational object transitions from an oscillating airfoil to a real rotating airfoil. These changes not only affect the physical rationality of the flow field solution but also directly determine the representativeness of the calculation results for the actual operating state of a vertical axis wind turbine (VAWT). Therefore, it is necessary to specifically discuss the scale characteristics of the rotating airfoil model.

First, the physical meaning of the inlet velocity undergoes a fundamental shift in the rotating airfoil model. In the oscillating airfoil model, the inlet velocity is typically interpreted as the equivalent relative inflow, used to reconstruct the local flow conditions experienced by the blade at a certain azimuth angle; however, in the rotating airfoil model, the inlet velocity can be directly considered as the ambient wind speed, i.e., the free inflow conditions experienced by the real VAWT. The change in the blade relative to the inflow is no longer artificially modulated by the inlet conditions but is naturally formed by the superposition of the blade tangential velocity and the inlet wind speed during the rotational motion. This shift makes the rotating airfoil model more direct in its physical interpretation but also implies the spontaneous formation of a complete rotor wake structure in the flow field.

The wake effect introduced by rotational motion places higher demands on the computational domain exit location. Because the blade continuously transmits momentum downstream during rotation, its wake exhibits a significant axial extension, and its attenuation length varies with rotor size and operating parameters. If the exit boundary is set too close, the wake will be truncated before it can fully develop, leading to non-physical reflections or pressure feedback at the exit, thus contaminating the flow field solution throughout the computational domain. Therefore, compared to the oscillating airfoil model, the rotating airfoil model requires a significantly longer computational domain in the downstream direction to ensure the wake can leave the computational region in a near-free-developing state.

Thus, the introduction of the rotating airfoil model inevitably leads to an increase in the overall computational scale. In the oscillating airfoil model, the computational domain scale is mainly determined by the airfoil chord length and its surrounding flow characteristics. In the rotating model, however, the characteristic length is dominated by the rotor diameter. With the introduction of the rotor radius, the spatial range covered by the blade within one rotation cycle significantly expands, requiring the computational domain to provide sufficient space in both the radial and tangential directions to accommodate the blade's motion trajectory and its wake structure. This scaling not only affects the geometric dimensions but also directly impacts the total mesh size, time step selection, and computational resource requirements.

From the perspective of the forward flow field, the in-situ DV deformation mechanism ensures that blade geometric modifications are always defined within the blade's local coordinate system and updated synchronously with its rotational motion to the current spatial position. This approach avoids the non-physical deformation or geometric discontinuities that might be introduced by directly applying geometric perturbations in the Eulerian reference frame. From the perspective of unsteady adjoint optimization, the in-situ DV deformation mechanism plays a decisive role in the sensitivity propagation path. In the adjoint method, the sensitivity of the objective function to design variables needs to be backpropagated across the entire time interval. If the geometric deformation is defined in the in-situ coordinate system, the in-situ DV deformation ensures that the design variables are always bound to the blade's physical position, allowing the adjoint sensitivity to accumulate backward along the blade's actual motion trajectory, thereby significantly improving the stability and physical interpretability of the gradient.

4.2.3 Synchronous Deformation Mechanism of Multiple Blades

When introducing geometric optimization based on design variables (DVs) into a rotating airfoil model, a core challenge is ensuring that geometric deformation retains clear physical meaning and numerical consistency despite continuous blade motion. Unlike stationary or oscillating airfoil models, rotating airfoils are in different spatial positions and attitudes at each time step. Applying design variable displacements directly to the global Euler coordinate system would cause non-physical shifts in the direction of geometric deformation over time, thus disrupting the correspondence between sensitivity information and actual geometric changes. Therefore, this study employs a synchronous deformation mechanism based on a rotational coordinate transformation matrix to ensure that design variables are always defined in the local coordinate system of the blade and maintain strict consistency in multi-blade scenarios.

(1) Construction of the In-situ Coordinate System Based on the Rotation Matrix

To ensure that design variable deformation always revolves around the airfoil itself, this study first introduces a time-varying local coordinate system for each rotating airfoil. This coordinate system uses the airfoil reference point (such as the quarter-chord point or geometric center) as its origin, and its coordinate axes always maintain a fixed relationship with the airfoil body. The positional changes of a rotating airfoil in the global coordinate system can be represented by a standard two-dimensional rotation matrix in Chapter 3.

In the numerical implementation, the geometric displacements caused by all design variables are first defined in the airfoil's local coordinate system. Let the displacement of a design variable at a certain node, calculated from the adjoint sensitivity in the local coordinate system, be multiplied by a matrix to obtain the corresponding displacement in the global coordinate system.

Through this transformation, the update direction of the design variables always remains consistent with the physical meaning of the airfoil surface normal or tangential, without distortion due to the airfoil's rotation in space. The sensitivity of the design variables changes in the local coordinate system without iteration, while the geometric update is mapped to the global space through the rotation matrix. This approach ensures that the physical orientation of the geometric deformation is not lost over time during unsteady rotation.

This matrix-based in-situ coordinate system processing is particularly important for unsteady adjoint optimization. Since the adjoint sensitivity essentially reflects the objective function's response to local geometric perturbations, without coordinate system separation, the sensitivity will be incorrectly projected onto the global direction over time, leading to uninterpretable or even invalid gradient information.

In a real VAWT rotor, multiple blades are typically identical in structure and aerodynamic design, and their design variable distributions should be physically consistent. Therefore, in the multi-bladed rotating model, this study introduces a multi-bladed synchronous deformation mechanism based on single-airfoil sensitivity to ensure that all blades undergo the same geometric updates during optimization.

Specifically, an independent wall boundary is defined for each blade in the numerical model, but only one reference blade is used to calculate the associated sensitivity and update its design variable distribution. The updated design variables on this reference blade are considered the "standard deformation mode" of the airfoil. In each optimization iteration, this deformation mode is automatically copied and applied to the remaining blades through coordinate transformation and index mapping. This update amount is entirely derived from the design variable update results of the reference blade. This process is executed automatically in each optimization iteration, ensuring that the deformation of all blades is completely consistent in the local coordinate system, exhibiting different geometric attitudes only in the global spatial position due to different rotation angles.

This synchronous deformation mechanism avoids the computational overhead of calculating the sensitivity for each blade separately, and also prevents asymmetric or non-physical geometric differences between multiple blades. More importantly, since all blades share the same set of design variables, the optimization results naturally satisfy the periodic symmetry requirements of the rotor structure and aerodynamic design.

4.2.4 Influence of Synchronous Deformation Mechanism on Multiple Blades

In multi-bladed rotating airfoil models, if a synchronous deformation mechanism is not employed, and only one blade undergoes geometric optimization based on design variables while the other retains its original shape, the rotor will exhibit a degree of asymmetry in both geometry and aerodynamics. In the case of a two-bladed vertical axis wind turbine (VAWT), this asymmetry manifests as different local aerodynamic responses generated by the two blades within the rotation cycle, thus introducing differences in instantaneous load distribution.

From a physics perspective, if only one blade is optimized, its local lift, drag, and tangential force characteristics will change within the corresponding azimuth angle range, while the other blade maintains its original aerodynamic characteristics. This difference can be identified at a single time step or local azimuth angle, particularly in the amplitude and phase of the instantaneous aerodynamic force curve. However, due to the inherent time-staggered nature of a two-bladed VAWT within a complete rotation cycle, the load contributions of the two blades are superimposed in a time integral sense, which significantly weakens the asymmetry effect introduced by the single-blade shape difference after periodic averaging.

From a flow field perspective, the asymmetry introduced by asynchronous updates is mainly reflected in the local differences in the wake structure. The wake intensity and structure formed downstream by the optimized blade differ slightly from those of the unoptimized blade, but due to diffusion and dissipation during wake propagation, these differences are partially smoothed out before reaching another blade. This wake diffusion mechanism further reduces the direct transmission efficiency of geometric asymmetry between blades, keeping the impact of asynchronous updates on the overall flow field structure within a limited range.

The above effects also exhibit significant scale dependence. As the turbine size increases, the rotor diameter increases significantly relative to the wake characteristic scale, and the influence range of a single blade's wake across the entire rotor scale relatively decreases. In large-scale VAWTs, increased blade spacing and extended wake diffusion paths further weaken the direct impact of one blade's geometric difference on the aerodynamic environment of another blade. Therefore, in larger-scale turbines, even without synchronous geometric optimization of all blades, the impact on overall performance and flow field statistical characteristics is often negligible.

This study employs a strategy of using single-airfoil design variables and simultaneously updating multiple blades. This approach is not only physically sound but also offers significant advantages in computational efficiency. Since calculating unsteady accompanying sensitivity is typically more time-consuming than forward CFD solutions, calculating sensitivity for each blade separately and updating design variables independently would significantly increase the overall optimization cost. By calculating the sensitivity for only one reference blade and synchronously mapping its design variable updates to the remaining blades, the computational overhead related to optimization can be approximately halved without sacrificing physical consistency.

From a physical perspective, once the rotating flow field reaches a periodic steady state, the downwind flow environment experienced by different blades in a two-bladed VAWT at different time steps statistically differs only in phase shift. In other words, the flow characteristics experienced by one blade when entering the downwind region at a certain time step will be completely experienced by the other blade within one rotation cycle through time shift. Therefore, when the optimization objective is time integral or periodic average, single-airfoil design variables can adequately represent the aerodynamic response of multiple blades throughout the entire rotation cycle.

It is worth noting that the modeling assumption based on single-airfoil design variables and simultaneous updates of multiple blades implicitly presupposes that the rotor flow field possesses statistical periodic translational invariance. However, under certain specific physical conditions, this assumption may no longer hold strictly. First, under strong blade-blade frequency-locking interference, the unsteady aerodynamic responses of adjacent blades may phase-lock through wake interactions, thereby disrupting the time translational symmetry between blades and causing fundamental differences in the flow environment experienced by different blades at the same azimuth angle. Second, under aperiodic stable dynamic stall chaotic conditions, blade aerodynamics may exhibit quasi-periodic or even chaotic characteristics. In this case, the flow field evolution is highly sensitive to initial conditions, making it difficult to establish equivalence relationships between different blades through simple phase translation. Furthermore, for very small-scale, closely spaced rotors with small blade spacing, the wake of a single blade may not have fully diffused before reaching the downstream blade. Its velocity deficit and vortex structure may directly dominate the inflow conditions of the downstream blade, thus significantly amplifying the impact of geometric or aerodynamic differences between blades. Finally, under asymmetric conditions (such as yaw inflow or significantly non-uniform inflow), the rotor no longer satisfies rotational symmetry in space. Different blades may experience systematically different aerodynamic environments within the same rotational cycle, making the synchronous renewal strategy based on a single airfoil physically inapplicable. The synchronous deformation mechanism used in this study explicitly excludes the above situations, limiting the research to VAWT conditions where geometry and operating conditions are symmetrical and the flow field reaches a periodic steady state.

Based on the above considerations, this study adopts a synchronous update strategy driven by single-wing design variables, which effectively reduces computational costs while ensuring the physical consistency of unsteady adjoint optimization, providing a feasible path for efficient optimization of large-scale VAWT.

4.3 Near-Wall Mesh Definition

Accurate resolution of unsteady flow structures and time-dependent sensitivities in VAWT adjoint optimization requires careful attention to both mesh design and the iterative numerical schemes employed in solving the governing and adjoint equations. In this study, the mesh generation and solver configuration are specifically tailored to support time-accurate, rotating, and deforming geometries under adjoint-based optimization.

The computational domain is divided into two regions: a stationary stator zone (housing the inflow boundary and outer domain) and a rotating inner rotor zone, where the blades are mounted and subjected to both physical motion and shape deformation. A circular sliding interface separates the two zones, allowing for relative motion without mesh disconnection. The mesh in the rotor region is structured to conform to the rotational geometry and boundary layer requirements of the blades.

To maintain high fidelity during unsteady simulations, the mesh must satisfy several key criteria:

Near-wall resolution is enforced using first-cell height targeting $y+\approx 1$ to ensure proper integration with turbulence models like k-w SST.

Spanwise resolution is increased near the blade tips and root regions to capture 3D flow separation and tip vortex structures, especially under dynamic deformation.

Temporal-consistent mesh deformation is supported within the rotor zone using radial basis function (RBF) interpolation or linear elastic smoothing, allowing for smooth transitions during free-form deformation (FFD) without introducing skewed or tangled elements.

Grid orthogonality and low aspect ratio are maintained in boundary layers to reduce numerical diffusion and preserve adjoint accuracy near solid surfaces.

Mesh quality is particularly critical in adjoint computations because gradient noise can be amplified by mesh irregularities, especially in regions with high curvature or abrupt motion-induced changes. As such, all FFD-based deformations are monitored for element Jacobian quality and adjusted through mesh smoothing if necessary before each primal-adjoint evaluation cycle.

In the aerodynamic simulation and adjoint optimization of unsteady vertical axis wind turbines (VAWT), the definition of the near-wall mesh directly determines the analytical accuracy of the boundary layer, the reliability of aerodynamic predictions, and the numerical stability of sensitivity calculations. Because VAWT blades experience a wide range of effective angle of attack variations within a single rotation cycle and frequently enter dynamic stall and reattachment processes, the near-wall flow characteristics exhibit significant unsteadiness and spatial gradient variations. Therefore, compared to steady horizontal axis wind turbine (HAWT) problems, VAWT places more stringent requirements on the quality of the near-wall mesh.

This section focuses on the near-wall mesh construction strategy for the optimized NACA0015 airfoil, including the first-layer mesh height (represented by y+), the normal mesh growth rate, the wall tangential resolution, and the mesh treatment of the trailing edge region. This mesh definition not only ensures the accuracy of the forward CFD calculations but is also a necessary prerequisite for the subsequent airfoil geometric constraint analysis and design variable deformation feasibility in Section 4.4.

A review of past VAWT numerical studies reveals that most works addressing dynamic stall and unsteady aerodynamic problems employ low Reynolds number near-wall treatments or wall-resolved turbulence models, thus requiring the first grid layer to be located within a viscous sublayer, i.e., the value of y+ does not exceed 1.

Based on the above research consensus, and considering the need for unsteady accompanying sensitivity calculations in this study, this paper suggests and adopts a y+ range of less than 1 as the target range for near-wall mesh design. During actual mesh generation, the height of the first mesh layer is conservatively selected based on the estimated combination of maximum inflow velocity and rotational tangential velocity to ensure that Y+ remains within this range throughout the entire rotation cycle.

Besides the initial mesh height, the quality of the near-wall mesh in both the normal and tangential directions significantly impacts the numerical results. In the normal direction, a progressively increasing structured or quasi-structured mesh is employed, with the growth rate kept within a small range to avoid abrupt changes in mesh scale within the boundary layer. Typically, the normal growth rate is limited to 1.1–1.2 to ensure smooth resolution of velocity and turbulent gradients near the wall.

In the tangential direction, the mesh distribution along the airfoil surface must accommodate both the high curvature region at the leading edge and the pressure gradient variation region in the mid-to-rear section. For the NACA0015 airfoil, a higher tangential resolution is required in the leading edge region due to strong acceleration and potential stall initiation points; while in the mid-chord to trailing edge region, sufficient mesh density is needed to resolve boundary layer separation and reattachment processes. This tangential distribution strategy also helps maintain mesh quality stability during subsequent geometric deformation.

For the standard NACA0015 airfoil, its theoretical geometric trailing edge is a sharp structure. In numerical implementation, directly using a geometrically perfectly sharp trailing edge would lead to significant mesh distortion at the trailing edge, thus affecting the computational stability of pressure and shear stress. Therefore, in this study, the trailing edge tip is not strictly modeled as a mathematically zero-thickness structure. Instead, numerical resolvability is achieved by introducing a very small but finite trailing edge thickness.

The selection principle for this trailing edge thickness is: its scale is much smaller than the airfoil chord length and boundary layer thickness, thus not significantly affecting the overall aerodynamic characteristics, while being sufficient to ensure the continuity and orthogonality of the mesh in the trailing edge region. It is important to emphasize that this study only discusses the optimized NACA0015 airfoil and does not involve special trailing edge configurations such as the J-shape or other modified baseline airfoils. Therefore, the trailing edge treatment strategy will remain consistent throughout, which is beneficial for subsequent systematic analysis of geometric deformation constraints.

After generating the near-wall mesh, subsequent chapters (Chapters 5, 6, and 7) systematically check the mesh quality, including parameters such as element orthogonality, distortion, and minimum element volume. The results show that the mesh quality parameters meet the requirements of unsteady CFD and associated calculations within the airfoil surface and its adjacent regions. Furthermore, the near-wall mesh maintains a reasonable quality level even after airfoil geometry undergoes design variable-driven deformation.

This is crucial for subsequent chapters. Since Section 4.4 will analyze airfoil geometric constraints and design variable distribution, the near-wall mesh must remain stable during geometric changes to avoid misinterpreting numerical errors as aerodynamic or optimization effects due to local mesh degradation.

4.4 Airfoil Constraints Analysis

In an adjoint optimization framework, the geometric update of an airfoil typically manifests as continuous deformation along the wall normal or control point direction. Without appropriate geometric constraints, optimization tends to seek short-term aerodynamic gains through local "extreme shapes," such as sudden reductions in thickness, trailing edge collapse, abrupt curvature changes, or chord length drift. While these shapes may numerically improve the objective function, they often lack structural manufacturability, strength margin, or mesh preservation, and significantly reduce the interpretability of unsteady adjoint gradients. Therefore, in the NACA0015 airfoil optimization of this study, constraint analysis is used as a prerequisite for the geometric update strategy to limit the design space and ensure the convergence and reproducibility of the optimization process.

In common optimization examples in SU2, aerodynamic optimization of wind turbine blade airfoils can be addressed. Several common types of constraints can be summarized as follows:

Scale constraints: Maintaining a constant chord length or limiting the range of chord length variation, ensuring that the dimensionless coefficient definition is consistent with the operating conditions, and avoiding obtaining non-target gains "through scaling geometry."

Thickness constraints: Limit maximum, minimum, or thickness distribution to ensure structural manufacturability and strength requirements, preventing localized thinning that could lead to mesh degradation and unreasonable separation features.

Leading/Tail Geometric Constraints (LE/TE constraints): Constrain the leading edge radius, trailing edge thickness/angle, and trailing edge position to avoid sharp corners or folds; simultaneously ensuring aerodynamic and mesh quality stability.

Smoothness/Curvature Constraints: Control the rate of change of curvature or the second derivative to prevent localized ripple deformation from introducing non-physical pressure oscillations and gradient noise.

Area/Volume Constraints: Maintain approximately constant cross-sectional area to avoid sacrificing aerodynamic benefits for material usage and ensure structural consistency.

Non-self-intersection/Single-valued Surface Constraints: Avoid intersections of upper and lower surfaces or negative thicknesses, ensuring the airfoil remains a definable closed section.

Based on the near-wall mesh strategy in 4.3, this study prioritizes the use of the constraints of chordlength and thickness, that are directly related to mesh quality and structural feasibility to ensure that unsteady CFD and adjoint optimization remain stable during multiple iterations.

For two-dimensional airfoil optimization, chord length constraints can be achieved by fixing key points at the leading and trailing edges. Let the leading edge point be x_{LE} and the trailing edge point be x_{TE}, and the chord length be defined as: $c = |x_{TE} - x_{LE}|$

In the geometry optimization process, the examples applicable to pitch airfoils typically do not penalize C at the objective function level. Instead, they directly fix the chord reference point through geometric parameterization and boundary conditions, preventing chord length drift at its source. Specifically, the following strategies can be adopted:

Fixed Leading and Trailing Edge Control Points/Nodes: Several key points located near x/c=0 (leading edge) and x/c=1 (tailing edge) are designated as "freeze points," ensuring their displacement is zero during design variable updates.

Geometric Parametric Definition in a Normalized Chord Coordinate System: For example, using x/c as the independent variable to represent the shape of the upper and lower surfaces, optimization only allows changes to the profile in the normal direction, disallowing translation of endpoints along the chord.

Constraining Trailing Edge Position: This requires x_{TE} to remain constant in the global coordinate system, preventing changes in chord length caused by global scaling or translation.

This method ensures that the chord length constraint is strictly satisfied during the iteration process. It avoids inconsistencies in the definition of dimensionless force coefficients caused by "chord length drift," thus guaranteeing the comparability of different iteration results.

For NACA0015, the thickness distribution determines not only the structural margin but also the triggering of dynamic stall and the scale of the separation bubble. Without thickness constraints during optimization, common non-physical tendencies include: local thinning to reduce drag, excessively sharp leading edges to enhance suction peaks, or tail-edge collapse leading to mesh deterioration. To avoid these problems, this study employs a constraint system centered on "thickness distribution."

The local thickness at the chordal position x is the difference between upper coordinate $y_{upper}(x)$ and $y_{lower}(x)$. The typical thickness constraints include:

- *Maximum thickness constraint: Keeps tmax close to the reference airfoil (or limits its variation range) to prevent overall thinning of the cross-section.*

- *Minimum thickness constraint: Limits t(x) ⩾ tmin(x) at critical chordal locations.*

- *Tail edge thickness constraint: Maintains a finite or minimum tail edge thickness to ensure mesh and numerical stability.*

There are generally two approaches to implementing thickness constraints in pitch airfoils:

1. Explicit geometric constraints (hard constraints): Thickness is defined as a constraint function at the parameterization level and treated as an inequality constraint in the optimizer. This requires parameterization and constraint evaluation to be calculated synchronously after each geometric update.

2. Projection/repair strategy: The thickness distribution is checked after each update. If $t(x) < t_{min}(x)$ or a trailing edge anomaly occurs, the local design variable update is rolled back or projected to the feasible region boundary.

For unsteady adjoint optimization, the second approach is often more robust: it avoids introducing additional constraint adjoint terms into the adjoint gradient and significantly reduces the risk of mesh collapse due to geometric infeasibility. Since this study focuses on the optimized NACA0015, a strategy of "lower thickness limit + minimum trailing edge thickness + local repair" can cover the main risks.

In sensitivity-based gradient optimization, geometry updates typically employ an update rule of the form of $\Delta x = -\alpha_{opt} g$.

Where g is the shape gradient (or the smoothed/filtered gradient), and α_{opt} is the step size or scaling factor. In practical engineering, the selection of α_{opt} is one of the key factors determining whether the optimization is stable. Its role is not only to control the geometric deformation amplitude of each iteration, but also to directly affect the mesh quality, the gradient noise of the time integration objective, and the convergence speed.

When α_{opt} is too large, a single geometric update becomes overly aggressive, easily triggering thickness constraint violations, tail collapse, or abrupt curvature changes. Near-wall mesh height and orthogonality deteriorate rapidly, making it difficult for forward CFD residuals to converge, leading to gradient distortion. Unsteady objectives (such as time-integrated C_T) are more sensitive to geometric perturbations; excessively large step sizes amplify high-frequency components of the load within a cycle, causing optimization oscillations or divergence.

When α_{opt} is too small, the single update amplitude is insufficient, the objective function decreases slowly, and the number of optimization iterations increases significantly. In the presence of unsteady load noise and accompanying discrete errors, excessively small step sizes can cause the "real improvement signal" to be submerged by numerical noise, resulting in a non-monotonic or nearly stagnant objective function. Due to minimal geometric changes, optimization may get stuck in a local flat region, making it difficult to overcome the performance bottleneck of the initial design.

Based on these trade-offs, this paper suggests using a normalized step size strategy to determine α_{opt}: using the chord length c or the maximum thickness tmax as a scale, the maximum normal displacement in a single cycle is controlled within a small dimensionless threshold range $max\|\Delta x\|$. It is typically on the order of 10^{-4} to 10^{-3} (the specific value should be determined in conjunction with the mesh resolution and thickness lower bound constraints). The essence of this strategy is to ensure that the magnitude of each update is on the same order of magnitude as the mesh resolution, thereby guaranteeing analyzable geometric changes.

4.5 DV Distribution and Airfoil Deformation

For the standard NACA0015 airfoil, its aerodynamically sensitive regions exhibit a distinctly non-uniform distribution along the chord direction. The leading edge region, due to its strong acceleration effect and significant pressure gradient, is a critical location for dynamic stall triggering, leading-edge separation bubble formation, and suction peak evolution. The trailing edge region significantly influences the wake structure, pressure recovery process, and overall drag level. In contrast, the flow changes in the airfoil's central region are relatively gentle, exhibiting lower sensitivity to local geometric disturbances.

Based on these physical characteristics, a non-uniform distribution strategy is typically adopted for the arrangement of discrete points on the airfoil surface: denser points at the leading and trailing edges, and relatively sparser points in the central region. This distribution improves the optimization's response to key aerodynamic regions without significantly increasing the total number of design variables, while avoiding the introduction of redundant degrees of freedom in regions with low aerodynamic sensitivity. In numerical implementation, this strategy also reduces the impact of geometric deformation on the near-wall mesh quality, allowing the mesh to maintain good orthogonality and smoothness after multiple iterations.

In this study, the distribution of points on the airfoil surface is nonlinearly mapped based on the chordal parameter x/c: the point spacing is significantly refined in the leading-edge region ($x/c < 0.1$) and the trailing-edge region ($x/c > 0.9$), while the spacing gradually widens in the mid-chordal region. This distribution method is consistent with the near-wall mesh refinement strategy in Section 4.3, thus ensuring the coordination between the geometric deformation scale and numerical resolution at both the physical and numerical levels.

In adjoint optimization literature, the number of design variables on the airfoil surface is usually much smaller than the total number of discrete points on the surface. The aim is to capture the main aerodynamic characteristics through low-dimensional parameterization while suppressing non-physical oscillations. In early airfoil optimization studies based on the continuous adjoint method, the number of design variables was mostly concentrated on the order of 20–50, and the airfoil shape was often described using B-spline control points or Fourier coefficients [122-138].

With the improvement of computing power and the development of parameterization methods, research on unsteady problems and complex aerodynamic phenomena has gradually adopted higher-resolution parameterization, but the overall trend remains to keep the number of design variables below the hundred level. Rezaeiha et al. [105-107], in their optimization of VAWT aerodynamic performance, also emphasized avoiding too many degrees of freedom to prevent the optimization results from being overly sensitive to mesh and turbulence model errors.

For unsteady adjoint optimization, the impact of the number of design variables is particularly significant. Since the adjoint equation needs to be integrated in reverse over the entire time interval, increasing the dimension of design variables amplifies the cumulative effect of gradient noise over time, thereby reducing the robustness of optimization convergence. Therefore, in the unsteady optimization of rotating and oscillating airfoils, a moderate number (20–50) of design variables with strong physical interpretability is generally preferred over pursuing extremely high geometric degrees of freedom.

In practical optimization, this DV distribution effectively adjusts the peak suction position and intensity in the leading edge region and improves pressure recovery characteristics in the trailing edge region, without introducing unnecessary high-frequency geometric fluctuations in the central region. Combined with the geometric constraints and scaling factor settings discussed in Section 4.4, this DV distribution provides the necessary conditions for the stable evolution of subsequent airfoil deformation.

4.6 Simulation Timestep & Unit Displacement

In VAWT's unsteady CFD/adjoint optimization, the "time step" is not merely a numerical parameter, but a key modeling quantity that couples the rotational motion (azimuth advance) with the time scale of unsteady separation/dynamic stall. In engineering, it's more common not to directly specify Δt , but rather to specify the azimuth increment $\Delta\theta$ (e.g., 1°, or 0.1 revolutions per step), and then convert the rotational angular velocity Ω into the actual time step.

The advantage of this definition method is that, under different TSR or different speed conditions, the same $\Delta\theta$ can maintain a constant number of sampling points per revolution, thus more directly controlling the "resolution per revolution", which is more in line with the physical structure of the VAWT's periodic load/wake-blade re-interaction.

Existing VAWT URANS/Hybrid RANS-LES studies generally show that the "minimum requirement" for time step (or $\Delta\theta$) depends on flow complexity, especially in low TSR (dynamic stall, strong vortex shedding) and downwind wake interference. Rezaeiha et al.'s conclusion on the sensitivity of systematic parameters is representative: at higher TSRs (where the flow is mostly attachment), $\Delta\theta \leq 0.5°$ is often sufficient; however, at low to medium TSRs (with dynamic stall and significant wake-blade effects), it is necessary to refine to $\Delta\theta \leq 0.1°$ to stably capture load abrupt changes and subsequent oscillations, thus making statistics such as power coefficient/moment coefficient less sensitive to time step [105-107].

In literature with a "given Δt", a common practice is to compare three or more Δt values, selecting the one with minimal difference in critical outputs (C_m, $\Delta\theta$) but significantly reduced computational cost. For example, Celik compared multiple sets of Δt values for the unsteady computation of the self-starting process and ultimately chose $\Delta t = 0.00072s$ as a compromise [151].

Similarly, in 3D studies of two-bladed straight-bladed VAWTs, the time resolution is often expressed as "$\Omega\Delta t$" and after weighing resolutions such as 4°, 2°, 1°, and 0.5°, 1° is chosen as the default setting that is acceptable for engineering applications.

For unsteady solvers like SU2, which are based on implicit/explicit time advancement, a true time step Δt often corresponds to several pseudo-time iterations. The purpose is not to "make the time advancement faster," but to reduce the residuals of the discrete equations to an acceptable level at this time level, so as to avoid conflating "time discrete errors" with "non-convergent algebraic errors." Smaller time steps result in:

weaker individual physical changes and easier convergence of individual equations;

but increased total number of steps leads to higher cumulative computational costs;

for unsteady adjoints, more time steps also mean higher storage/reconstruction pressure (especially for discrete adjoints requiring playback or storage of forward flow history).

Therefore, engineering practices typically employ a strategy of "first finding periodic stability with a coarser $\Delta\theta$, then gradually refining it": first ensuring the rotor reaches statistical stability (C_m, C_P) after a certain number of revolutions, then refining $\Delta\theta$ to a level where dynamic stall is analytical, thus reducing unnecessary computation. Rezaeiha et al. also emphasized that, in addition to $\Delta\theta$, the "number of revolutions required for statistical stability" is itself a result-sensitive term [105-107].

In your workflow, unit displacement can be understood as the minimum amount of motion required to update the geometric/motion boundary within each time step, which is $\Delta\theta$ in a pure rotation problem; in problems involving deformation (DV) or pitch, it also includes the displacement/rotation increment per step (e.g., $\Delta\theta$). Its core functions are:

- *Controlling the "step smoothness" of dynamic mesh or geometric updates, avoiding sudden drops in local mesh quality (negative volume, strong non-orthogonality, near-wall distortion) due to excessive geometric changes at each step, thus inducing unsteady divergence;*

- *In unsteady adjoint optimization, ensuring that the gradient of the objective functional with respect to design variables is approximately within the "linear response range," reducing adjoint noise caused by coarse time discretization.*

The reason for choosing displacement per unit time as the scale is that many VAWT CFDs use $\Delta\theta$ (the azimuth angle rotated per step) to control the time resolution, because it is inherently tied to the rotor motion scale; the same $\Delta\theta$ will correspond to different Δt under different TSRs and different D.

4.7 Initial Conditions and Residuals

In most VAWT unsteady numerical studies, the initial conditions typically employ a uniform inflow field plus a static fluid assumption. That is, at the start of the calculation, the velocity field across the entire computational domain is initialized to the inlet inflow velocity, the pressure field to the reference static pressure, and the turbulent fluxes are given based on the inlet turbulence intensity or empirical formulas. This initialization method is advantageous because it is simple to implement and numerically stable, but its physical drawback is that the initial stage does not include any rotor wake information.

Therefore, almost all reliable VAWT unsteady studies explicitly state that the initial conditions themselves do not represent a physically steady state. The flow field only enters a statistically stable state after several complete rotational cycles. During this process, the rotor wake gradually establishes itself, and the flow environment experienced by the blades in the upwind and downwind regions begins to exhibit periodic repetition. Only after this process do the extracted aerodynamic forces, torques, or power coefficients have physical meaning.

In rotating airfoil or full-scale VAWT models, the initial azimuth angle $\Phi 0$ of the blades can usually be arbitrarily chosen because, under periodic steady-state conditions, this choice only results in a phase shift of the time series without altering the periodic averaging results. However, when performing instantaneous load or dynamic stall phase analysis, the initial azimuth angle is usually explicitly given in the literature to ensure the repeatability of the results.

For studies using single-blade pitch or equivalent oscillating airfoil models, the definition of initial conditions differs from that of rotating models. Since these models do not involve actual rotational motion but instead simulate the local aerodynamic behavior of the blades in a VAWT through time-varying pitch angles and equivalent relative flow, the initial conditions need to simultaneously consider flow field initialization and kinematic state initialization.

In the literature, a common practice is to set the initial pitch angle of the airfoil to a physically reasonable and numerically smooth value, such as the average angle of attack or the initial phase angle of the pitch function. Subsequently, the pitch angle evolves gradually over time according to a predefined periodic function. This approach avoids introducing non-physical transient pressure waves or numerical oscillations due to abrupt changes in the pitch angle during the initial calculation phase [139-150].

Similar to rotating models, oscillating airfoil models also require several oscillation cycles to reach statistical stability. Only when the time histories of lift, drag, or tangential force essentially coincide within consecutive periods can the influence of the initial conditions be considered eliminated.

In unsteady CFD calculations, the meaning of residuals differs from that in steady problems. For each true time step, the solver typically reduces the algebraic residuals of the discrete equations through several pseudo-time iterations (inner iterations). It is generally accepted in the literature that the residuals should decrease by at least 3–4 orders of magnitude within each time step to avoid coupling between time-progression errors and algebraic errors [151-153].

However, relying solely on residual decrease is insufficient to determine whether VAWT unsteady calculations have truly converged. Since the flow itself is periodically unsteady, the residuals do not decrease monotonically between different time steps. Therefore, most studies combine the periodic consistency of physical quantities as the primary convergence criterion, such as:

The power coefficient C_P essentially coincides within three or more consecutive rotational cycles:

- *The time histories of lift, drag, or tangential force repeat in phase;*
- *The change in the periodic average quantity is below a given threshold (e.g., <1%).*
- *This dual criterion of "residuals + physical quantities" has become the standard practice in VAWT unsteady numerical studies.*

In the framework of unsteady adjoint optimization, the importance of initial conditions and residual convergence is further amplified. Since the adjoint equation requires backward integration along time, any numerical noise or non-convergence error in the forward calculation will be amplified during backpropagation, thus contaminating gradient information. Therefore, before proceeding to the adjoint solution, it must be ensured that the forward unsteady calculation has reached a stable periodic solution.

In practice, this typically means running several complete rotational cycles (or oscillation cycles) before starting the adjoint calculation and updating the design variables, and confirming that the key aerodynamic parameters have converged to a periodic steady state. This strategy is widely adopted in unsteady optimization studies of VAWT and is considered a necessary condition for obtaining reliable gradients and stable optimization convergence.

4.8 Scale Analysis of Model Boundaries

In unsteady CFD simulations of VAWT, the choice of the computational domain shell (inlet/outlet/far-field) has a decisive impact on the accuracy of the flow field. Because vertical-axis wind turbines generate strong asymmetric separation, vortex shedding, and significant wake diffusion in the upwind and downwind regions within a single rotational cycle, the requirements for the computational domain size are typically more stringent than for steady-airfoil or horizontal-axis wind turbines. If the shell size is insufficient, boundary conditions will cause non-physical disturbances to the pressure field, induced velocity, and wake evolution near the rotor, thus affecting the convergence of aerodynamic predictions and unsteady statistics.

In existing VAWT numerical studies, the computational domain size is typically defined dimensionlessly based on the rotor diameter D. Numerous studies have shown that in two-dimensional or three-dimensional rotating VAWT models, the inlet boundary is typically set 5D–10D from the rotor center, while the outlet boundary needs to be significantly farther, usually 10D–50D, and even further under low TSR or strong dynamic stall conditions [18] [105-107] [154].

The core reason for this asymmetric arrangement of inlet and outlet lies in the physical characteristics of the VAWT wake. Compared to horizontal axis fans, the VAWT wake not only contains an axial velocity deficit but also features a significant lateral velocity component, periodic vortex structures, and a low-speed recirculation region formed in the downwind region. These wake structures need to fully develop and gradually diffuse within the computational domain to approach a "quasi-uniform flow" state before reaching the outlet boundary. If the exit distance is too short, exit boundary conditions (such as constant pressure or zero gradient conditions) will forcibly truncate the wake, leading to non-physical pressure reflections or induced velocity deviations, thus affecting the overall rotor load prediction.

Therefore, the literature generally recommends that the exit boundary distance should be significantly larger than the inlet distance to reduce the wake's sensitivity to boundary conditions. This requirement is particularly important under low TSR conditions, where the wake velocity deficit is greater, diffusion is slower, and the wake length increases significantly [155].

Multiple parameter sensitivity studies show that when the computational domain size is insufficient, even if the instantaneous residuals converge within each time step, the periodically averaged aerodynamic and power coefficients still exhibit a significant dependence on the shell size. Specific issues include:

The downwind tangential force and moment coefficient are underestimated or overestimated.

The power coefficient C_P changes monotonically with the expansion of the computational domain, making it difficult to reach the plateau region.

The unsteady load time history exhibits phase or amplitude differences between different periods.

Therefore, in unsteady VAWT calculations, the independence analysis of the shell scale is generally considered as important as mesh independence and time step independence. Only when the sensitivity of key aerodynamic parameters to further expansion of the computational domain is negligible can the choice of shell scale be considered reasonable [156-158].

For single-blade pitching or equivalent oscillating airfoil models, their flow characteristics differ significantly from those of a fully rotating VAWT. These models typically do not include the actual superposition of multi-blade wakes and downwind re-interaction, but rather focus on the local unsteady aerodynamic behavior of a single airfoil under given relative inflow and pitching motions. Therefore, their requirements for the computational domain scale are relatively relaxed.

The commonly adopted approach in the literature is to set the far-field boundary within the range of 10D–20D of the equivalent rotor diameter, or, in the case of a two-dimensional oscillating airfoil problem, to set upstream, downstream, and lateral distances of at least 15c, based on the airfoil chord length c. Within this scale range, the unsteady vortex structure generated by the oscillating airfoil has significantly decayed before reaching the far-field boundary, thus avoiding interference from boundary conditions on the time histories of lift, drag, or tangential force.

It should be noted that although the shell scale of a single-blade pitching model can usually be smaller than that of a full VAWT model, when the pitch amplitude is large or the research focus involves the shedding and convection processes of dynamic stall vortices, it is still necessary to appropriately increase the far-field distance to ensure that the separated vortices can evolve completely within the computational domain.

Based on the above literature conclusions and the unsteady rotation and pitch conditions focused on in this study, the selection of the computational domain shell scale follows these principles:

For the rotating VAWT model, the inlet boundary distance is no less than 5D, and the outlet boundary distance is significantly greater than the inlet distance to ensure sufficient wake development;

For the single-blade pitch model, the far-field boundary is set above O (10D) of the equivalent rotor scale to ensure that the unsteady vortex structure has significantly attenuated before reaching the boundary;

Sensitivity analysis of key aerodynamic parameters verifies that the changes in results are negligible when the shell scale is further increased.

This shell scale analysis provides a reliable computational domain foundation for subsequent three-dimensional flow field extension and surface definition (Section 4.9).

4.9 Effect on 3D Flowfield and Surface Definition

VAWT blades are inevitably affected by three-dimensional effects under real-world operating conditions, including tip-induced vortices, spanwise pressure gradients, support arm/hub disturbances, and spanwise non-uniform stall and reattachment. Compared to two-dimensional (2D) models, three-dimensional (3D) CFD can explicitly analyze these phenomena and is therefore widely used for: assessing tip losses, studying the influence of support structures, analyzing the three-dimensional structure of wakes, and providing more reliable power and load predictions under asymmetric conditions such as yaw/tilt axes [159-161].

Based on publicly available literature, the following types of research represent the main development trends in 3D VAWT numerical simulation. In experimental comparisons and engineering-scale analyses, Li et al., in their Part I/Part II series published in Energy, conducted three-dimensional numerical and wind tunnel comparative studies on straight-bladed VAWTs, focusing on load/performance and flow field/performance predictions respectively [162-163]. 3D Influence of Structural Details/Auxiliary Components: Marsh et al. used 3D CFD to evaluate the influence of the support structure on power, torque fluctuations, and loads in a straight-blade vertical-axis turbine (where tidal currents and wind energy are both cross-flow), providing a quantitative framework for three-dimensional losses caused by "non-blade body geometry" [164].

These studies collectively demonstrate that 3D models are often necessary when the research objective involves end losses, spanwise load distribution, three-dimensional wake structures, skewed inflows, or the influence of auxiliary components; while when focusing on two-dimensional cross-sectional aerodynamic mechanisms or requiring efficient iterative optimization, 2D/equivalent models can be used, and a consistency bridge can be established between the two by "extracting 2D cross-sectional information from 3D".

When it is necessary to convert the flow field and load information of a 3D VAWT into "2D usable" input (e.g., for single-section analysis, equivalent pitch airfoil model calibration, or verification of 2D/quasi-2D model assumptions), the core idea is to extract the phase condition statistics at representative spanwise locations, while avoiding the strongly three-dimensional regions at the ends and attached components as much as possible, and to maintain consistency with the 2D reference coordinates/force coefficient definitions. The following workflow is typically used:

Choosing the Span Section Location: The most common practice is to select a section at the mid-span of the blade or at a certain distance from the tip (e.g., > 1–2 local chord lengths from the tip) to avoid the end vortex-dominated region. If the model contains support arms/connectors, sections near them should be avoided, and a "pure blade section region" should be selected [165-168].

Defining Section Slices and Coordinate Transformation: During CFD post-processing, a two-dimensional slice plane is established at a fixed z (span) direction, and the velocity, pressure, vorticity, and other fields on this plane are output. Simultaneously, the velocity vector is transformed from the global coordinate system to the local blade coordinate system (chordal/normal) or the tangential/radial system that rotates with the blade to ensure that the CT, C_m, and C_P calculated subsequently are consistent with the 2D definitions [166].

Phase Alignment and Phase-Locked Averaging: 3D unsteady flows exhibit significant periodicity and a certain degree of turbulent fluctuations. To obtain a "deterministic response" comparable to the 2D model, phase averaging of cross-sectional data at the same azimuth angle θ over multiple stable periods is performed. This filters out random fluctuations and retains unsteady characteristics locked to rotor motion.

If it is necessary to map 3D data to the boundary input of a 2D oscillating airfoil (e.g., equivalent $V_{rel}(t)$, equivalent angle of attack $\alpha(t)$, reference sampling points or sampling lines can be defined near the cross section (e.g., the inflow point at a certain distance in front of the blade leading edge, or several monitoring points around the cross section). The velocity vector is extracted and projected onto local coordinates to construct $U_{eff}(\theta, z)$ and $\alpha_{eff}(\theta, z)$. In scenarios requiring "2D equivalence," the mid-span phase average is typically used as a representative.

Through these steps, the unsteady flow field and load information of the 3D VAWT can be statistically compressed into a set of 2D data sequences associated with azimuth/time, providing a foundation for subsequent consistency comparison, error attribution, and parameter calibration from the "2D cross section model to the 3D VAWT model.

It is worth noting that this study employs a so-called 2.5D modeling strategy to investigate the aerodynamic advantages of optimized airfoils under three-dimensional flow conditions while avoiding the complexity of full three-dimensional rotor simulation. Currently, the 2.5D method based on finite-span blades and spanwise symmetric boundaries follows commonly used quasi-three-dimensional modeling methods to separate cross-sectional aerodynamic effects while preserving basic three-dimensional flow characteristics This model includes blades of finite height with symmetric boundary conditions applied to their upper and lower surfaces, and excludes winglets or endplates. This configuration effectively eliminates free-end pressure leakage and classic tip vortex formation, allowing the analysis to focus on three-dimensional flow phenomena related to spanwise pressure gradients, vortex stretching, and non-uniform separation along the blade span [169-170].

The rationale for this assumption is that the primary objective of this study is to evaluate the aerodynamic advantages resulting from airfoil shape optimization, rather than quantifying the effects of end-point losses or tip devices. By applying symmetric boundary conditions at both ends of the spanwise axis, this model represents an idealized blade segment embedded in an infinitely repeating spanwise environment. Under this assumption, the main 3D effects captured by the simulation originate from inherent unsteady separation and vortex dynamics caused by rotation or equivalent pitch motion, rather than geometric end effects. This approach enables controlled comparisons between baseline and optimized airfoils, attributing differences in performance and flow structure primarily to airfoil geometry.

Although the current model does not include free blade tips, it still allows for the formation of 3D flow structures within the computational domain. The finite blade height allows for the emergence of spanwise velocity components and 3D vortex deformation, making the model more representative than rigorous 2D simulations while incurring significantly lower computational costs than full 3D rotor calculations. Therefore, the 2.5D method offers a suitable balance between physical accuracy and computational efficiency for evaluating the impact of airfoil optimization.

Regarding the use of steady-state or quasi-steady-state simulations for 3D flow visualization, it is important to note that when the goal is to compare the relative aerodynamic advantages of different airfoil geometries under the same numerical settings, steady-state solutions considered "important snapshots" in historical studies can still provide crucial information about the spatial structure of the separated region and 3D vortex patterns. Unsteady-state simulations are used to further verify selected operating conditions to ensure that conclusions drawn from steady-state simulations are not necessarily the result of model assumptions.

In Chapter 7, span length independence is used for verification. By comparing 2–3 different heights (H/c) under the same mesh and model, the statistics of C_T, C_M, and C_P at the mid-span are compared, as well as the stability of the main scales of the three-dimensional vortex structure (e.g., Q-criterion or vorticity isosurface morphology). If the mid-span results vary little with height, it indicates that the model captures a "local three-dimensional effect" rather than an end effect. Simultaneously, in symmetric boundaries, if the normal velocity near the upper and lower boundaries is close to 0, and the pressure/velocity field does not exhibit end leakage characteristics, then... This demonstrates the validity of the 2.5D "de-endpointing" assumption, allowing for subsequent data acquisition.

Finally, it is important to emphasize that the current 2.5D framework is not intended to predict absolute end losses, wingtip vortex intensity, or the aerodynamic performance of winglets. Instead, it aims to isolate and evaluate the impact of airfoil shape optimization on three-dimensional flow behavior and performance trends under ideal spanwise conditions. Therefore, this assumption is considered applicable to the scope and objectives of this study.

4.10 Continuous and Discrete Adjoints

In unsteady adjoint optimization, there are two main approaches to constructing the adjoint equation: continuous adjoint and discrete adjoint. The core difference lies in whether to discretize first or perform variational analysis first: continuous adjoint first derives the adjoint PDE from the continuous governing equations, then discretizes the adjoint equation; discrete adjoint directly differentiates the discretized residual equation (numerical scheme), obtaining an adjoint system that is strictly consistent with the discrete forward solver.

The greatest advantage of discrete adjoint is its strict consistency with the given numerical scheme: if the forward equation, objective function, and boundary treatment are all consistently differentiated at the discrete level, the resulting gradient is numerically closer to the "true discrete optimization gradient," which is more conducive to stable convergence and repeatability. The advantage of continuous adjoint derivations lies in their clearer derivation forms and stronger interpretability. However, if the discretization is not entirely consistent with the continuous derivation (e.g., upwind schemes, limiters, wall functions, time-discrete details, etc.), gradient deviations may occur, requiring additional verification and correction.

Complex numerical details (turbulence models, nonlinear limiters, multigrids, etc.) For solvers containing complex numerical "patches," discrete adjoint derivations are easier to maintain consistency because they, in principle, differentiate with respect to the "discrete residuals of the code implementation." Continuous adjoint derivations, on the other hand, require equivalent processing of each numerical detail at the continuous level, resulting in a greater workload and a higher likelihood of omissions.

Continuous adjoints offer a more direct theoretical derivation for "custom objective functions/constraints," especially when the objective is a continuous functional (e.g., time-integral torque, loss functionals in a specific region). Continuous derivations often more clearly articulate their variational structure. Discrete adjoints, on the other hand, require ensuring the objective function is differentiable in the discrete implementation and consistent with the previous discretization method; otherwise, the gradient may introduce noise or non-differentiable points.

In unsteady adjoints, regardless of whether they are continuous or discrete, the adjoint integral requires access to the previous time history (either stored or recalculated). Discrete adjoints, strictly adhering to discrete-time progression, offer a more "natural" replay strategy, but are more reliant on time-discrete details. Continuous adjoints, theoretically rewritten in a time-continuous form, still ultimately require discretization and addressing the same history dependency issues.

For unsteady, strongly segregated/dynamically stalled scenarios like VAWT, which involve rotation/geometric updates and custom C_T as an objective, discrete adjoints are more suitable if stable, repeatable optimization convergence is the primary objective.

This is because unsteady flows in VAWT involve strong nonlinearity and (numerically) more sensitive segregation/reattachment processes, making gradients easily amplified by discretization errors, time step errors, and locally non-differentiable numerical processing. Discrete adjoints exhibit stronger consistency with a given solver's discretization scheme and are generally less prone to problems such as "correct gradient direction but magnitude drift" or "gradient noise leading to extremely small step sizes". Therefore, the recommended strategy for VAWT is usually: "The derivation and mechanism explanation in the paper are more continuous (for easier interpretation), while the convergence of engineering solutions and optimizations is less discrete (to ensure consistency)." This also aligns with the practical path of many industrial/engineering CFD optimizations: using a continuous framework to explain the functionals and physical meaning, and using a discrete framework to implement them in code and ensure gradient reliability.

4.11 Turbulence Models and Experiments

In unsteady numerical studies of vertical axis wind turbines (VAWTs) and oscillating airfoils, the choice of turbulence model and experimental verification methods directly determine the reliability of overall performance indicators such as the power coefficient. Compared to local transient vortex structures or high-frequency pressure fluctuations, the power coefficient is essentially a highly integrated quantity over time and space, and its sensitivity to small-scale turbulent details is relatively limited. Therefore, numerous studies over the years have shown that, for performance prediction and optimization, the RANS/URANS framework combined with the k-ω SST model can provide sufficiently accurate and stable results.

The unsteady flow of VAWTs is mainly dominated by periodic angle-of-attack variations, dynamic stall, and wake-blade interactions, and its timescale is usually related to rotor speed or pitch period. For periodically averaged quantities such as power coefficient and torque coefficient, the key lies in the phase and duration of separation and its combined effect on tangential force, rather than the fine turbulent structure within the separation vortex. The URANS method, through time-stepping, can resolve the main unsteady separation and reattachment processes, while the k-ω SST model exhibits good robustness in attachment-separation transitions, adverse pressure gradient handling, and near-wall behavior, and is therefore widely used.

Similar conclusions hold for single-blade pitching or equivalent oscillating airfoil models. Multiple studies show that, under reasonable time steps and near-wall resolution, URANS/SST can predict lift, drag, and their periodic variation trends well, and is consistent with experimental results in a periodically average sense. For the evaluation of power coefficient or equivalent tangential force, the improvement brought by further introducing LES or Hybrid RANS–LES is often limited, but the computational cost increases significantly. Therefore, from the perspective of engineering optimization and parameter research, RANS/URANS + k-ω SST is generally considered a reasonable choice in terms of accuracy-efficiency balance.

Particle Image Velocimetry (PIV) is one of the most commonly used flow field measurement methods in VAWT experimental research, especially playing a key role in the study of dynamic stall and wake. Ferreira et al. systematically measured the velocity field and vortex structure of straight-bladed VAWTs at different azimuth angles using PIV, and compared the results with 2D URANS simulations phase by phase, providing important verification evidence for the unsteady separation prediction of numerical models [25].

In subsequent studies, PIV data are often used to validate the following types of CFD results:

The formation location and shedding phase of dynamic stall vortices;

The basic distribution characteristics of the velocity fields in the upwind and downwind regions;

The macroscopic structure of velocity deficit and vorticity distribution near the wake.

Multiple studies have shown that, provided the time step and grid resolution are reasonable, URANS/SST exhibits good consistency with PIV in these "macroscopic unsteady characteristics," thus supporting its rationality in power coefficient prediction.

Although PIV provides important experimental evidence for CFD validation, it still has several inherent limitations in the VAWT scenario, which have been repeatedly pointed out in numerical-experimental comparative studies over the years.

First, spatial resolution is limited. Near the leading edge or very close to the wall where dynamic stall occurs, PIV often struggles to obtain reliable velocity data, limiting the experimental resolution of details within the boundary layer. Therefore, even if CFD deviates from the actual flow in the near-wall region, it may not be directly identifiable by PIV.

Secondly, there are limitations imposed by the two-dimensional measurement assumptions. Most VAWT PIV experiments employ planar PIV (2D-2C), measuring only the velocity components within a single cross-section while ignoring spanwise velocities and three-dimensional structures. For situations with significant three-dimensional effects (end vortices, support arm disturbances, or yaw conditions), the consistency between experimental and 2D CFD results does not necessarily mean that the actual three-dimensional flow has been fully captured.

Thirdly, there is a lack of complete consistency between experimental and numerical conditions. Wind tunnel blockage effects, turbulence intensity, inflow non-uniformity, and the presence of model support structures all influence PIV measurement results, factors that are often idealized or simplified in CFD. Therefore, PIV validation is generally more suitable for qualitative or semi-quantitative comparisons than for point-by-point error assessment.

Finally, PIV data primarily focus on the velocity field itself, while overall performance indicators such as the power coefficient often still rely on force measurements or numerical integration. This further illustrates that in studies with the power coefficient as the core objective, a reasonably validated URANS/SST model can meet engineering accuracy requirements, without necessarily resorting to high-cost, high-fidelity turbulence simulations [171-177].

4.12 Summary

This chapter systematically reviews the construction and verification of numerical models for the key modeling elements required for unsteady adjoint optimization of VAWT blades. By introducing an objective function centered on the time-dependent tangential force coefficient and combining it with user-defined functions to achieve a unified description of rotation/pitch motion, equivalent inflow, and boundary conditions, an unsteady optimization framework directly related to VAWT power output is established. Simultaneously, in terms of grid, time step, and computational domain scale, the chapter follows the common guidelines in existing literature regarding dynamic stall and wake development, ensuring that unsteady flow characteristics can be stably analyzed.

Building on this foundation, this chapter further discusses the selection principles for design variable distribution, geometric constraints, and continuous versus discrete adjoint methods, pointing out that in engineering-scale VAWT optimization, the URANS-based discrete adjoint method has a greater advantage in balancing gradient consistency and computational efficiency. Combined with the verification results of CFD in existing PIV experiments, it can be concluded that the modeling strategy adopted in the study with the power coefficient as the core performance indicator possesses sufficient physical credibility and numerical robustness, providing a reliable foundation for the subsequent analysis and discussion of unsteady optimization results.

Chapter 5

VAWT Oscillation Airfoil Optimization

5.1 Overview

Vertical axis wind turbines (VAWTs) exhibit significantly different blade aerodynamic characteristics under complex inflow conditions compared to traditional two-dimensional airfoils operating under steady inflow. Because the blades undergo periodic changes in both the inflow direction and relative angle of attack during rotation, VAWT blades are essentially in a strongly unsteady, periodically oscillating aerodynamic environment. This is particularly pronounced at low tip speed ratios (TSRs) and downwind conditions, where dynamic stall, induced velocity variations, and multi-blade interference are especially significant. Therefore, blade design and performance prediction based on steady airfoil pole curves often fail to accurately reflect the aerodynamic behavior under real VAWT conditions.

Based on this background, this chapter systematically conducts airfoil aerodynamic optimization research for VAWT conditions, using the oscillating airfoil model as the core intermediate level. Furthermore, the optimization results are mapped and validated onto a complete VAWT numerical model, thus constructing a complete research path from "airfoil optimization based on a single-blade approximation model to rotor-level validation." The objective of this chapter is to explore airfoil optimization methods suitable for the unsteady operation environment of VAWT (Vehicle Air Wheel Drive) and evaluate their potential for improving aerodynamic performance in a real rotor model.

First, in Section 5.2, a numerical model of an oscillating airfoil is established and validated. Based on the local aerodynamic characteristics of a reference VAWT, this model, through reasonable settings of the airfoil's oscillating motion form and parameters, enables the two-dimensional oscillating airfoil to, to a certain extent, equivalently characterize the unsteady inflow conditions of the VAWT blade during rotation. This section systematically introduces the selection of the reference turbine, the numerical modeling method, and the configuration of motion and geometric parameters. Through a series of numerical validation studies, including time step, CFL number, mesh independence, computational domain size, and periodic solution convergence, the oscillating airfoil model is ensured to have sufficient numerical accuracy and stability under unsteady conditions. Simultaneously, through comparative analysis with the complete VAWT numerical model, the rationality and representativeness of this oscillating airfoil model at the aerodynamic response level are further verified.

Building upon this foundation, Section 5.3 introduces the unsteady adjoint optimization method to conduct a systematic study of airfoil geometry optimization for oscillating airfoils. This section first defines the optimization objective function for the VAWT condition, focusing on the aerodynamic output characteristics during the unsteady period. It then details the optimization process, the selection principles for design variables (DV) and constraints, and the application strategy of window controlling in unsteady adjoint solutions. Furthermore, a pilot test is conducted on a reference airfoil to verify the effectiveness of the constructed optimization framework in terms of numerical stability and design trends, laying the foundation for subsequent systematic optimization of candidate airfoils.

Section 5.4 focuses on analyzing the aerodynamic performance of different candidate airfoils under oscillating conditions. By comparing the performance changes of the airfoil before and after optimization in terms of periodic average aerodynamic forces, transient aerodynamic responses, and performance under different operating parameters, the adaptability and robustness of the optimized airfoil under oscillating conditions are evaluated. Simultaneously, considering the complex induced flow environment of the VAWT downwind blades, a downwind inflow correction is introduced to further examine the airfoil's aerodynamic performance under conditions closer to real rotor operation. Furthermore, this section systematically analyzes the impact of different tip velocity ratios and variations in inflow conditions on airfoil performance to evaluate the applicability of the optimization results across a wide operating range.

After completing the study of the oscillating airfoil level, Section 5.5 establishes and validates the complete VAWT numerical model. This section employs the same numerical methods as before to systematically model and validate the VAWT rotor model, including studies on time step, mesh independence, computational domain size, and periodic solution convergence. The reliability of the rotor-level numerical model is ensured by comparing it with existing experimental or literature data.

Section 5.6 further discusses the key prerequisites required for transitioning from the oscillating airfoil model to the VAWT rotor model, focusing on analyzing the near-field inflow velocity and induced velocity characteristics of the blades, as well as the aerodynamic interaction mechanisms between multiple blades. This section provides the physical basis for a reasonable interpretation of airfoil performance in the rotor-level model.

Subsequently, in Section 5.7, the candidate airfoils obtained from the aforementioned optimization are applied to the complete VAWT model, and their overall aerodynamic performance is systematically evaluated under both shaftless and shafted two-bladed rotor configurations. By comparing the performance of different airfoils in terms of rotor power output and aerodynamic loads, the practical effect of the oscillating airfoil optimization strategy at the rotor scale is verified.

Finally, Section 5.8 summarizes the main research content and conclusions of this chapter, outlining the advantages and limitations of the oscillating airfoil optimization method in VAWT applications, and providing references and prospects for future research.

5.2 Modeling and Validation of Oscillating Airfoils

This section establishes and validates an oscillating airfoil numerical model for characterizing the unsteady aerodynamic properties of VAWT blades. By introducing periodic oscillating motion, a two-dimensional airfoil simulates the unsteady incoming flow environment experienced by a VAWT blade during rotation under controlled conditions. During model construction, the influence of numerical modeling methods, motion parameter settings, and computational configuration on the unsteady aerodynamic response was systematically investigated. A series of numerical validation studies, including periodic solution convergence, time step and CFL number, mesh independence, and computational domain size, ensured the model's stability and reliability under unsteady conditions. Furthermore, comparative analysis with the results of the complete VAWT numerical model verifies the rationality of the oscillating airfoil model in capturing key unsteady aerodynamic characteristics, providing a reliable physical basis for subsequent airfoil optimization research.

5.2.1 Reference Turbine

To illustrate and validate the proposed oscillating airfoil modeling and optimization method, a vertical axis wind turbine (VAWT) with sufficient numerical and experimental data support is selected as a reference example. This VAWT model originates from the research of Angell et al. [78], and its numerical simulation results are based on wind tunnel experiments, thus possessing high reliability and suitable as a benchmark for CFD model validation and subsequent optimization method explanation. Using turbines with large dimensions and lower solidity helps ensure the rationality and persuasiveness of the single-blade approximation model. These blades experience less velocity loss from the incoming flow in the leeward section and are less prone to inter-blade interactions (such as the lateral crossing of the leading blade wake). Simultaneously, choosing a higher tip speed ratio (TSR) keeps the blade angle of attack and the approximate angle of attack in the Darrieus formula at a low level, essentially avoiding entry into the flow separation zone. This makes them more suitable for modeling and optimization, minimizing modeling errors while saving computational costs.

Angell et al. [29] have carried out a comprehensive set of experimental tests in the Glasgow University wind tunnel on symmetrical NACA airfoils performing Darrieus pitch motions that simulate the conditions experienced by a VAWT. The data gathered involves the lift and drag coefficients as a function of the blade angle of attack and other useful aerodynamic information. This experimental data is comprehensive and well suited as a baseline case for blade aerodynamics optimization studies in this investigation. Table 2.1 shows one of the oscillating airfoil cases tested in the wind tunnel experiments which models the performance of the Carmarthen Bay 130 kW VAWT. It is thus employed as the baseline case for both the CFD model validation and for the development of the adjoint blade optimization in this study.

The airfoil employed was a standard NACA0015 symmetric airfoil with a chord length 0.55 m which pitched about its quarter length chord point. The mean angle of attack representing the fixed pitch of the blade on the turbine is zero degree. The tip speed ratio of the turbine simulated in the experiments is 3.25. The time histories of the blade angle of attack was determined using the Darreius function and the induced factor is derived from single streamtube model [19], in order to simulate the blade motion of the turbine.

This wind speed was employed in the CFD simulations and blade optimization of the oscillating airfoil employed in this paper, and this is the same as what was employed in the experimental tests of Angell et al. [29]. The freestream wind speed V_∞ employed is 9.66 m/s and the value taken for the a was 0.224. Table 5.1 shows the detail parameters of the tested turbine.

Table 5.1 Details of the Darrieus Pitch Airfoil for VAWT-130.

Turbine Blade Profile	NACA0015
Chord length	0.55 m
Number of Blades	2
Height	18 m
Experimental Span	1.61 m
Radius	12.5 m
Motion type	Darrieus Function
Mean angle of attack	0°
Representative TSR	3.25
Representative freestream wind speed	9.66
Pitching amplitude	13.80°

5.2.2 Modelling and Analysis

As explained in the previous sections, design optimization using adjoint methods is a powerful technique that can efficiently find an optimal solution for problems with multiple geometrical design variables, such as points that form the surface of an airfoil. For a blade optimization problem, the adjoint method involves solving two sets of equations: the original equations representing the flow physics and the adjoint equations representing the sensitivity of the objective function, such as the lift of an airfoil with respect to the blade geometrical design variables. The design variables, or geometry of the blade, are then adjusted to maximize the objective function, i.e. the lift of an airfoil.

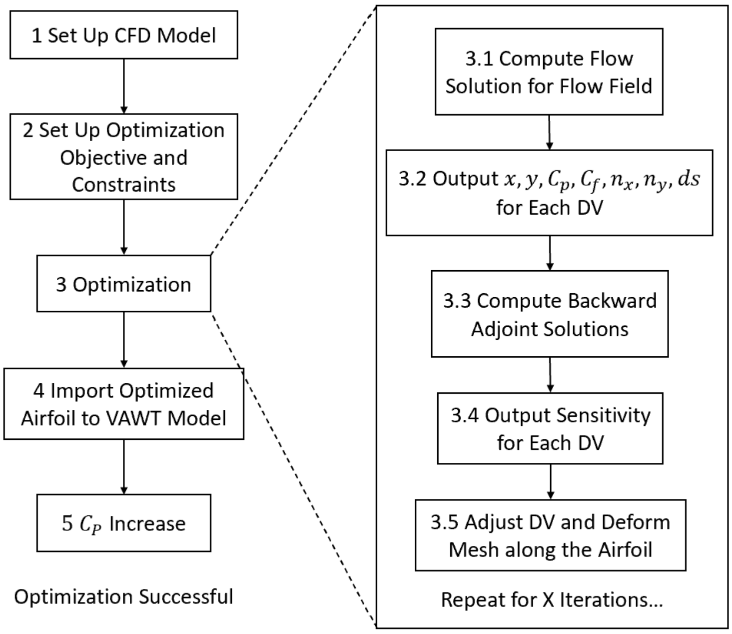

Fig. 5.1: Overview of the Transient Adjoint Optimization Procedure.

Fig. 5.1 shows the major steps taken in this investigation to perform blade aerodynamics optimization using the adjoint method when it is combined with computation fluid dynamics analysis. The optimization process aims to adjust the design variables to maximize the tangential force coefficient of the airfoil. The unsteady, incompressible Navier-Stokes equations are solved using the open-source CFD software SU2. The adjoint equations are also solved using the solver built in the SU2.

As illustrated in Fig 5.1, the optimization process starts with setting up the CFD model for the flow over the blade to be optimized and the objective function with any constraints. Then the CFD modelling of the fluid flow, backward adjoint solutions for sensitivity analysis, and modifications of the blade geometry are conducted iteratively until a converged optimal solution is found.

The main objective of a VAWT blade optimization is to find the optimum airfoil geometry that can maximize the torque of the turbine. Fig. 5.2 illustrates the components of the aerodynamic forces acting on a blade when it is travelling around the axis of the VAWT in the wind.

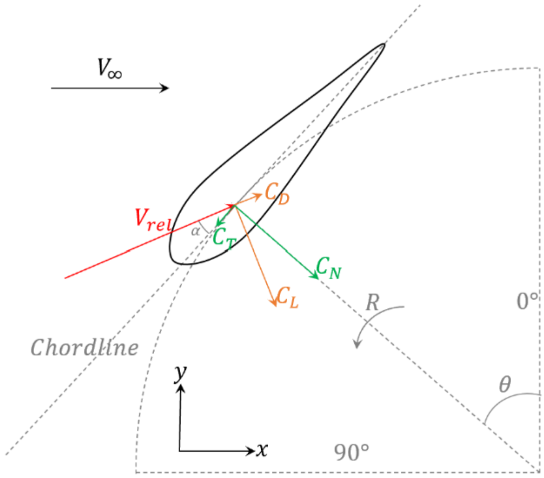

Fig.5.2: Schematic of the components of the force coefficients for a VAWT airfoil.

The significance of the torque generated can be expressed using the tangential force coefficient as follows:

$$C_T = C_L sin\alpha - C_D cos\alpha \quad \text{[Eq. 5.1]}$$

Where C_T is the tangential force coefficient, C_L is the lift coefficient, C_D is the drag coefficient, and α is the angle of attack.

A fixed induction factor a was employed to model the effect of the presence of the turbine on the freestream wind speed encountered by the turbine blade. The blade angle of attack constantly changes while the blade is travelling around and it can be expressed as follows:

$$\alpha = tan^{-1}\left(\frac{sin\theta}{\frac{\lambda}{1-a} + cos\theta}\right) \quad \text{[Eq. 5.2]}$$

where θ is the azimuthal angle, a is the induction factor, and λ is the blade tip speed ratio of the blade speed and freestream wind speed.

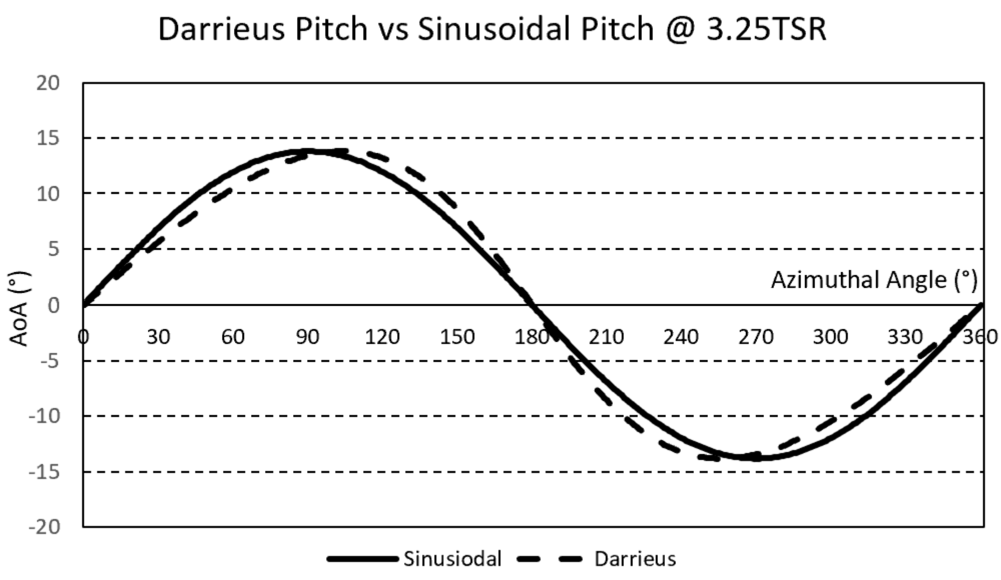

Fig. 5.3: The Angle of Attack Distribution in Darrieus Pitch Function and Sinusoidal Pitch Function at 3.25 TSR.

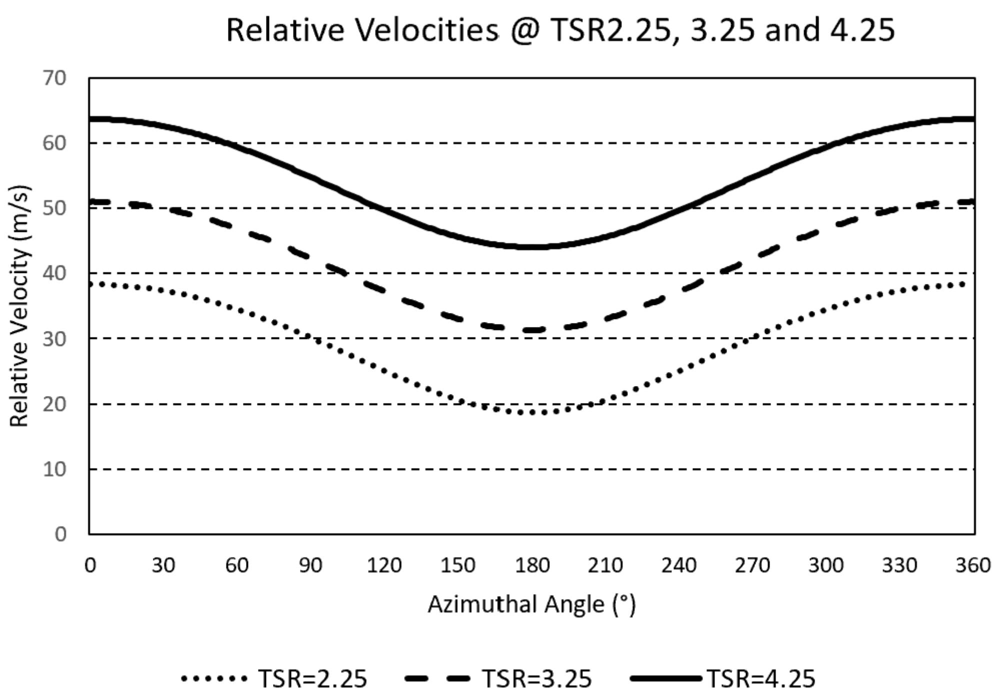

Fig. 5.4: The Reletive Wind Speed in Darrieus Pitch Function at various TSR.

Fig 5.3 and 5.4 shows the change in the angle of attack and relative wind speed as a function of the azimuthal angle at different tip speed ratios. When the blade tip speed ratio increases, the curve moves more closely to a sinusoidal profile. The positive and negative sections of the cycle represents the turbine blade located at the upwind and downwind sections of the wind turbine, respectively.

According to the single stream tube concept, the axial flow velocity, V_a across the wind turbine is estimated to be as follows:

$$V_a = V_\infty(1 - a) \qquad \text{[Eq. 5.3]}$$

where a is the induction factor which takes different values for different rotational speeds of the turbine.

The blade tip speed ratio of the VAWT is related to the freestream wind speed V_∞ as follows:

$$\lambda = \frac{R\omega}{V_\infty} \qquad \text{[Eq. 5.4]}$$

where ω is the angular velocity, R is the radius of the VAWT, and V_∞ is the freestream wind speed. On a relative coordinate system that is fixed on the turbine blade and rotates with the blade, the relative wind velocity to the blade V_{rel} is also changing and it is given as follows:

$$V_{rel} = V_a\sqrt{\left(\frac{\lambda}{1-a}\right)^2 + 2\frac{\lambda}{1-a}cos\theta + 1} \qquad \text{[Eq. 5.5]}$$

The power coefficient is defined as the ratio of the mechanical power delivered by the turbine to the total kinetic energy of the wind flow through the turbine. The magnitude is positively correlated with the torque.

$$C_P = \frac{T\omega}{\frac{1}{2}\rho V_\infty^3 S} \qquad \text{[Eq. 5.6]}$$

Where T is the total torque experienced by all blades, ω is the angular velocity, S is the VAWT sweeping area, and V_∞ is the freestream wind speed.

$$T = N\overline{F_T}R \qquad \text{[Eq. 5.7]}$$

Where N is the number of blades, $\overline{F_T}$ is the average force experienced by a blade through a rotation cycle, and R is the radius of the turbine. $\overline{F_T}$ can be calculated as follows:

$$\overline{F_T} = \frac{1}{2\pi}\int_0^{2\pi} F_T(\theta)d\theta \qquad \text{[Eq. 5.8]}$$

Where θ is the azimuthal angle of a blade and F_T is the tangential force of a blade at a specific azimuthal angle, which can be calculated as follows:

$$F_T = \frac{1}{2}C_T\rho cHV_{rel}^2 \qquad \text{[Eq. 5.9]}$$

Where c is the chord length of a blade cross-sectional airfoil and H is the height of the blade.

Although the single-blade Darrieus pitch model simplification ignores certain eddy and blade-blade interactions, it significantly reduces the calculation time and improves the stability of the adjoint solver. Moreover, research suggests that the Darrieus pitch model can have sufficient accuracy.

Therefore, if a turbine blade is oscillating up and down following the angle of attack defined by Eq 5.2 in a wind speed defined by Eq 5.3, i.e. performing the Darrieus pitch motion, then the force acting on the blade would be the same as it would be on the blade rotating with the turbine. Therefore, in order to maximize the tangential force acting on the blade performing the Darrieus pitch motion. The objective function of the optimization problem can be defined as follows:

$$C_T = C_L sin\left(tan^{-1}\left(\frac{\sin(\omega t)}{\frac{\lambda}{1-a}+\cos(\omega t)}\right)\right) - C_D cos\left(tan^{-1}\left(\frac{\sin(\omega t)}{\frac{\lambda}{1-a}+\cos(\omega t)}\right)\right) \qquad \text{[Eq. 5.10]}$$

Where ω is a constant, t is time, and $C_L(x,t)$ and $C_D(x,t)$ are functions of the design variables x which representing the geometric points that define the shape of the blade.
The sensitivity of the objective function with respect to the design variables x can be expressed as:

$$\frac{dC_T}{dx} = \left(\frac{1}{\omega}cos(\omega t_0) - \frac{1}{\omega}cos(\omega T)\right)\frac{\partial C_L}{\partial x} + \left(\frac{1}{\omega}sin(\omega t_0) - \frac{1}{\omega}sin(\omega T)\right)\frac{\partial C_D}{\partial x} \qquad [Eq. 5.11]$$

where t_0 and T can be defined as the initial time, and the final time of one cycle of oscillation respectively. To optimise the airfoil shape, the design variables x are updated using the gradient information obtained from the sensitivity analysis from the adjoint calculations. A simple update rule could be, for example:

$$x_{new} = x_{old} - \alpha \frac{dC_T}{dx} \qquad \text{[Eq. 5.12]}$$

where α is the step size taken for determining the magnitude of the step to take in the direction of the steepest descent.

There are a range of different airfoil shape parameterization methods. The Hicks–Henne bump functions was employed in this study because when compared with other airfoil parameterization methods, it is more computationally efficient. If the Hicks–Henne bump functions are used, the parameterized airfoil must have at least 12 shape parameters, or variables to achieve acceptable accuracy. In this investigation 20 shape design variables were employed to perform the parameterization and optimization of the airfoil. A range of values of the shape variables have been tested from 20-100 and it is find that increase the number of shape design variable beyond 20 has little effect on the final optimised airfoil.

Once the sensitivity gradient of the objective function with respect to the design variables x is calculated using Eq. 5.13, the shape of the airfoil can be updated using the Hicks–Henne bump function equations 2.14-2.15 as follows:

$$y = y_{basis} + \sum_{i=1}^{i=n} a_i f_i(x) \qquad \text{[Eq. 5.13]}$$

$$f_i(x) = \left[\sin\left(\pi x^{\frac{\log\frac{1}{2}}{\log t_1}}\right)\right]^{t_2}, 0 \leq x \leq 1 \qquad \text{[Eq. 5.14]}$$

Where y is the y-coordinate of each design variable along the airfoil, t_1 is the maximum thickness location of the bump, t_2 is the width of the bump and a_i is the shape parameter.

Hicks–Henne can be configured with single-sensitivity and dual-sensitivity. Single-sensitivity, i.e., the thickness mode, causes the upper and lower surfaces of the airfoil to move synchronously, changing only the thickness distribution at other nodes due to the deformation of different DVs, while keeping the camber line unchanged. Dual-sensitivity adds a camber mode, which allows the upper and lower surfaces of the airfoil to displace in the same direction, thus changing the camber and also controlling the thickness. In VAWT simulations, the flow field experienced by the upper and lower surfaces differs significantly, particularly in the windward or leeward regions where the pressure difference between the upper and lower surfaces is greatest. Even with periodically averaged values, the difference in incoming flow velocity between the windward and leeward regions leads to a significant degree of non-uniform sensitivity distribution between the upper and lower surfaces.

5.2.3 Configurations

Incompressible RANS modeling is used in this type of problem primarily because the incoming Mach number of the studied object is relatively low (e.g., 40 m/s corresponds to $M \ll 0.3$), and density variations in the flow can be neglected. The incompressibility assumption significantly reduces the nonlinearity of the governing equations, decoupling the energy equation from the density-pressure coupling in the solution system, thereby improving numerical stability and reducing computational costs. Simultaneously, this assumption is also more favorable for the convergence of unsteady moving meshes and slip-interface problems. For the turbulence model, the $k-\omega$ SST (Shear Stress Transport) model is chosen because it inherits the good predictive ability of the $k-\omega$ model for boundary layer separation in the near-wall region, while smoothly transitioning to $k-\varepsilon$ behavior in the free flow region through a mixing function, avoiding excessive sensitivity of the free flow to turbulence. This makes SST particularly suitable for unsteady phenomena such as strong adverse pressure gradients and dynamic stall that may occur during airfoil pitching motions, thus becoming the mainstream engineering choice for incompressible RANS airfoil problems.

In the incompressible RANS implementation of SU2, although the energy equation is not solved, the configuration file and some boundary condition interfaces still require the provision of temperature parameters. This is because SU2 uses a unified data structure for compressible/incompressible and laminar/turbulent flow in its software architecture, and temperature is preserved as part of the fluid state to ensure interface consistency and the integrity of the physical property model. For this problem, temperature does not participate in the momentum equation, nor does it affect the turbulent transport equation or the associated linearization process; its value exists only as a placeholder. Therefore, in incompressible airfoil examples, temperature is usually simply set to a reasonable constant (such as 300 K), which will not have any practical impact on the flow field solution, the associated equation, or the geometric sensitivity.

In terms of numerical solution, a pressure-based solver combined with a coupled pressure-velocity algorithm is used to improve the convergence efficiency of unsteady calculations. A second-order upwind scheme is used for spatial discretization, and a bounded second-order implicit scheme is used for time advancement to balance computational stability and time accuracy.

In solving the incompressible RANS + $k-\omega$ SST, the SU2 restart_flow file stores the complete original state vector required for linearization. For the 2D case, each mesh node (or control volume) contains at least 5 scalar unknowns. These are the velocity components (x and y), pressure, turbulent kinetic energy, and specific dissipation rate, respectively. This restart flow defines the linearization point of the adjoint problem: all convection, diffusion, turbulence source, and wall/damping functions, such as the blending function of SST, are frozen and differentiated in this state. Therefore, these five columns of variables in restart_flow collectively determine all the coefficients of the Jacobian matrix in the subsequent adjoint system.

The five variables in `restart_flow` are used to construct and freeze the partial derivatives of the residuals with respect to these five states. Velocity and pressure determine the convection-diffusion Jacobian of the momentum/continuity equation, while k and ω determine the turbulent transport equation and its coupling terms with the master equation. The resulting adjoint field λ is then multiplied by the residual change caused by geometric perturbation to obtain the optimized target rate of change of the surface normal.

5.2.4 Grid Independence Study

This study did not employ a square or sector-shaped computational domain, but instead chose a circular computational domain combined with an O-grid topology. The main reason for this is that for vertical axis fan flow fields with significant flow direction changes and rotational effects, square boundaries and their symmetrical boundary conditions would greatly interfere with the evolution of the incoming velocity direction. This is especially true for the approximate relative velocity of the changing-direction incoming flow, where the impact is very severe, necessitating a very large far-field and defined boundaries.

In a square computational domain, symmetrical boundary conditions implicitly assume symmetry in velocity direction and flow field structure. When strong induced velocities, recirculation zones, or periodic directional changes exist in the flow field, this assumption often no longer holds, leading to boundary reflection effects and non-physical constraints. Unless the far-field boundary is set extremely far, the airfoil and its wake may still be affected by the boundary conditions, which not only significantly increases the computational domain size but also raises computational costs.

In contrast, a circular computational domain is geometrically more compatible with rotating flows, and its boundaries have consistent normal characteristics in all orientations, effectively mitigating the boundary condition interference caused by flow direction changes. Under the same far-field radius, the influence of a circular boundary on the flow field is significantly less than that of a square boundary, thus reducing dependence on the far-field scale while maintaining computational accuracy. Furthermore, using a circular computational domain makes the construction of the O-grid topology more natural and efficient. The O-grid offers the following significant advantages:

The circular computational domain has high near-wall resolution. The O-grid can form a regular annular grid layer around the airfoil or blade surface, facilitating precise control of the initial layer height and normal grid growth rate, thereby better resolving boundary layer flows, which is particularly crucial for lift, drag, and moment calculations. Compared to structured grids that force transitions within a square domain, the O-grid exhibits higher orthogonality and lower element distortion near the airfoil, contributing to improved numerical stability and convergence. The surrounding grid topology can more smoothly capture flow characteristics, reducing numerical dissipation caused by grid distortion, and has significant advantages for predicting separated flows, wake evolution, and unsteady moments.

The grid independence check is first established on the basis that the computational domain is large enough to ensure that the flow solution around the turbine is as unaffected as possible.

When the size of the far field gradually reaches 40 times the size of the rotor, the moment coefficient of its direct output no longer changes under the same physical conditions. In addition, five meshes of different number of computational cells are used to study mesh independence to determine the effect of the mesh size on the numerical results. The total number of grids corresponding to the 5 grid systems used in this experiment are from 1k to around 20k respectively. The resulting periodical tangential coefficients of the turbine remain almost the same with increasing the computational cells from 9.8k to 19.1k. Therefore, for the results presented in this paper, the mesh with 9.8k computational cells was employed. Figure 5.5 and 5.6 shows the structure of both O-Grids and the closer view of the airfoils.

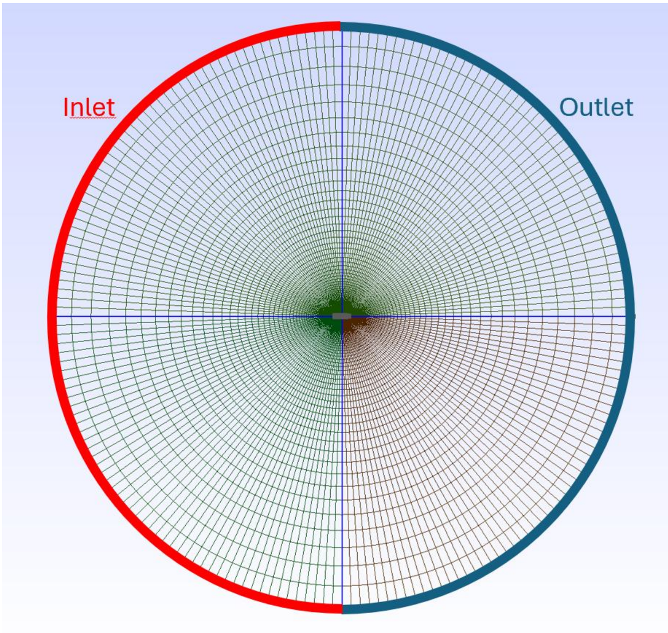

Fig 5.5: Single-Blade Model Mesh Structure (Without Rotor).

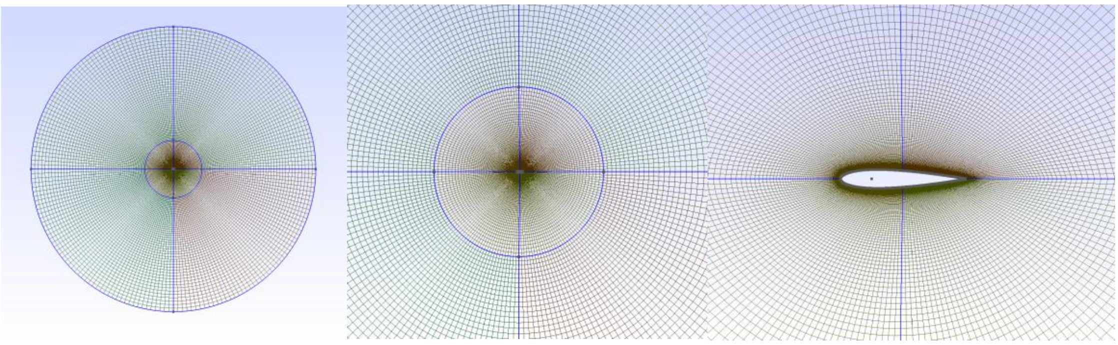

(A) (B) (C)

Fig 5.6: Single-Blade Model Mesh Structure (Without Rotor) around the (A) Farfield, (B) Rotor, and (C) Airfoil Surface.

Table 5.2: Single-Blade Model Grid Size Independence Study

Type	1	2	3	4	5
O-Grid	1.2k	**2.3k**	4.8k	9.8k	19.1k
O-Grid with Rotor	1.2k	**2.4k**	4.9k	9.9k	19.7k

5.2.5 Domain Size Study

To evaluate the impact of far-field computational domain size on the numerical simulation results of oscillating airfoils and to eliminate non-physical interferences from boundary conditions on flow field development, this paper further investigates the independence of computational domain size. By comparing aerodynamic performance prediction results under different external computational domain scales, the adequacy of the selected computational domain in capturing unsteady aerodynamic characteristics is verified.

In each computational domain setting, the mesh refinement strategy for the near-wall region and local areas of the airfoil remains consistent to ensure that domain size variation is the only influencing factor. It is worth mentioning that the solver using the square model has difficulty achieving convergence, and the time-averaged tangential coefficients derived after 3 cycles fail to achieve periodic convergence. In contrast, the circular model was tested with far-field diameters ranging from 20 to 80 times the chord length. The results show that the incoming flow field can achieve stable velocity fluctuations with a far-field diameter of 40 times the chord length.

5.2.6 Timestep and CFL Number

After verifying mesh independence and determining the final mesh configuration, the impact of time step and Courant–Friedrichs–Lewy (CFL) number on the numerical simulation results of oscillating airfoils was further investigated. This study aimed to evaluate the sensitivity of time discretization settings to unsteady aerodynamic performance prediction and to achieve a reasonable balance between numerical accuracy and computational efficiency.

While maintaining the spatial discretization settings and computational domain size, different time step configurations were selected, corresponding to different unit displacements and CFL number levels. By comparing the power coefficient C_P calculated under different time step conditions, the impact of time step selection on the unsteady aerodynamic response prediction results was quantitatively evaluated. The relevant time steps, unit linear displacements, and corresponding C_P results are summarized in the table.

Based on the aforementioned comparative analysis, and balancing computational accuracy and cost, this study systematically evaluates the unsteady numerical simulation results under different time step settings. The results show that when the time step value is within the range of 0.001–0.01, the main aerodynamic responses (including lift, torque, and their phase characteristics) of the oscillating airfoil and vertical axis wind turbine (VAWT) models can achieve good convergence, and the calculation results meet the research requirements in terms of numerical stability and temporal accuracy.

It should be noted that for large vertical axis wind turbine models, due to their large characteristic scale, the corresponding angular displacement per unit time is small. To ensure the continuity of azimuth angle changes and the temporal resolution of the aerodynamic response during rotor rotation, a smaller time step is usually required to avoid phase errors or numerical oscillations introduced by excessively coarse time discretization. However, in the single-airfoil pitch motion problem involved in this study, there is no strict requirement for unit angular displacement limited by the overall rotor scale. This type of problem focuses on the range of angle-of-attack variation covered by the airfoil within one oscillation cycle and its corresponding unsteady aerodynamic characteristics. As long as the time step can reasonably analyze the angle-of-attack variation process, the physical reliability of the results can be guaranteed.

Considering the above factors, a time step of 0.001 was selected in the initial stage of the numerical simulation to ensure sufficient capture of unsteady flow details and transient aerodynamic changes. Further comparative results show that appropriately widening the time step to 0.01 does not significantly affect the main aerodynamic characteristics, thus providing a feasible range for time step selection for subsequent parametric studies under computational cost constraints.

5.2.7 Periodic Solution Convergence Study

Without specifying a restart file (RESTART_SOL = NO), SU2 typically initializes with a uniform free-flow, meaning the flow field variables across the entire computational domain are initialized to a free-flow state consistent with the incoming boundary conditions. However, for problems with periodic motion (such as airfoil pitch, flapping, or rotation), this initial condition is difficult to represent the true periodic steady-state flow field.

For unsteady problems, SU2 more often uses the steady-state solution or the solution from the previous cycle as the initial condition, with the following format:

```
RESTART_SOL = YES
SOLUTION_FILENAME = solution.dat
```

This approach can significantly shorten the initial transition phase and reduce non-physical transient responses in the first cycle. Due to the difference between the initial condition and the true periodic steady-state flow field, unsteady calculations typically experience a periodic change in lift, drag, and their corresponding tangential forces in the first few cycles. With inlet velocity reversal, convergence requires more than three cycles, while for oscillating airfoils, this configuration typically requires only half a cycle.

5.2.8 Model Validation

When using incoming wind speed profiles together with the operating conditions shown in Table 2.1, and the AoA defined by Eq. 2.2, the CFD predicted lift coefficient and drag coefficient as a function of the equivalent azimuthal position of the turbine blade when it is travelling around the axis of the turbine is shown in Fig. 2.2. The experimental data [29] are also shown in the Figure for comparison. Bearing in mind that θ = 0 is the location when the blade is located at the top of a blade rotation cycle. The azimuthal angle at 0-180° represent the upwind side of a blade rotation cycle when the AoAs are positive, and 180-360° represents the downwind side of a blade rotation cycle when the AoAs are negative.

It should be noted that the CFD predicted and the experimental measured lift and drag coefficients show approximately an antisymmetric and symmetric profile, respectively. The upstream and downstream sections of a blade rotation cycle have the same absolute value of AoA, and the force coefficients. These are exactly as expected when the single stream tube model condition is employed. The predictions of the lift and drag coefficient are largely matched with the experimental data although some minor discrepancies can be observed. It is noted that the peak values of both force coefficients are slightly different for the upstream and downstream sections. This indicates some inaccuracy in the experimental data.

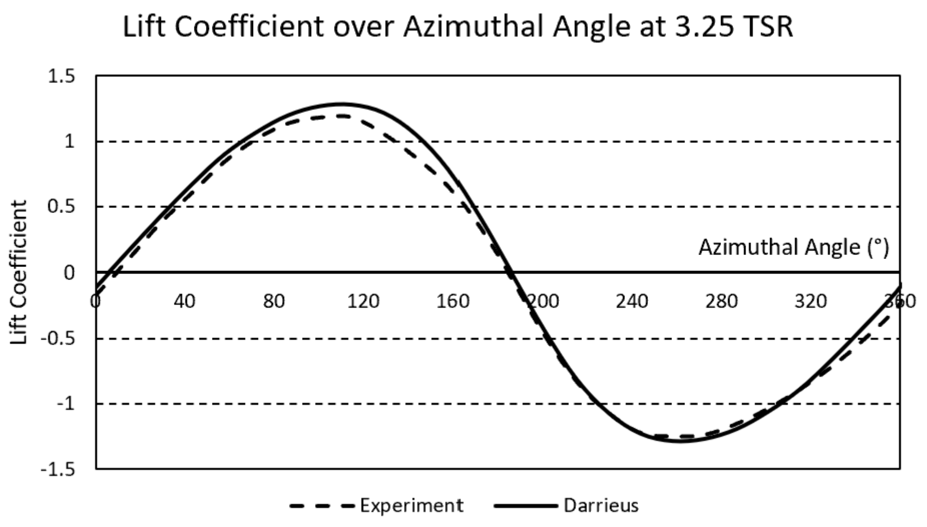

(A)

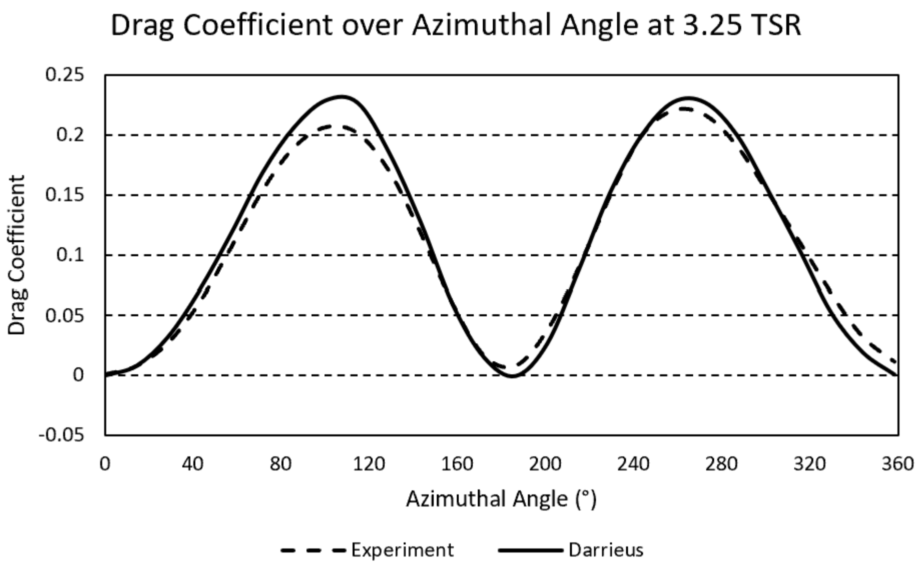

(B)

Fig. 5.7: Lift (A) and drag (B) coefficient as a function of the azimuthal angle (rad) at 3.25 TSR (360 deg).

Fig. 5.7 shows the measured angle of attack as a function of the azimuthal angle during the test of the oscillating airfoil and it is compared with the theoretical angle of attack using the single streamtube model. A lower angle of attack at the azimuthal angles around 100° employed in the experiments could lead to a reduction in both the lift and the drag acting on the airfoil. This explanation matches with what is observed compared with the CFD predicted lift and drag coefficients. Therefore it is concluded that the CFD model developed can accurately predict the aerodynamic force acting on the airfoil when it is performing a Darrieus oscillation.

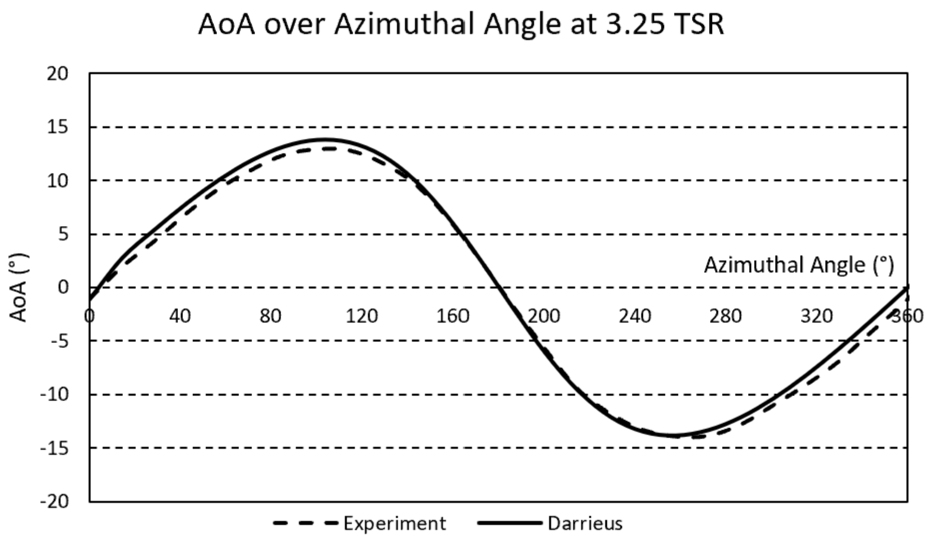

Fig. 5.8: AoA (degree) as a function of the Azimuthal Angle (rad) at 3.25 TSR.

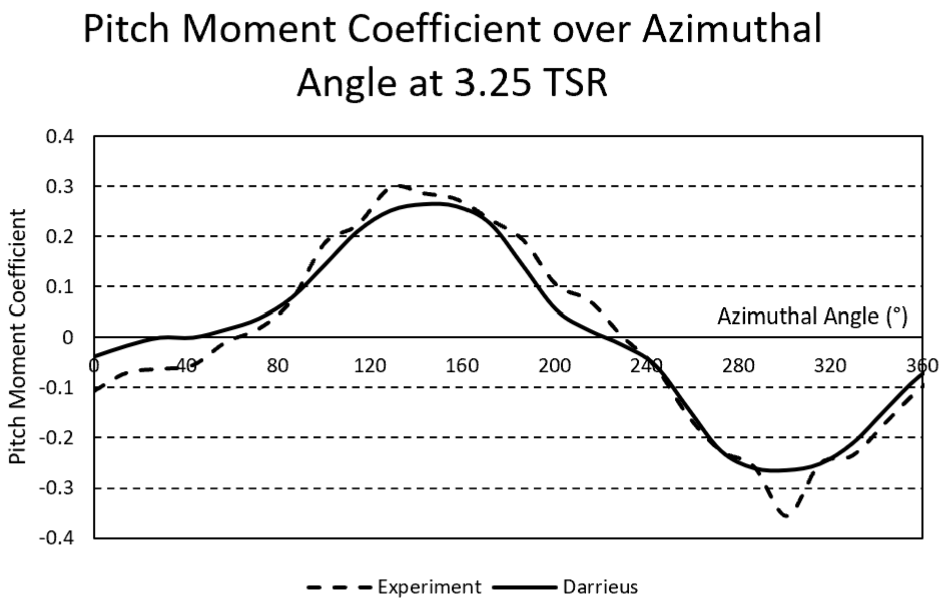

Fig. 5.9: Pitch Moment Coefficient over Azimuthal Angle at 3.25 TSR.

5.2.9 Comparative Study with VAWT Model

To further evaluate the rationality of the single-blade oscillation model in characterizing the unsteady aerodynamic characteristics of VAWT, this paper compares and analyzes the numerical results of the single-blade model with those of the full VAWT numerical model and the results reported by Day et al. [18] This comparison aims to examine the ability of the single-blade model to capture key aerodynamic trends at different modeling levels and to provide a basis for subsequent airfoil optimization research based on the single-blade model.

The comparison results will be shown in Section 5.6 in conjunction with the aerodynamic performance of oscillating airfoils. The comparisons in this section are primarily used to verify the applicability of the single-blade model at the methodological level, rather than to quantitatively evaluate specific performance differences.

5.3 Unsteady Adjoint Optimization

This study employs the Adjoint solver in SU2 to achieve aerodynamic optimization of an oscillating airfoil. It should be noted that while existing literature provides systematic guidance on the practical configuration methods and application procedures of the SU2 module for strongly unsteady problems (oscillating aircraft wings), it has not yet been applied to VAWT. Therefore, the Adjoint module settings and optimization procedures for VAWT adopted in this paper require extensive preliminary numerical experiments and parameter testing to determine.

5.3.1 Objective Functions

This study aims to directly improve the aerodynamic performance of the VAWT under real-world operating conditions. Unlike traditional airfoil optimization that targets steady lift coefficient or lift-to-drag ratio, this paper defines the objective function as the tangential force contribution directly related to rotor power output, thus ensuring the optimization results have clear physical meaning.

During the algorithm development phase, two optimization objectives were used: a tangential force coefficient based on time-transformed lift and drag coefficients, and a custom force function. The optimization effects were compared and analyzed. The differences in mathematical form and physical meaning of the relevant objective functions are discussed in detail in Chapter 4. The above comparative study verifies the rationality of the selected objective function in describing the unsteady aerodynamic performance of the

VAWT and ensures that the established optimization problem is mathematically self-consistent and feasible.

It should be noted that the objective change defined in this paper corresponds to the performance improvement in the time-averaged sense of the rotor. However, different airfoils may exhibit higher local performance under specific instantaneous flow field conditions. Therefore, in subsequent studies, the sensitivity information under different flow stages was repeatedly calculated by adjusting the time window length in order to enhance the applicability of the optimization results under multiple operating conditions.

5.3.2 Optimization Procedure and Setup

This study employs the unsteady adjoint solver in SU2 to achieve aerodynamic optimization of oscillating airfoils. The adjoint solution itself does not directly provide the optimized airfoil geometry, but rather generates sensitivity distribution information regarding the objective function. This sensitivity data needs to be applied to the airfoil surface through a subsequent mesh deformation process to achieve geometric updates.

The mesh deformation region is set as a rotor region surrounding the airfoil wall and its surrounding local mesh, excluding the stator in the computational domain. The size of this region was determined through preliminary testing in section 5.2.4. This setting ensures that airfoil geometric changes are smoothly absorbed by the surrounding mesh while avoiding impact on other regions in the computational domain.

Once all sensitivity information and constrained sensitivity information are obtained, mesh deformation is performed under a unified reference attitude to generate a new airfoil geometry. The transient calculation is then restarted, and numerical simulations are performed again on the new geometry for at least three rotational cycles. The aerodynamic performance of the updated airfoil is evaluated using the results of the last cycle. This process is repeated several times iteratively to gradually form a series of candidate airfoils, whose actual performance needs to be further verified using a complete VAWT model.

5.3.3 Design Variables and Constraints

This study does not employ traditional geometric parameterization methods. Sensitivity information is calculated at the node level, and mesh deformation is also implemented at the node level through design variables (DVs). Design variables can be set in both the X and Y directions, with a total of 20 variables, which are uniformly distributed within the deformation region in this paper. Chord length and thickness constraints can be directly input in the configuration file, with a default scaling factor of 0.001.

5.3.4 Window Controlling

Considering that different airfoils may exhibit different performance advantages in the upwind and downwind flow fields, this paper further repeats the sensitivity calculation process by changing the window length and position. Specifically, window settings including only the upwind section, only the downwind section, and both the upwind and downwind sections are used to evaluate the impact of different flow stages on the optimization results. Through the above window control strategy, the optimizer can extract more representative sensitivity information for different flow characteristics, thereby improving the overall performance of the optimized airfoil under multiple operating conditions.

5.3.5 Optimization Workflow

Based on the aforementioned unsteady adjoint modeling method and parameter settings, this paper constructs an aerodynamic optimization process suitable for oscillating airfoils, the overall idea of which is as follows:

Stage 1: Create a single-blade CFD mesh model and configuration file.

Stage 2: After the baseline single-blade model completes three rotational cycles, plot the tangential force coefficient of the baseline airfoil as a function of time and angle of attack (AoA).

Stage 3: Using the last cycle as a window, calculate sensitivity through discretization. If additional constraints exist, apply constraint penalties.

Stage 4: Perform corresponding airfoil deformation based on the scaling factor.

Stage 5: Re-output the configuration file and continue calculations. After the new blade completes three rotational cycles, plot the tangential force coefficient of the baseline airfoil as a function of time and angle of attack (AoA).

Stage 6: Repeat stages 3-5, iterating sequentially. Manual or automatic operation can be used until the airfoil approaches the optimized shape.

Stage 7: This stage repeats simulation operation 1, requiring changes to the window settings, specifically using both upwind and downwind modes.

Stage 8: This stage repeats simulation operation 2, changing the TSR (Transient Stream Ratio), i.e., the pitch-equivalent AoA profile.

Stage 9: This stage repeats simulation operation 3, changing the free-flow wind speed value, i.e., the pitch-equivalent relative wind speed function.

Stage 10: This stage repeats simulation operation 4, changing the leeward correction wind speed, and then the pitch-equivalent relative wind speed function.

During algorithm development, we conducted numerous tests to ensure that the optimized blade shape correctly achieved the expected goals. Initially, we used direct CL, CD, and time-transformed CT, and also defined a force function to observe the changes in the optimized blade performance under each objective. The theoretical differences between these two objectives are explained in Chapter 4, thus ensuring the feasibility of the established mathematical problem.

5.4 Aerodynamic Performance on Oscillating Airfoils

After establishing and validating the unsteady adjoint optimization method, this section systematically evaluates the aerodynamic performance of the obtained candidate airfoils under oscillating airfoil conditions. By comparing and analyzing the geometric evolution characteristics of the airfoils and their corresponding tangential force coefficient changes under different optimization settings, the focus is on examining the improvement effect of the optimization process on unsteady aerodynamic performance and its sensitivity to different operating condition assumptions.

After establishing and validating the unsteady adjoint optimization method, this section systematically evaluates the aerodynamic performance of the obtained candidate airfoils under oscillating airfoil conditions. By comparing and analyzing the geometric evolution characteristics of the airfoils and their corresponding tangential force coefficient changes under different optimization settings, the focus is on examining the improvement effect of the optimization process on unsteady aerodynamic performance and its sensitivity to different operating condition assumptions.

5.4.1 Candidate Airfoil Performance on Oscillating Airfoils

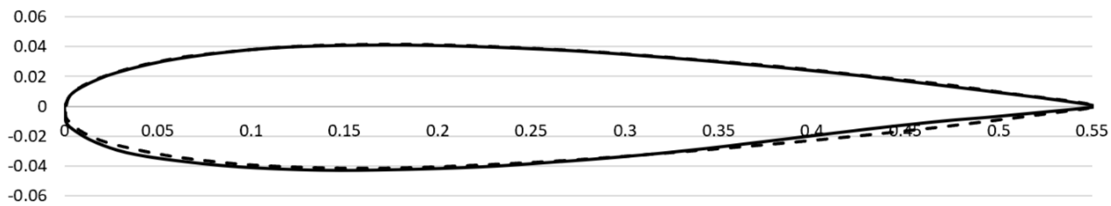

Fig. 5.10: Profiles Comparison between 1st Generated Optimized Airfoil and NACA0015 Airfoil.

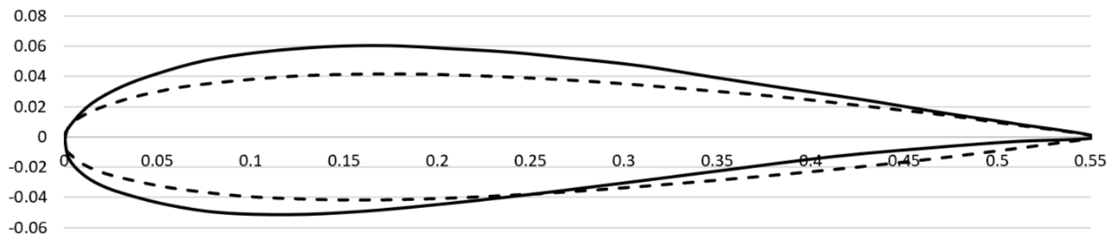

Fig. 5.11: Profiles Comparison between the Final Optimized Airfoil and NACA0015 Airfoil.

Figures 5.10 and 5.11 show the airfoil geometry obtained in the first and final iterations, respectively, under the condition of a complete oscillation cycle as the optimization window. It can be observed that as the optimization iteration progresses, the airfoil gradually forms asymmetrical local geometric adjustments in the leading edge and suction surface regions, reflecting the optimizer's response to local aerodynamic characteristics under unsteady inflow conditions. This geometric change is not a simple overall thickness or chordal scaling, but rather exhibits local deformation characteristics closely related to the oscillating motion stage.

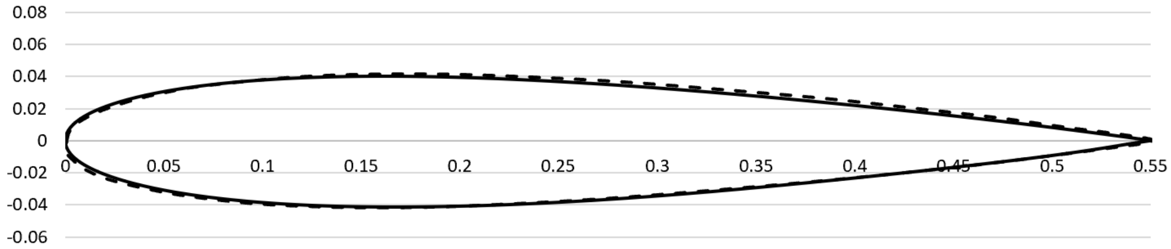

Fig. 5.12: Profiles Comparison between 1st Generated Upwind Optimized Airfoil and NACA0015 Airfoil.

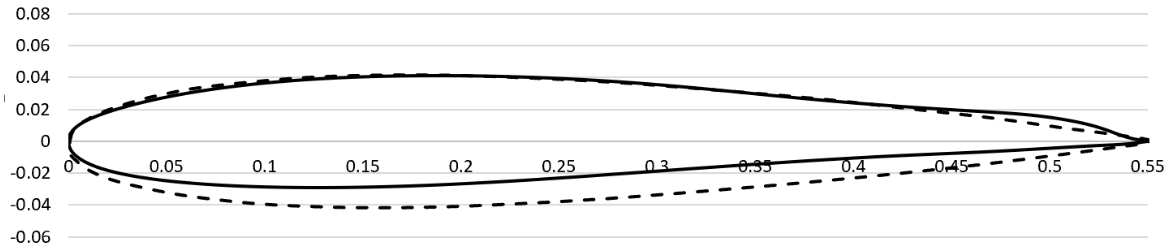

Fig. 5.13: Profiles Comparison between the Final Upwind Optimized Airfoil and NACA0015 Airfoil.

To further examine the impact of window selection on the optimization results, Fig. 5.12 and Fig. 5.13 show a comparison of the airfoil performance in the initial and final iterations when only the upwind section (0-180°) is used as the optimization window. Compared to full-cycle optimization, the geometric changes of the airfoil under this setting are more concentrated in the region dominated by the upwind condition, particularly in the adjustment of the leading edge curvature and the local distribution of the suction surface. This indicates that window control can significantly affect the accumulation mode of the accompanying sensitivity, thereby guiding the airfoil towards its optimal performance in a specific flow stage.

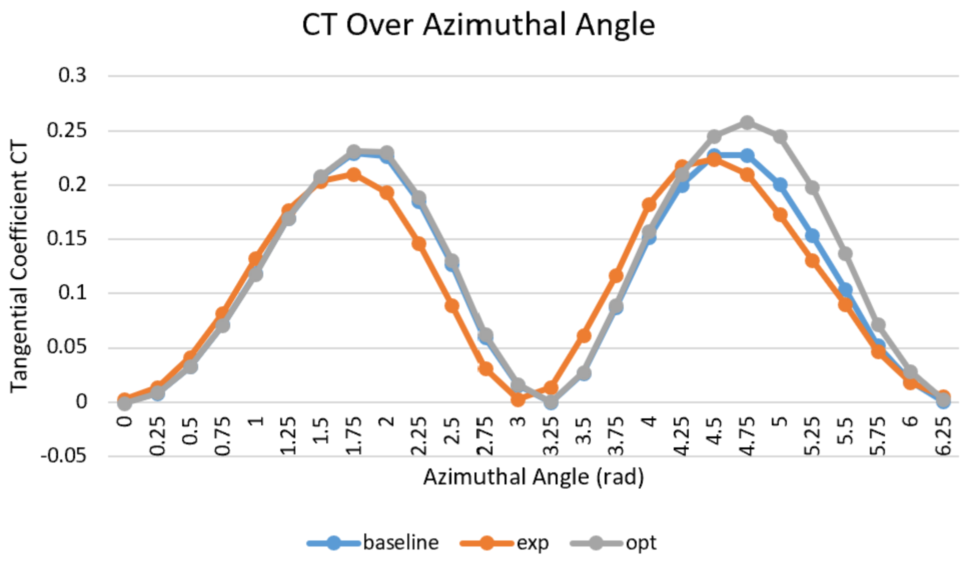

Fig. 5.14: Comparison of the Tangential Force Coefficient (CT) Versus Time.

Fig. 5.14 shows a comparison of the tangential force coefficient (C_T) versus time (or equivalent angle of attack) for different candidate airfoils under oscillating conditions. It can be seen that compared to the baseline airfoil, the optimized airfoil exhibits a higher C_T level throughout most oscillation cycles, especially in the upwind section and during periods of drastic angle of attack changes, where the performance improvement is more significant. This demonstrates that the unsteady accompanying optimization method effectively captures the aerodynamic characteristics that contribute most to rotor power during oscillation.

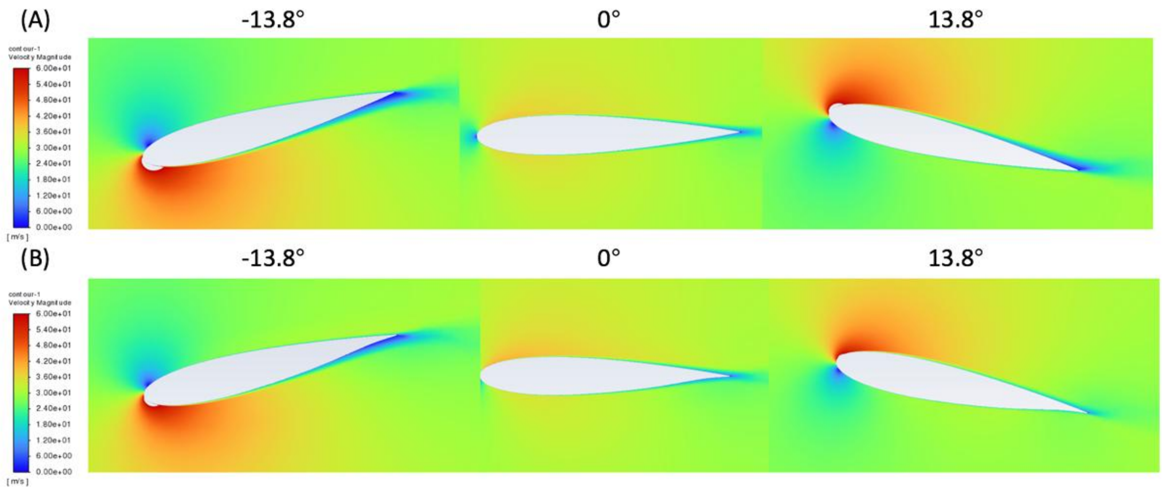

Fig. 5.15: Pitch-down Flow Physics around (A) NACA0015 Airfoils, (B) Optimized Airfoils.

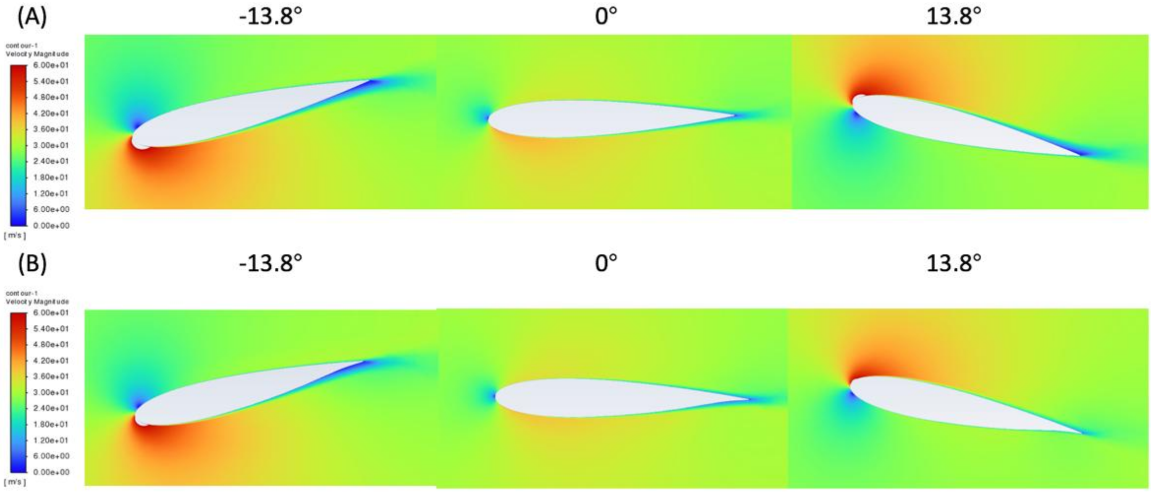

Fig. 5.16: Pitch-up Flow Physics around (A) NACA0015 Airfoils, (B) Optimized Airfoils.

Furthermore, to gain a deeper understanding of the aerodynamic behavior of the optimized airfoil in different oscillation stages, Fig. 5.15 and Fig. 5.16 show a comparison of the aerodynamic response of the airfoil during pitch-up and pitch-down processes, respectively. The results show that the optimized airfoil effectively delays flow separation during the pitch-up stage, while exhibiting a smoother aerodynamic force decay trend during the pitch-down stage. This performance improvement during the bidirectional oscillation process indicates that the optimized airfoil not only improves peak aerodynamic performance but also improves the overall characteristics of unsteady load variations.

In summary, the results in this section demonstrate that unsteady adjoint optimization based on the oscillating airfoil model can significantly improve the tangential force contribution of the airfoil throughout the entire oscillation period, and the selection of the optimization window has a significant impact on the final airfoil geometry and performance distribution. This lays the foundation for subsequent introduction of leeward inflow correction and multi-condition analysis.

5.5 Modeling and Validation of VAWT Model

After completing the modeling, verification, and optimization methods for the oscillating airfoil and single-blade models, this section further establishes and verifies a complete VAWT numerical model to evaluate the aerodynamic performance of the optimized airfoil under a real rotor configuration. This VAWT model is a two-dimensional cross-section, two-blade, shaft-equipped configuration. Its computational scale, flow complexity, and numerical cost are significantly higher than the single-blade oscillating model; therefore, it is necessary to independently verify its numerical settings and reliability.

Similar to Section 5.2, this section systematically evaluates the numerical reliability of the VAWT model, starting with the modeling method, selection of numerical parameters, and several numerical sensitivity studies. Unless otherwise specified, the numerical methods and verification approach are consistent with Section 5.2. Figure 22 shows the variables used in the VAWT model.

The experimentation of the oscillating airfoil by Angell et al. [78] and the blade optimization performed in the previous section are based on the Carmarthen Bay 130 kW VAWT when it is operating at a tip speed ratio of 3.25 in the freestream wind speed of 9.66 m/s. In order to verify the improvements in the VAWT when the original NACA0015 is replaced with the optimised airfoil derived from the adjoint optimization described in the previous section, the performance of the VAWT was simulated using the ANSYS Fluent software. The turbine was originally fixed with two straight NACA0015 blades. The diameter of the wind turbine is 25 m. The blade chord length is 0.55m with no fixed pitching. Since there is no experimental data for the turbine that is available in the public domain, only numerical simulation results of the turbine fitted with the optimised airfoil are compared with those of the original NACA0015. The CFD simulations are performed in 2D and a schematic of the turbine blade layout is shown in Fig. 5.17.

Fig. 5.17 shows the schematic of the computational domain computational domain. It employed a rectangular domain. The wind is coming from the left and flows down to the right, where a velocity inlet condition and a pressure condition is employed at these boundaries, respectively. The top and bottom boundaries are non-friction walls. The turbine is located at 37.5m downstream of the inlet boundary. The mesh around the airfoil is locally refined with a 40-layer near wall boundary cells which are orthogonal to the wall, characterized by a growth factor of 1.25, in order to resolve the velocity gradients in the immediate vicinity of the wall. The y+ values are kept around or below 1. During the optimization, the mesh around the airfoil is automatically adjusted within this locally refined mesh region. The local refinement region in the rotor consists of 180,000 triangular meshes, and 370,000 triangular meshes are defined far from the local refined area, and this acts as the far field.

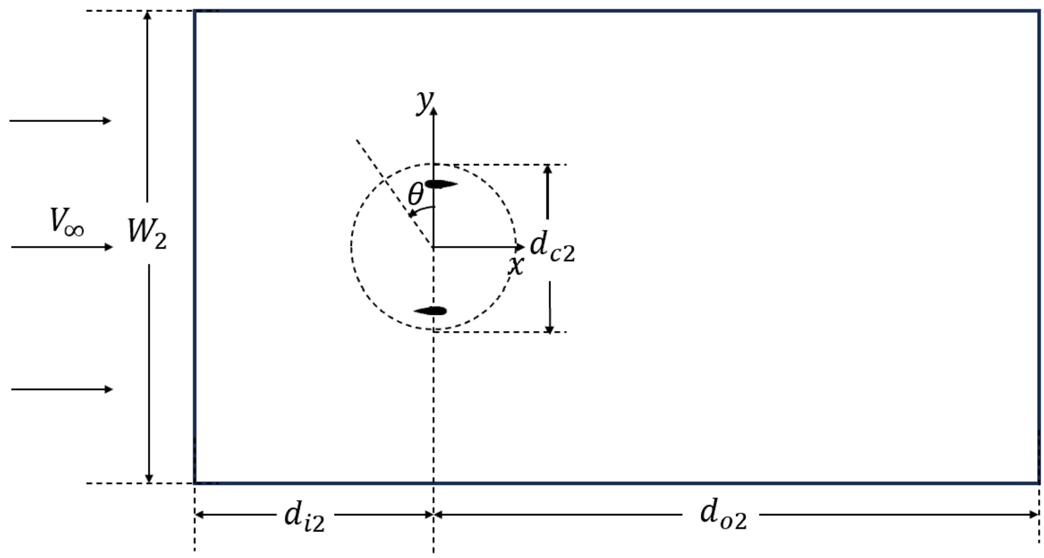

Fig. 5.17: Schematic of the computational domain: d_{i1}, distance from the inlet to the VAWT interface center; d_{o1}, distance from the VAWT interface center to the outlet; d_{c1}, diameter of the interface; W_1, width of the computational domain.

The original airfoil is modelled parametrically by using the Gmsh software which facilitates access to the SU2 software. This makes the update of the blade shape and the computational mesh easier. The morphing of the blade is achieved by displacing the nodes on the surface of the airfoil in the direction normal to the chord. The chord length of the airfoil is fixed to ensure that when it is applied to the VAWT, the solidity of the turbine remains unchanged. This is the only geometric constraint that is imposed for the airfoil shape optimization.

Before the optimizer participates in the calculation, CFD-based transient flow solutions, also known as the direct solution, are obtained. Then the optimizer obtains the sensitivity of each deformation node of the airfoil according to the flow solutions. This is used to determine the degree to which the change in each of the nodes is required to find an optimum airfoil shape.

Then the transient flow solutions over the modified airfoil are obtained and the optimization process continues until an optimum airfoil shape is identified. In a previous study [62], the optimizer found the optimal lift-to-drag ratio solution for NACA64A010 through 12 iterations under transient conditions.

The VAWT numerical model uses a two-dimensional unsteady CFD method to simulate the aerodynamic behavior of the two-blade rotor in the cross-sectional plane. The model explicitly includes the rotor shaft structure, and compared to the single-blade model, there are more significant wake development, blade-blade interactions, and shaft-induced effects in the flow field. Figure 5.18 shows the mesh used in the VAWT model and the visualization of local refinement. Table 5.3 shows the density values used in the mesh-independent analysis and the local refinement strategy.

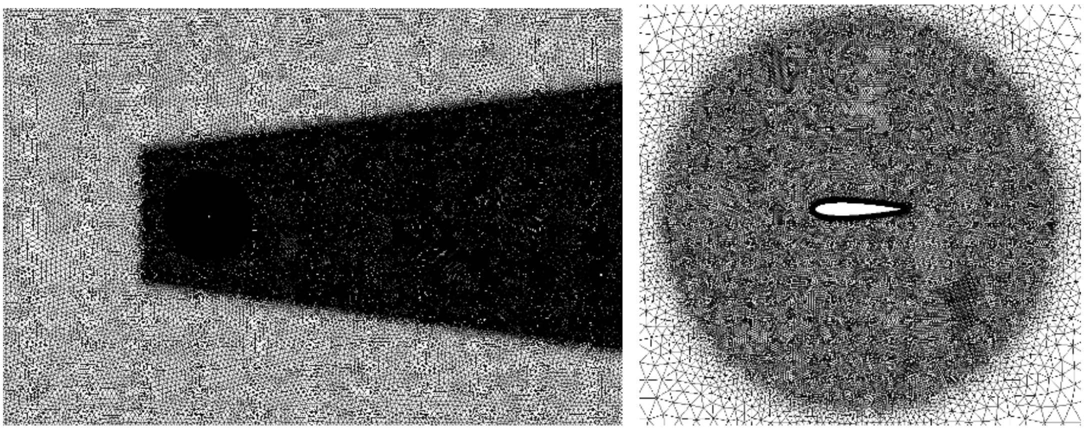

(A) (B)

Fig. 5.18: 2-Blade VAWT (A) Model Mesh Structure, (B) Model Mesh Structure around the Airfoil.

Table 5.3: Summary of the Mesh Independence Study

Model	Grid	Local Refinement	Grid Type	Size (mm)	Distance To Boundary
2-Blade VAWT	0.4M	With local refinement	Triangular	1	10X
	0.7M		Triangular	1.3	10X
	1.15M		Triangular	1.7	10X
	1.93M		Triangular	2.2	10X

To assess the sensitivity of numerical results to grid resolution and ensure the reliability of subsequent numerical simulations of oscillating airfoils and VAWT, this paper conducts a systematic study on grid independence. By progressively refining the airfoil's near-wall region and the overall computational domain grid, aerodynamic performance predictions under different grid densities are compared and analyzed to verify the rationality of the selected grid configuration between accuracy and computational cost.

The locally refined region in the rotor consists of quadrilateral grids around 200 nodes of the airfoil, with increases and decreases proportionally to the total number of grids. The optimized airfoil grid is automatically adjusted within this locally refined region. Larger quadrilateral grids are defined further away from the locally refined region as the far field. The node data around the airfoil uses a node distribution number converted according to the same distribution ratio, which can be added or subtracted, as shown in Appendix E.

The grid independence check is first established on the basis that the computational domain is large enough to ensure that the flow solution around the turbine is as unaffected as possible. When the size of the far field gradually reaches 10 times the size of the rotor, the moment coefficient of its direct output no longer changes under the same physical conditions. In addition, five meshes of different number of computational cells are used to study mesh independence to determine the effect of the mesh size on the numerical results. The total number of grids corresponding to the 5 grid systems used in this experiment are 24k, 40k, 68k, 114k and 193k, respectively. The resulting moment coefficient of the turbine remain almost the same with increasing the computational cells from 114k to 193k. Therefore, for the results presented in this paper, the mesh with 193k computational cells was employed.

Since the complete VAWT model needs to simultaneously resolve multi-blade interactions and the complex downwind inflow environment, its computational domain size and mesh scale are significantly larger than those of the single-blade model. Except for differences in geometric configuration, the governing equations, turbulence model, and time-progression method remain consistent with the single-blade model described in Section 5.2 to ensure comparability of results across different model levels.

The CFD computational configuration of the VAWT model is generally consistent with the settings of the single-blade model in Section 5.2.3, including solver type, discretization scheme, and boundary conditions. The main differences lie in the computational domain scale, rotating subdomain settings, and mesh density distribution, to accommodate the geometric complexity of the complete rotor model.

Due to the significantly increased rotor diameter and wake development range, the VAWT model employs a larger computational domain size and local mesh refinement near the blades, around the shaft, and in the wake region. The corresponding mesh count and configuration parameters are summarized in the table, maintaining consistency in structure and presentation with the verification table used in Section 5.2.

Similar to the single-blade oscillation model, the full VAWT numerical simulation is also a typical unsteady periodic problem. Therefore, the periodic convergence was verified before extracting aerodynamic performance indicators.

Comparative analysis of the rotor aerodynamic performance over several consecutive rotational cycles revealed that after several initial rotational cycles, the flow field gradually escapes the influence of initial conditions and tends towards a stable periodic state. The results show that from the third rotational cycle onwards, the changes in key aerodynamic performance indicators between adjacent cycles are within acceptable limits. Based on this result, subsequent analyses uniformly use the results after periodic convergence for evaluation, consistent with the processing method in Section 5.2.

After determining the final grid configuration of the VAWT model, the influence of the time step and CFL number on the numerical results was evaluated. This research method is consistent with the time step study of the single-blade model in Section 5.2.6, only adjusting the time step size and corresponding CFL number level appropriately according to the rotor scale.

The results show that within the selected time step range, the rotor aerodynamic performance prediction results are insensitive to the time discretization setting. The final selected time step balances stability and time accuracy of the unsteady solution with computational efficiency.

A mesh independence study was conducted on the full VAWT model to evaluate the impact of mesh resolution on rotor aerodynamic performance predictions. Compared to the single-blade model, the VAWT model requires higher mesh resolution near the blades, in the shaft region, and along the wake development direction.

Comparative analysis of rotor aerodynamic performance under different mesh densities revealed that key performance indicators tend to stabilize after a certain mesh count. Based on this result, a mesh configuration that achieves a reasonable balance between accuracy and computational cost was selected for all subsequent VAWT numerical simulations.

Considering the longer wake development region of the full VAWT model, the computational domain size was independently validated. By changing the size of the external computational domain and comparing the rotor aerodynamic performance results, the impact of boundary positions on flow field predictions was evaluated.

The results show that within the selected computational domain size range, further increasing the computational domain size has a negligible impact on aerodynamic performance predictions. Therefore, this paper adopts a computational domain size configuration that strikes a balance between accuracy and computational efficiency.

To verify the reliability of the complete VAWT numerical model, the numerical simulation results presented in this research were compared with experimental or numerical results in existing literature. The comparison results show that the established VAWT model maintains good consistency with the reference data in terms of overall performance level and variation trend.

These verification results demonstrate that the two-dimensional double-bladed VAWT model with a shaft can reasonably reflect the main aerodynamic characteristics of the rotor under unsteady operating conditions and can serve as a reliable tool for subsequent airfoil performance evaluation and comparative studies.

Similar to the simulation of the oscillating airfoils, the *k-ω* SST turbulence model was employed in this study. The sliding mesh method was employed to enable the rotation of the turbine. A freestream wind velocity of 9.66 m/s was specified at the inlet boundary in the left and a zero pressure condition was employed on the downstream boundary. The rotational speed of 2.54 rad/s is specified to keep the blade tip speed ratio to 3.25. All the simulation results were collected after 20 simulated turbine rotational cycles when the turbine torque profile stabilized and repeated itself from cycle to cycle in order to ensure that the impact of the initial conditions were eliminated.

In summary, all simulations presented in this chapter were performed using SU2 version 7.3.1 by solving the unsteady Reynolds-averaged Navier–Stokes (URANS) equations coupled with the SST k-ω model. All settings are shown in Table 5.4, which were selected based on the mesh and time-step independence studies presented in Chapter 5/6/7 and were applied consistently throughout the optimisation and validation cases.

Table 5.4: Summary of the General CFD Setup

Parameter	Value
Solver	SU2 7.3.1
Governing equations	URANS
Turbulence model	SST k-ω
Convective flux scheme	JST
Spatial discretization	Second-order MUSCL reconstruction
Temporal discretization	Second-order dual-time stepping
Time step size	0.01s

Physical CFL	1-2
Pseudo iterations per step	2-5
Mesh type	200/400/800
Wall treatment	Structured / O-Grid
Maximum y+	<1
Boundary conditions	Velocity inlet / Pressure outlet
Convergence criterion	Residual $<10^{-6}$

5.6 Prerequisites for Incoming Flow Velocity Correction

In the aforementioned study, the oscillating airfoil model was used to characterize the local aerodynamic behavior of VAWT blades under unsteady conditions and served as an intermediate-level model for airfoil optimization. However, before mapping the aerodynamic performance and optimization results of the oscillating airfoil to the full VAWT model, it is necessary to further examine the fundamental differences in incoming flow conditions between the two. Especially in real rotor conditions, the local incoming flow velocity experienced by the blade is not equivalent to the free incoming flow velocity, but is significantly affected by both induced velocity effects and multi-blade interactions.

In VAWT, during blade motion, the local incoming flow is jointly determined by the free incoming flow velocity, rotor induced velocity, and other blade wakes. Particularly in the leeward region, the incoming flow velocity is often significantly weakened, leading to a deviation between the equivalent incoming flow conditions assumed in the oscillating airfoil model and the actual rotor environment. Therefore, without reasonable correction for the incoming flow velocity, directly applying the optimization results of the oscillating airfoil level to the full VAWT model may introduce systematic errors, affecting the accuracy of performance evaluation.

Based on the above understanding, this section discusses the preconditions for incoming flow velocity correction from a physical mechanism perspective. First, it analyzes the composition of the actual incoming flow velocity and the characteristics of the induced velocity in the near-field region of the blade. Second, it discusses the influence of inter-blade interactions on the local incoming flow under multi-blade configurations. These analyses lay the physical foundation for establishing a reasonable incoming flow velocity correction method and provide the necessary prerequisites for performance mapping between the oscillating airfoil model and the complete VAWT model.

5.6.1 Near-Airfoil Wind Speed and Induced Velocity

In the real operating environment of a vertical axis wind turbine, the local incoming flow velocity experienced by the blades is not equivalent to the free incoming flow velocity. It is determined by the interaction of the free incoming flow, rotor-induced effects, and wake. The induced velocity typically refers to the velocity disturbance component near the blades caused by the momentum change exerted by the rotor on the flow field. Its essence originates from the pressure field and vortex structure formed under the aerodynamic forces of the blades. This induced velocity is superimposed on the free incoming flow, thus altering the effective incoming flow velocity and direction perceived by the blades.

In numerical simulations, whether the induced velocity needs to be explicitly introduced depends on the physical integrity and mathematical descriptive power of the model used. In computational fluid dynamics (CFD)-based simulations, the induced velocity does not need to be explicitly set as an input quantity but is naturally generated as part of the solution to the governing equations. However, in momentum-theoretic flow tube models (such as streamtube, DMST, or BEM), the induced velocity must be explicitly introduced to compensate for the limitations of the model's physical descriptive power.

In CFD simulations, the solutions are the continuity equations and the momentum conservation equations (Navier–Stokes equations), combined with an appropriate turbulence model to enclose the flow. The blades interact with the flow field through wall boundary conditions, and their aerodynamic effects create a non-uniform pressure distribution and vortex structure within the flow field, thus inducing momentum changes in the fluid. As a direct result of this process, velocity deficit regions, wake structures, and induced velocity components in the near-field of the blades naturally form in the flow field. Therefore, within the CFD framework, induced velocities are not pre-specified input parameters but are physical quantities automatically calculated by the governing equations under given free-flow conditions.

In other words, in CFD simulations, researchers only need to specify the free-flow velocity in the far-field boundary conditions; all other velocity variations (including near-field induced effects and velocity deficits in the downstream wake) are obtained by self-consistently solving the equations. Introducing a induced velocity into the inlet conditions in CFD simulations would lead to the repeated calculation of induced effects, which is physically incorrect and significantly distorts numerical results. Therefore, explicitly specifying the induced velocity in CFD simulations is unreasonable.

In contrast, flow tube models (streamtube, DMST, or BEM) have fundamental limitations in their physical description capabilities. These models are typically zero-dimensional or one-dimensional, do not directly solve the Navier–Stokes equations, and cannot analyze pressure field distribution, wake structure, vortex evolution, or describe the interactions between multiple blades. Within this framework, the only physical constraint available to the model is the momentum conservation relationship within the control volume. However, relying solely on momentum conservation, the model itself cannot determine the actual magnitude of the incoming flow velocity sensed by the blades.

To address this issue, flow tube models must introduce the induced velocity as an additional unknown and solve it in conjunction with the momentum conservation equations. The induced velocity is essentially an algebraic approximation of the pressure field, wake development, and vortex-induced effects in the real flow field; it is a necessary closure assumption. Without the induced velocity, the blades would always face with the free-flow velocity, leading to unphysically predicted power. Therefore, in flow tube models, the induced velocity is not a solution result but a necessary compensation term to maintain the model's physical plausibility.

This difference also explains why models like DMST must explicitly distinguish between upwind and leeward induced effects. In the upwind region, the induced velocity is relatively weak; while in the leeward region, wake development and multi-blade interactions significantly enhance the induced effect. Since flow tube models cannot directly analyze these flow structures, they can only approximate the actual flow field by artificially setting induced velocities for different regions.

It should be noted that even in the upwind region, the near-field velocity of the blades is not strictly equal to the free-flow velocity. The blades have already begun extracting energy from the flow field on the upwind side, and the pressure field and induced effects have already formed. Therefore, the local effective velocity will exist. However, the magnitude of the induced velocity is a key factor in determining whether it is negligible. Under high tip speed ratio (TSR) conditions, the flow is dominated by lift, and the dynamic stall effect is weak; the induced velocity on the upwind side typically accounts for only about 5–10% or less of the free flow velocity. Under these conditions, the local inflow velocity near the blade is numerically very close to the free flow velocity.

Therefore, when using a single-blade oscillation model under high TSR conditions, directly using the free flow velocity as the equivalent inflow velocity for the upwind blade is a reasonable approximation, and this is a common practice in many studies. However, in the downwind region, with the development of the wake, the superposition of multi-blade disturbances, and the accumulation of momentum deficit, the effective inflow velocity near the blade will be significantly lower than the free flow velocity, exhibiting obvious nonlinear and non-uniform variations with azimuth. In this case, simply using a fixed scaling factor (e.g., 0.5) to correct the free flow is insufficient to reflect the true physical process, and it is necessary to directly extract the local inflow velocity characteristics using CFD simulation.

In single-blade oscillation models, free-flow velocity is typically used directly as the model input to establish a controllable and repeatable unsteady aerodynamic environment. However, it's important to note that this approach only has good physical validity in the upwind region. In a full VAWT rotor, the blade continuously inputs momentum into the flow field during rotation, resulting in significant velocity deficit zones within the rotor and on the leeward side. Therefore, even if a constant free-flow velocity is applied in the CFD simulation, the actual inflow velocity in the near-field region of the blade will still deviate significantly from the free-flow value due to induced effects.

This difference is particularly pronounced on the leeward side (azimuth 180-360°). After passing the upwind side, the blade's wake extends downstream and superimposes with the internal rotor flow field, placing the leeward blade in an inflow environment already disturbed by the rotor itself, thus significantly reducing the effective inflow velocity around the airfoil. Some early studies approximate this reduction in leeward inflow velocity by introducing a fixed empirical reduction factor (e.g., multiplying the free-flow velocity by 0.5). However, this method ignores the significant variation in incoming velocity at different azimuth angles, making it difficult to reflect the non-uniformity of the real flow field, and therefore physically inaccurate.

Based on the above problems, this paper does not adopt an empirical model with a fixed reduction coefficient, but directly extracts and analyzes the incoming velocity in the near-field region of the blade through CFD numerical simulation. Specifically, at different azimuth angles, the local velocity distribution near the airfoil is measured to quantify the difference between the free incoming flow and the actual perceived incoming flow of the blade, and to clarify the spatial evolution characteristics of the wake effect. This method can more realistically reflect the rotor-induced effect and the variation of leeward velocity deficit with azimuth angle.

Furthermore, this paper also analyzes the directionality of the near-field incoming velocity of the blade. The results show that under most operating conditions, the local incoming velocity is still dominated by the global x-direction component; however, in the leeward region, especially in the 270-360 azimuth angle range, the y-direction component of the velocity shows a slight positive increase, while in the 180-270 range, it shows a slight negative component. This phenomenon reflects the existence of wake-induced deflection and local streamline bending. However, since the amplitude of this lateral velocity component is extremely small compared to the mainstream directional component, its impact on the airfoil's aerodynamic performance is negligible. Therefore, in the subsequent inflow velocity correction, only the change in velocity magnitude is considered, without explicitly introducing directional correction.

Through the above analysis, this section clarifies that introducing numerically simulated inflow velocity correction is necessary when associating the oscillating airfoil model with the complete VAWT model, and lays the physical foundation for further discussion of multi-blade interactions.

5.6.2 Multi-Airfoil Interaction

When comparing VAWT numerical results at different scales and configurations, a noteworthy phenomenon emerges: under the same free-flow velocity $\sigma \infty$, larger-scale rotors exhibit less local velocity attenuation in the leeward region. It is important to emphasize that this phenomenon should not be simply attributed to "larger airfoil size," as airfoil shape itself is not the dominant factor determining leeward velocity loss. A more reasonable explanation is that leeward flow characteristics are jointly determined by the overall rotor scale, solidity σ, number of blades N, shaft geometry, and wake development and recovery characteristics. When the model is scaled up from small-scale rotors to larger scales, solidity may decrease with geometric scaling, or the wake may recover faster in a relative-scale sense, resulting in a relatively weaker leeward velocity loss.

In multi-bladed VAWT, the fundamental physical mechanism of leeward flow attenuation stems from multi-bladed wake overlap and blade-wake interaction. For a VAWT with N blades, each blade generates a shear layer, vortex shearing, and a velocity deficit wake associated with energy extraction during its upwind operation. These wake structures are transported downstream at convective velocities and overlap with the trajectories of other blades within the rotor and in the leeward region. As a result, subsequent blades inevitably enter the wake and vortex structures generated by the previous blade (or its previous rotation cycle) during leeward operation, causing the local inflow to exhibit characteristics significantly different from the free inflow.

Extensive experimental and numerical studies have shown that this blade-wake interaction induces three typical effects on the leeward side: first, a reduction in local velocity amplitude (velocity deficit), as the blade operates in a flow field where momentum has been extracted; second, a significant enhancement in turbulence and velocity fluctuations, reflecting the superposition and fragmentation of complex vortex structures in the wake; and third, a deflection of the inflow direction, causing the local velocity to no longer strictly follow the global mainstream direction. The research by Rezaeiha et al. clearly points out that the significant aerodynamic fluctuations observed in straight-bladed VAWTs within a specific azimuth range on the leeward side are closely related to blade-wake interactions, and further emphasizes the influence of the shaft wake on the leeward flow structure [105-107].

At the engineering parameter level, these effects are often discussed using **rotor solidity** and the number of blades N. For H-type/straight-blade VAWTs, solidity is typically written as:

$\sigma \approx Nc/2R$

Where c is the chord length and R is the rotor radius. When the number of blades or the chord length is increased while other conditions remain constant, the circumferential area "occupied" by the blades within a unit rotation angle increases. This leads to more frequent generation of wake structures within the rotor, making it easier for subsequent blades to enter a stronger, less fully recovered wake region on the leeward side. This significantly increases the probability of wake overlap, resulting in a greater velocity deficit on the leeward side and stronger unsteady fluctuations. It is precisely because engineering-grade models (such as DMS or DMST) cannot explicitly analyze this complex multi-bladed wake interference process that it is necessary to introduce zonal induced velocities or empirical interference factors to treat the leeward side as an independent region.

The impact of wake overlap on the local incoming flow is reflected not only in the velocity amplitude but also in the velocity direction. Consistent conclusions from PIV and CFD studies indicate that the VAWT near-wake region exhibits a significant asymmetric and non-uniform velocity distribution. The leeward blades often operate in a flow field where the velocity deficit has not yet recovered, which aligns with our observations in the 180-360 azimuth range that near-airfoil velocities are lower than far-field wind speeds. Simultaneously, the vortex structures and shear layers carried in the wake cause local streamline bending, resulting in a slight deflection of the inflow direction relative to the global mainstream direction. High-resolution experimental and numerical studies show that the vortex structure trajectories in the VAWT wake exhibit significant variations across different rotational periods, accompanied by complex local velocity component distributions.

Based on this, a reasonable explanation can be provided for the phenomenon that "downward attenuation is smaller with larger scales." Without altering the fundamental physical mechanisms, larger-scale rotors often possess lower relative solidity (e.g., reduced c/R), leading to more dispersed momentum extraction per unit circumferential area, thus weakening the intensity of wake superposition. Furthermore, with increasing scale and Reynolds number, the relative thickness of the wake and the vortex scale may change, allowing the velocity deficit to recover more quickly in a relative distance sense. If the shaft size is not scaled up proportionally, its relative blocking effect may weaken with increasing scale. Research has shown that the shaft wake has a non-negligible impact on leeward flow; therefore, explicitly considering the shaft's role is necessary when comparing different scales or configurations.

Based on the above analysis, a crucial conclusion for subsequent modeling can be drawn: there is no fixed scaling factor universally applicable across scales and configurations for leeward inflow velocity attenuation. The comparative results in this paper show that, at different scales and configurations, the leeward local velocity deficit extracted by CFD exhibits significant differences in both amplitude and azimuth distribution. This fact indicates that using fixed empirical factors (e.g., uniformly reducing the leeward inflow to $0.5\ \lambda\ \infty$) is insufficient to reflect the true physical process. Instead, it is necessary to establish a more physically consistent rotational-blade model based on the azimuth-related local inflow characteristics extracted by CFD, providing a reliable foundation for mapping the oscillating airfoil optimization results to the complete VAWT model.

5.6.3 Equivalent Incoming Wind Speed Correction

Based on the aforementioned analysis of the near-field incoming flow characteristics of the blades (Section 5.6.1) and multi-blade interactions (Section 5.6.2), it can be concluded that under the complete VAWT condition, the local incoming flow velocity sensed by the blades deviates significantly from the free incoming flow velocity $\Phi\ \infty$ in both amplitude and azimuth distribution. This deviation mainly originates from rotor-induced effects, wake superposition, and shaft interference. Directly using the free incoming flow velocity to construct the relative motion incoming flow in the single-blade oscillation model will fail to reflect the downwind aerodynamic characteristics under real rotor conditions.

However, explicitly introducing the multi-blade and shaft geometry of the complete VAWT directly into the single-blade model will significantly increase the computational scale and numerical cost, weakening the efficiency advantage of this intermediate-layer model in the optimization process. To achieve a balance between physical consistency and computational efficiency, this paper proposes an equivalent incoming wind speed correction method to approximate the actual incoming flow conditions of the blades under the complete VAWT model in the single-blade model. This correction method uses the blade azimuth angle as the independent variable to map the free-flow velocity to an equivalent inflow velocity, which is then used to calculate the relative inflow velocity of the blades. Considering the fundamental differences in flow mechanisms between the upwind and leeward sides, the equivalent inflow velocity is defined as a piecewise function: in the upwind region, the near-field inflow velocity is close to the free-flow velocity, thus the correction magnitude is small; in the leeward region, a velocity attenuation term based on CFD extraction results is introduced to reflect the reduction in actual inflow velocity caused by wake overlap and induced effects.

To avoid introducing non-physical discontinuous changes at the boundary of the piecewise function and to ensure the smoothness of the equivalent inflow velocity throughout the entire rotation cycle, this paper further employs a smoothing function to transition the piecewise definition. This smoothing curve is used to construct a continuously differentiable equivalent inflow velocity distribution, thereby avoiding numerical oscillations or unreasonable transient aerodynamic fluctuations when calculating the relative inflow velocity. The specific mathematical expression of the equivalent inflow velocity and its smooth transition is detailed in Appendix A.

Through the above processing, the single-blade model, while maintaining a smaller computational scale and good numerical stability, can statistically more closely approximate the actual incoming flow environment experienced by the blades in the full VAWT model. This equivalent incoming flow correction method provides a crucial bridge for subsequently mapping the optimization results of oscillating airfoils to the full VAWT model, and also provides an effective way to reduce computational costs during the optimization process.

Table 5.5 shows the estimated wind speed at the downwind side of the turbine from the CFD simulations of the turbine. It is assumed that the freestream wind speed is unaffected at the upwind side. The wind speed at the downwind side is calculated by directly extracting the wind speed values at the front of the airfoil from the CFD solutions. The obtained wind speed values are written in the form of a continuous function (or a piecewise function?) representing the speed change in front of the airfoil throughout the cycle, Fig. 5.3.10 shows the corresponding AoA profile when wake effect is considered.

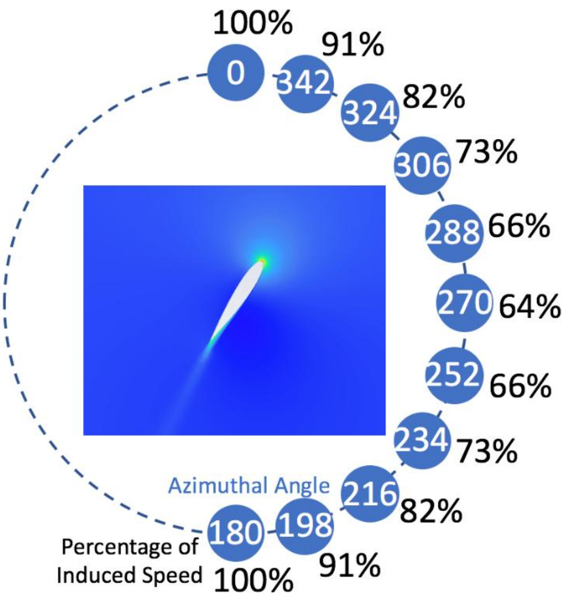

Fig. 5.19: Induced Speed Percentage Value over Different Azimuthal Angles.

Table 5.5 Induced Speed Percentage Value over Different Azimuthal Angles

Azimuthal Angle (°)	Wind Speed
0-180	100%
198	91%
216	82%
234	73%
252	66%
270	64%
288	66%
306	73%
324	82%
342	91%

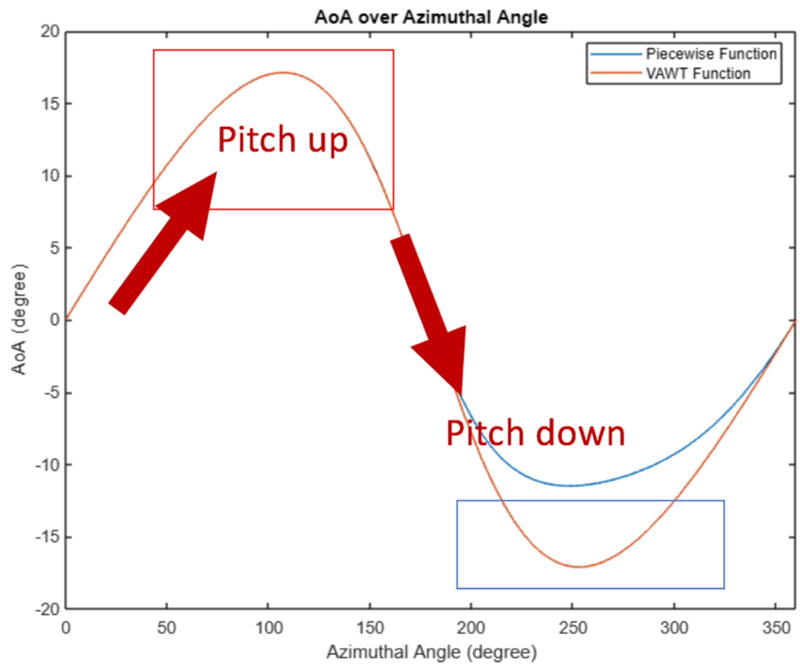

Fig. 5.20: Wake Affected AoA Profiles over Different Azimuthal Angles.

Fig. 5.3.11 shows the optimization of the airfoil when the modified incoming velocity file and the angles of attack profile are implemented in the oscillating airfoil model. This is compared with the original NACA0015. Fig. 5.3.12 Comparison of the C_T of the turbine with the new optimised airfoil and those of the NACA0015.

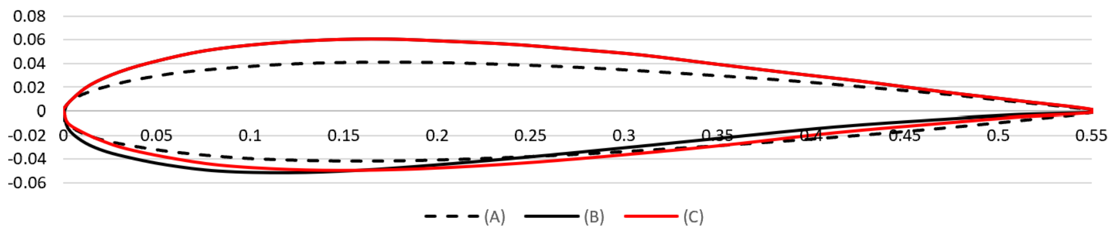

Fig. 5.21: Profiles Comparison among the (A) NACA0015, (B) Optimized Airfoils and (C) Optimized Airfoils in the Wake Affected Condition.

5.7 Aerodynamic Performance on VAWT Model

After completing the unsteady adjoint optimization and systematically evaluating its aerodynamic performance in the aforementioned oscillating airfoil model, it is necessary to further introduce the optimized airfoil into the complete VAWT numerical model to verify its impact on overall power output under real rotor conditions. This section directly compares and analyzes the oscillatingly optimized airfoil with the initial baseline airfoil based on a two-dimensional two-blade VAWT model.

Fig. 5.22 presents a typical flow field around the turbine fitted with the original NACA0015 blade. There is not a significant change in the overall picture of the flow when the optimised airfoil is employed since the modification to the airfoil shape is relatively small. As expected, the freestream flow is less disturbed when the blade is travelling at the upwind locations. The blade indeed will travel into the wake region when it travels in the downwind locations. The reduction in the wind speed was not considered in the optimization presented in the previous section but this will be assessed later.

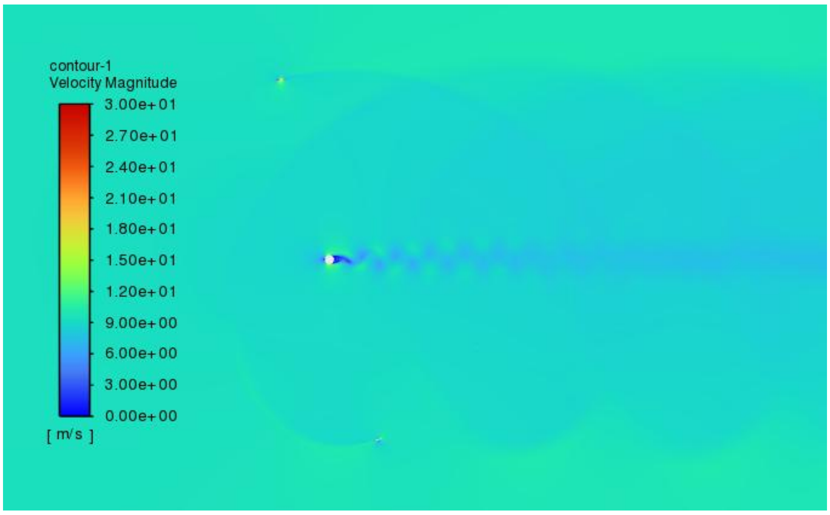

Fig. 5.22: Airfoil Contour Diagram of the VAWT-130.

In Fig. 5.23, the force and moment of the third cycle is recorded, which is applied in other subsequent optimization cases to eliminate the influence of initial conditions. This simulation recorded 20 cycles, which confirmed that the simulation results of the third cycle are exactly the same as those of the subsequent cycles.

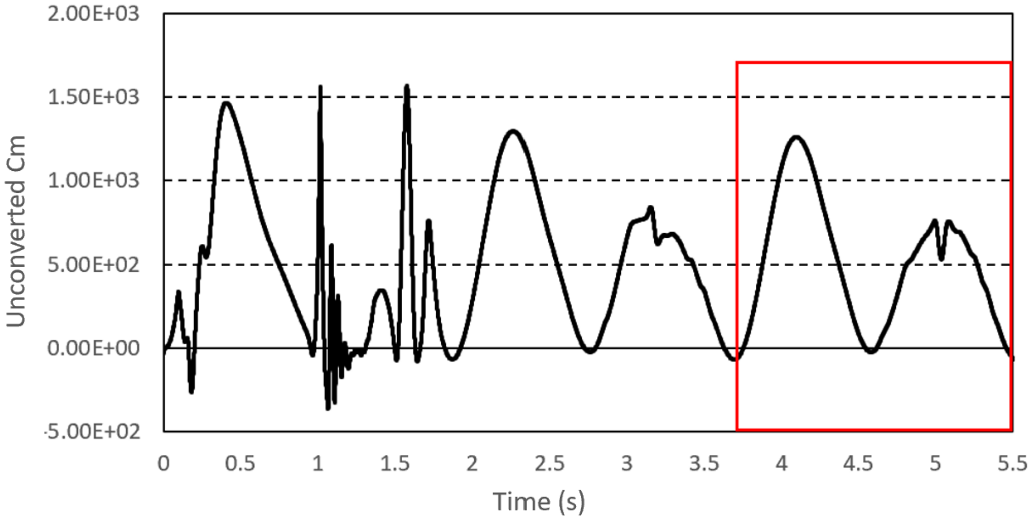

Fig. 5.23: Recorded Simulation Cycles of the VAWT-130.

It is worth noticing that when simulating a vertical-axis wind turbine (VAWT) in Fluent, special attention should be paid to the interpretation of the monitored torque coefficient C_M when hybrid initialization is used as the initial condition. The C_M value displayed in the Fluent monitor is not always directly comparable to the standard non-dimensional torque coefficient reported in the wind turbine literature, because it may be based on Fluent's internal reference values rather than on the physical normalization convention commonly adopted for VAWTs. As a result, the monitored C_M may not be in the same non-dimensional form as the torque coefficient used for aerodynamic performance analysis, and direct comparison with published results can therefore be misleading. To obtain a physically meaningful and standardized torque coefficient, the monitored torque or the reported C_M are converted using the conventional VAWT definition. Only after this conversion can the resulting C_M be regarded as the standard torque coefficient suitable for evaluating the instantaneous torque behavior of the VAWT and for subsequent calculation of the mean torque coefficient, power coefficient, and comparison with experimental or numerical results from the literature.

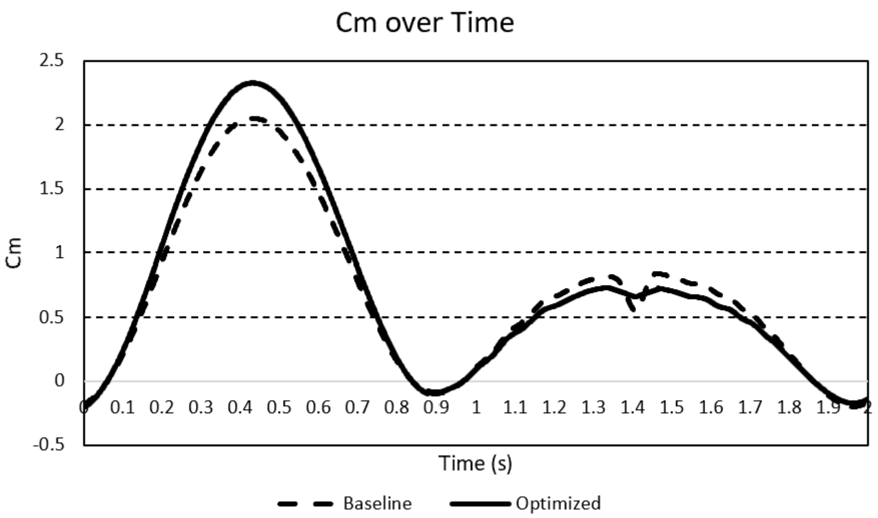

Fig. 5.24: Moment Coefficient in the VAWT-130 Model over time at 9.66m/s.

Fig. 5.24 compares the moment generated by the original NACA0015 and the optimised airfoil. It can be seen that the peak moment coefficient of the airfoil increases significantly when the blade is at the upwind side of the turbine with the peak moment increased by over 10%, while the peak tangential coefficient of the airfoil at the downwind side experiences almost no change. These results indicate that the optimized airfoil is most effective when the blade is at the upwind side and this is where most of the turbine power is generated. The average increase in the moment over the full cycle is approximately 7% over the original NACA0015. It is also demonstrated that the adjoint optimization method proposed using an oscillating airfoil is promising.

Fig. 5.25 compares the instantaneous velocity distribution around NACA0015 and optimised airfoils when they are at the azimuthal angle of 90° where the maximum improvements in the momentum occurs. It can be observed that since the surface curvature on one side of the airfoil shape is significantly reduced, the speed of the air around it passing through the surface is significantly reduced, resulting in the airfoil in the upwind condition generating in a smaller lift component, but a larger lift component is generated in the downwind condition. This effect makes the lift and drag of the airfoil contributing a higher degree of improvement to the total value.

(A) (B)

Fig. 5.25: Velocity distribution around (A) NACA0015 and (B) optimized airfoils when VAWT-130 at 90^o azimuthal angle where maximum improvements in the momentum occurs.

The observed improvement in the tangential coefficient, particularly in the upwind region, signifies promising advantages in the employment of the optimised aeorfoil in the VAWT design. Enhancing the tangential coefficient in the upwind region is of paramount importance because it directly correlates with the ability of the VAWT to capture more wind energy from the prevailing wind direction, thereby increasing its overall power generation efficiency. The optimization process effectively tailors the airfoil shape to extract the maximum energy during the upwind conditions, making it a crucial component for boosting the VAWT's power coefficient. It also underscores the significance of the fine-tuning airfoil designs that leads to a net gain in the power production potential.

When the other physical conditions remain unchanged, the optimized airfoil will be placed in exactly the same 2-blade VAWT model for obtaining the moment coefficients. Table 5.5 shows a numerical comparison of the moment coefficients obtained in the VAWT models for the airfoil optimized using this method. It can be seen that under certain wind speed conditions, the optimized blades using the new AoA profiles can obtain a larger power coefficient, which has made a certain degree of improvement for the equivalent downwind condition under the oscillation airfoil model.

Table 5.6: Averaged Moment Coefficient of the Airfoils overall one rotational cycle with a constant wind speed of 9.66 m/s.

TSR	NACA0015	Optimized	% increase
2.25	0.0421	0.0434	3.09%
3.25	0.0911	**0.0972**	6.70%
4.25	0.0810	0.0823	1.02%

It can be shown in the Table 5.6 that under a certain speed condition, the optimized blade can still obtain a greater power coefficient under similar wind speed conditions. As shown and discussed in Figure 5.3.9, in most cases the blade will pass through the wake of the blade ahead in the downwind side of the turbine where the wind speed is substantially lower than the freestream wind stream in the upwind side of the turbine and where there is more turbulence. A lower wind speed results in a decrease in the blade angle of attack at the downwind side of the turbine. These issues were not considered in the optimization of the oscillating blade.

5.8 Summary

This chapter focuses on the aerodynamic optimization problem of oscillating airfoils under the unsteady operating environment of the VAWT (Vacuum-and-Wide Aircraft World) system. A numerical model of the oscillating airfoil is systematically established and validated, and based on this, a set of unsteady adjoint optimization methods is constructed. By verifying key factors such as the mesh independence, time step, computational domain size, and convergence of periodic solutions, the numerical reliability of the oscillating airfoil model under unsteady conditions is ensured. Subsequently, the model is compared with existing experimental data and the complete VAWT numerical model, verifying its rationality in predicting relevant aerodynamic characteristics of VAWT.

The main goal of changing the curvature of an airfoil is to modify the lift and drag characteristics of the airfoil. The tangential coefficient resulting from the combination of the lift and drag is responsible for generating the force that drives the turbine to rotate. However, what is different from other oscillating airfoil problems is that in VAWT applications, the lift and drag change more obviously and regularly with time. When the curvature of an airfoil changes, it affects the tangential coefficient of the airfoil. In the application of VAWT, optimizing the airfoil curvature takes into account the effects of the upwind and downwind sides of the airfoil. Among them, the shape change on the upwind side is mainly to break through the value of the tangential coefficient, while the shape change on the downwind side is to reduce the turbulence and flow separation and promote better flow adhesion and control. However, under the upwind condition of 0-180 degrees and the downwind condition of 180-360 degrees, the upwind side and downwind side of the airfoil are exchanged with each other. This means that a certain upwind side shape can break through the tangential coefficient well during the upwind phase, but cannot reduce the turbulence and flow separation on the downwind side. Therefore, in order to increase the tangential coefficient throughout the cycle, the deformation on both sides of the airfoil needs to reach a balanced state.

It can be seen from the results that whether the turbine operates at the high wind speed or low wind speed, the optimized airfoil shape is no longer symmetrical. The shape of the airfoil is more affected by the upwind range of one equivalent rotation period, that is, its optimization improvement in the upwind range is the main contribution to the optimization of the airfoil power coefficient. In the flow solution of the new blade, it can be found that due to the chord length constraint, the blade gradually tends to have a small curvature, and the trailing edge of the blade also points to the normal direction of the side with greater curvature. This asymmetrical shape plays a huge role in the upwind conditions, but the performance is the average in the downwind conditions, but the tangential coefficient of the airfoil does not decrease significantly in the downwind conditions. This is because the blade generates a larger high-pressure region than the original NACA0015 in the upwind condition and obtains a more favourable pressure gradient size and direction. However, under the downwind condition of the blade, most of the area facing the wind is a high-pressure region with a curvature, and only the trailing edge of the airfoil does not perform well. In addition, the flow separation caused by the shaft further affects the initial velocity of the NACA0015 airfoil and the optimized airfoil under the downwind condition.

Methodologically, based on unsteady adjoint solutions and mesh deformation techniques, an optimization process suitable for oscillating airfoils is constructed, and key issues such as the objective function, design variables, constraints, and time window control are systematically discussed. Pilot tests verify the stability and feasibility of the optimization process, laying a methodological foundation for subsequent airfoil performance evaluation and its application in the complete VAWT model.

Chapter 6

VAWT Rotational Blade Optimization

6.1 Overview

Since the single-blade model based on oscillating airfoils mentioned in the previous chapter still relies on equivalent inflow correction to approximate the rotor environment, it is difficult to characterize the interaction between blades and its impact on the optimization process in the rotating coordinate system corresponding to VAWT. To further narrow the gap between the intermediate layer model and the actual VAWT operating condition, this chapter proposes and studies an in-situ optimization method for rotating blades.

This chapter establishes single-blade and double-blade rotating models to directly model and optimize the aerodynamic performance of the blades in a rotating reference frame, thereby avoiding empirical corrections to the inflow conditions. Numerical modeling and verification work were systematically carried out around this rotating blade model, and the unsteady adjoint optimization method was extended to the rotating blade scenario.

6.1.1 Advantages of In-Situ Blade Optimization

The study of wake flows in VAWTs has a rich history, with the early investigations using wind tunnel measurements and flow visualization techniques to identify the dominant vortical structures shed during operation. Subsequent numerical studies related to CFD demonstrated that the VAWT wake exhibits faster momentum recovery compared with the HAWT wakes, and this is due to the enhanced turbulent mixing induced by strong periodic shedding.

More recent studies have emphasized the interplay between blade kinematics, airfoil shape, and wake development. For instance, optimization of blade pitch trajectories and flexible blade structures has been shown to mitigate unsteady load fluctuations and improve energy capture [129]. Parallel research into airfoil design has demonstrated that tailored geometries can delay stall onset, suppress adverse vortex shedding, and thereby enhance the power coefficient under a range of operating conditions [130]. Nevertheless, these studies often treat wake effects indirectly, rather than embedding them as explicit constraints or objectives in the optimization process. This research gap highlights the necessity for a integrated approach in which wake dynamics are directly incorporated into the optimization framework.

By enabling efficient sensitivity evaluation across thousands of design variables, such methods allow the exploration of turbine geometries that simultaneously improve local aerodynamic efficiency, stabilize vortex shedding, and promote favorable wake recovery. The present work builds on this foundation to advance the state of the VAWT design through comprehensive aerodynamic optimization strategies that explicitly integrate the wake flow analysis.

The role of the wake in the aerodynamic performance of vertical axis wind turbines (VAWTs) has been investigated extensively over the past four decades, yet significant challenges remain in fully integrating wake dynamics into design methodologies. Early experimental studies in the 1980s and 1990s used hot-wire anemometry and flow visualization to identify the dominant vortex structures shed by rotating blades and their downstream evolution [131]. These investigations revealed that VAWT wakes are characterized by strong periodic shedding, rapid mixing, and a relatively fast recovery compared with horizontal axis wind turbines (HAWTs). Such properties suggested that VAWTs could achieve higher power densities in array configurations [132]. However, most of these studies focused on near-wake structures and did not fully quantify the impact of the wake on system-level performance or blade–wake feedback mechanisms.

Furthermore, induction effects, which describe the reduction in the local wind velocity due to energy extraction by the turbine, have been widely addressed in HAWT modeling through momentum theory and its extensions. In the VAWT literature, however, induced factors have often been treated with significant simplifications. The classical double multiple streamtube (DMST) model assumes uniform induction factors for upstream and downstream passes, neglecting the inherently unsteady and azimuthally varying nature of the induced velocity field. While more advanced formulations have introduced azimuthal variation and dynamic stall corrections, they still fall short of capturing the time-dependent wake-induced velocities that strongly influence instantaneous blade loading. High-fidelity CFD studies have shown that neglecting the spatial and temporal variation of induction leads to underprediction of unsteady loads and overprediction of the power coefficient. Consequently, induced factors remain one of the central uncertainties in reduced-order VAWT models and a persistent limitation in their application to optimization tasks.

Another critical issue is the treatment of multiblade interactions. In practice, VAWTs often employ two or three blades to balance aerodynamic efficiency with structural considerations. The flow field generated by one blade significantly alters the environment experienced by subsequent blades, particularly through the advection of vortices and wake structures across the rotor disk [133]. Despite this, much of the early optimization research treated blades in isolation or assumed that blade–blade interactions could be approximated by uniform inflow conditions. Even contemporary optimization studies frequently rely on two-dimensional, single-blade simulations to reduce computational expense [134]. While such simplifications yield insights into sectional airfoil performance, they fail to capture the cumulative effects of multiple blades interacting through shared wakes, especially under high tip-speed ratio operation where vortices from one blade may impinge directly on another. Recent stereoscopic PIV studies have highlighted the complex coupling between successive blades, showing that these interactions can either amplify or suppress dynamic stall depending on the phasing [135]. Yet, these effects are rarely incorporated into design optimization frameworks.

With increasing computational resources, high-fidelity CFD-based optimization has gained popularity. Two-dimensional unsteady Reynolds-averaged Navier–Stokes (URANS) and, more recently, large-eddy simulations (LES) have been employed to evaluate the aerodynamic performance of candidate airfoils under cyclic loading. In these studies, optimization frameworks are typically limited to sectional airfoil shapes, where the wake is implicitly accounted for through boundary conditions but not directly resolved at the system level. As such, the complex blade–wake interactions and induced velocity variations that dominate rotor-scale performance will not be explicitly incorporated into the optimization objectives.

Overall, the existing body of work on VAWT aerodynamics provides valuable characterizations of wake behavior, induction, and multiblade effects, but these aspects have largely been studied in isolation. The literature highlights a persistent research gap: the absence of comprehensive optimization frameworks that simultaneously account for unsteady wake development, induction variability, and multiblade interaction in complete VAWT systems. Most optimization efforts to date have either prioritized computational efficiency by using reduced-order models or focused narrowly on sectional airfoil shapes without incorporating feedback from the wake dynamics. This has resulted in designs that may perform well under idealized inflow but fail to address the full complexity of the complete VAWT model.

The unsteady structures caused by vortex shedding and wake effects alter the inflow conditions to subsequent blades, thus affecting aerodynamic forces and power output. Furthermore, the interaction between multiple blades leads to uneven aerodynamic load distribution, impacting lift-to-drag ratio and overall energy capture efficiency. Therefore, as demonstrated in Chapter 5, even after considering wake effects and correcting for relative inflow velocity during optimization, the performance improvements achieved with a single blade or simplified model are still difficult to reproduce in actual wind turbines. Therefore, introducing wake and multi-blade effects during the optimization process improves the applicability and stability of the results, making the optimization more realistic.

The core advantage of in-situ blade optimization lies in the fact that the evaluation and optimization of blade aerodynamic performance are performed directly within a rotating reference frame and under actual rotor motion conditions, thus avoiding the approximate assumptions about equivalent incoming flow conditions found in intermediate-level models. Compared to optimization methods based on oscillating airfoils or single-blade static models, this method naturally incorporates rotor-induced effects, inter-blade interactions, and possible shaft influences, making the optimization process physically closer to real VAWT conditions. Furthermore, the in-situ optimization method can simultaneously consider aerodynamic responses at different blade azimuth angles within a unified numerical framework, reducing uncertainties introduced by incoming flow corrections or empirical models.

6.1.2 Assumptions of Single-Blade Rotation

In numerical studies of VAWT (Variable Aerodynamic Weighted Wheatstone) systems, due to considerations of computational cost and problem controllability, many existing works employ two-dimensional cross-sectional models to analyze the rotor aerodynamic characteristics. Although three-dimensional effects are not negligible in practical VAWTs, two-dimensional models have been widely proven to capture key physical characteristics for studying blade aerodynamic mechanisms, unsteady load characteristics, and methodological verification. Therefore, in CFD studies of VAWTs over the years, two-dimensional cross-sectional models, small-scale rotors, and simplified configurations have been commonly used, especially in scenarios requiring extensive parameter scans or optimization iterations.

Based on this research background, this paper first establishes a single-blade rotating model for direct in-situ blade optimization in a rotating reference frame. This model contains only one rotating blade within a two-dimensional cross-section, and its rotation mode, relative motion description, and unsteady solution strategy are consistent with the complete VAWT model. The resulting near-field flow solution is comparable to the single-blade flow field in the complete VAWT cross-section in a local aerodynamic sense, only omitting the direct interference from other blades and the shaft in terms of geometric configuration.

A key motivation for using a single-blade rotating model is to significantly reduce computational scale. Compared to the multi-bladed rotor model, this model significantly reduces the computational domain size, mesh count, and time progression cost, enabling unsteady adjoint optimization to complete multiple iterations within a reasonable computational time. This is particularly crucial for method development and parameter sensitivity studies. It should be noted that the rotor size used in this paper is a relatively small turbine configuration; its purpose is not to directly reproduce a specific engineering model, but rather to repeatedly test and validate the proposed optimization method under controllable computational costs. The method's physical modeling and numerical framework settings are scale-independent, thus allowing it to be extended to larger-scale VAWTs while maintaining similarity criteria (such as Reynolds number and reasonable TSR ranges).

In the kinematic description, the single-bladed rotating model adopts the iso-TSR assumption, meaning the blade angular velocity maintains a constant proportional relationship with the free flow velocity. This assumption is consistent with the settings used in the complete VAWT numerical model discussed earlier, ensuring comparability of aerodynamic conditions across different model levels. Under this assumption, the relative flow velocity change experienced by the blade during rotation is entirely determined by its azimuth angle, thus providing a clear and repeatable basis for subsequent unsteady sensitivity analysis and optimization.

It is important to reiterate that a VAWT consisting of a single blade does not exist in reality. The single-blade rotation model in this paper is not intended to represent a real rotor configuration, but rather serves as an intermediate-level model to verify the feasibility of in-situ optimization methods in a rotating reference frame, and to provide a benchmark for subsequent research on dual-blade rotation models that more closely approximate the real configuration.

6.1.3 Assumptions of Double-Blade Rotation

Building upon the validation of the single-blade rotating model, this paper further introduces a two-blade rotating model to more realistically reflect the fundamental geometric characteristics of VAWT while maintaining controllable computational costs. The two-blade configuration is one of the most common and fundamental rotor configurations in VAWT research, widely adopted in experimental and numerical studies over the years, and particularly suitable for methodological research and model validation.

The two-blade rotating model established in this paper is also based on a two-dimensional cross-sectional description, with the two blades arranged symmetrically along the rotor circumference, differing in azimuth by 180°. Under the assumption of equal TSR, when the numerical solution reaches periodic convergence, this configuration exhibits clear physical symmetry in the sense of rotational symmetry: at any given time, the local flow structures experienced by the two blades are spatially equivalent, with only a 180° phase difference. This characteristic provides an important basis for simplifying the in-situ optimization process.

Based on the above symmetry assumption, this paper performs flow field monitoring and associated sensitivity extraction on only one blade in the two-blade rotating model, and simultaneously applies the resulting geometric deformation to the other blade. In other words, the two blades maintain geometric consistency throughout the optimization process, experiencing different flow stages only due to differences in rotation phase. This approach is physically consistent with the periodic symmetry of the two-blade configuration, while significantly reducing the complexity and computational cost of the optimization problem numerically.

It is important to note that this simplification relies on the two-blade structure and its strict geometric and operational symmetry. When the number of blades increases to three or more, the azimuth angles of different blades at the same time are no longer simply symmetrical. The flow field conditions experienced by each blade also become significantly different. At this point, the method of synchronous deformation based on the sensitivity of a single blade is no longer applicable. Instead, it is necessary to monitor multiple blades simultaneously and extract their sensitivity information separately. This greatly increases the complexity of the optimization process. Since this paper focuses on the establishment and validation of the method, this chapter will not discuss the case of more than two blades.

Similar to the single-blade rotating model, the two-blade rotating model also employs a relatively small-scale turbine configuration to allow for multiple rounds of optimization iterations and parameter testing at a reasonable computational cost. The purpose of this model is to verify the effectiveness of the in-situ rotation optimization method under conditions closer to the actual rotor configuration, rather than to predict performance at a specific engineering scale. Therefore, the conclusions obtained in this paper should be understood as methodological conclusions, and their application to larger-scale VAWTs requires consideration of the corresponding scale and Reynolds number effects.

6.1.4 Coordinate Transformation Mechanism of the Monitoring Area

Transient adjoint optimization combined with unsteady flow field solution and finally using FFD deformation provides an efficient method for VAWT airfoil optimization. The core of the optimization process is to calculate the sensitivity through the adjoint method, flexibly adjust the geometry with FFD technology, and find the optimal value through an iterative optimization algorithm. The parameter used for the airfoil optimization objective, the power coefficient, is calculated by the time-averaged torque $T(t)$ and the input power. The optimization process adjusts the airfoil shape through the sensitivity information so that the objective function J reaches the minimum value, that is, the maximum value of the power coefficient.

$$J = -\int_0^T \frac{\int_s F_t ds}{\frac{1}{2}\rho U_\infty^2 A} dt \qquad \text{[Eq. 6.1]}$$

Where F_t is the component of the airfoil surface force F in the tangential direction and s is the airfoil surface.

The component of the surface force F_t in the tangential direction can be expressed as follows if it is analyzed by the forces on the discrete grid and the area of the discrete elements.

$$J = -\int_0^T \frac{\sum_i (F_i \cdot e_{\theta,i}) \Delta s_i}{\frac{1}{2}\rho U_\infty^2 A} dt \qquad \text{[Eq. 6.2]}$$

Where $F_i \cdot e_{\theta,i}$ is the forces on the discrete grid and Δs_i is the area of the discrete elements.

From the definition of the objective function J, the gradient d of the objective function on the flow field variables can be expressed. Assuming that F is composed of the pressure p and shear stress τ, then:

$$\frac{\partial J}{\partial u} = -\frac{1}{\frac{1}{2}\rho U_\infty^2 A} \cdot \sum_i \frac{\partial}{\partial u} \left[(-p n_i + \tau) \cdot e_{\theta,i} \Delta s_i \right] \qquad \text{[Eq. 6.3]}$$

Where u is the flow field variable.

The optimization process aims to adjust the design variables to minimize the objective function. The primal equations represent the flow physics. For the unsteady, incompressible Navier-Stokes equations, the sensitivity of the objective function J with respect to the design variables x is given by:

$$\frac{dJ}{dx} = \int_\Omega \frac{\partial J}{\partial u} \frac{\partial u}{\partial x} d\Omega \qquad \text{[Eq. 6.4]}$$

In the study of the VAWT oscillation airfoil model, it is clear that the optimization process aims to adjust the design variables to minimize the objective function. The primal equations represent the flow physics. For the unsteady, incompressible Navier-Stokes equations, the sensitivity of the objective function J with respect to the design variables x is given by:

$$\frac{dC_t}{dx} = \int_{t_0}^T \left(sin(\omega t) \frac{\partial C_L}{\partial x} - cos(\omega t) \frac{\partial C_D}{\partial x} \right) dt \qquad \text{[Eq. 6.5]}$$

Where T is the final time and t_0 is the initial time, C_L is the lift coefficient and C_D is the drag coefficient.

When calculating the gradient of the objective function in the rotating grid plane, it is necessary to introduce the coordinate transformation of the rotating grid. It is assumed that the plane where the airfoil is located rotates with the rotating grid at an angular velocity ω, which changes the relationship between the global coordinates and the local coordinates. The adjoint gradients $\frac{\partial C_L}{\partial x}$ and $\frac{\partial C_D}{\partial x}$ need to be projected into the rotating coordinate system. Assume that the center of rotation is O, the rotation angle of the airfoil local coordinate system (X, Y) at a certain time t is θ, and the global coordinate system of the rotation center is (X_c, Y_c), then the local coordinate system (x', y') can be expressed as:

$$\begin{bmatrix} X \\ Y \end{bmatrix} = \begin{bmatrix} cos\theta & -sin\theta \\ sin\theta & cos\theta \end{bmatrix} \begin{bmatrix} x' \\ y' \end{bmatrix} + \begin{bmatrix} X_c \\ Y_c \end{bmatrix} \quad \text{[Eq. 6.6]}$$

The position of the geometric design variable (x', y') in the rotating coordinate system is affected by time:

$$x'(t) = x' + \Delta x'(t) \quad \text{[Eq. 6.7]}$$

The local lift coefficient C'_L and the local drag coefficient C'_D can be expressed as:

$$\begin{bmatrix} C'_L \\ C'_D \end{bmatrix} = \begin{bmatrix} cos\theta & sin\theta \\ -sin\theta & cos\theta \end{bmatrix} \begin{bmatrix} C_L \\ C_D \end{bmatrix} \quad \text{[Eq. 6.8]}$$

The complete formula of the objective function gradient in the rotated grid is given by:

$$\frac{dC_t}{dx'} = \int_{t_0}^{T} \left(sin(\omega t) \frac{\partial C'_L}{\partial x'} - cos(\omega t) \frac{\partial C'_D}{\partial x'} \right) dt \quad \text{[Eq. 6.9]}$$

Free Shape Deformation (FFD) is a common geometry parameterization technique used to adjust the geometry based on the sensitivity in adjoint optimization. Its main advantage is that modelling can be done in a relative coordinate system, while a mesh around the control airfoil needs to be defined. Here, a Cartesian control mesh is constructed around the airfoil, and the control points G define the mesh shape. Points on the airfoil are interpolated using the basis functions B of the control point mesh G.

In this deformation, there is an interface area between the stationary plane and the rotational plane, and the mesh in the circular area moves with the rotational plane. It is necessary to combine the rotation transformation and the deformation mapping of the FFD to describe the new position of the mesh point. Let G be the control point of the FFD, the control mesh covers the entire rotational plane, and the position of the mesh point can be expressed by the FFD mapping formula:

$$P(x, y, z) = \sum_{i=0}^{l} \sum_{j=0}^{m} \sum_{k=0}^{n} B_i^l(u) B_j^m(v) B_k^n(w) G_{ijk} \quad \text{[Eq. 6.10]}$$

Where x, y, z are the parameter coordinates of the original point, u, v, w map the point x, y, z to the position in the control grid coordinate system B is the Bernstein basis function, l, m, n is the resolution of the control mesh in the parametric space and i, j, k is the position of a specific control point in the grid.

In the rotation plane within the model, the original coordinates of the mesh points before rotation are assumed to be:

$$X_{old} = (x_{old}, y_{old}, z_{old}) \quad \text{[Eq. 6.11]}$$

The center of the rotation plane is given by:

$$C = (x_c, y_c, z_c) \quad \text{[Eq. 6.12]}$$

On the two-dimensional model plane, the rotation angle is θ about the z-axis, so the rotation transformation function is given by:

$$X_{rot} = \begin{bmatrix} cos\theta & -sin\theta & 0 \\ sin\theta & cos\theta & 0 \\ 0 & 0 & 1 \end{bmatrix} \cdot (X_{old} - C) + C \quad \text{[Eq. 6.13]}$$

For the mesh points in the rotation plane, the initial geometric position of the rotation plane is first deformed by the FFD, and then the deformed points are subjected to rotation transformation. The expression is given by:

$$X_{new} = \begin{bmatrix} cos\theta & -sin\theta & 0 \\ sin\theta & cos\theta & 0 \\ 0 & 0 & 1 \end{bmatrix} \cdot (P(X_{old}) - C) + C \quad \text{[Eq. 6.14]}$$

Sensitivity-driven deformation adjusts the position of the control point G through the sensitivity gradient $\frac{\partial J}{\partial q}$ to update the geometry:

$$G_{ijk}^{new} = G_{ijk} - \alpha \frac{\partial J}{\partial G_{ijk}} \quad \text{[Eq. 6.15]}$$

Where α is the step size.

The goal of the optimization problem is to minimize or maximize the objective function J. The gradient $\nabla J = \frac{dJ}{dx}$ of the objective function with respect to the design variable x describes the direction and magnitude of the improvement of the current design point. When the optimization reaches the optimal point, the gradient approaches zero. When the gradient is less than the threshold, if the condition is met, the optimization stops, otherwise the iterations continue.

It should be noted that the scenario discussed in this section primarily addresses an extreme and idealized situation. Its purpose is to illustrate the potential impact of optimization strategies under different phase and time allocation assumptions, rather than attempting to comprehensively cover all practical configurations. For a two-bladed vertical axis wind turbine, due to the spatial distance between the two blades, the direct interaction between them is weak, and their motion has a strict 180° phase difference. Under these conditions, the aerodynamic processes experienced by the two blades within a complete cycle are highly symmetrical, and therefore their periodic average aerodynamic loads are theoretically identical. Based on this characteristic, the optimization process for a two-bladed configuration does not require the introduction of additional coordinate or phase transformations in practical applications.

However, when the number of blades increases to three or more, the above simplifying assumptions no longer hold strictly. Although a three-bladed configuration typically employs a 120° phase difference, this phase relationship is insufficient to fully describe the aerodynamic response of the blades in complex unsteady flow fields. Because blades may experience the wake region, the region of significant induced velocity changes, or the region of strongly unsteady flow in different sequences, their aerodynamic loads may vary in sensitivity to the flow field structure, thus rendering the blades no longer strictly equivalent in a period-average sense.

Therefore, the analysis in this section primarily aims to provide ideas and theoretical references for optimization problems with higher blade numbers and more complex configurations, rather than offering directly applicable engineering conclusions. Due to the limitations of this research focus, the numerical simulations conducted in Chapter 6 will not further discuss the aforementioned complex multi-bladed cases.

6.2 Modeling and Validation of Single-Blade Rotational Airfoils

In Chapter 5, the oscillating airfoil model was used to establish an unsteady adjoint optimization method, and its effectiveness in capturing local unsteady aerodynamic characteristics was verified. However, this model is still based on equivalent oscillating motion, which limits its ability to reproduce real rotational motion. To further narrow the gap between the model assumptions and actual VAWT operating conditions, while avoiding the high computational cost of the full multi-bladed rotor model, this chapter introduces a single-bladed rotating airfoil model.

This model directly applies real rotational motion to a single airfoil, causing it to experience relative flow changes in the inertial coordinate system equivalent to those of a VAWT blade. This achieves more physically consistent rotational aerodynamic characteristics without introducing multi-bladed wake superposition and shaft interference. Compared to the full VAWT model, this method significantly reduces the computational scale while maintaining key unsteady physical mechanisms, providing a feasible numerical platform for subsequent in-situ unsteady adjoint optimization.

To avoid complex wake interference caused by multiple blades and the shaft, and to ensure that the changes in incoming flow perceived by the blade during rotation are primarily determined by its own motion, the single-blade rotating model employs a significantly enlarged rotor radius and computational domain scale. In this way, the wake generated by the blade within one rotation cycle gradually decays in regions far from the blade, effectively reducing its reverse interference in subsequent rotational phases. This contrasts sharply with the multi-blade wake interaction and shaft wake superposition in the complete VAWT model with a shaft.

A significant advantage of this modeling strategy is that it achieves an unsteady aerodynamic response highly consistent with the rotational motion of the VAWT cross section using only a single blade, while avoiding the additional uncertainties introduced by multi-blade interactions and the presence of the shaft. This makes the model more suitable for unsteady adjoint optimization studies, and the resulting sensitivity information more directly reflects the aerodynamic contribution of a single blade during rotation.

Figure 6.1 shows the overall configuration and key geometric parameters of the single-blade rotating airfoil model, including the rotor radius, computational domain size, and the definition of the rotating reference frame. Based on this model construction method, subsequent sections will systematically verify its numerical properties, such as periodic convergence and time step independence.

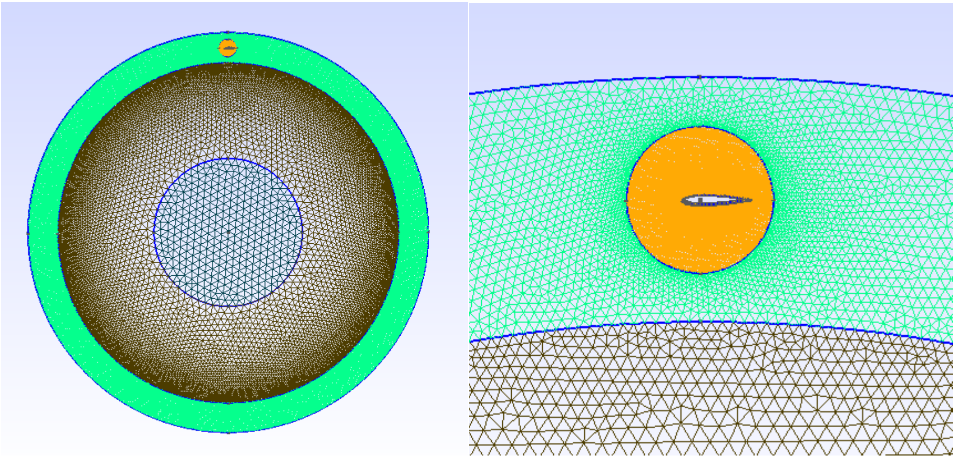

(A) (B)

Fig. 6.1: Mesh Scheme1-Single Bladed Rotating Circular Model.

The computational domain consists of a rotating region containing the single blade and an external stationary region, with momentum and mass exchanged between them via a non-conformal interface. The size of the rotating region is significantly larger than in the oscillating airfoil model to reduce the influence of the blade's wake on its subsequent position within a single rotation cycle, thus more closely approximating the aerodynamic response of an "isolated rotating blade." The size of the external computational domain is also correspondingly enlarged to avoid interference from the inlet and outlet boundaries on the rotating flow field.

In the near-wall region, a multi-layered, finely meshed grid is applied to the blade surface to ensure that the boundary layer resolution meets the requirements of the turbulence model. The height of the first layer of mesh on the wall is controlled within a suitable range to maintain a low y+ value, thereby avoiding the use of wall functions and improving the prediction accuracy of unsteady aerodynamic forces. The relevant near-wall modeling strategies and parameter selections have been validated in the preceding chapters.

Regarding boundary conditions, a uniform free-flow velocity is applied at the inlet, a pressure outlet condition is used at the outlet, and lateral boundaries are set to far-field or symmetric conditions to reduce the influence of lateral constraints on the flow field. Rotational motion is applied directly to the rotor region by specifying an angular velocity, allowing the blades to rotate continuously in the inertial coordinate system.

The single-bladed rotating airfoil model uses the same numerical settings as the aforementioned VAWT model for the time step and the Courant–Friedrichs–Lewy (CFL) number. This time-progression scheme has been systematically tested and verified in the multi-bladed VAWT numerical simulation in the previous chapter, and it can accurately capture the unsteady evolution characteristics of aerodynamic forces and flow fields during rotation while ensuring numerical stability.

It should be noted that compared with the complete VAWT model, the number of rotating blades in this section is reduced to a single blade. However, since the linear and angular displacements of the blade per unit time during rotation remain consistent with the aforementioned model, its local time scale and numerical stability requirements have not changed fundamentally. Therefore, it is reasonable to continue using the time step and CFL number settings verified above.

Based on the above considerations, this paper does not make additional parameter adjustments to the time step and CFL number in the single-bladed rotating airfoil model. The relevant numerical settings effectively avoid unnecessary repeated verification while ensuring computational accuracy, providing a stable and reliable numerical foundation for subsequent periodic convergence analysis and unsteady adjoint optimization.

To verify the periodic convergence of the single-bladed rotating airfoil model in unsteady calculations, the variation of its aerodynamic moment coefficient with the rotation period was monitored and analyzed. Transient calculations were performed starting from the initial conditions, continuously calculating multiple complete rotation periods, with the periodically averaged aerodynamic moment coefficient used as the primary indicator of convergence.

The results show that the single-bladed rotating airfoil model achieves periodic convergence within a relatively short number of rotation periods. Compared to the two-dimensional two-bladed VAWT model used in Chapter 5, its aerodynamic moment coefficient rapidly stabilizes after the initial few periods, and the difference between adjacent periods is significantly reduced. This indicates that the flow field development process of this model is more stable, and the periodic solution is established faster.

It can be clearly seen that the single-bladed model requires significantly fewer convergence periods than the multi-bladed VAWT model. This phenomenon is physically plausible: the single-blade model lacks the cumulative effect of wakes between multiple blades and is free from interference from axial wakes. The flow field is primarily dominated by the single rotating blade, resulting in relatively simple induced effects and wake structures, making it easier to establish stable periodic flow patterns.

In the latest progress, several key adjustments were made to improve the accuracy and reliability of the rotating airfoil simulations. The optimization objective was shifted from the moment (M) to the moment coefficient (C_M), the timestep was reduced from 0.01 to 0.00174533, and stationary domains with explicit inlet and outlet boundary conditions were introduced. Additionally, efforts were made to clarify the proportional relationship between M and C_M observed in Fluent and to carry out model size independence tests.

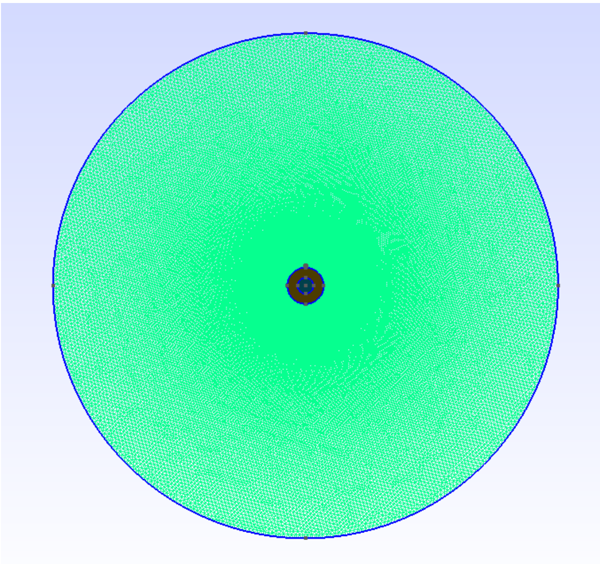

Fig. 6.2: Rotor Mesh Size Definition

A series of parametric studies were conducted to evaluate boundary definitions and domain scaling. For the farfield, the size was redefined relative to the airfoil chord length, with diameters of 50x, 100x, and 200x tested. The results indicated the sensitivity of the force predictions to the farfield distance.

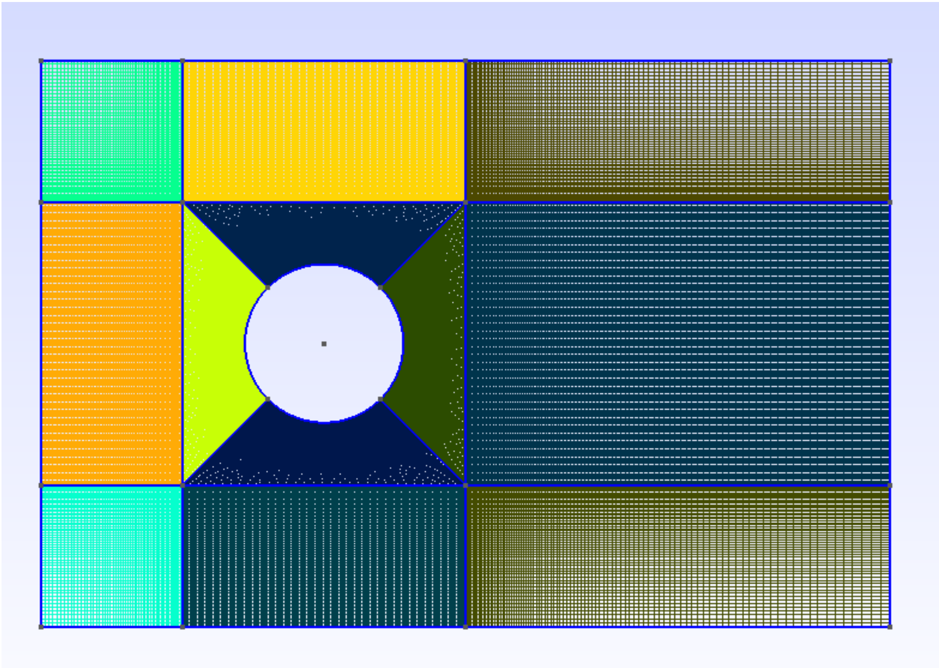

Fig. 6.3: Stator Mesh Size Definition

Table 6.1: Stator Mesh Sizing Study

Model	Grid	Local Refinement	Grid Type	Size (x)	Stationary
1-Blade	123200	Only the grid near the	quad	1/80	4x
Rotational	277200	rotating domain is	quad	1/80	6x
Airfoil	770000	refined	quad	1/80	10x

For the stationary domain, three relative diameters (4x, 6x, and 10x, where x is the diameter of the rotating domain) were assessed, along with three inlet unit lengths (also 4x, 6x, and 10x). These variations provided valuable insight into the influence of the computational domain size on the solution stability and accuracy.

Table 6.2: Reviews on Timestep, Radius, Omega and Airfoil Unit Displacement Study

Study	Timesteps per cycle	Radius/Omega	Unit Disp
Day et al. [18]	0.00174533s	0.5m/83.8rad/s	**0.07312m**
Angell et al. [78]	0.001s	12.5m/2.54rad/s	0.03175m
Celik et al. [151]	0.00072-0.00144s	0.375m/36.6rad/s	0.01979m

A refined timestep of 0.00174533 was used for displacement studies, which improvedthe temporal resolution of unsteady aerodynamic loads. Furthermore, model size independence tests were performed with different mesh resolutions, particularly varying the number of cells along the interface (400 and 800 units) to evaluate convergence of the average force on the baseline NACA0015 airfoil over one full rotation cycle. These tests confirmed trends in grid and domain scaling, thus helping to establish reliable meshing and timestep parameters for future optimization runs.

Table 6.3: Rotor Mesh Sizing Study

Model	Grid	Local Refinement	Grid Type	Max Size	Interface
1-Blade	43000	0.000001mm	Triangular	400	50x
VAWT	84000	initial height, 40	Triangular	400	100x
	176000	layers with 1.25		400	200x
	123000	height ratio	Triangular	800	50x
	286000		Triangular	800	100x
	614000			800	200x

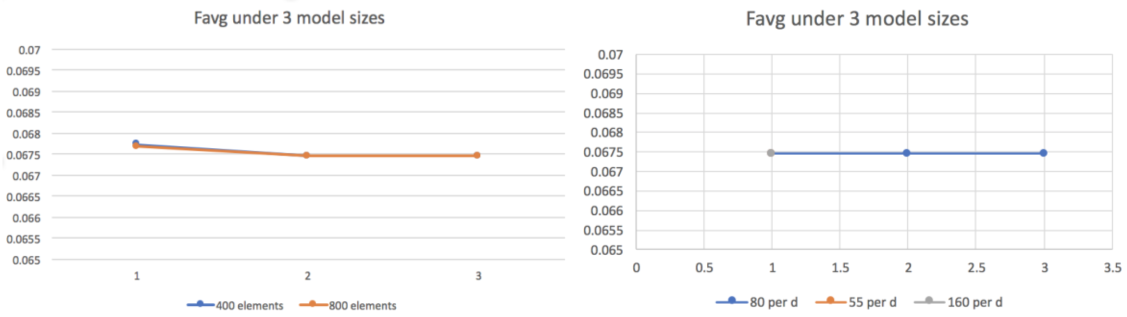

(A) (B)

Fig. 6.4: Airfoil and Stator Grid Element Independece Study on Favg.

According to the Fig. 6.4, the investigation has advanced the simulation framework by finalizing the use of the average force as the optimization metric, refining the temporal resolution, and systematically testing domain sizes and farfield definitions. These adjustments build a stronger foundation for consistent and accurate aerodynamic performance predictions of rotating airfoils in subsequent optimization studies.

6.3 Modeling and Validation of Double-Blade Rotational Airfoils

In contrast, in the multi-blade VAWT model, the wakes of each blade continuously superimpose and interact with each other inside the rotor and on the leeward side. Simultaneously, the axial wake further enhances the unsteadiness of the flow field, requiring the overall flow field to undergo more rotational cycles to reach statistical stability.

Scheme 1 employed a simplified Rotating-Circular model to represent a single blade moving within a steady inflow field. This prototype mesh consisted of relatively coarse, unstructured elements that could be quickly generated and modified. The key feature of this scheme was the use of a dynamic size ratio adjustment method in Gmsh, which allowed rapid scaling of the element density in critical flow regions such as the blade surface and wake zone, while maintaining coarser resolution in the far-field. This approach significantly reduced the computational time, making it ideal for the initial tests and parametric studies. The boundary conditions were implemented on a circular far-field boundary, with the blade rotating around a central axis. Although this mesh was relatively coarse, it proved effective in capturing the global aerodynamic trends, and it was especially useful for testing if the optimizer can operate during the trial-running.

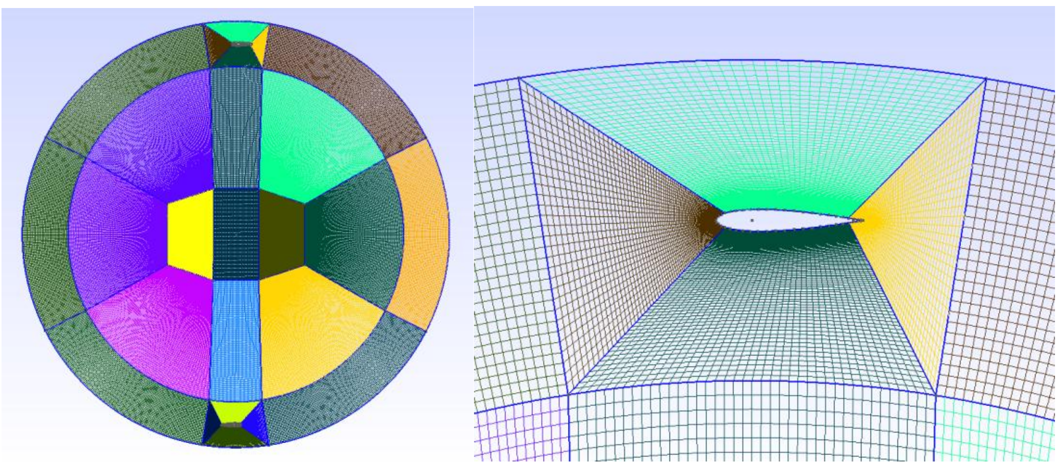

Fig. 6.5: Mesh Scheme2-Double Bladed Rotating Circular Model.

Scheme 2 was developed to improve the accuracy and capture finer details of the blade–wake interaction. A structured mesh was generated, with two distinct rotational zones: the inner rotor region containing the blades, and an outer stator region that enforced far-field boundary conditions. The use of multiple rotation domains allowed precise modeling of the relative motion between the blades and surrounding flow. Moreover, the mesh included a carefully modified size ratio, ensuring high resolution along the blade surfaces and in the near-wake, while gradually expanding to larger cells in the outer field. This hierarchical resolution not only enhanced the numerical accuracy but also stabilized the solver by avoiding abrupt element size jumps.

Both schemes were tested in the SU2 CFD framework, with pySU2 serving as the Python-based interface for case management and preliminary parallel computation tests. The workflow demonstrated that the meshes could be efficiently deployed for parallelized numerical simulation, and the code infrastructure can be readily extended to high-performance computing (HPC) environments if needed. The integration of Gmsh with pySU2 created a flexible pipeline: meshing, solver setup, and optimization routines could be coupled seamlessly, ensuring reproducibility and scalability of the simulations.

There are three main reasons for omitting the shaft. First, the shaft wake significantly enhances the flow field unsteadiness on the leeward side, thus delaying the establishment of periodic solutions. In this study, the focus is on the aerodynamic behavior of the rotating blades themselves and their impact on the optimization process; therefore, shaft interference is deliberately eliminated to obtain faster and clearer periodic convergence characteristics. Second, removing the shaft effectively reduces the complexity of wake superposition, ensuring that the interaction between the two blades is primarily blade-to-blade wake interference rather than multi-source wake coupling. Third, at the optimization implementation level, the shaftless geometric configuration is more conducive to the symmetrical mapping and synchronous update of the accompanying sensitivity, thus simplifying the optimization process.

Similar to the single-blade rotating model, in the two-blade model, both airfoils move at a constant angular velocity within the same rotational region, and their instantaneous relative inflow is entirely determined by the rotational motion. Since the two airfoils are geometrically and kinematically symmetrical, their aerodynamic response should have only a 180° phase difference under ideal periodic convergence conditions. Based on this symmetry, this study only performs aerodynamic monitoring and sensitivity calculations on one airfoil, while the aerodynamic behavior of the other airfoil is implicitly included through phase translation.

Regarding the implementation of unsteady adjoint optimization, SU2's design variables and mesh deformation (DEFORM) module allows the same set of sensitivity fields to be mapped to multiple geometric entities. In this study, after the adjoint solver calculates the sensitivity distribution of the monitored airfoil over a complete 0-360° rotation cycle, this sensitivity information is simultaneously applied to the geometric updates of both airfoils. Specifically, the node updates of the second airfoil are achieved by applying a 180° angular phase difference to the sensitivity field of the first airfoil, thus ensuring that the two airfoils always maintain strict consistency in shape changes.

This approach is physically reasonable: for a two-blade rotating system, the aerodynamic process experienced by one airfoil from 0-180° is completely equivalent to the process of the other airfoil from 180-540° (discussed in later Section 6.3 and Section 6.5), with a phase difference only in the windward and leeward sequence. Therefore, by performing sensitivity calculations on a single airfoil and simultaneously updating both airfoils, the computational costs of adjoint solutions and geometric updates can be significantly reduced, while also avoiding asymmetric deformation problems caused by numerical noise.

In the two-bladed rotating airfoil model, the two airfoils satisfy the following conditions: perfect geometric consistency and identical rotational angular velocities. Flows with a fixed spatial phase difference of 180° satisfy rotational symmetry after periodic convergence.

Therefore, the same initial blades have an aerodynamic history theoretically equivalent to those with an aerodynamic history of $\theta \in [180,540] \approx 0,360$. The difference lies only in whether the leeward or frontal flow occurs first (phase difference), not in the flow physics. Therefore, for any complete cycle, the objective function, such as the periodic average C_M or CT, is expressed as follows:

$$\frac{\partial J}{\partial x_1} = \frac{\partial J}{\partial x_2} \qquad [Eq. 6.22]$$

This equation holds numerically under periodic convergence conditions. If the two airfoils share the same set of design variables, their deformation directions and amplitudes are completely identical and automatically maintain symmetry, which is most conducive to maintaining stable values. The reason this study did not choose to calculate the adjoints for each airfoil separately, besides saving half the adjoint cost, is that numerical noise causes the airfoil shapes to be inconsistent, easily violating rotational symmetry. This method is only necessary when monitoring only a specific window region during optimization.

In summary, the two-bladed rotating airfoil model, while maintaining numerical efficiency and convergence, introduces fundamental multi-bladed interaction characteristics and provides a suitable numerical platform for subsequent in-situ unsteady adjoint optimization that is more representative of engineering applications.

6.4 Unsteady Adjoint Optimization

This section, building upon the unsteady adjoint optimization framework established in Chapter 5, further extends and applies this method to the rotational airfoil model. Unlike oscillating airfoil optimization, the optimization process in this chapter is performed directly in the rotating reference frame, with the blades always in a true rotor motion state. This allows for the extraction of more physically consistent sensitivity information without the need for equivalent inflow correction. It should be noted that although adjoint solvers have been systematically applied to strongly unsteady problems (such as oscillating airfoils), their application in in-situ optimization of VAWT rotating blades has been limited to snapshot studies. Therefore, the adjoint settings and optimization process for the rotational airfoil model in this chapter need to be redesigned to ensure numerical stability and the repeatability of optimization results.

6.4.1 Objective Functions

This chapter continues the basic idea from Chapter 5, directly using the tangential force contribution related to rotor power output as the optimization objective. In the rotating airfoil model, the objective function is defined as the tangential force coefficient of the blade during rotation. Its calculation is based on the projection of instantaneous aerodynamic forces onto the rotor's tangential direction, and is performed through time integration or averaging within a given time window.

It should be noted that the objective change defined in this chapter still corresponds to a performance improvement in the time-averaged sense. However, since the flow characteristics experienced by the rotating airfoil at different azimuth angles vary significantly, an improvement in local instantaneous performance is not necessarily equivalent to an improvement in overall average performance. Therefore, unlike Chapter 5, the subsequent optimization process adjusts the time window settings multiple times and extracts sensitivity information for different flow stages multiple times to enhance the applicability of the optimization results under different operating conditions.

6.4.2 Optimization Procedure and Setup

This chapter employs SU2's unsteady adjoint solver for aerodynamic optimization of a rotating airfoil model. Similar to Chapter 5, the adjoint solver does not directly output the optimized blade geometry; instead, it generates sensitivity distribution information of the objective function relative to nodal displacements on the blade surface. This sensitivity information is then applied to the blade surface via a mesh deformation module to achieve geometric updates.

In the rotating airfoil model, the mesh deformation region is defined as the area surrounding the blade wall and its local rotating subdomain, excluding the external static flow field region. This setting ensures that blade geometric changes are smoothly absorbed by the surrounding mesh, while avoiding unnecessary impacts on the far-field boundary and rotating interface. However, the size of the deformation region differs from that in Chapter 5, although the degree of local mesh refinement around the blade remains the same.

After completing the sensitivity calculations and applying geometric constraints, all sensitivity information is processed under a unified reference attitude to avoid orientation inconsistencies introduced by the rotating coordinate system. Mesh deformation is then performed to generate a new rotating airfoil geometry. The updated geometry model is then recalculated unsteadily and undergoes at least three complete rotational cycles. The evaluation of the optimization effect is based on the aerodynamic results of the last cycle, thus ensuring that the performance indicators being compared correspond to the cycle convergence state.

6.4.3 Design Variables and Constraints

Similar to Chapter 5, nodal displacements on the blade surface and within the deformation region are used as design variables in the optimization process. Sensitivity information and mesh deformation are both completed at the nodal level.

In shape optimization, DV is commonly defined in two ways: parametric DV (e.g., the Hicks–Henne bump) and FFD (Freeform Factorization) control points (described using FFD box names and control point indices). Design variables are defined in the local geometric parameter space that moves with the blade (e.g., FFD control points or chord-direction parameter positions), moving synchronously with the blade geometry during rotation, rather than applying displacement along fixed global x, y directions.

The accompanying surface sensitivity is defined through the airfoil's local normal, which is the rate of change of the objective function with respect to the infinitesimal displacement of the surface along the normal. The key to its application is that after the gradient is mapped to DV, the direction of the moving surface nodes during the mesh deformation stage needs to be redefined.

This study defines the geometric update as the displacement scalar of surface nodes along the local normal, and recalculates the surface normal based on the current shape during each geometric update, ensuring that the deformation direction is always perpendicular to the local surface.

For the two-blade rotating model, based on its geometric and operational symmetry, sensitivity is extracted for only one blade, and geometric deformation is applied synchronously to the other blade, thereby maintaining rotor configuration consistency without introducing additional design variables.

6.4.4 Window Controlling

Given the significant differences in flow characteristics experienced by rotating airfoils at different azimuth angles, this chapter introduces more time window control strategies to selectively extract sensitivity information for specific flow stages. By adjusting the length and position of the time window, optimization can be performed separately for the upwind side, leeward side, or the entire rotation cycle. Specifically, this paper sets up multiple window formats, including only the upwind azimuth interval, only the leeward interval, and covering the entire rotation cycle, to study the impact of different flow stages on the optimization results.

6.4.5 Optimization Workflow

Based on the aforementioned unsteady adjoint modeling method and parameter settings, this paper constructs an aerodynamic optimization process suitable for rotational airfoils, the overall idea of which is as follows:

Stage 1: Create a single-blade CFD mesh model and configuration file. Then create a double-blade CFD mesh model and configuration file with the same sizing.

Stage 2: After the baseline single-blade model completes three rotational cycles, plot the tangential force coefficient of the baseline airfoil as a function of time and angle of attack (AoA).

Stage 3: Using the last cycle as a window, calculate sensitivity through discretization. If additional constraints exist, apply constraint penalties.

Stage 4: Perform corresponding airfoil deformation based on the scaling factor. The double-blade CFD mesh model requires additional programming for synchronized deformation.

Stage 5: Re-output the configuration file and continue calculations. After the new blade completes three rotational cycles, plot the tangential force coefficient of the baseline airfoil as a function of time and angle of attack (AoA).

Stage 6: Repeat stages 3-5, iterating sequentially. Manual or automatic operation can be used until the airfoil approaches the optimized shape.

Stage 7: This stage repeats simulation operation 1, requiring changes to the window settings, specifically using both upwind and downwind modes.

Stage 8: This stage repeats simulation operation 2, changing the TSR (Transient Stream Ratio), i.e., the pitch-equivalent AoA profile.

Stage 9: This stage repeats simulation operation 3, changing the free-flow wind speed value, i.e., the pitch-equivalent relative wind speed function.

Through the above process, this paper systematically verifies the feasibility of the unsteady adjoint optimization method in rotating airfoil models and lays the methodological foundation for optimization research based on the complete VAWT configuration. The reason for adopting repeated simulations is explained in Appendix G.

6.5 Aerodynamic Performance on Rotational Airfoils

After establishing and performing unsteady adjoint optimization on single-blade and two-blade rotating airfoil models, this section systematically evaluates the aerodynamic performance of the candidate optimized airfoils under rotating conditions. By comparing the aerodynamic response and time-averaged performance indices of the optimized airfoil and the baseline airfoil during rotation, the effectiveness of in-situ optimization of the rotating airfoil in improving tangential force contribution and overall aerodynamic stability is examined.

This section analyzes the single-blade and two-blade rotating airfoil models separately, evaluating the consistency and differences of the optimization results under different rotating configurations. The results not only verify the effectiveness of the proposed optimization method under rotating conditions but also provide necessary evidence for subsequent performance comparisons with the complete VAWT model.

6.5.1 Candidate Airfoil Performance on Single-Blade Rotational Airfoils

After unsteady adjoint optimization based on a single-blade rotating airfoil model, the aerodynamic performance of the resulting candidate airfoils was systematically evaluated. The results show that, compared with the baseline airfoil, the optimized airfoil achieves stable performance improvement in the single-blade rotating model, verifying the effectiveness of the in-situ rotating optimization method in improving tangential force contribution.

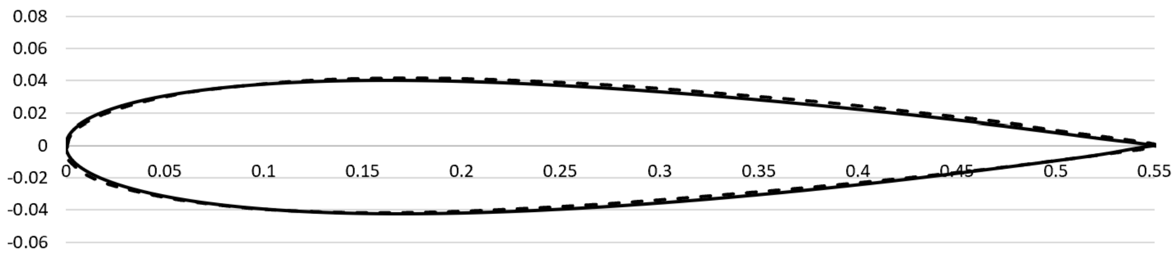

Fig. 6.6: 1st Generated Optimized Airfoil NACA0015 in Single Bladed Rotaional Model

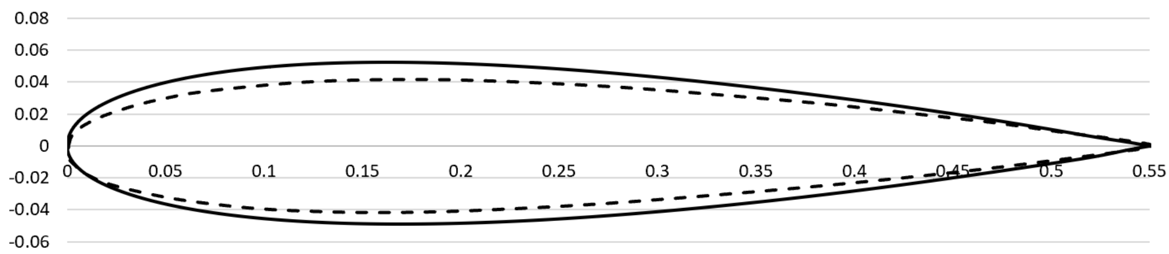

Fig. 6.7: Final Optimized Airfoil NACA0015 in Single Bladed Rotaional Model

Figures 6.6 and 6.7 show the geometric shape comparison of the airfoil obtained in the first and final iterations of the optimization process, respectively. It can be observed that as the optimization iterations progress, the airfoil gradually forms local geometric adjustments with asymmetric characteristics in the leading edge and suction surface regions. These changes reflect the optimizer's response to unsteady incoming flow conditions during rotation, and its geometric evolution trend differs from the results obtained based on the oscillating airfoil model, more directly reflecting the influence of actual rotational motion on the airfoil's aerodynamic characteristics.

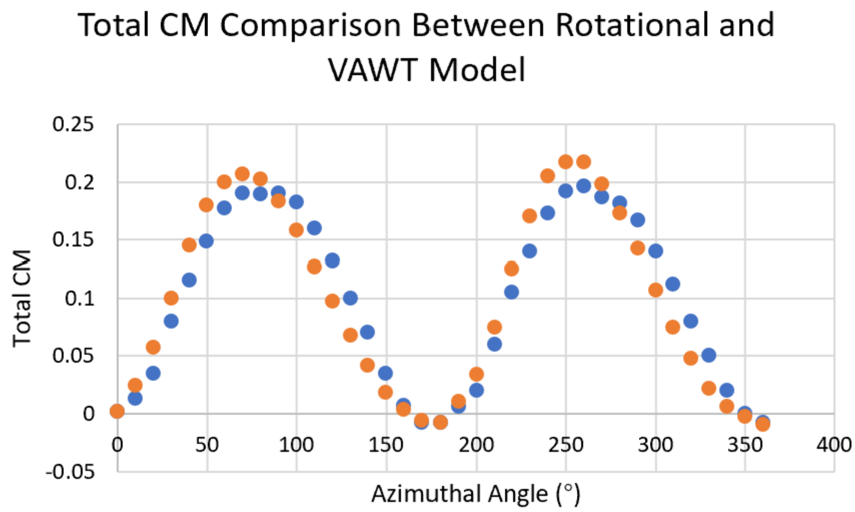

Fig. 6.8: Total C_M Comparison Between Rotational and VAWT Model.

To further understand the aerodynamic mechanisms resulting from geometric changes, Figure 6.8 shows a comparison of the moment coefficient of the airfoil at different azimuth angles from 0 to 360°. The results show that in the windward direction, the optimized airfoil effectively improves the pressure distribution near the leading edge and maintains more stable attached flow over a wider angle of attack. In the leeward direction, although the flow is significantly affected by wake and induced effects, the optimized airfoil still exhibits a relatively reduced separation region and a smoother flow structure. This indicates that airfoil optimization not only enhances local peak aerodynamic forces but also improves flow stability throughout the entire rotation cycle.

Overall, the performance evaluation results under the single-blade rotating airfoil model demonstrate that unsteady adjoint optimization can effectively improve the aerodynamic torque and power output of the airfoil under real rotating conditions. These results provide important reference for performance verification in subsequent two-blade rotating airfoil models and the complete VAWT model.

6.5.2 Candidate Airfoil Performance on Double-Blade Rotational Airfoils

In the two-bladed rotating airfoil model, the blades not only experience unsteady incoming flow induced by themselves during rotation, but also periodically traverse the wake region generated by the other blade, making their aerodynamic behavior more complex than that of the single-bladed model. This section focuses on analyzing the instantaneous flow characteristics and overall performance of the optimized airfoil under two-bladed rotating conditions to evaluate the effectiveness of in-situ rotation optimization under multi-bladed interaction conditions.

Table 6.4: Total Moment Coefficient of the Airfoils at Specific Azimuthal Angle.

Azimuthal Angle	Baseline	Optimized	% increase
60°	0.0342	0.0365	6.73%
90°	0.0342	**0.0374**	9.36%
120°	0.0342	0.0354	3.51%
210°	0.0342	0.0356	4.09%

Table 6.4 shows instantaneous flow snapshots data of the airfoil at typical azimuth angles of 60, 90, 120, and 210. These azimuth angles correspond to key positions of the blade in the windward section, the windward-leeward transition zone, and after traversing the wake of the preceding blade in the leeward section. It can be observed that at azimuth angles related to wake traversal (especially around 165 and 195), the incoming flow velocity decreases significantly and the turbulence intensity increases, leading to significant changes in the pressure distribution and separation morphology on the airfoil surface. Compared to the baseline airfoil, the optimized airfoil exhibits a smoother flow reorganization process and a reduced local separation region under these wake-dominated conditions, indicating a stronger adaptability to wake interference.

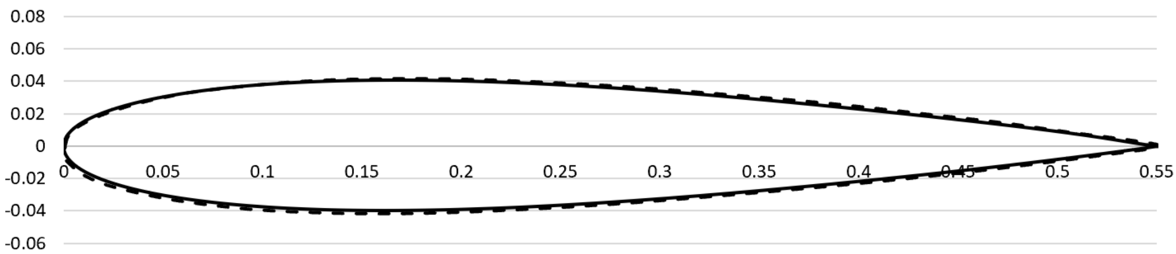

Fig. 6.9: 1st Generated Optimized Airfoil NACA0015 in Double Bladed Rotaional Model

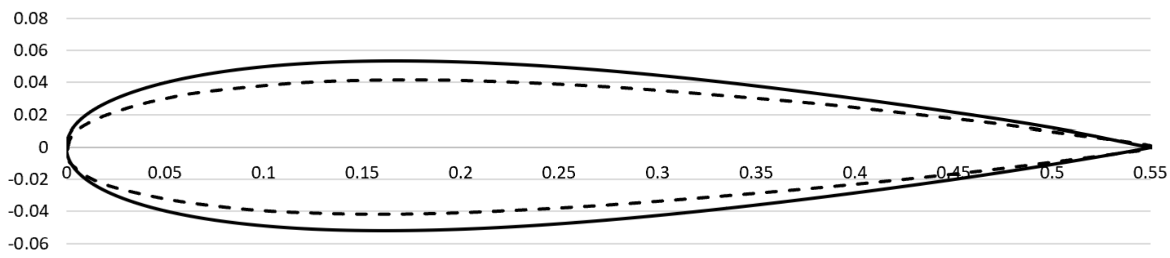

Fig. 6.10: Final Optimized Airfoil NACA0015 in Double Bladed Rotaional Model

Figures 6.9 and 6.10 show the geometric shape comparison of the airfoil obtained in the first and final iterations of the optimization process in the two-blade rotating model, respectively. It can be seen that the airfoil undergoes a geometric adjustment with obvious asymmetric characteristics during optimization. This adjustment is not simply aimed at improving the performance of the frontal section, but also considers the aerodynamic response of the blades after passing through the wake. This geometric evolution trend reflects the optimizer's comprehensive trade-off of the unsteady aerodynamic characteristics caused by multi-blade interactions in a periodically averaged sense.

The results show that although the wake superposition effect is enhanced and the flow complexity is increased under the two-blade configuration, the optimized airfoil still achieves a stable performance improvement compared to the baseline airfoil. This demonstrates that the unsteady adjoint optimization method based on single-blade and two-blade rotating models can extract geometric adjustment directions beneficial to overall power output even under conditions with significant blade-wake interactions.

After the optimization process, the baseline NACA0015 airfoil gradually evolved into a thinner section. After 4 iterations, the profile showed reduced thickness and smoother camber adjustments, aligning more closely with a NACA0012-type shape. Continuing the optimization, by around 8 iterations, the geometry effectively converged towards the NACA0012 profile, indicating that the adjoint-based deformation consistently guided the airfoil from the original thicker section towards a more aerodynamically efficient thinner configuration.

The optimization results demonstrate a clear improvement in the power coefficient for both baseline airfoils. For the NACA0015, the average power coefficient increased from 0.3121 to 0.3174 after optimization, reflecting a modest but consistent gain in aerodynamic efficiency. In comparison, the NACA0012 exhibited a larger improvement, with its power coefficient increasing from 0.2711 to 0.3010. These outcomes indicate that the adjoint-based optimization framework is effective in enhancing the turbine performance, and that thinner initial profiles such as the NACA0012 may benefit more significantly from shape optimization than thicker profiles such as the NACA0015.

6.6 Summary

This study validates the feasibility and effectiveness of directly applying the fully unsteady adjoint optimization method to the aerodynamic optimization problem of vertical axis wind turbine (VAWT) blades. By introducing a rotating airfoil model, the optimization process can directly consider key unsteady effects such as wake evolution, multi-blade interactions, and true induced velocities within a rotating reference frame. In contrast, these factors exhibit only limited influence in simplified models such as oscillating airfoils, but are crucial to the reliability and robustness of the optimization results at the full rotor scale.

In the rotating airfoil model, the temporal evolution characteristics of blade aerodynamics are more accurately characterized. Specifically, the angle of attack corresponding to different blade rotation positions exhibits a clear and continuous variation law, and the induced velocity is naturally generated by the flow field solution, rather than relying on piecewise empirical function fitting. This makes the rotating airfoil model physically more consistent with traditional piecewise or quasi-steady methods in describing the unsteady aerodynamic behavior of VAWTs. Optimization based on this model significantly improves the rotor's average power coefficient, with performance significantly superior to the benchmark NACA0015 airfoil. Meanwhile, with the advancement of optimization iterations, the shape changes of the blades on both the upwind and leeward sides became more significant, exhibiting stronger asymmetric characteristics compared to the aforementioned candidate airfoils.

Further analysis shows that the airfoils obtained from partial-cycle optimization and full-cycle optimization exhibit significantly different aerodynamic performance characteristics under high and low wind speed conditions. The results indicate that the airfoil geometry is highly sensitive to the local inflow velocity around the blades, meaning that optimization on the leeward side can also substantially contribute to overall performance, not just in areas difficult to explain scientifically (such as low-torque regions like 0 or 180 degrees, where performance improvements may be due to errors). Flow field analysis of the optimized airfoil shows that localized periodic optimization can effectively suppress flow separation, and the resulting asymmetric airfoil exhibits superior aerodynamic performance compared to other airfoils under wake conditions. The full-cycle optimized airfoil achieved an improvement in power coefficient throughout the entire rotation cycle. This improvement is reflected not only in performance enhancement under complex wake and multi-blade interference conditions but also in the overall enhancement of the tangential force coefficient under the original inflow wind speed conditions.

The innovation of this study lies in its first systematic application of a fully unsteady adjoint optimization framework directly to rotating VAWT blades, rather than relying on simplified or quasi-steady models. By introducing real-time, precise blade kinematics, naturally formed induced velocities, and full-cycle aerodynamic behavior encompassing wake interactions and multi-blade effects, this method captures key physical mechanisms that traditional steady-state or piecewise methods struggle to reflect. This not only significantly improves the reliability of the optimization results but also deepens the physical understanding of how periodic asymmetric airfoils enhance performance throughout the rotor cycle.

Chapter 7

Towards 2.5D VAWT: Performance of the 2D Optimized Airfoil

7.1 Overview

The preceding chapters, based on a two-dimensional cross-sectional model, systematically conducted unsteady adjoint optimization studies under oscillating and rotating airfoil conditions, and verified the aerodynamic rationality of the proposed method at the rotor scale. However, the aerodynamic performance of actual VAWTs is not only affected by the aerodynamic characteristics of the two-dimensional cross-section, but also significantly constrained by finite span, end effects, and three-dimensional flow structures. Therefore, it is necessary to further introduce the airfoil obtained from the two-dimensional optimization into a three-dimensional rotor model to evaluate its performance and applicability under more realistic operating conditions.

This chapter constructs a three-dimensional numerical model of a H-blade VAWT, systematically modeling and verifying its aerodynamic characteristics. Based on this, the candidate optimized airfoils obtained in the previous sections are applied to the three-dimensional rotor model and compared with the benchmark airfoil, focusing on evaluating their impact on overall power output and aerodynamic force distribution. Through this three-dimensional verification process, this chapter aims to verify the generalizability of the two-dimensional unsteady optimization method in a real rotor environment and provide more convincing performance evidence for the engineering application of optimized airfoils.

7.2 3D-Modelling of H-Blade VAWTs

This chapter optimizes a two-dimensional airfoil cross section using a transient adjoint method and extends the study to the three-dimensional performance of the optimized airfoil when applied to a full vertical-axis wind turbine (VAWT) model. While two-dimensional optimization captures key unsteady aerodynamic mechanisms of oscillating and rotating airfoils, such as lift-drag variations, flow separation, and tangential force enhancement, it inherently ignores the complex three-dimensional flow phenomena that occur in real turbine operation. These phenomena include spanwise flow migration, tip vortices, and induced velocity gradients, all of which affect the effective angle of attack and the rotor's overall aerodynamic efficiency.

The primary objective of this chapter is to evaluate how the aerodynamic advantages gained from the two-dimensional optimization translate to a real three-dimensional environment to ensure that the improvement in the blade-cycle-averaged power coefficient is not due to errors introduced by simplifications in the 2D model. The optimized airfoil is implemented spanwise in a full three-dimensional CFD model, and its performance is compared to a baseline NACA0015 configuration under identical operating conditions. The analysis focuses on the improvement in power coefficient, the pressure and velocity field distributions, and the vortex dynamics during both the upwind and downwind phases of rotation.

Theoretically, because the optimized airfoil retains its excellent aerodynamic properties in the mid-span region, the local flow conditions in this region are very similar to those assumed in 2D simulations. The enhanced curvature and asymmetric pressure distribution of the optimized airfoil promote delayed flow separation and enhanced tangential coefficient in this region, resulting in significant improvements in turbine torque and total power output. However, a key detail is that at the blade tip and root, three-dimensional effects dominate. In particular, the presence of tip vortices, radial velocity components, and wake interference alter the local flow topology, thereby reducing the magnitude of the 2D CFD gains.

Despite these spanwise variations, 3D CFD simulations confirm that the adjoint-optimized airfoil provides measurable and physically consistent performance improvements compared to the baseline design. The first part of this chapter describes the performance of existing candidate airfoils in a 3D model. The second part proposes a layered optimization approach and reshapes the model to mitigate some potential issues introduced by 3D effects. The presented analysis establishes the critical connection between cross-sectional aerodynamic optimization and overall turbine performance, highlighting both the effectiveness and inherent limitations of directly applying 2D transient adjoint optimization results to 3D rotating systems.

From a physical standpoint, steady-state simulation is not scientifically sound for the VAWT model because it cannot account for the principal velocity components of the blades, especially when the airfoil is at 90° and 270°. Previous steady-state simulation snapshot studies [18] have shown that direct aerodynamic optimization on in-situ turbines can produce significant errors; however, in 3D models, it can be used for prior testing. By simulating the flow field variation along the z-axis of the blade, the optimal thickness for a 2.5D model can be accurately determined. Therefore, this study first performed steady-state simulations, and then conducted two full-cycle transient simulations at a specific thickness to compare the characteristics of the optimized airfoil.

Currently, there are two mature methods for 3D optimization: one is layered optimization of the 2D cross-section, suitable for blades with a small cross-section-to-length ratio; the other is based on FFD, which is generally more practical and easier to deform the mesh. The implementation method and approach can be found in the manual extraction method in Chapter 6, but it requires significant computational power to complete the numerical solution of the flow field.

Since the focus of this study is to propose an optimization methodology applicable to vertical axis wind turbine airfoil design and to verify its effectiveness, the complex and computationally expensive shape optimization process based on numerical solutions of three-dimensional unsteady flow fields is not discussed in this paper. This study uses a two-dimensional optimized airfoil as input and constructs a three-dimensional H-type VAWT numerical model through geometric extrapolation. Specifically, the optimized airfoil is imported into the three-dimensional modeling process as coordinate parameters and stretched along the span to generate a straight-blade structure with a finite span, thus forming a two-blade H-blade rotor configuration. This modeling method ensures the consistency of the airfoil cross-sectional geometry in the spanwise direction, allowing the three-dimensional model to directly reflect the aerodynamic performance of the two-dimensional optimization results in the space structure.

The established three-dimensional VAWT model contains two straight blades, symmetrically arranged along the rotor circumference, and their rotation mode is consistent with the aforementioned two-dimensional model. To avoid introducing additional end controls or unnecessary complex structures, this study does not include winglets. In the spanwise direction, symmetrical boundary conditions are used for both the upper and lower boundaries, with an approximate idealized infinite span assumption, and the three-dimensional effects are mainly limited to the influence caused by the finite span and the development of spatial flow.

The main geometric and operational parameters of the 3D model, including rotor dimensions, blade chord length, span, rotational speed, and incoming flow conditions, are consistent with the aforementioned 2D study, and their specific values are listed in Table 7.1. In this way, the impact of airfoil geometry optimization itself on the overall aerodynamic performance of the 3D rotor can be evaluated with minimal interference from variables.

The three-dimensional (3D) computational model in this study is based on the Delft University H-type vertical axis wind turbine (VAWT) prototype, which has become a canonical configuration for validating CFD simulations of straight-bladed VAWTs. The turbine was designed to reproduce realistic Reynolds numbers for small-scale wind energy systems while remaining compatible with both experimental and numerical analysis environments. It serves as a well-characterized physical reference for the present 3D CFD investigation.

The turbine consists of two straight blades mounted on diametrically opposite sides of a central shaft, forming a classic H-type rotor with a diameter $D = 1.0$ m and a blade span $H = 1.0$ m, resulting in an aspect ratio (AR) = 1.0. Each blade is a straight extrusion of an aluminum NACA 0015 airfoil profile with a constant chord length $c = 0.06\ m$.

The overall solidity of the rotor is thus given by:

$$\sigma = \frac{Nc}{\pi D} = \frac{2 \times 0.06}{3.14 \times 1.0} = 0.11 \qquad [Eq. 7.1]$$

which lies within the moderate-solidity range suitable for efficient energy extraction at the tip speed ratios (TSR) of 4.5.

A Cartesian coordinate system is adopted with the origin at the turbine's rotation center. The x-axis is aligned with the freestream wind direction (positive downstream), the y-axis points toward the upwind side, and the z-axis points upward. The turbine rotates counterclockwise when viewed from above, corresponding to a positive rotational direction.

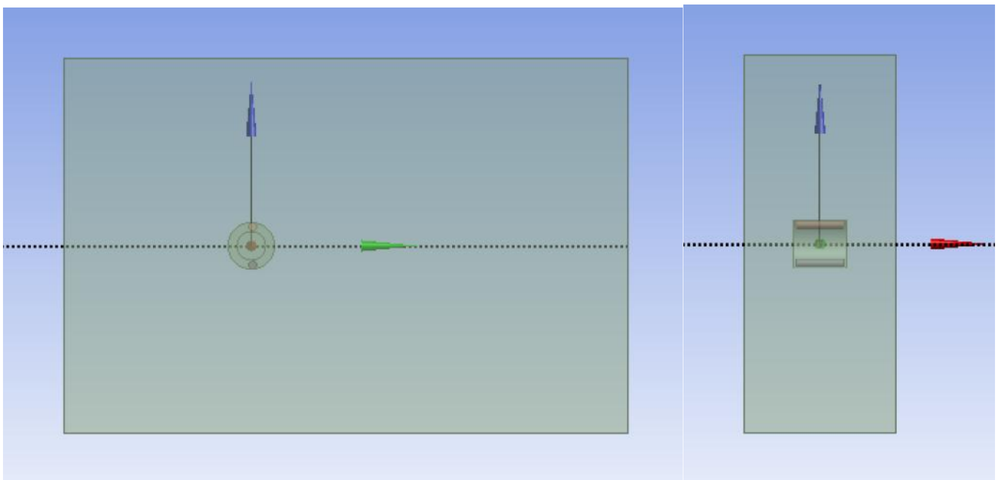

(A) (B)

Figure 7.1: (A) Top view and (B) Left view of the 3D VAWT model.

The computational domain was constructed to reproduce open-jet wind tunnel conditions, while minimizing blockage and reflection effects. A cylindrical domain with a diameter of 10D and a length of 15D was used. The upstream inflow boundary was positioned at 5D ahead of the rotor plane, and the outlet was placed 10D downstream to capture wake recovery. Side and top boundaries were treated as symmetry planes or pressure outlets depending on the specific simulation, and the bottom boundary was modeled as a smooth no-slip wall to emulate the floor of the test section.

At the inlet, a uniform velocity of 9.3m/s and turbulence intensity of 0.5% were prescribed, consistent with the Open Jet Facility (OJF) conditions reported by Delft University [138]. The pressure outlet was set at zero gauge pressure. The turbine blades and struts were assigned rotating wall boundary conditions with no-slip surfaces, and the motion of the rotor was driven by a prescribed angular velocity corresponding to the desired TSR.

A hybrid unstructured grid was generated using tetrahedral elements with prism layers near the blade surfaces to resolve the boundary layer accurately. The first-layer thickness was set to maintain y^+≈ 1, ensuring wall-resolved turbulence modeling without wall functions. Local refinement was applied around the blade tips and strut–blade intersections to capture tip vortices and interaction effects. The total cell count for the final grid was approximately 1.25 million elements, which was verified for grid convergence by comparing torque coefficient and instantaneous pressure distributions across three grid densities.

When using transient simulation, The turbine motion was simulated using time-accurate URANS with second-order implicit time stepping. Each revolution was divided into 720 steps, providing a temporal resolution of 0.5° in the azimuth. Simulations were advanced until periodic convergence was achieved after 3 revolutions, with the last revolution used for data averaging. The instantaneous torque Q(θ) on each blade was integrated over one revolution to obtain the mean power coefficient:

$$C_P = \frac{Q\,\omega}{\frac{1}{2}\rho U_\infty^3 A} \qquad [Eq. 7.2]$$

where $A = D \times H$ is the rotor swept area, the tangential coefficient and azimuthal variations of aerodynamic forces were also extracted for analysis.

7.3 Candidate Airfoil Performance

After establishing and validating the 3D H-blade VAWT numerical model, this section introduces the candidate optimized airfoils obtained in the preceding chapters into the 3D rotor model to systematically evaluate their aerodynamic performance under real 3D operating conditions. This analysis aims to verify the generalizability of the results obtained from 2D unsteady optimization and in-situ optimization of rotating airfoils in a 3D environment, and further compare the impact of different optimization strategies on overall rotor performance.

Specifically, this section examines the performance of airfoils based on pitch-optimized and rotation-optimized airfoils in the 3D H-blade VAWT, respectively, and compares them with the baseline airfoil. Performance evaluation not only focuses on time-averaged power or torque indices but also analyzes the stability and consistency of the optimized airfoil throughout the entire rotation cycle, incorporating periodic aerodynamic force variations.

Through these comparisons, this section provides direct evidence for subsequently summarizing the correlation between 2D and 3D optimization results.

7.3.1 Snapshot Aerodynamic Performance of Candidate Airfoils

In steady-state three-dimensional numerical simulation, the flow of a single blade of an H-type vertical axis wind turbine exhibits significant spatial non-uniformity, but also has a spanwise region with obvious two-dimensional characteristics. Based on the three-dimensional steady-state flow field results, this study systematically analyzed the aerodynamic response of the blade at different azimuth angles and spanwise positions. The results show that the blade aerodynamic performance is most sensitive to geometric changes at an azimuth angle of approximately 120°. This conclusion has been verified by the aforementioned snapshot-based optimization: near this azimuth angle, the peak moment coefficientC_M of the optimized blade is significantly improved, with a maximum increase of approximately 0.06, while the power coefficient C_P is also significantly improved, with an increase of approximately 0.023 [18]. Although the relative inflow velocity in this region is not the maximum value over the entire circumference, its response to airfoil geometric changes is extremely sensitive, exhibiting the typical characteristics of "low relative velocity – high aerodynamic sensitivity," and is therefore considered the key azimuth angle region most suitable for two-dimensional or 2.5D parametric modeling and optimization.

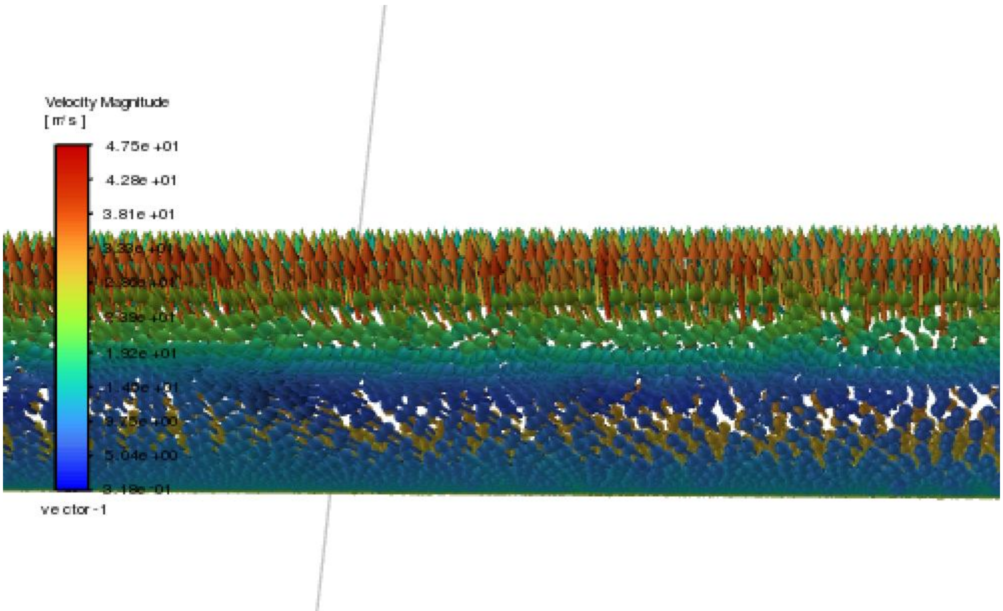

Figure 7.2: Surface Velocity Vectors at 30%-70% of the Airfoil Midsection at the Snapshot of 120°.

Figure 7.2 shows the distribution characteristics of the blade surface velocity vector along the spanwise (z-direction). It can be observed that within the spanwise region of the mid-blade, the direction and magnitude of the velocity vector change very little along the z-direction, indicating that the flow in this region has strong two-dimensionality, and the influence of spanwise flow and three-dimensional effects on local aerodynamic characteristics can be ignored.

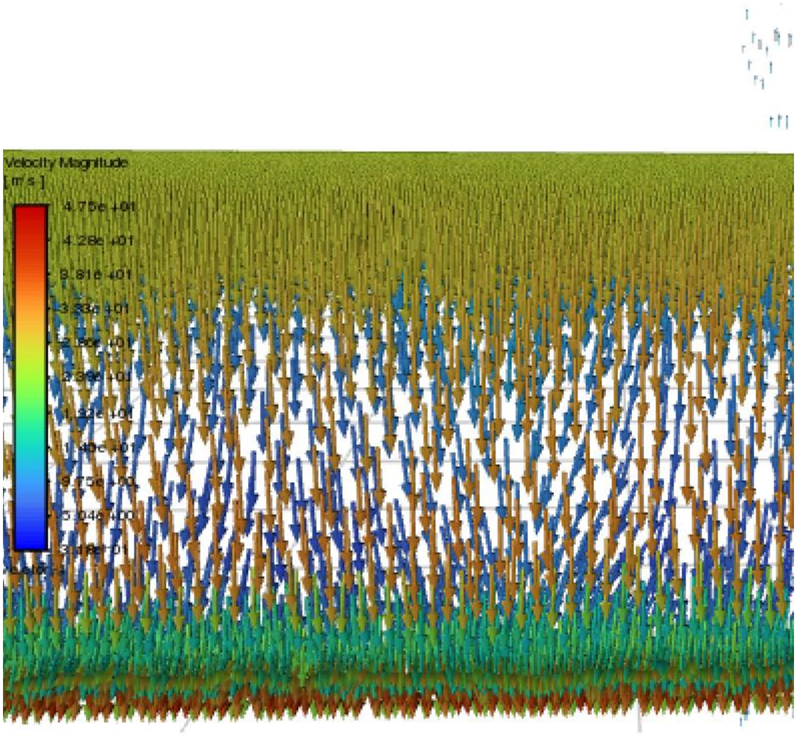

Figure. 7.3: Surface Velocity Vectors at 40%-60% of the Airfoil Midsection at the Snapshot of 120°.

Figure 7.3 is a magnified view of this region, further demonstrating that even under the extreme condition of maximum velocity on the upper surface and minimum velocity on the lower surface of the airfoil at a negative angle of attack, the surface velocity field maintains a high degree of consistency along the spanwise direction, without significant spanwise shear or velocity gradient. This phenomenon indicates that within this spanwise range, the aerodynamic load on the airfoil is mainly dominated by the two-dimensional flow of the cross-section.

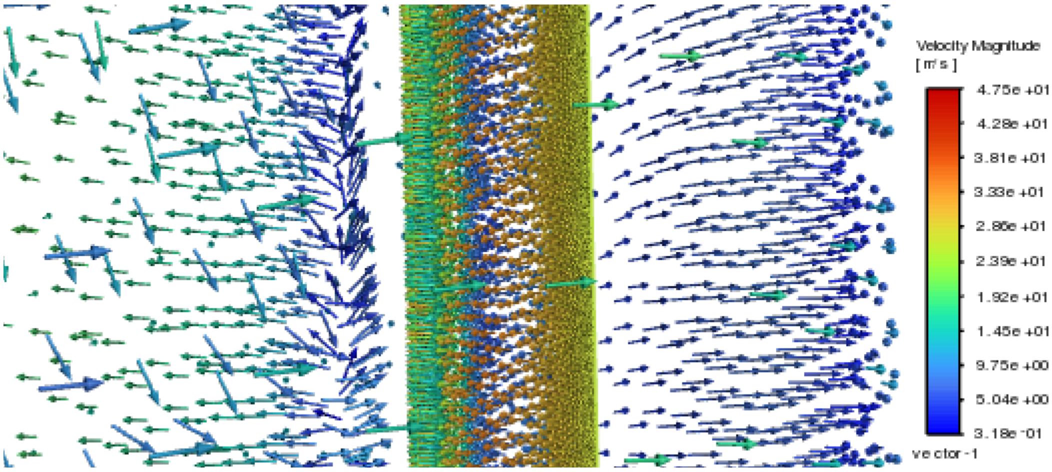

Figure. 7.4: Surrounding Velocity Vectors at 30%-50% of the Airfoil Midsection at the Snapshot of 120°.

Figures 7.4 and 7.5 show the overall motion characteristics of the three-dimensional flow field around the airfoil. From the inner side of the blade (near the pivot point), a small local region shows a relatively turbulent distribution of airflow velocity direction and magnitude, exhibiting obvious unsteady and non-uniform characteristics. This is closely related to the complex induced velocity field and wake interference near the pivot point. In contrast, in the outer region of the blade, the z-component of velocity in the flow field increases significantly as the spanwise position approaches the blade tip, indicating that the tip effect and three-dimensional induced flow dominate in this region. This trend implies that the closer to the blade edge, the greater the error introduced by using two-dimensional or even steady-state two-dimensional models for aerodynamic prediction.

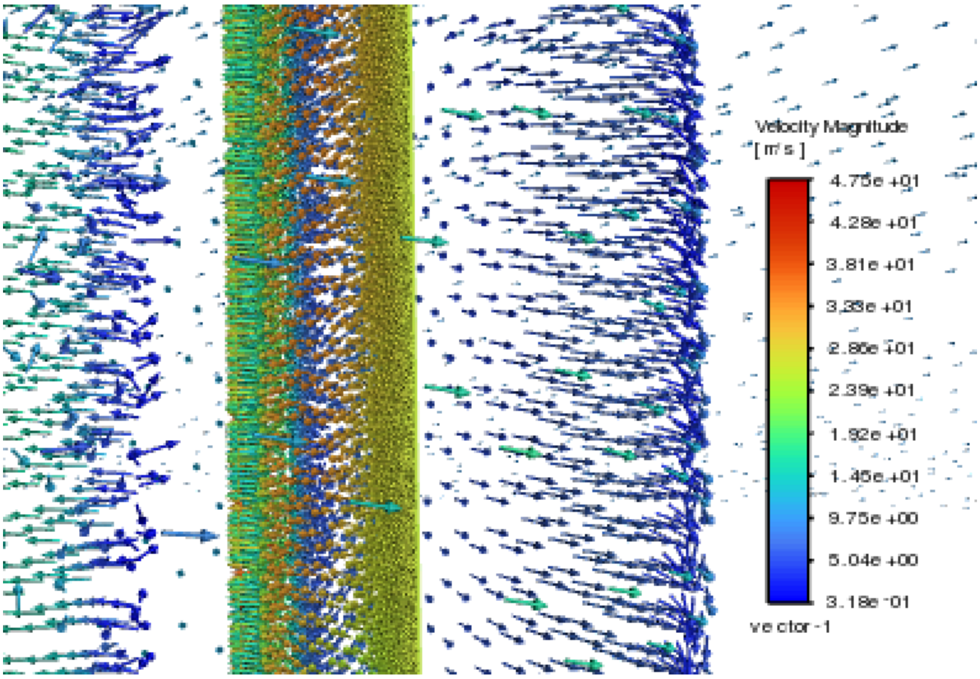

Figure. 7.5: Surrounding Velocity Vectors at 50%-80% of the Airfoil Midsection at the Snapshot of 120°.

Based on the above analysis, it can be concluded that high-fidelity aerodynamic optimization of a three-dimensional single blade requires constructing an equivalent incoming flow model that includes velocity components in the X, Y, and Z directions to accurately describe the impact of spanwise non-uniformity on aerodynamic loads. However, in the approximately 40% spanwise region of the blade (approximately 0.3–0.7m), the z-component of velocity in the airfoil surface and surrounding flow field remains at a low level, and the three-dimensional effect is relatively weak. Therefore, in the subsequent calculation and modeling of the power coefficient C_P, only the flow data within this spanwise range is selected as representative, which can significantly reduce model complexity while ensuring computational accuracy, providing a reasonable basis for 2.5D aerodynamic modeling and optimization.

For the 3D simulation of the VAWT, particular attention should be paid to the axial velocity distribution at each spanwise section, because the presence of a non-negligible spanwise velocity component (z-velocity) is generally undesirable when the aerodynamic behavior is to be interpreted using a 2D blade-section assumption. If a blade section in the 3D model is to be represented by a 2D airfoil simulation, it is therefore necessary to examine the proportion of the spanwise velocity component in the vicinity of the airfoil under the same inlet velocity condition. Based on the preliminary 3D results for the selected airfoil, three main conclusions can be drawn.

First, in the vicinity of the trailing edge, the flow becomes increasingly unstable due to the development of three-dimensional turbulent structures. Although the detailed vortical structures cannot be fully resolved within the present RANS framework, the highly irregular and rapidly changing velocity vectors indicate that the flow field becomes markedly more unstable as the location approaches the trailing-edge region. Second, near the leading edge, the spanwise velocity component becomes larger as the observation point moves closer to the blade tip. However, when the axial velocity is extracted at a location with a small upstream offset from the airfoil surface, the contribution of the spanwise velocity component is significantly reduced. This trend is consistent with the axial-velocity sampling strategy adopted in the 2D simulations, suggesting that the axial-velocity extraction position defined in the previous chapter remains applicable in the subsequent 3D simulations. Third, owing to computational resource limitations, the present optimized airfoil was assessed only using a blade geometry generated by extruding the identical 2D optimized cross-section along the span, without accounting for spanwise geometric variation. Therefore, the current 3D analysis can only demonstrate the influence of the reduced axial velocity component on the performance of the optimized airfoil, but it cannot be used to establish the influence of spanwise velocity effects on the airfoil optimization itself.

As summarized in Table 7.1, which presents the proportion of the spanwise velocity component relative to the axial velocity, the z-velocity component remains relatively small and regular near the leading edge, whereas it becomes highly scattered and irregular near the trailing edge. This behavior strongly suggests the onset of three-dimensional turbulent flow structures in the trailing-edge region. A more refined future investigation may quantify this phenomenon through the distribution of turbulent kinetic energy.

Table 7.1: Proportion of the spanwise velocity component to the axial velocity.

% Span	% V_z/V Leading	% V_z/V Trailing
20	-0.3650	-0.8135
30	-0.2500	-0.6445
40	-0.2334	-0.1233
50	-0.1226	-0.0884
60	0.1234	-0.0157
70	0.2443	-0.1107
80	0.2876	0.4413

Overall, since the 2D model, lacking spanwise degrees of freedom, cannot describe the spread and recombination of the wake in the spanwise direction, often overestimating or underestimating the magnitude of local aerodynamic changes. In contrast, the finite span effect and three-dimensional vortex structure in the 3D model allow for the redistribution of some energy in the spanwise direction, significantly altering the local pressure field and torque response. Therefore, at this azimuth angle, the 3D effect has the most significant impact on the aerodynamic torque, leading to the deviation between the 2D and 3D results.

7.3.2 Transient Aerodynamic Performance of Candidate Airfoils

Based on the steady-state snapshot analysis, the full-cycle transient aerodynamic performance of candidate airfoils in a three-dimensional H-blade VAWT was further evaluated and compared with the results of a two-dimensional VAWT cross-sectional model. This analysis focuses on the variation characteristics of the aerodynamic moment coefficient C_M and the power coefficient calculated from it over the complete rotational cycle.

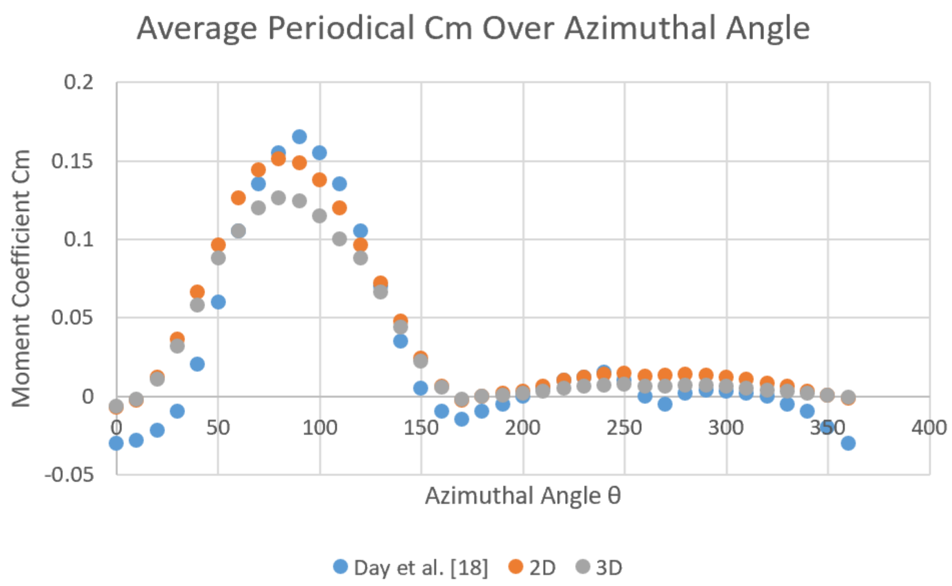

Fig. 7.6: Comparison of Moment Coefficients between 3D and 2D VAWT Models.

Figure 7.6 shows the comparison results of the periodically averaged aerodynamic moment coefficients obtained for the same airfoil in two-dimensional and three-dimensional models. It can be observed that for both the baseline and optimized airfoils, the periodically averaged C_M predicted by the three-dimensional model is slightly lower than the two-dimensional result, with a difference of approximately 8%. This trend is consistent in both types of airfoils, indicating that the three-dimensional effect has a systematic characteristic on the overall aerodynamic performance, rather than being caused by individual airfoil geometry.

Table 7.2: Moment and power coefficient at percentage of L.

Conditions @ 4.5 TSR	10%L	25%L	50%L	2D
C_M, Iteration2	0.0302	0.0295	0.0326	
C_P, Iteration2	0.2718	0.2655	0.2934	
C_M, Iteration3	0.0256	0.0255	0.0276	Always at the
C_P, Iteration3	0.2304	0.2295	0.2484	last iteration
C_M, Iteration4	**0.0234**	**0.0243**	**0.0270**	**0.0274**
C_P, Iteration4	**0.2106**	**0.2187**	**0.2430**	**0.2466**

To further analyze the sources of the above differences, Table 7.1 summarizes the results of local aerodynamic moments and power coefficients extracted at different spanwise height percentages, and also provides a comparison between the overall three-dimensional integral results and the predictions of the two-dimensional model. This stratified analysis shows that the local aerodynamic moment is close to the two-dimensional result near the mid-span region; however, the aerodynamic moment decreases slightly near the upper and lower symmetry boundaries. This distribution characteristic reflects the modulating effect of finite span and three-dimensional flow structure on local aerodynamic loads.

By integrating the results at different spanwise positions, the aerodynamic moment and power coefficient of the overall three-dimensional rotor can be obtained, and their values are consistent with the overall results directly output by the three-dimensional solver. This further illustrates that the reduction in overall performance in the three-dimensional model mainly stems from the non-uniform distribution of aerodynamic loads in the spanwise direction, rather than errors introduced by the numerical extraction method. In contrast, the two-dimensional model, due to its assumption of infinite span and neglect of the effects of spanwise momentum transport and three-dimensional vortex structure, often overestimates the overall rotor performance to some extent.

Table 7.2: Optimized moment and power coefficient at percentage of L.

Conditions @ 4.5 TSR	10%L	25%L	50%L	2D
C_M, Iteration2	0.0276	0.0258	0.0267	
C_P, Iteration2	0.2484	0.2322	0.2403	
C_M, Iteration3	0.0257	0.0256	0.0278	Always at the
C_P, Iteration3	0.2313	0.2304	0.2502	last iteration
C_M, Iteration4	**0.0250**	**0.0275**	**0.0280**	**0.0283**
C_P, Iteration4	**0.2250**	**0.2475**	**0.2520**	**0.2547**

Table 7.2 further presents the aerodynamic moment and power coefficient results of the optimized airfoil at different spanwise height percentages and compares them with the

baseline airfoil. The results show that although the three-dimensional effect reduces the overall aerodynamic moment level, the optimized airfoil consistently outperforms the baseline airfoil at all spanwise positions, and its performance improvement is retained in the overall integral results. This indicates that the airfoil advantages obtained from the aforementioned two-dimensional and rotating airfoil optimization methods do not disappear due to three-dimensional effects, but are continued in the more realistic three-dimensional rotor environment.

Three-dimensional flow visualization reveals several important physical differences between the baseline and optimized cases. For the baseline NACA0015 blades, large-scale tip vortices form at the upper and lower blade ends during both upwind and downwind passes, creating strong radial outflow and wake expansion. These vortices persist far downstream, reducing energy recovery efficiency and promoting unsteady torque oscillations. In contrast, the optimized airfoil demonstrates a smoother pressure recovery near the trailing edge, which weakens vortex shedding intensity and delays the onset of tip-vortex roll-up.

Instantaneous vorticity contours at 50%, 75% (25%), and 90% (10%) span positions show that the optimized blade maintains better flow attachment on the suction surface during the upwind half of the rotation. The pressure distribution indicates a stronger suction peak near the mid-chord and a gentler gradient near the trailing edge, reducing adverse pressure recovery and mitigating dynamic stall phenomena. The net result is a more coherent wake structure and reduced aerodynamic losses.

As summarized in Table 7.1 and Table 7.2, the simulation results indicate that at locations further away from the blade tip, the computed power coefficient C_P values are slightly lower than, yet closely approach, those obtained from the corresponding two-dimensional simulations. This trend suggests that the three-dimensional effects such as tip-vortex dissipation and radial flow, introduce limited but measurable energy losses compared with the idealized 2D condition. Nevertheless, the agreement between mid-span sections and 2D predictions confirms that the optimized airfoil maintains consistent aerodynamic efficiency across most of the blade span. Examination of the iterative convergence histories further shows that the solution begins to stabilize from approximately the third to fourth revolution, indicating that a quasi-periodic flow state is reached beyond this point. Minor oscillations with intermittent peaks are still observed in some azimuthal regions, corresponding to transient vortex interactions and local dynamic stall events, but their amplitudes remain small and do not affect the overall convergence or the averaged aerodynamic performance of the turbine.

At the turbine level, the azimuthally averaged power contribution per blade reveals a more uniform torque distribution, with smaller phase lag between the upwind and downwind sectors. This not only increases mean efficiency but also contributes to mechanical smoothness, potentially lowering fatigue loading on the shaft and bearings.

To isolate the contribution of true 3D flow phenomena, additional quasi-3D simulations were performed by extruding 2D sections with periodic boundary conditions along the span, effectively removing tip effects. In this configuration, the optimized airfoil achieved a 3.1% increase in C_P relative to NACA0015, closely matching the improvement predicted in the purely 2D optimization. The slightly lower gain observed in the full 3D model thus arises from genuine three-dimensional losses associated with finite aspect ratio and tip-vortex energy dissipation.

This finding confirms that the aerodynamic benefits of the 2D adjoint-optimized airfoil are preserved under full 3D conditions, albeit slightly reduced due to physical effects not captured in two-dimensional analysis. Importantly, no unexpected degradation or instability was observed, indicating that the optimized shape generalizes well across dimensional scales and remains aerodynamically robust in realistic operating environments.

In summary, transient full-cycle analysis shows that the three-dimensional H-blade VAWT model exhibits a certain degree of reduction in predicted aerodynamic torque and power coefficient compared to the two-dimensional model. This is mainly attributed to the finite span effect and the influence of the three-dimensional flow structure. However, the optimized airfoil shows a consistent performance improvement trend in both two-dimensional and three-dimensional models, verifying the effectiveness and generalizability of the aforementioned optimization methods under actual three-dimensional rotor conditions.

7.4 Summary

A three-dimensional analysis of a vertical-axis wind turbine (VAWT) airfoil optimized using a transient adjoint provides a comprehensive understanding of how cross-sectional aerodynamic improvements translate into overall turbine performance. The results confirm that the aerodynamic advantages predicted by the two-dimensional optimization. It can increase tangential and power coefficients, delay flow separation, and enhance pressure recovery. With flow conditions in the mid-blade region closely resembling those assumed in the two-dimensional simulation. This validates the effectiveness of the two-dimensional transient adjoint approach as a fundamental approach to improving the local aerodynamic efficiency of vertical-axis wind turbine blades.

However, the three-dimensional simulation also reveals several important flow phenomena that are missing from the two-dimensional analysis. The presence of tip vortices, radial flow migration, and spanwise pressure gradients redistribute the annular flow across the blade span and lead to local variations in the effective angle of attack. These effects reduce cross-sectional lift near the blade tip and alter the total torque generation compared to the two-dimensional predictions. Furthermore, enhanced rotation and induced downwash introduce spatially dependent unsteady loads, resulting in phase shifts and amplitude variations in the aerodynamic forces throughout the rotation cycle. As a result, while the average power coefficient of the optimized turbine remains higher than that of the baseline configuration, the magnitude of the improvement is reduced in a three-dimensional environment.

Chapter 8

Recommendations for Optimizing Blade Body Manufacturing

Based on the discussion in the Chapter 5, 6 and 7, we hypothesize that vertical axis wind turbines can efficiently collect energy generated by wind in all directions if they rely on advanced aerodynamic design. When it undergoes CFD optimization to adjust the blade shape to maximize the power coefficient, the blade structure will change significantly. These changes typically include increasing curvature, adjusting cross-sectional thickness distribution, and optimizing twist profiles. After these optimization efforts were completed, turning this shape into a manufacturable part presented additional challenges. In particular, there is the question of whether money can be saved by increasing power output as processing or test costs increase. This requires careful planning of composite layups, molds, and quality assurance during production. Additionally, ensuring that these complex blades maintain performance, reduce costs, and do not fail under fatigue loads is important to commercial success.

8.1 Manufacturing Techniques

VAWT blades are typically manufactured using glass fiber fabric reinforced epoxy resin due to their good strength-to-weight ratio, corrosion resistance, and cost-effectiveness. To meet structural stiffness and fatigue requirements (especially in designs with large curvatures), blade designs often incorporate PVC or PU foam cores to reduce weight while maintaining cross-sectional stiffness [178-180]. The primary load paths within VAWT blades are bending moments along the vertical axis and torsional shear from wind loads. A multi-layer layup structure is employed, typically containing 0° unidirectional fibers to resist bending and ±45° fibers to mitigate torsional loads [181]. This layup strategy not only ensures load-bearing efficiency but also provides damping capacity to suppress vibration resonances. Resin transfer molding (RTM) or vacuum-assisted resin transfer molding (VARM) are considered the most suitable processes for manufacturing such blades, especially after CFD-driven morphological changes. These methods allow for precise control of fiber wetting, reduced porosity, and repeatability [182]. However, these processes require additional high-precision 3D molds during the machining process, which are not available for conventional VAWT blade production and are essential for handling the non-developable surfaces commonly found in optimized VAWT blades. The molds themselves are typically made from CNC machined foam blocks, post-processed by grinding and surface polishing, or from 3D printed modular shell components [183]. The mold halves must maintain sufficient dimensional accuracy to ensure the consistency of the airfoil, as slight deformations caused by each optimization of the airfoil will affect the final aerodynamic efficiency. For small batches or prototype production, hybrid mold manufacturing methods can be used to integrate low-cost mold plates and rapid prototyping materials, such as PLA or ABS shells reinforced with epoxy putty [184], to minimize production costs without sacrificing geometric accuracy. The non-uniform shape characteristics of VAWT blades complicate standard manufacturing, especially during layup and vacuum bagging. Areas with large curvature are prone to fiber wrinkling, resin accumulation, or inconsistent consolidation pressure [185]. Countermeasures include: using customized preforms for segmented layup [186], using biaxial or triaxial fabrics that better conform to the curvature [187], using 3D stitched or woven reinforcements in stress concentration areas (e.g., blade root or mid-span bend) [188], and performing drape analysis based on 3D simulation before layup [189], which can also help predict fiber deformation and optimize layup orientation.

Quality assurance is important to ensure that the manufacturing process accurately replicates the optimized design and achieves structural reliability. For example, 3D geometric accuracy testing uses structured light or laser scanning systems to generate point cloud data on the blade surface. Then, the deviation map compares the point cloud data with the CAD model, and the tolerance is usually controlled within ±0.5 mm [190]. Non-destructive testing also includes ultrasonic C-scans to detect internal porosity and delamination, and infrared thermography to evaluate resin-enriched or dry areas after curing [190]. In addition, digital image correlation is combined with full-scale load testing to map surface strain distribution, helping to identify problem-prone areas, or where strain may be unexpectedly concentrated due to manufacturing defects [190]. After the prototype blades pass dimensional and visual inspections, they undergo comprehensive structural testing to see if they can withstand operating loads. The test is based on the IEC 61400-23 standard, which specifies methods for static load, fatigue life and natural frequency identification [190]. Testing focuses on first-order bending and torsion modes as they directly affect noise, vibration and structural fatigue in practical applications. Modal testing uses accelerometers and shaking table excitations to extract the natural frequencies of the blades, and then compare them with the original FEA modal results to ensure structural integrity and avoid resonance with wind-induced excitation frequencies. Many methods can optimize the cost-effective production of blades. To commercialize CFD-optimized VAWT blades, the manufacturing process needs to find a balance between precision, material efficiency, and cost reduction. The following strategies can reduce costs without sacrificing quality: Batch RTM process based on modular molds: achieve economies of scale by producing multiple blades with interchangeable mold inserts, accommodating blades of different lengths or twisted profiles. Use prepregs in high curvature areas: Resin-preimpregnated prepreg fabrics can improve layup consistency and reduce waste in hard-to-reach mold areas. Automatic infusion monitoring: Real-time flow sensors during vacuum infusion can improve resin distribution control and reduce rework due to incomplete infusion. Digital twin manufacturing: Use simulation software to map production changes, correlate them with blade performance, and create a closed-loop optimization system between design, manufacturing, and operations [191-193]. If these methods are implemented systematically, they can improve energy capture efficiency, reduce operation and maintenance costs, and improve the return on investment (ROI) of the turbine's entire life cycle.

In general, manufacturing vertical axis wind turbine (VAWT) blades requires high-precision manufacturing processes, integrated testing procedures, and smart cost control strategies. By using advanced composite material molding techniques such as RTM and infusion, combined with rigorous geometric and structural verification, manufacturers can theoretically ensure that the final product maintains its designed aerodynamic performance while meeting fatigue and safety requirements.

8.2 Testing and Regulation Standards

Those VAWTs optimized using CFD and advanced structural simulation must undergo rigorous verification and certification processes. This will ensure safety, performance and grid compatibility. In the UK, small wind systems (generally less than 50kW) are governed by international standards (such as the IEC 61400 series), British standards (such as BS EN 61400-2) and domestic regulatory frameworks (such as the Microgeneration Certification Scheme MCS). This framework is responsible for feed-in tariffs and eligibility for planning permission. Compliance is not only a legal requirement, but also a prerequisite for market access and investment [194-196].

Testing includes dimensional fidelity, structural integrity, vibration response, fatigue durability, electrical performance, which are verified in a certified environment accredited to UKAS/ISO 17065 [197]. See Appendix H for test requirements.

Chapter 9

Conclusions and Future Work

This study comprehensively investigates the transient adjoint aerodynamic optimization of vertical-axis wind turbine (VAWT) blades using computational fluid dynamics (CFD). The primary goal is to improve the aerodynamic efficiency and total power coefficient of VAWTs through a time-dependent sensitivity analysis framework that captures the inherent unsteady flow phenomena in turbine motion.

Unlike traditional steady-state or simplified quasi-steady optimization methods, the fully transient adjoint approach directly accounts for unsteady effects such as flow separation, dynamic stall, and the cyclical variations in lift and drag during turbine rotation. By combining this approach with a high-fidelity SU2-based CFD solver, this study successfully demonstrates an efficient and robust method for optimizing airfoil geometry under realistic time-varying aerodynamic loads.

Through a series of numerical experiments, this study confirms that curvature modifications and asymmetric airfoil shaping can significantly improve the tangential force distribution and total power coefficient of VAWT blades. The results demonstrate that, even within the single-blade approximation, the transient adjoint approach effectively identifies optimal design trends that are consistent with physical intuition and experimental observations.

9.1 Evaluation and Limitations

The conclusions drawn from this study provide both quantitative evidence of improved aerodynamic performance and qualitative insights into blade shape evolution and flow physics. Furthermore, the method developed here lays the foundation for future optimization research on multi-blade and fully coupled vertical-axis wind turbines.

The following sections summarize the evaluation and limitations of the proposed method in various test cases (oscillation, rotation, and a three-dimensional representation of a two-dimensional optimized airfoil) and outlines potential directions for future research and practical applications in advancing vertical-axis wind turbine aerodynamic design.

9.1.1 Evaluation on Oscillation Airfoils

A Darrieus oscillating airfoil was optimized using a transient adjoint method, primarily to improve the average cyclic power coefficient of vertical-axis wind turbine (VAWT) blades. CFD results directly reveal that adjustments to the airfoil curvature directly affect lift and drag characteristics, which together determine the total force exerted on each blade and its tangential component. Unlike traditional oscillating airfoil problems, the aerodynamic behavior of the blade pitching angular acceleration exhibits significant time-dependent periodicity due to the unique periodicity of the blade's upwind and downwind motion.

Numerical analysis results demonstrate that for a Darius-type vertical-axis wind turbine (VAWT), the actual pitching motion derived from the turbine kinematics follows a non-sinusoidal, asymmetric curve due to the combined effects of rotational motion and the changing relative wind speed vector. This deviation from regular sinusoidal behavior makes the angular acceleration non-uniform. Therefore, the airfoil will be subject to asymmetric aerodynamic loads. This asymmetry changes the time and intensity of airflow separation and reattachment. These two key phenomena determine the unstable lift and drag characteristics of turbine blades.

Theoretically, this behavior can be explained by the unsteady Bernoulli principle and vorticity dynamics. When the pitch acceleration is high, the effective angle of attack changes quickly. Eddy convection and boundary layer adaptation take time, and local flow pressure recovery lags. This results in the formation of leading edge vortices (LEVs) and transient flow separation. On the contrary, at low angular acceleration, the air flow is relatively stable, which facilitates reattachment and the pressure recovery along the suction surface is also enhanced. Therefore, the non-sinusoidal Darrieus oscillation changes the lift-drag relationship, adding a time-varying hysteresis loop.

Ultimately, this unique cyclical aerodynamic response affects the turbine's overall performance. It explains why optimized airfoil geometry balances the curvature on both sides to maintain high tangential force efficiency throughout the rotation. Analysis of the periodic power coefficient curve shows that changes in airfoil curvature significantly affect the tangential coefficient. The optimization process shows that performance improvement depends largely on the balance of aerodynamic behavior on the upwind and downwind sides of the airfoil. On the upwind side, curvature adjustment increases tangential force by improving lift production and maintaining a favorable pressure gradient. On the downwind side, the goals of shape modification are to suppress flow separation, reduce turbulence, and improve flow reattachment. However, as the blades rotate, the upwind and downwind surfaces alternate between 0 degrees and 360 degrees, so the optimal airfoil must meet the aerodynamic requirements under headwind and tailwind conditions. This inevitably introduces design trade-offs that require balancing deformation to maximize overall cycle performance rather than instantaneous gain.

Another key finding is that the optimized airfoil exhibits a significant improvement in power coefficient compared to the baseline configuration at both high and low wind speeds. This improvement is achieved while maintaining chord length constraints and ensuring structural feasibility. The transient adjoint-based optimization method effectively captures dynamic aerodynamic interactions throughout the entire oscillation cycle, providing more realistic and comprehensive optimization results than steady-state or quasi-steady-state methods.

Notably, the evaluation also highlighted some of its limitations. The optimization employed a single-blade model, ignoring the complex flow interactions between multiple blades in a real vertical-axis wind turbine system. Furthermore, while a Darius pitching motion was used to approximate actual pitching behavior, the actual angle of attack variation may not strictly follow this function. Despite these simplifications, the transient adjoint method successfully demonstrates its ability to handle highly unsteady flow conditions and irregular airfoil motions, validating its applicability in the aerodynamic design of vertical-axis wind turbines.

9.1.2 Evaluation on Rotational Airfoils

In the evaluation of rotating airfoils, an optimization method based on a transient adjoint optimization framework is extended to account for the realistic unsteady incoming flow environment experienced by rotating blades. Unlike traditional Darrieus models, which assume a regular, idealized sinusoidal or analytical variation of the angle of attack (AoA) with azimuthal position, this study analyzes the transient aerodynamic state of the airfoil under a continuously varying relative velocity vector. In reality, the incoming flow at each blade section is the result of the superposition of the freestream wind speed and the local rotational velocity, both of which vary dynamically with time and position. As a result, the actual angle of attack fluctuates irregularly and is no longer synchronized with the idealized Darrieus motion cycle.

In the real vertical-axis wind turbine (VAWT) environment, the transient flow field around the blades is highly nonuniform and influenced by wake interactions and multi-blade effects. By incorporating the full transient flow field into the adjoint optimization process, this study effectively addresses the limitations of traditional quasi-steady or kinematic Darrieus assumptions. The resulting aerodynamic behavior better reflects the true physics of blade rotation, capturing the asynchronous evolution of lift, drag, and pressure distributions throughout the rotation process.

Regarding the formation and shedding of vortices near the leading and trailing edges, these are quite pronounced in both the upwind and downwind phases of the baseline NACA0015 configuration. This leads to dynamic stall occurring at certain times due to local Reynolds number and angle of attack variations. These vortices cause significant unsteady loads and energy losses, thereby reducing the effective tangential coefficient and overall power coefficient of the turbine. After optimization using the transient adjoint method, the average power coefficient of the airfoil is improved. It exhibits a smoother pressure gradient and delayed flow separation, resulting in a more stable and weaker vortex shedding pattern. The leading-edge vortices are smaller and more periodic, and they reattach earlier on the suction surface. This reduces aerodynamic hysteresis, making the tangential force more consistent throughout the rotation. Furthermore, the asymmetry in the optimized profile helps to readjust the pressure distribution, achieving a good balance between increased lift in the upwind phase and reduced drag in the downwind phase.

From a theoretical perspective, the optimization reshapes the blade geometry so that the local curvature and pressure recovery zone naturally suppress the occurrence of large-scale vortex shedding. This mitigates the sudden aerodynamic loads associated with vortex shedding, thereby improving the turbine's efficiency and structural stability. Essentially, the rotating airfoil optimization based on transient adjoints not only captures the non-periodic and time-varying aerodynamic environment but also actively modifies the airfoil geometry to accommodate the unsteady flow physics, rather than relying on the simplifying assumption of a regular angle of attack variation.

It is important to note that during certain phases of the rotation cycle, the local Reynolds number and instantaneous angle of attack may reach a critical combination, triggering dynamic stall. While the optimized airfoil exhibits improved aerodynamic performance during specific time intervals (particularly when favorable flow attachment and pressure gradients are achieved), the advantages are not fully maintained throughout the entire rotation cycle. This limitation arises because the optimization is performed on a static airfoil geometry and no dynamic shape adaptation or deformation is introduced during operation. Therefore, optimized design is a compromise. It can deliver excellent performance during the main aerodynamic phase, but it cannot simultaneously optimize all local flow conditions throughout the entire cycle. This finding demonstrates the limitations of static geometric optimization for unsteady rotating systems. When flow characteristics vary significantly over time, a single fixed airfoil shape cannot meet the aerodynamic requirements at different azimuthal positions.

A further consideration concerns the potential modeling and numerical errors introduced by the use of a movable monitored body and a dynamic mesh framework. In this study, the airfoil motion is realized through a time-dependent coordinate transformation, where each node position is updated according to the instantaneous rotational matrix and translational displacement of the moving reference frame. While this approach enables the accurate representation of blade motion and time-resolved sensitivity evaluation, it inevitably introduces additional numerical complexity. In a dynamic mesh environment, maintaining geometric conservation is essential; inconsistencies between mesh velocity, control-volume deformation, and flux evaluation may violate the geometric conservation law (GCL), resulting in spurious residual drift even in steady flow conditions. Moreover, the interpolation of mesh motion, particularly in regions of strong curvature or large deformation, can generate non-orthogonal or skewed cells, amplifying local truncation errors and potentially degrading the accuracy of both the primal and adjoint solutions.

From a theoretical perspective, the transformation between the inertial and rotating coordinate systems introduces metric terms and fictitious forces that must be treated consistently in both the flow and adjoint equations. Any mismatch in their discrete representation leads to dual inconsistency, producing inaccurate gradient information. Additionally, the mapping between design variables and nodal coordinates is inherently nonlinear: when shape parameters such as thickness, camber, or curvature are projected onto the moving mesh, even small interpolation or remeshing errors can alter the sensitivity chain and cause gradient noise. Using static parameterization, the adjoint derivatives of the mesh motion solver are approximate and not explicitly differentiated. This further reduces gradient fidelity.

In summary, movable monitoring volumes and dynamic meshes greatly improve the physical realism of the simulations, allowing transient adjoint methods to capture true unsteady aerodynamics. But this also brings geometric, numerical and coordinate transformation errors, which need to be carefully controlled. In order to ensure the accuracy and stability of the optimization results, it is necessary to ensure strict geometric conservation, consistent coordinate measurement, and smooth design and physical space mapping.

9.1.3 Evaluation of 3D Behaviors

To further evaluate the aerodynamic performance and physical validity of the optimized 2D airfoil, a 3D CFD analysis was performed on a full vertical axis wind turbine (VAWT) configuration. This step bridges the gap between idealized 2D blade cross-section optimization and the complex, fully 3D flow environment of actual turbine operation. The goal was to assess how the aerodynamic improvements achieved through transient adjoint 2D optimization translate to actual 3D turbine performance, where spanwise flow and induced velocity effects become significant.

The 3D simulation primarily monitored spanwise flow parameters using line probes. The monitoring results showed that while the optimized 2D airfoil maintained its excellent aerodynamic characteristics in the mid-span region, its performance gradually degraded toward the blade tip due to radial flow effects. These phenomena altered the local angle of attack and pressure distribution, resulting in a partial loss of the lift and tangential force improvements predicted by the 2D optimization. The interaction between the tip vortex system and the downwind blade passage leads to additional unsteady effects that were not captured by the 2D analysis. Despite the three-dimensional complexity, the optimized airfoil allows the turbine to achieve a significantly higher average power coefficient. This proves that the two-dimensional transient adjoint optimization has a positive effect on the overall aerodynamic efficiency of the entire rotor system.

In the 3D CFD model, the flow field visualization shows that the optimized airfoil delays flow separation, reduces the intensity of the trailing edge vortex in the mid-span area, and helps stabilize the overall wake structure. However, near the blade root and tip, the induced velocity gradient promotes flow migration in the spanwise direction and cross-plane vortex transmission, resulting in energy dissipation and a reduction in local aerodynamic efficiency. This shows that pure two-dimensional optimization cannot completely solve the problem of radial flow redistribution in a three-dimensional rotating system. In other words, the 2D derived shape function effectively improves cross-sectional performance but does not incorporate spanwise flow control mechanisms such as torsion or chord length changes.

From a theoretical perspective, the transition from 2D to 3D introduces additional terms in the momentum balance related to radially induced and tip-loss effects, which redistribute the circulation across the blade span. Optimizing the airfoil geometry changes the local lift distribution and reduces large-scale vortex shedding, but induced flow imbalances persist without concurrent optimization of the spanwise geometry. Therefore, while this study shows that 2D optimization based on transient adjoints can effectively improve baseline aerodynamic performance, to achieve a globally optimal turbine design, a complete 3D adjoint optimization framework is required, taking into account both cross-sectional shape and spanwise parameters.

In conclusion, the 3D evaluation demonstrates that the aerodynamic improvements resulting from 2D transient adjoint optimization are justified and can lead to real performance improvements in full turbine simulations. However, the effects of wingtip vortices, spanwise flow coupling, and radial pressure gradients limit the extent of improvements achievable with purely 2D optimization. These findings highlight the need to extend the transient adjoint approach to 3D multi-parameter optimization to fully account for the coupled effects of rotation, wake dynamics, and structural constraints.

9.2 Future Work

This study proves that the full transient adjoint method can effectively optimize the aerodynamic performance of vertical axis wind turbine (VAWT) blades. Although great progress has been made in capturing the unsteady physics of oscillating and rotating airfoils, there are still research directions that require further exploration and improvement.

(i) Extension to full 3D adjoint optimization

The most direct continuation of this work is to extend the transient adjoint framework from two-dimensional sectional optimization to a fully three-dimensional blade optimization. This will allow simultaneous consideration of spanwise twist, chord distribution, and thickness variation, which are strongly coupled with the radial induction and tip-loss effects observed in the 3D evaluation. A consistent 3D adjoint formulation would enable the optimization of both sectional aerodynamics and global circulation distribution, leading to a more physically complete and efficient turbine design.

(ii) Combination of fluid-structure coupling and dynamic deformation. The optimization now assumes that the blades are rigid and the airfoil geometry is static. But in fact, turbine blades will produce elastic deformation and vibration due to unsteady aerodynamic loads. If structural dynamics can be added and a coupled aeroelastic adjoint solver is developed, shape optimization of deformable or flexible blades can be performed. In this way, the geometry can adapt to the instantaneous flow field in real time, maintaining optimal aerodynamic conditions throughout the rotation cycle.

(iii) Improved modeling of unsteady flow phenomena. The current simulation captures the main transient characteristics. But it can be improved by higher fidelity turbulence modeling (e.g. DES, hybrid RANS-LES) and better dynamic grid algorithms. These algorithms can better maintain geometric conservation and mesh quality under large deformations. Future work should also analyze the vortex dynamics, dynamic stall occurrence and flow reattachment mechanisms in detail, and ensure the reliability of the model through experimental verification.

(iv) Development of reduced-order and surrogate models for optimization efficiency

Transient adjoint simulations are computationally intensive. Constructing reduced-order models (ROMs) or machine-learning-based surrogate models trained on adjoint sensitivities could greatly accelerate the optimization process while retaining physical accuracy. Such hybrid approaches would enable multi-objective optimization involving power coefficient, structural stress, and noise simultaneously, thus improving both performance and manufacturability.

(v) Apply optimized airfoils in body-manufacturing

The integration of design-for-manufacturing (DfM) principles into the optimization process should be explored. Future work can establish a coupled optimization framework that simultaneously considers aerodynamic performance, material layout, manufacturability, and cost. While CFD optimization enhances power output, the increased tooling complexity and material consumption associated with highly curved designs may offset some of these benefits. Future work should develop quantitative models linking manufacturing cost, fatigue life, and aerodynamic gain, to identify the economically optimal design point for commercial deployment.

In conclusion, future work should focus on developing a fully coupled, three-dimensional, and multi-physics transient adjoint optimization framework. Such an approach will enable not only higher aerodynamic efficiency but also structural reliability and adaptability of VAWT blades, pushing forward the practical application of adjoint-based optimization in the next-generation wind energy systems.

References

[1] Ashwill, T.D., Sutherland, H.J. and Berg, D.E. (2012) A retrospective of VAWT technology. Sandia National Laboratories Report No. SAND2012-0304. Albuquerque, NM: Sandia National Laboratories.

[2] Kumar, P.M., Sivalingam, K., Narasimalu, S., Lim, T.C., Ramakrishna, S. and Wei, H. (2019) A review on the evolution of Darrieus vertical axis wind turbine: large wind turbines. Clean Technologies, 1(1), pp. 205–223.

[3] Sandia National Laboratories (2012) Offshore use of vertical-axis wind turbines gets closer look. Albuquerque, NM: Sandia National Laboratories.

[4] Barter, G.E., Sethuraman, L., Bortolotti, P., Keller, J. and Torrey, D.A. (2023) 'Beyond 15 MW: a cost of energy perspective on the next generation of wind turbines', *Applied Energy*, 344, article 121272.

[5] Sandia National Laboratories (1987) Structural design and fabrication of the Sandia 34-meter vertical axis wind turbine. Technical Report SAND86-2618. Albuquerque, NM: Sandia National Laboratories.

[6] Ali, S., Park, H. and Lee, D. (2024) Investigating the structural and power performance of a 15 MW class wind energy generation system under experimental wind and marine loading. Journal of Marine Science and Engineering, 12(9), Article 1485.

[7] Möllerström, E., Ottermo, F. and Bernhoff, H. (2019) A historical review of vertical axis wind turbines rated 100 kW and above. Renewable and Sustainable Energy Reviews, 105, pp. 1–13.

[8] Sandia National Laboratories (2022) *Vertical-axis wind turbines for offshore wind energy*. SAND2022-11833 O. Albuquerque, NM: Sandia National Laboratories. Available at: https://www.sandia.gov/app/uploads/sites/273/2024/02/Vertical-Axis-Wind-Turbines.pdf.

[9] Maydew, R.C. and Klimas, P.C. (2012) Aerodynamic performance of vertical and horizontal axis wind turbines. Journal of Energy, 2012, Article ID 62496.

[10] Borg, M. and Collu, M. (2015) 'A comparison between the dynamics of horizontal and vertical axis offshore floating wind turbines', *Philosophical Transactions of the Royal Society A: Mathematical, Physical and Engineering Sciences*, 373(2035), article 20140076.

[11] Tchakoua, P., Wamkeue, R., Ouhrouche, M., Slaoui-Hasnaoui, F., Tameghe, T.A. and Ekemb, G. (2014) Wind turbine condition monitoring: state-of-the-art review, new trends and future challenges. Energies, 7(4), pp. 2595–2630.
[12] de Azevedo, H.D.M., Araújo, A.M. and Bouchonneau, N. (2016) 'A review of wind turbine bearing condition monitoring: state of the art and challenges', *Renewable and Sustainable Energy Reviews*, 56, pp. 368–379.
[13] Van Dam, J. and Bond, L.J. (2015) 'Economics of online structural health monitoring of wind turbines: cost benefit analysis', *AIP Conference Proceedings*, 1650 (1), pp. 899–908.
[14] Scheel, M., Santos, I.F. and Achiche, S. (2013) Wind turbine condition monitoring based on SCADA data using normal behaviour models – part 1: system description. Applied Soft Computing, 13, pp. 259–270. https://doi.org/10.1016/j.asoc.2012.08.024.
[15] Muralidharan, P., Thakur, G., Shalini, M., Sharma, V., Abootharmahmoodshakir and Dhablia, A. (2024) 'A review on condition monitoring of wind turbines using machine learning techniques', *E3S Web of Conferences*, 540, article 03003.
[16] Al-Rawajfeh, M.A. and Gomaa, M.R. (2023) 'Comparison between horizontal and vertical axis wind turbine', *International Journal of Applied Power Engineering*, 12(1), pp. 13–23.
[17] Abbasi, S. and Daraee, M.A. (2024) 'Improving vertical-axis wind turbine performance through innovative combination of deflector and plasma actuator', *Physics of Fluids*, 36 (4).
[18] Day, H. (2021) Aerodynamic optimisation of vertical axis wind turbines using adjoint methods in CFD. PhD thesis. Sheffield: University of Sheffield.
[19] Savonius, S.J. (1922) The Savonius wind rotor. Finnish Patent FI 14206.
[20] Darrieus, G.J.M. (1931) Turbine having its rotating shaft transverse to the flow of the current. U.S. Patent 1,835,018.
[21] Yergin, D. (1991) The prize: the epic quest for oil, money and power. New York, NY: Simon & Schuster.
[22] Hand, B. and Cashman, A. (2020) 'A review on the historical development of the lift-type vertical axis wind turbine: from onshore to offshore floating application', *Sustainable Energy Technologies and Assessments*, 42, article 100744.
[23] Möllerström, E., Gipe, P., Beurskens, J. and Ottermo, F. (2019) 'A historical review of vertical axis wind turbines rated 100 kW and above', *Renewable and Sustainable Energy Reviews*, 105, pp. 1–13.

[24] Islam, M., Ting, D.S.-K. and Fartaj, A. (2008) Aerodynamic models for Darrieus-type vertical axis wind turbines: a comparative study. Renewable and Sustainable Energy Reviews, 12(4), pp. 1087–1109.
[25] Ferreira, C.S., van Kuik, G.A.M., van Bussel, G.J.W. and Scarano, F. (2009) Visualization by PIV of dynamic stall on vertical axis wind turbine blades. Experiments in Fluids, 46(1), pp. 97–108.
[26] Mertens, S. (2006) Wind energy in the built environment: concentrator effects of buildings. Delft: Delft University Press.
[27] Claessens, M.C. (2006) The design and testing of airfoils for application in small vertical axis wind turbines. MSc thesis. Delft: Delft University of Technology.
[28] Zhang, A., Yu, H., Zeng, J., Zhao, W., Wen, H. and Zheng, J. (2026) 'Numerical investigation of dynamics stall on vertical axis wind turbine', *Applied Mathematics and Mechanics (English Edition)*.
[29] Bazilevs, Y., Hsu, M.-C., Akkerman, I., Wright, S., Takizawa, K., Henicke, B., Spielman, T. and Tezduyar, T.E. (2011) 3D simulation of wind turbine rotors at full scale. Computers and Fluids, 50(1), pp. 93–103.
[30] ANSYS Inc. (2020) ANSYS Fluent theory guide. Available at: https://www.ansys.com (Accessed: 10 June 2025).
[31] Jasak, H., Jemcov, A. and Tukovic, Z. (2007) OpenFOAM: a C++ library for complex physics simulations. Proceedings of the International Workshop on Coupled Methods in Numerical Dynamics, Dubrovnik, Croatia.
[32] Drela, M. (1989) XFOIL: an analysis and design system for low Reynolds number airfoils. Proceedings of the Conference on Low Reynolds Number Airfoil Aerodynamics. Notre Dame, IN: University of Notre Dame, pp. 1–12.
[33] Ben Jaber, M. and Arfaoui, M.F. (2015) 'Parametric study of vertical axis wind turbine', in *Proceedings of the 6th International Congress Design and Modelling of Mechanical Systems (CMSM 2015)*, Hammamet, Tunisia, 23–25 March 2015.
[34] Vassberg, J.C. and Jameson, A. (2016) *Aerodynamic shape optimization Part II: sample applications*. VKI Lecture-II, Brussels, Belgium, 24 May. (Accessed: 10 June 2025).
[35] Paraschivoiu, I. (1988) 'Double-multiple streamtube model for studying vertical-axis wind turbines', *Journal of Propulsion and Power*, 4 (4), pp. 370–377.
[36] Rezaeiha, A., Kalkman, I. and Blocken, B. (2017) Effect of pitch angle on power performance and aerodynamics of a vertical axis wind turbine. Applied Energy, 197, pp. 132–150.

[37] Peng, H.Y., Zhong, B.W., Hu, G. and Liu, H.J. (2022) ‘Optimization analysis of straight-bladed vertical axis wind turbines in turbulent environments by wind tunnel testing’, *Energy Conversion and Management*, 257, article 115411.
[38] Ertem, S., Simão Ferreira, C.J., Gaunaa, M. and Madsen, H.A. (2016) ‘Aerodynamic optimization of vertical axis wind turbine with trailing edge flap’, in *Proceedings of the 34th Wind Energy Symposium*. Reston, VA: American Institute of Aeronautics and Astronautics (AIAA), pp. 1–23. Paper AIAA 2016-1735.
[39] MacPhee, D.W. and Beyene, A. (2019) ‘Performance analysis of a small wind turbine equipped with flexible blades’, *Renewable Energy*, 132, pp. 497–508.
[40] Marten, D., Pechlivanoglou, G., Nayeri, C.N. and Paschereit, C.O. (2013) QBlade: an open source tool for design and simulation of horizontal and vertical axis wind turbines. International Journal of Emerging Technology and Advanced Engineering, 3(3), pp. 264–269.
[41] Windspire Energy (2010) Windspire vertical wind turbine product brochure. Available at: https://www.windspireenergy.com (Accessed: 10 June 2025).
[42] Jawahar, H.K., Ai, Q. and Azarpeyvand, M. (2018) Experimental and numerical investigation of aerodynamic performance for airfoils with morphed trailing edges. Renewable Energy, 127, pp. 355–367.
[43] Kirke, B.K. and Lazauskas, L. (1991) Enhancing the performance of vertical axis wind turbines using a simple variable pitch system. Wind Engineering, 15(4), pp. 187–195.
[44] Raciti Castelli, M., Englaro, A. and Benini, E. (2011) The Darrieus wind turbine: proposal for a new performance prediction model based on CFD. Energy, 36(8), pp. 4919–4934.
[45] Ferreira, C.S., Bijl, H., van Bussel, G.J.W. and van Kuik, G.A.M. (2007) Simulating dynamic stall in a two-dimensional vertical-axis wind turbine: verification and validation with particle image velocimetry data. Wind Energy, 10(6), pp. 629–647.
[46] Howell, R., Qin, N., Edwards, J. and Durrani, N. (2010) Wind tunnel and numerical study of a small vertical axis wind turbine. Renewable Energy, 35(2), pp. 412–422.
[47] Lighthill, M.J. (1945) A new method of two-dimensional aerodynamic design. Aeronautical Research Council Reports and Memoranda, No. 2112.
[48] Luo, J., Xiong, J., Liu, F. and McBean, I. (2011) Three-dimensional aerodynamic design optimization of a turbine blade by using an adjoint method. Journal of Turbomachinery, 133, Article 011026.

[49] Rathore, M.K., Agrawal, M. and Baredar, P. (2021) 'Pitch control mechanism in various type of vertical axis wind turbines: a review', *Journal of Vibration Engineering & Technologies*, 10, pp. 3105–3124.
[50] Wang, L., Kolios, A., Nishino, T., Delafin, P.-L. and Bird, T. (2016) 'Structural optimisation of vertical-axis wind turbine composite blades based on finite element analysis and genetic algorithm', *Composite Structures*, 153, pp. 123–138.
[51] Zhang, L.-X., Liang, Y.-B. and Liu, X.-H. (2014) 'Effect of blade pitch angle on aerodynamic performance of straight-bladed vertical axis wind turbine', *Journal of Central South University*, 21(4), pp. 1417–1427.
[52] Howell, R. and Qin, N. (2011) Wind tunnel and numerical study of a vertical axis wind turbine with different blade profiles in urban environments. Journal of Wind Engineering and Industrial Aerodynamics, 99(9), pp. 979–990.
[53] Rezaeiha, A., Montazeri, H. and Blocken, B. (2018) Towards optimal aerodynamic design of vertical axis wind turbines: impact of blade number and solidity on performance. Energy Conversion and Management, 169, pp. 45–65.
[54] Balduzzi, F., Bianchini, A. and Ferrari, L. (2016) Feasibility analysis of a vertical-axis wind turbine with self-starting capability via hybridization. Applied Energy, 161, pp. 560–569.
[55] Castellani, F., Astolfi, D., Natili, F. and Sayed, A. (2019) 'Experimental vibration analysis of a small-scale vertical axis wind turbine under interaction with a turbulent flow generated by a building', *Machines*, 7(2), article 35.
[56] Rubino, A., Vitale, S., Colonna, P. and Pini, M. (2020) 'Fully-turbulent adjoint method for the unsteady shape optimization of multi-row turbomachinery', *Aerospace Science and Technology*, 106, article 106132.
[57] Mavriplis, D.J. (2013) *Adjoint-based sensitivity analysis for computational fluid dynamics* [presentation]. Available at: s https://scientific-sims.com/cfdlab/Dimitri_Mavriplis/HOME/assets/presentations/musaf2.final.2013.pdf.
[58] Giles, M.B. and Pierce, N.A. (2001) An introduction to the adjoint approach to design. Flow, Turbulence and Combustion, 65(3), pp. 393–415.
[59] Tam, C.K.W. (1995) Computational aeroacoustics: issues and methods. AIAA Journal, 36(5), pp. 681–693.
[60] Giles, M.B., Duta, M.C., Müller, J.-D. and Pierce, N.A. (2003) 'Algorithm developments for discrete adjoint methods', *AIAA Journal*, 41(2), pp. 198–205.

[61] Dwight, R.P. and Brezillon, J. (2006) 'Effect of approximations of the discrete adjoint on gradient-based optimization', *AIAA Journal*, 44(12), pp. 3022–3031.

[62] Economon, T.D., Palacios, F., Copeland, S.R., Lukaczyk, T.W. and Alonso, J.J. (2016) SU2: an open-source suite for multiphysics simulation and design. AIAA Journal, 54(3), pp. 828–846.

[63] He, P., Mader, C.A., Martins, J.R.R.A. and Maki, K.J. (2020) 'DAFoam: an open-source adjoint framework for multidisciplinary design optimization with OpenFOAM', *AIAA Journal*, 58(3), pp. 1254–1268.

[64] Shires, A. (2013) Design optimisation of an offshore vertical axis wind turbine. ICE Energy, 166, pp. 7–18.

[65] Kenway, G.K.W., Mader, C.A., He, P. and Martins, J.R.R.A. (2019) 'Effective adjoint approaches for computational fluid dynamics', *Progress in Aerospace Sciences*, 110, article 100542.

[66] Colonno, M.R., Palacios, F., Economon, T.D., Lonkar, A.K. and Alonso, J.J. (2013) 'An adjoint-based aerodynamic shape optimization methodology for fairing systems', in *31st AIAA Applied Aerodynamics Conference*. Reston, VA: American Institute of Aeronautics and Astronautics, Paper AIAA 2013-2649.

[67] Belme, A. 2011. *Unsteady Aerodynamics and Adjoint Method*. PhD thesis.

[68] Venditti, D.A. and Darmofal, D.L. (2000) Adjoint error estimation and grid adaptation for functional outputs: application to quasi-one-dimensional flow. Journal of Computational Physics, 164(1), pp. 204–227.

[69] Chen, F., Cheng, X., Zhang, K., Chen, Y. and Zhang, X. (2024) 'Unsteady aerodynamic shape optimization of a vertical axis wind turbine under the framework of DAFoam', in *2023 Asia-Pacific International Symposium on Aerospace Technology (APISAT 2023) Proceedings*. Singapore: Springer Nature Singapore.

[70] van Stratan, G.S.M., Roy, S., Lee, V.C.C. and San, Y.K. (2024) 'Adjoint method shape optimization of a vertical axis wind turbine', *Journal of Physics: Conference Series*, 2818(1), p. 012023. doi: 10.1088/1742-6596/2818/1/012023.

[71] Templin, R.J. (1974) Aerodynamic performance theory for the NRC vertical-axis wind turbine. National Research Council of Canada Report No. LTR-LA-160.

[72] Paraschivoiu, M. (1981) Aerodynamic design and optimization of the Darrieus vertical axis wind turbine. Journal of Energy, 5(1), pp. 41–46.

[73] Paraschivoiu, M. (2002) Wind turbine design: with emphasis on Darrieus concept. Montreal: Polytechnic International Press.

[74] Kirke, B.K. and Lazauskas, L. (2011) Limitations of fixed pitch Darrieus hydrokinetic turbines and the challenge of efficiency prediction using streamtube theory. Renewable Energy, 36(3), pp. 893–898.
[75] Vavalle, A. and Qin, N. (2007) Iterative response surface based optimization scheme for transonic airfoil design. Journal of Aircraft, 44, pp. 365–376.
[76] Balduzzi, F., Bianchini, A., Carnevale, E.A. and Ferrara, G. (2016) Critical issues in the CFD simulation of Darrieus wind turbines. Renewable Energy, 85, pp. 419–435.
[77] Migliore, P.G., Fanucci, J.B. and Fielding, J.C. (1980) 'Wind-tunnel tests of vertical-axis wind turbine blades', *Journal of Energy*, 4(5), pp. 240–244.
[78] Angell, R.K., Musgrove, P.J., Galbraith, R.A. and Green, R.B. (1990) Summary of the collected data for tests on the NACA 0015, NACA 0018, NACA 0021, NACA 0025 and NACA 0030 airfoils. National Technical Reports Library, United States.
[79] Wang, S., Ingham, D.B., Ma, L., Pourkashanian, M. and Tao, Z. (2010) Numerical investigations on dynamic stall of low Reynolds number flow around oscillating airfoils. Computers and Fluids, 39, pp. 1529–1541.
[80] Wang, S., Ingham, D.B., Ma, L., Pourkashanian, M. and Tao, Z. (2012) Turbulence modelling of deep dynamic stall at relatively low Reynolds number. Journal of Fluids and Structures, 33, pp. 191–209.
[81] Alnaieli, H.A., Jadallah, A.A. and Alsamarraie, D.Y. (2022) 'Theoretical and experimental investigation on the performance of a designed vertical axis wind turbine', *AIP Conference Proceedings*, 2415(1), p. 020004.
[82] Elsakka, M., Rezaeiha, A. and Blocken, B. (2021) Influence of turbulence intensity and inflow conditions on angle of attack and performance of vertical axis wind turbines. Renewable Energy, 163, pp. 1932–1947.
[83] Balduzzi, F., Bianchini, A. and Ferrara, G. (2015) Blade aerodynamic performance assessment of a straight-bladed vertical axis wind turbine through wind tunnel experiments. Renewable Energy, 78, pp. 617–626.
[84] Abraham, J.P., Mowry, G.S., Plourde, B.D., Sparrow, E.M. and Minkowycz, W.J. (2011) 'Numerical simulation of fluid flow around a vertical-axis turbine', *Journal of Renewable and Sustainable Energy*, 3(3).
[85] Ferreira, C.S., van Bussel, G.J.W. and van Kuik, G.A.M. (2006) Wind tunnel hotwire measurements, flow visualization and thrust measurement of a VAWT. Renewable Energy, 128(4), pp. 487–497.

[86] Rezaeiha, A., Kalkman, I. and Blocken, B. (2017) CFD simulation of a vertical axis wind turbine operating under various yaw angles. Energy Conversion and Management, 148, pp. 1054–1070.

[87] Moore, K.R. and Ennis, B.L. (2021) 'Vertical-axis wind turbine steady and unsteady aerodynamics for curved deforming blades', *AIAA Journal*, 59(8), pp. 2998–3010.

[88] Mulleners, K. and Raffel, M. (2013) Dynamic stall development. Experiments in Fluids, 54(2), pp. 1469–1477.

[89] Balduzzi, F., Bianchini, A., Gigante, F.A., Ferrara, G., Campobasso, M.S. and Ferrari, L. (2015) 'Parametric and comparative assessment of Navier–Stokes CFD methodologies for Darrieus wind turbine performance analysis', in *ASME Turbo Expo 2015: Turbine Technical Conference and Exposition*, Montreal, Canada, 15–19 June 2015. New York: American Society of Mechanical Engineers. ISBN 9780791856802.

[90] Mohammed, A.A., Sahin, A.Z. and Ouakad, H.M. (2020) 'Numerical investigation of a vertical axis wind turbine performance characterization using new variable pitch control scheme', *Journal of Energy Resources Technology, Transactions of the ASME*, 142(3).

[91] Simão Ferreira, C.J. (2009) The near wake of the VAWT: 2D and 3D views of the VAWT aerodynamics. PhD thesis. Delft: Delft University of Technology.

[92] Mishra, A., Economon, T.D., He, L. and Alonso, J.J. (2019) Efficient unsteady adjoint-based optimization for rotorcraft using SU2. AIAA Journal, 57(2), pp. 675–688.

[93] Albring, T., Sagebaum, M. and Gauger, N.R. (2016) 'Efficient aerodynamic design using the discrete adjoint method in SU2', in *17th AIAA/ISSMO Multidisciplinary Analysis and Optimization Conference*. Reston, VA: American Institute of Aeronautics and Astronautics. doi:10.2514/6.2016-3518.

[94] Papoutsis-Kiachagias, E.M., Giannakoglou, K.C. and Economon, T.D. (2014) Continuous adjoint methods for turbulent flows: applications and extensions using the SU2 suite. Computers and Fluids, 105, pp. 1–20.

[95] Economon, T.D. (2015) *An unsteady continuous adjoint approach for aerodynamic design*. NASA AMS Seminar, 9 June 2015. Available at: N
https://www.nas.nasa.gov/assets/nas/pdf/ams/2015/AMS_20150609_Economon.pdf.

[96] Kapellos, C.S., Papoutsis-Kiachagias, E.M., Giannakoglou, K.C. and Hartmann, M. (2019) 'The unsteady continuous adjoint method for minimizing flow-induced sound radiation', *Journal of Computational Physics*, 397, 108838.

[97] Jain, S. and Saha, U.K. (2020) 'The state-of-the-art technology of H-type Darrieus wind turbine rotors', *Journal of Energy Resources Technology*, 142(6), 060801.

[98] Nielsen, E.J., Diskin, B. and Yamaleev, N.K. (2012) 'Discrete adjoint-based design optimization of unsteady turbulent flows on dynamic unstructured grids'.
[99] Samareh, J.A. (2001) Survey of shape parameterization techniques for high-fidelity multidisciplinary shape optimization. AIAA Paper 2001-532, Proceedings of the 39th AIAA Aerospace Sciences Meeting and Exhibit, Reno, NV.
[100] Jameson, A. (2003) Aerodynamic shape optimization using the adjoint method. Lecture Series 2003-04. Rhode-Saint-Genèse: Von Karman Institute for Fluid Dynamics.
[101] Quagliarella, D., D'Ambrosio, D. and Iollo, A. (2003) 'Airfoil design using Navier–Stokes equations and hybrid evolutionary optimization techniques', in *Evolutionary Methods for Design, Optimisation and Control with Applications to Industrial Problems (EUROMECH 411)*, Madrid, Spain, 10–13 June 2002. Barcelona: CIMNE.
[102] Xisto, C.M., Pascoa, J.C. and Leger, J.A. (2014) Wind energy production using an optimized variable pitch vertical axis rotor. Proceedings of the ASME 2014 International Mechanical Engineering Congress and Exposition.
[103] Rendall, T.C.S. and Allen, C.B. (2007) Unified interpolation for mesh deformation in computational fluid dynamics. AIAA Journal, 44(6), pp. 1326–1335.
[104] Dhert, T., Ashuri, T. and Martins, J.R.R.A. (2017) 'Aerodynamic shape optimization of wind turbine blades using a Reynolds-averaged Navier–Stokes model and an adjoint method', *Wind Energy*, 20(5), pp. 909–926. doi:10.1002/we.2070.
[105] Rezaeiha, A., Kalkman, I. and Blocken, B. (2017) CFD simulation of a vertical axis wind turbine operating at a moderate tip speed ratio: guidelines for minimum domain size and azimuthal increment. Renewable Energy, 107, pp. 373–385.
[106] Rezaeiha, A., Kalkman, I. and Blocken, B. (2017) Effect of pitch angle on power performance and aerodynamics of a vertical axis wind turbine. Applied Energy, 197, pp. 132–150.
[107] Rezaeiha, A., Montazeri, H. and Blocken, B. (2018) Towards accurate CFD simulations of vertical axis wind turbines at different tip speed ratios and solidities: guidelines for azimuthal increment, domain size and convergence. Energy Conversion and Management, 156, pp. 301–316.
[108] Selvan, K. (2015) On the effect of shape parameterization on airfoil shape optimization. International Journal of Research in Engineering and Technology, 4(2), pp. 123–133.
[109] Buchner, A.J., Lohry, M.W., Martinelli, L., Soria, J. and Smits, A.J. (2015) Dynamic stall in vertical axis wind turbines: comparing experiments and computations. Journal of Wind Engineering and Industrial Aerodynamics, 146, pp. 163–171.

[110] Brown, R. and Scheurich, F. (2011) ‘Effect of dynamic stall on the aerodynamics of vertical-axis wind turbines’, *AIAA Journal*, 49(11), pp. 2511–2521.

[111] Lee, T. and Gerontakos, P. (2004) Investigation of flow over an oscillating airfoil. Journal of Fluid Mechanics, 512, pp. 313–341.

[112] McCroskey, W.J. (1981) The phenomenon of dynamic stall. NASA Technical Memorandum 81264.

[113] Leishman, J.G. and Beddoes, T.S. (1989) A semi-empirical model for dynamic stall. Journal of the American Helicopter Society, 34(3), pp. 3–17.

[114] Sharma, A. and Visbal, M. (2019) Numerical investigation of the effect of airfoil thickness on onset of dynamic stall. Journal of Fluid Mechanics, 870, pp. 870–900.

[115] Hand, B., Kelly, G. and Cashman, A. (2017) Numerical simulation of a vertical axis wind turbine airfoil experiencing dynamic stall at high Reynolds numbers. Computers and Fluids, 149, pp. 12–30.

[116] Edwards, J.M. (2012) The influence of aerodynamic stall on the performance of vertical axis wind turbines. PhD thesis. Sheffield: University of Sheffield.

[117] Edwards, J.M., Danao, L.A. and Howell, R.J. (2013) PIV measurements and CFD simulation of the performance and flow physics of a small-scale vertical axis wind turbine. Wind Energy, 18, pp. 201–217.

[118] Rosado Hau, N. (2021) Unsteady aerodynamics of vertical axis wind turbines. PhD thesis. Sheffield: University of Sheffield.

[119] Almohammadi, K.M., Ingham, D.B., Ma, L. and Pourkashanian, M. (2012) CFD sensitivity of a straight-blade vertical axis wind turbine. Wind Engineering, 36, pp. 571–588.

[120] Almohammadi, K.M., Ingham, D.B., Ma, L. and Pourkashanian, M. (2015) 2D CFD analysis of the effect of trailing edge shape on the performance of a straight-blade vertical axis wind turbine. IEEE Transactions on Sustainable Energy, 6, pp. 228–235.

[121] Coton, F.N., Galbraith, R.A.M. and Jiang, D. (1996) The influence of detailed blade design on the aerodynamic performance of straight-bladed vertical axis wind turbines. Proceedings of the Institution of Mechanical Engineers, Part A: Journal of Power and Energy, 210, pp. 65–74.

[122] Gosselin, R., Dumas, G. and Boudreau, M. (2016) Parametric study of H-Darrieus vertical-axis turbines using CFD simulations. Journal of Renewable and Sustainable Energy, 8(5), Article 053301.

[123] Danao, L.A., Edwards, J., Eboibi, O. and Howell, R.J. (2013) A numerical investigation into the influence of unsteady wind on the performance and aerodynamics of a vertical axis wind turbine. Applied Energy, 116, pp. 111–124.
[124] Scheurich, F. and Brown, R.E. (2013) Modelling the aerodynamics of vertical-axis wind turbines in unsteady wind conditions. Wind Energy, 16, pp. 91–107.
[125] Vassberg, J.C., Gopinath, A.K. and Jameson, A. (2005) Revisiting the vertical-axis wind turbine design using advanced computational fluid dynamics. AIAA Journal, 43(9), pp. 1907–1917.
[126] Zhang, L., Liang, Y., Liu, X. and Guo, J. (2014) Effect of blade pitch angle on aerodynamic performance of straight-bladed vertical axis wind turbine. Journal of Central South University, 21, pp. 1417–1427.
[127] Lanzafame, R., Mauro, S. and Messina, M. (2014) 2D CFD modelling of H-Darrieus wind turbines using a transition turbulence model. Energy Procedia, 45, pp. 131–140.
[128] Ning, S.A., Damiani, R. and Moriarty, P.J. (2013) Objectives and constraints for wind turbine optimization. Journal of Solar Energy Engineering, 136(4), Article 041010.
[129] Chehouri, A., Younes, R., Ilinca, A. and Perron, J. (2015) Review of performance optimization techniques applied to wind turbines. Applied Energy, 142, pp. 361–388.
[130] Orman, E. and Durmus, G. (2016) Comparison of shape optimization techniques coupled with genetic algorithm for a wind turbine airfoil. Proceedings of the 2016 IEEE International Conference on Renewable Energy Research and Applications (ICRERA), Birmingham, UK, pp. 1–7.
[131] Ram, K.R., Lal, S. and Ahmed, M.R. (2009) Low Reynolds number airfoil optimization for wind turbine applications using genetic algorithm. Journal of Renewable and Sustainable Energy, 5, Article 052007.
[132] Ram, K.R., Lal, S. and Ahmed, M.R. (2012) Airfoil optimization for small wind turbines using multi-objective genetic algorithm. Proceedings of the ASME 2012 International Mechanical Engineering Congress and Exposition, Paper IMECE2012-88788, pp. 1–9.
[133] Lachenal, X., Daynes, S. and Weaver, P.M. (2013) Review of morphing concepts and materials for wind turbine blade applications. Wind Energy, 16, pp. 283–307.
[134] Kear, M., Evans, B., Ellis, R. and Rolland, S. (2016) Computational aerodynamic optimisation of vertical axis wind turbine blades. Applied Mathematical Modelling, 40, pp. 1038–1051.

[135] Carpentieri, G. (2009) An adjoint-based shape-optimization method for aerodynamic design. PhD thesis. Delft: Delft University of Technology.

[136] Ritlop, R.M. and Nadarajah, S.K. (2009) Toward the aerodynamic shape optimization of wind turbine profiles. MEng thesis. Montreal: McGill University.

[137] Coppin, J. (2014) Aerodynamics, stability and shape optimisation of unmanned combat air vehicles. PhD thesis. Sheffield: University of Sheffield.

[138] Lei, J. and He, J. (2016) Adjoint-based aerodynamic shape optimization for low Reynolds number airfoils. Journal of Fluids Engineering, 138, Article 021401.

[139] Rajagopal, S. and Ganguli, R. (2011) 'Multidisciplinary design optimization of long endurance unmanned aerial vehicle wing', *Computer Modeling in Engineering & Sciences*, 81(1), pp. 1–22.

[140] Hicks, R.M. and Henne, P.A. (1978) Wing design by numerical optimization. Journal of Aircraft, 15(7), pp. 407–412.

[141] Kim, S., Alonso, J.J. and Jameson, A. (2007) Design optimization of unsteady flow problems using the continuous adjoint method. AIAA Journal, 45(6), pp. 1466–1480.

[142] Martins, J.R.R.A., Sturdza, P. and Alonso, J.J. (2003) The complex-step derivative approximation. ACM Transactions on Mathematical Software, 29(3), pp. 245–262.

[143] Mohammadi, B. and Pironneau, O. (2001) Applied shape optimization for fluids. Oxford: Oxford University Press.

[144] Nadarajah, S. and Jameson, A. (2000) A comparison of the continuous and discrete adjoint approach to automatic aerodynamic optimization. AIAA Paper 2000-0667.

[145] Nadarajah, S. and Jameson, A. (2001) Optimum shape design for unsteady flows using time-accurate adjoint equations. AIAA Journal, 39(6), pp. 1184–1192.

[146] Pironneau, O. (1974) On optimum profiles in Stokes flow. Journal of Fluid Mechanics, 59(1), pp. 117–128.

[147] Selig, M.S. and McGranahan, B.D. (2004) Wind tunnel aerodynamic tests of six airfoils for use on small wind turbines. Journal of Solar Energy Engineering, 126(4), pp. 986–1001.

[148] van Rooij, R.P.J.O.M. and Timmer, W.A. (2003) Roughness sensitivity considerations for thick rotor blade airfoils. Journal of Solar Energy Engineering, 125(4), pp. 468–478.

[149] Gosselin, R., Dumas, G. and Boudreau, M. (2016) Parametric study of H-Darrieus vertical axis turbines using uRANS simulations. Proceedings of the 21st Annual Conference of the CFD Society of Canada, Paper 178, Session 13-6.

[150] Li, C., Zhu, S., Xu, Y.-L. and Xiao, Y. (2014) 2.5D large eddy simulation of vertical axis wind turbine in consideration of high angle of attack flow. Renewable Energy, 63, pp. 317–329.
[151] Celik, Y. (2020) Aerodynamic investigation of the start-up process of H-type vertical axis wind turbines using CFD. PhD thesis. Sheffield: University of Sheffield. Available at: White Rose Research Online.
[152] Miao, W., Liu, Q., Zhang, Q., Xu, Z., Li, C., Yue, M., Zhang, W. and Ye, Z. (2022) 'Recommendation for strut designs of vertical axis wind turbines: Effects of strut profiles and connecting configurations on the aerodynamic performance', *Energy Conversion and Management*, 276, 116436. doi:10.1016/j.enconman.2022.116436.
[153] McLaren, K., Tullis, S. and Ziada, S. (2012) Computational fluid dynamics simulation of the aerodynamics of a high solidity vertical axis wind turbine. Wind Energy, 15(3), pp. 349–361.
[154] ElSakka, M. (2020) The aerodynamics of fixed and variable pitch vertical axis wind turbines. PhD thesis. Sheffield: University of Sheffield.
[155] Le Moigne, A. (2003) A discrete Navier–Stokes adjoint method for aerodynamic optimisation of blended wing-body configurations. PhD thesis. Sheffield: University of Sheffield.
[156] Peter, J.E.V. and Dwight, R.P. (2010) Numerical sensitivity analysis for aerodynamic optimization: a survey of approaches. Computers and Fluids, 39, pp. 373–391.
[157] Walther, B. and Nadarajah, S. (2015) An adjoint-based multi-point optimization method for robust turbomachinery design. Proceedings of the ASME Turbo Expo 2015, Paper GT2015-44142, pp. 1–12.
[158] Lee, B.J. and Liou, M. (2012) Unsteady adjoint approach for design optimization of flapping airfoils. AIAA Journal, 50, pp. 2460–2475.
[159] Hascoët, L. and Pascual, V. (2013) The Tapenade automatic differentiation tool: principles, model, and specification. ACM Transactions on Mathematical Software, 39(3), Article 20.
[160] Guo, J., et al. (2020) Flow characteristics of a straight-bladed vertical axis wind turbine with inclined pitch axes. Energies, 13(23), Article 6281.
[161] Lam, H.F. and Peng, H.Y. (2016) Study of wake characteristics of a vertical axis wind turbine by two- and three-dimensional computational fluid dynamics simulations. Renewable Energy, 90, pp. 386–398.

[162] Li, Q., Maeda, T., Kamada, Y., Murata, J., Kawabata, T., Shimizu, K., Ogasawara, T., Nakai, A. and Kasuya, T. (2016a) Wind tunnel and numerical study of a straight-bladed vertical axis wind turbine in three-dimensional analysis (part I: for predicting aerodynamic loads and performance). Energy, 106, pp. 443–452.
[163] Li, Q., Maeda, T., Kamada, Y., Murata, J., Kawabata, T., Shimizu, K., Ogasawara, T., Nakai, A. and Kasuya, T. (2016b) Wind tunnel and numerical study of a straight-bladed vertical axis wind turbine in three-dimensional analysis (part II: for predicting flow field and performance). Energy, 104, pp. 295–307.
[164] Marsh, P., Ranmuthugala, D., Penesis, I. and Thomas, G. (2015) Three-dimensional numerical simulations of straight-bladed vertical axis tidal turbines investigating power output, torque ripple and mounting forces. Renewable Energy, 83, pp. 67–77.
[165] Zanforlin, S. and Nishino, T. (2016) 'Fluid dynamic mechanisms of enhanced power generation by closely spaced vertical axis wind turbines', *Renewable Energy*, 99, pp. 1213–1226.
[166] Orlandi, A., Collu, M., Zanforlin, S. and Shires, A. (2015) 3D URANS analysis of a vertical axis wind turbine in skewed flows. Journal of Wind Engineering and Industrial Aerodynamics, 144, pp. 138–155.
[167] Posa, A., Parker, C.M., Leftwich, M.C. and Balaras, E. (2018) Large eddy simulation of an isolated vertical axis wind turbine. Journal of Wind Engineering and Industrial Aerodynamics, 174, pp. 139–155.
[168] Wang, S., Ingham, D.B., Ma, L., Pourkashanian, M. and Tao, Z. (2014) Large eddy simulation of the dynamic stall process of a vertical axis wind turbine. Energy, 64, pp. 356–366.
[169] Ferziger, J.H. and Perić, M. (2002) Computational methods for fluid dynamics. 3rd edn. Berlin: Springer.
[170] Spalart, P.R. (2009) Detached-eddy simulation. Annual Review of Fluid Mechanics, 41, pp. 181–202.
[171] Sagaut, P. (2006) Large eddy simulation for incompressible flows: an introduction. 3rd edn. Berlin: Springer.
[172] Dhamankar, N.S., Blaisdell, G.A. and Lyrintzis, A.S. (2015) 'An overview of turbulent inflow boundary conditions for large eddy simulations', in *22nd AIAA Computational Fluid Dynamics Conference*, Dallas, Texas, June 2015. Reston, VA: American Institute of Aeronautics and Astronautics.

[173] Nielsen, E.J. and Kleb, B. (2005) 'Efficient construction of discrete adjoint operators on unstructured grids by using complex variables', in *43rd AIAA Aerospace Sciences Meeting and Exhibit*, Reno, Nevada, 10–13 January 2005. AIAA Paper 2005-0324. Reston, VA: American Institute of Aeronautics and Astronautics.

[174] Menter, F.R. (1994) Two-equation eddy-viscosity turbulence models for engineering applications. AIAA Journal, 32(8), pp. 1598–1605.

[175] Rezaeiha, A., Montazeri, H. and Blocken, B. (2018) Characterization of aerodynamic performance of vertical axis wind turbines: impact of operational parameters. Energy Conversion and Management, 169, pp. 45–65.

[176] Rezaeiha, A., Montazeri, H. and Blocken, B. (2019) On the accuracy of turbulence models for CFD simulations of vertical axis wind turbines. Energy, 180, pp. 838–857.

[177] Rezaeiha, A., Montazeri, H. and Blocken, B. (2019) Active flow control for power enhancement of vertical axis wind turbines: leading-edge slot suction. Energy, 189, Article 116131.

[178] Yang, Z.-J., Gu, Y.-Z., Li, M., Li, Y.-X., Lu, J. and Zhang, Z.-G. (2014) 'Design and analysis of small-scale lift-type vertical-axis wind turbine using composite blade', *Polymers and Polymer Composites*, 22(4), pp. 423–430.

[179] Mishnaevsky, L., Branner, K., Petersen, H.N., Beauson, J., McGugan, M. and Sørensen, B.F. (2017) 'Materials for wind turbine blades: An overview', *Materials*, 10(11), 1285.

[180] Reddy, S.S.P., Suresh, R., Hanamantraygouda, M.B. and Shivakumar, B.P. (2021) 'Use of composite materials and hybrid composites in wind turbine blades', *Materials Today: Proceedings*, 46(Part 8), pp. 2827–2830.

[181] Sutherland, H.J., Berg, D.E. and Ashwill, T.D. (2012) A retrospective of VAWT technology. Sandia National Laboratories Technical Report SAND2012-0304. Albuquerque, NM: Sandia National Laboratories.

[182] Barbero, E.J. (2010) Introduction to composite materials design. Boca Raton, FL: CRC Press.

[183] Mandell, J.F., Samborsky, D.D. and Agastra, P. (2008) Composite materials fatigue issues in wind turbine blade construction. Proceedings of the SAMPE Conference.

[184] Eiríksson, E.R., Wilm, J., Pedersen, D.B. and Aanæs, H. (2016) 'Precision and accuracy parameters in structured light 3-D scanning', *The International Archives of the Photogrammetry, Remote Sensing and Spatial Information Sciences*, XL-5/W8, pp. 7–15.

[185] Stanciu, M.D., Nastac, S.M. and Tesula, I. (2022) ‘Prediction of the damage effect on fiberglass-reinforced polymer matrix composites for wind turbine blades’, *Polymers*, 14(7), 1471.
[186] Dabachi, M.A., Rouway, M., Rahmouni, A., Bouksour, O., Sbai, S.J., Laaouidi, H., Tarfaoui, M., Aamir, A. and Lagdani, O. (2022) ‘Numerical investigation of the structural behavior of an innovative offshore floating Darrieus-type wind turbines with three-stage rotors’, Journal of Composites Science, 6(6), 167.
[187] Rezaeiha, A., Kalkman, I. and Blocken, B. (2018) ‘CFD simulation of a vertical axis wind turbine operating at a moderate tip speed ratio: Guidelines for minimum domain size and azimuthal increment’, *Renewable Energy*, 107, pp. 373–385.
[188] Brøndsted, P. and Nijssen, R. (2013) Fatigue damage in wind turbine blade composites. Wind Energy, 16(7), pp. 1033–1046.
[189] Ashwill, T.D. (2009) Materials and innovations for large blade structures: research opportunities in wind energy technology. Wind Energy, 12(7), pp. 620–632.
[190] Gere, J.M. and Goodno, B.J. (2012) Mechanics of materials. 8th edn. Stamford, CT: Cengage Learning.
[191] Mandell, J.F., Samborsky, D.D. and Sutherland, H.J. (1999) ‘Effects of materials parameters and design details on the fatigue of composite materials for wind turbine blades’, conference paper, Sandia National Laboratories / U.S. Department of Energy. Report no. SAND98-1997C, OSTI ID 4194.
[192] Veers, P.S. (1990) ‘Fatigue reliability of wind turbine components’.
[193] de Oliveira, I., Amico, S.C., Souza, J.A. and de Lima, A. (2013) ‘Resin transfer molding process: a numerical and experimental investigation’, *The International Journal of Multiphysics*, 7(2), pp. 125–136.
[194] Kang, H. and Guo, W. (2013) ‘Three dimensional numerical simulation for hydrodynamic response of vertical axis tidal current turbine’, *Taiyangneng Xuebao/Acta Energiae Solaris Sinica*, 34(3), pp. 537–541.
[195] Wang, L., Kolios, A.J., Nishino, T., Delafin, P.-L. and Bird, T. (2016) ‘Structural optimisation of vertical-axis wind turbine composite blades based on finite element analysis and genetic algorithm’, *Composite Structures*, 153, pp. 123–138.
[196] Larsen, G.C., Hansen, M.H., Baumgart, A. and Carlen, I. (2002) *Modal analysis of wind turbine blades*. Roskilde, Denmark: Risø National Laboratory.
[197] International Electrotechnical Commission (2014) IEC 61400-23: Wind turbines – part 23: full-scale structural testing of rotor blades. Geneva: IEC.

Appendix A:
Definition of Upwind and Downwind Regions in VAWT Model

In some studies, in the case of vertical axis wind turbines (VAWT), the distribution of wind speed around the airfoil will change significantly, whether upwind (45°-135°) or downwind (225°-315°), and on the upwind (315°-45°) and downwind (135°-225°) sides. Fig. A.1 shows the segmentation of the wind turbine path.

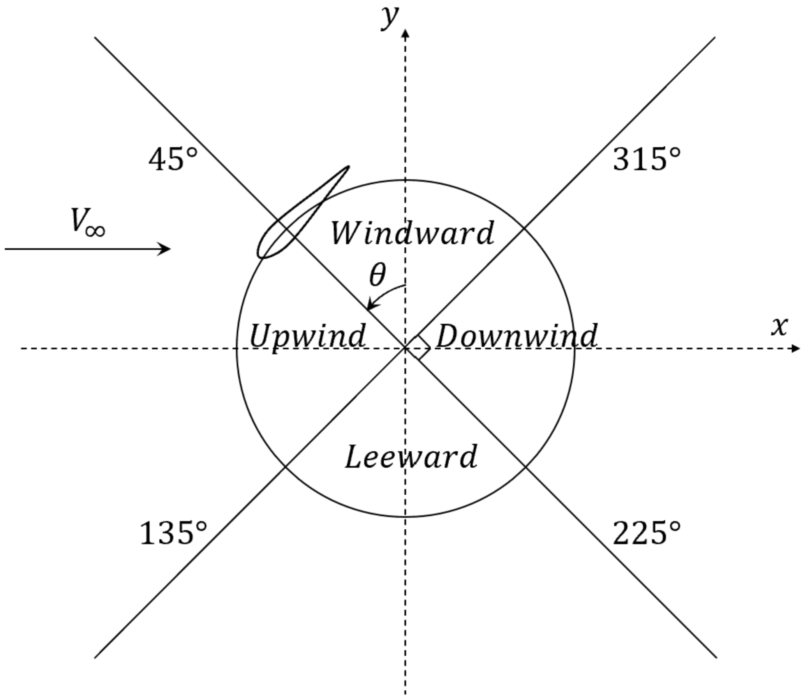

Fig. A1: A Controversial Definition: Segmentation of the Wind Turbine Path.

However, such definitions are controversial in academia. Therefore, the terms "upwind" and "downwind" are not used in this study. In this study, the upwind region is defined as the half of the rotor disk that directly faces the incoming free-stream wind (0°-180°), while the downwind region refers to the half located in the wake of the rotor (180°-360°).

For a free-stream velocity aligned with the positive x-direction, the upwind and downwind regions correspond to $x < 0$ and $x > 0$, respectively, if the pivot point of the VAWT is taken as the origin.

The wind speed on the upwind side is relatively stable and high when approaching the airfoil. When the wind flow hits the airfoil, it will slow down due to the obstruction of the airfoil, and the ratio of its deceleration is related to the induction factor. A low speed area will form in front of the airfoil.

After the wind flow on the downwind side passes through the airfoil, vortices and turbulence will form on the back of the airfoil, which makes the wind speed on the downwind side unstable and usually low. At this time, it is necessary to control to ensure that the angle of attack of the airfoil is not too high. In addition, in the VAWT model considering the shaft, the fluid behind the shaft will form vortices, which will affect the peak power coefficient on the downwind side.

After the wind flow on the upwind side passes through the airfoil, its relative wind speed is higher due to the wind force acting on the airfoil.

The downwind side located on the other side of the airfoil, which forms turbulence and eddies after wind passes through the airfoil, and its relative wind speed is lower.

The flow solution is used to directly extract the wind speed value from the front of the airfoil, and the obtained speed value is written in the form of a continuous function, and a piecewise function is used to represent the speed change in front of the airfoil throughout the cycle. Such AoA distribution has an obvious advantage, that is, it can simulate a more realistic downwind airfoil AoA in the oscillation airfoil model, which is closer to the VAWT rotating blade model, so that in the subsequent calculations with optimization, the airfoil The original pitch-down amplitude will be maintained, but its pitch-up amplitude will be reduced to a certain extent based on the distribution value curve of the inlet velocity.

In the study of oscillation airfoil, since the axial wind speed of the airfoil in different areas is different, before the optimization of the rotational airfoil model, there is a custom speed curve, which is represented by a piecewise function of the cosine function, so that it can match the value of the angle of attack of the common airfoil in the downwind direction.

$$V_{rel} = \begin{cases} V_{\infty}(1-a)\sqrt{{\frac{\lambda}{1-a}}^{2} + 2\frac{\lambda}{1-a}cos\theta + 1}, & 0 \le \theta < 180 \\ V_{\infty}(1-a)(1+ksin\theta)\sqrt{{\frac{\lambda}{1-a}}^{2} + 2\frac{\lambda}{1-a}cos\theta + 1}, & 180 \le \theta < 360 \end{cases} \qquad \text{[Eq. A1]}$$

Where k is the scaling factor, determined by minimum wind speed value over a cycle.

In the large offshore VAWT, the environmental characteristics of high wind speed make the VAWT in a high tip speed ratio under normal working conditions. Its main feature is that the angle of attack is small and gradually approaches a sinusoidal motion, and its efficiency is relatively high. Theoretically, it is less susceptible to deceleration caused by wake in the downwind section, so its k value will be smaller. In addition, the effect of flow separation is present but not large at smaller angle of attack changes. Overall, in the normal operation state, the whole motion is cyclically stable, as the periodically change of the angle of attack over the azmuthal angle is shown.

Appendix B:

Study on TSR-AoA Matching for Experimental Verification

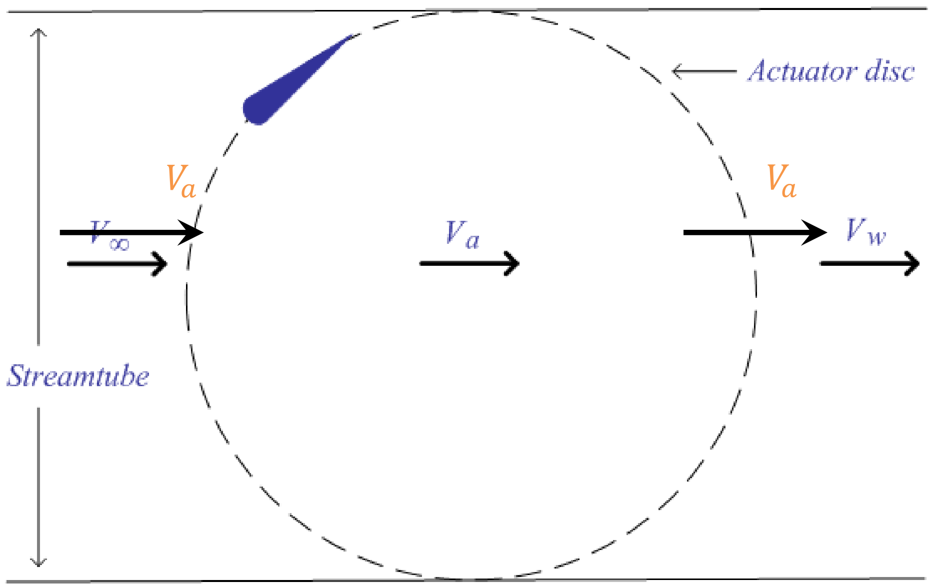

Fig. B1: Single Streamtube Velocity.

Fig. B1 shows the difference between the axial flow velocity V_a and the freestream velocity V_∞ in the VAWT model. The difference between the two can be explained by the single streamtube model. In single streamtube, if the wind speed near airfoil is different from the freestream wind speed, under the effect of induction factor, the expression of the AoA is:

$$\alpha = tan^{-1}\left(\frac{sin\theta}{\frac{\lambda}{1-a} + cos\theta}\right) \qquad \text{[Eq. B1]}$$

Where α is the angle of attack, θ is the azimuthal angle, λ is the tip speed ratio, V_D is the wind speed near airfoil and V_∞ is the freestream wind speed.

But tip speed ratio is still only related to the freestream wind speed.

$$\lambda = \frac{R\omega}{V_\infty} \qquad \text{[Eq. B2]}$$

Where ω is the angular velocity, R is the radius of the VAWT, and V_∞ is the freestream wind speed.

The induction factor u can be expressed as follow:

$$u = 1 - a = \frac{V_D}{V_\infty} \quad \text{[Eq. B3]}$$

According to Glauert's theory the velocity through a windmill disk V_D is the arithmetic mean of the undisturbed velocity V_∞ and the velocity in the wake. The wind turbine drag D is given by:

$$D = 2\rho A V_D (V_\infty - V_D) \quad \text{[Eq. B4]}$$

Where ρ is the air density, A is the area, and D is the wind turbine drag.

A disk drag coefficient based on the dynamic pressure and the disk area is defined as:

$$C_{DD} = \frac{D}{\frac{1}{2}\rho V_D^2 A} \quad \text{[Eq. B5]}$$

and from Eq. F5:

$$C_{DD} = 4(\frac{1}{u} - 1) \quad \text{[Eq. B6]}$$

In the experimental data, it can obtain what $\frac{\lambda}{V_D/V_\infty}$ equals to reach its peak angle of attack, that is, oscillation amplitude. The TSR divided by the $\frac{\lambda}{V_D/V_\infty}$ is the induction factor. The specific value is shown in Table B1.

Table B1: Comparison between Experimental F and Theoretical F.

TSR	u	Cdd	F (exp)	F
6	0.571	3.00525394	41.0553817	103.6139627
4	0.69	1.797101449	24.55056625	31.53623188
3.5	0.74	1.405405405	19.1995274	20.99233017
3.25	0.776	1.154639175	15.77375922	16.46005487

2.8	0.838	0.77326969	10.56379358	10.47649535
2.33	0.896	0.464285714	6.342701015	6.345762616
1.75	0.945	0.232804233	3.180385694	3.218106996

C_{DD} can be obtained theoretically and it is related to solidity factor by combining the blade element theory and momentum theory. A dimensionless force coefficient is defined as F, also known as the streamwise force coefficient, obtained by projecting the blade normal and tangential force coefficients onto the streamtube direction. If we define a function under the integral of that process by:

$$F = \frac{q}{\frac{1}{2}\rho V_D^2}(C_N sin\theta - C_T cos\theta) \qquad \text{[Eq. B7]}$$

Where q is the dynamic pressure of the airfoil, C_N is the normal coefficient and C_D is the tangential coefficient.

The q is related to the relative velocity of the airfoil and the $(C_N sin\theta - C_T cos\theta)$ can be rewritten as $C_D(\theta)$.

This equation is computed at the centre point of each element, Eq. F7 can be written as:

$$C_{DD} = \frac{3}{4}\frac{Nc}{R}\bar{F} \qquad \text{[Eq. B8]}$$

Where $\frac{Nc}{R}$ is the solidity factor of the turbine, C_N is the normal coefficient and C_D is the tangential coefficient, $\bar{F}$ is the arithmetic average of F.

Since the VAWT-450 (130kW) has 2 blades, the chordlength of 0.61m and the radius of 12.5m, the solidity factor is 0.0976. The experimental $\bar{F}$ at each TSR can be obtained from Eq. F8 and experimental C_{DD} from the table 1.

From Eq. F7, the drag coefficients over azimuthal angles $C_D(\theta)$ can be obtained from the SU2 CFD simulation (since there is no table provided) and the $q = \frac{1}{2}\rho V_{rel}^2$ in oscillation airfoil model. The relative velocity V_{rel} can be expressed as follow:

$$V_{rel} = V_\infty\sqrt{\frac{\lambda^2}{u} + 2\frac{\lambda}{u}cos\theta + 1} \qquad \text{[Eq. B9]}$$

Since in the single streamtube model, the same u value is shared under upwind and downwind conditions, so only the average value of 0-180° needs to be calculated. Based on Eq. F7, the $\bar{F}$ at a specific tip speed ratio can be written as

$$\bar{F} = \frac{1}{n}\sum_{\theta=1}^{n}\frac{\sqrt{\lambda^2 + 2\lambda cos\theta + 1}}{u^2}C_D(\theta) \qquad \text{[Eq. B10]}$$

The $\bar{F}$ value at each TSR is summarized in table 1.

When comparing the average F values obtained by the two methods in Fig. F2, it was found that they overlap when the TSR is less than 3.5. According to Ion's conclusion, the theoretical formula of single streamtube has its TSR range limitation. In the case of a small turbine in Fig. F3, under any solidity factor, TSR exceeding 3.5 will lead to inaccurate $C_D(\theta)$ prediction, but the predicted value should be higher than the experimental value.

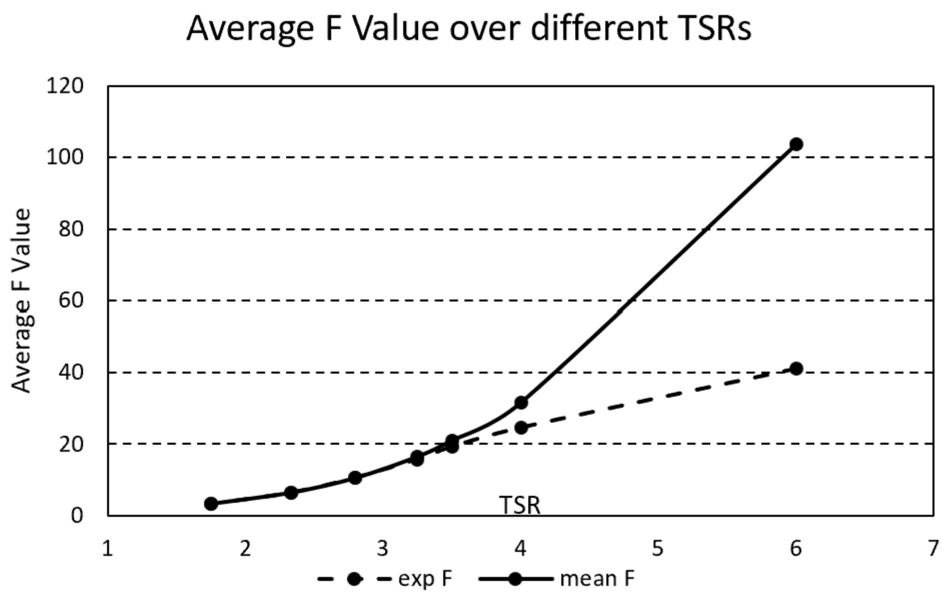

Fig. B2: Average F Value over Different TSRs.

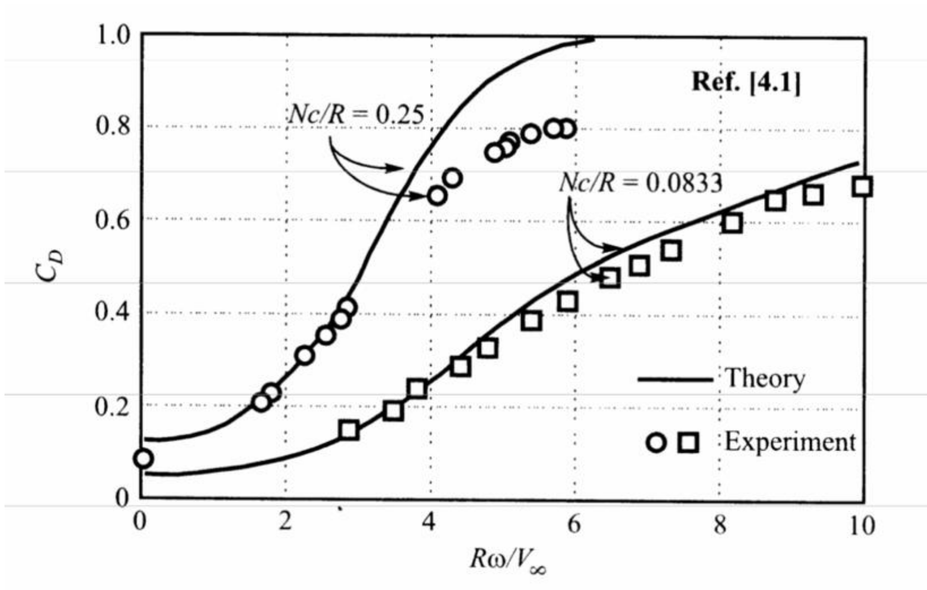

Fig. B3: C_D over Different TSRs.

Appendix C:

RANS Equations and SST k-ω Turbulence Model

The original Navier-Stokes equations describe the flow of Newtonian fluids, including the continuity equation and the momentum equation. For continuous media, the momentum equation expresses the relationship between the acceleration of fluid particles and the forces acting on them. Consider a fluid element: the inertial force (the time change of momentum) and the convection force (the spatial change of momentum in the fluid motion) together form the total acceleration of the fluid element. The external forces acting on the fluid element include the pressure force acting on the fluid interface and the viscous force from the internal friction of the fluid. That is, the total acceleration of the fluid element is equal to the resultant force of all external forces.

For incompressible fluids, the momentum equation can be written as:

$$\rho\left(\frac{\partial \mathrm{u}}{\partial t}+\mathrm{u}\cdot\nabla\mathrm{u}\right)=-\nabla p+\mu\nabla^2\mathrm{u}=0 \qquad \text{[Eq. C1]}$$

Where p is the pressure and μ is the dynamic viscosity.

For any control volume, the mass flowing into the volume must be equal to the mass flowing out of the volume plus the increase or decrease in the mass in the volume. The continuity equation can thus be expressed as:

$$\frac{\partial \rho}{\partial t}+\nabla\cdot(\rho\mathrm{u})=0 \qquad \text{[Eq. C2]}$$

Where ρ is the density, and u is the velocity vector.

The RANS equations are obtained by time averaging the Navier-Stokes equations, and are mainly used to deal with turbulent flow fields. Its basic steps include decomposing the velocity and pressure, substituting them into the Navier-Stokes equations, and then time averaging the equations. The processing expression after the introduction of Reynolds decomposition is as follows:

$$\mathrm{u}=\bar{\mathrm{u}}+\mathrm{u}' \qquad \text{[Eq. C3]}$$

$$p=\bar{p}+p' \qquad \text{[Eq. C4]}$$

Where the horizontal bar indicates the time average and the prime symbol indicates the eddy component.

The convection term is expanded as follows:

$$\mathrm{u} \cdot \nabla \mathrm{u} = (\bar{\mathrm{u}} + \mathrm{u}') \cdot \nabla(\bar{\mathrm{u}} + \mathrm{u}') \qquad \text{[Eq. C5]}$$

Considering that the average value of the vortex velocity is zero, we have:

$$\overline{\mathrm{u} \cdot \nabla \mathrm{u}} = \bar{\mathrm{u}} \cdot \nabla \bar{\mathrm{u}} + \overline{\mathrm{u}' \cdot \nabla \mathrm{u}'} \qquad \text{[Eq. C6]}$$

The entire convection term is processed by time averaging, and we get:

$$\rho\left(\frac{\partial \bar{\mathrm{u}}}{\partial t} + \bar{\mathrm{u}} \cdot \nabla \bar{\mathrm{u}}\right) = -\nabla \bar{p} + \mu \nabla^2 \bar{\mathrm{u}} - \nabla \cdot (\rho \overline{\mathrm{u}'\mathrm{u}'}) = 0 \qquad \text{[Eq. C7]}$$

Where $\rho\overline{\mathrm{u}'\mathrm{u}'}$ is the Reynolds stress tensor, which represents the additional stress due to velocity vortex.

Wherein, the last term $\overline{\mathrm{u}' \cdot \nabla \mathrm{u}'}$ represents the additional stress caused by the velocity vortex, also known as the Reynolds stress, represented by $-\rho\overline{u_i u_j}$, where the negative sign indicates that this stress is in the opposite direction of the average flow.

So, in the end, we get the RANS equation:

$$\rho\left(\frac{\partial \overline{u_i}}{\partial t} + \overline{u_j}\frac{\partial \overline{u_i}}{\partial x_j}\right) = -\frac{\partial \bar{p}}{\partial x_i} + \mu\frac{\partial^2 \overline{u_i}}{\partial x_j^2} - \frac{\partial}{\partial x_j}(\rho\overline{u_i u_j}) \qquad \text{[Eq. C8]}$$

Where i and j represent the components of the fluid velocity vector.

This shows that the treatment of turbulence needs to consider the influence of Reynolds stress, and these stresses usually need to be closed by appropriate turbulence models to make the equations solvable.

The $k-\omega$ SST model was developed by Menter, combining the advantages of the $k-\varepsilon$ model in far-field processing and the accuracy of the $k-\omega$ model in near-wall processing. The model describes the turbulent kinetic energy (k) and specific dissipation rate (ω) through two transport equations. By applying the product rule to the eddy part of the Reynolds decomposed Navier-Stokes equations and performing time averaging, the equation involving turbulent kinetic energy can be obtained, which is expressed as follows:

$$\frac{\partial(pk)}{\partial t} + \nabla \cdot (pku) = P_k - \beta^* \rho\omega k + \nabla \cdot [(\mu + \sigma_k \mu_t)\nabla k] \qquad \text{[Eq. C9]}$$

Where P_k represents the turbulent kinetic energy generated by the mean velocity gradient, $\beta^* \rho\omega k$ is the dissipation term, σ_k is the turbulent Prandtl number with the k equation, and μ_t is the turbulent viscosity.

The equation for the change of the specific dissipation rate (the dissipation rate of unit turbulent kinetic energy) is derived from the dissipation rate and production rate of turbulent kinetic energy, which is expressed as follows:

$$\frac{\partial(p\omega)}{\partial t} + \nabla \cdot (p\omega u) = \gamma \frac{P_k}{\nu_t} - \beta\rho\omega^2 + \nabla \cdot [(\mu + \sigma_\omega \mu_t)\nabla\omega] \qquad \text{[Eq. C10]}$$

Where γ and β are model constants that adjust the production and dissipation of ω, and σ_ω is the turbulent Prandtl number associated with the ω equation.

The dissipation term represents the process of converting turbulent kinetic energy into internal energy (heat) due to viscosity effects. In turbulence, the energy of large-scale eddies is gradually transferred to small-scale eddies, and finally dissipated into heat energy through viscosity at the microscopic level. The diffusion term describes the spatial distribution and transmission of turbulent kinetic energy in the flow field. This includes diffusion caused by molecular viscosity and turbulent viscosity.

The core of the $k - \omega$ model is that these two equations are interdependent and jointly describe the turbulent state. The turbulent viscosity μ_t is calculated from these two equations and is usually expressed as:

$$\mu_t = \rho \frac{k}{\omega} \qquad \text{[Eq. C11]}$$

In this way, the equations of k and ω are coupled to provide a relatively simple turbulence model suitable for the near-wall region.

The $k - \omega$ model is naturally suitable for handling flows near the wall because it simulates the wall directly, so the model is less sensitive to the y+ value (dimensionless wall distance). The SST model introduces a mixing function that automatically adjusts the weights of the $k - \omega$ and $k - \varepsilon$ models according to the viscous effects of the flow field. This adaptive adjustment means that the $k - \omega$ model is naturally used more near the wall, while the $k - \varepsilon$ model is gradually transitioned to the area far from the wall.

Appendix D: Overview of VAWT Testing and Certification Landscape

Dimensional verification requires the use of structured light or laser scanning systems to generate a complete 3D point cloud of the blade surface. The scan results are then compared to the CAD model to check if the optimized airfoil exceeds an error of ±0.5 mm. Non-destructive testing (NDT) can detect internal problems in advance, such as porosity, delamination, or insufficient resin. Ultrasonic C-scanning can reveal internal porosity and bonding quality. Infrared thermography can show dry patches or resin accumulation. Shear interferometry and digital image correlation (DIC) techniques are often used to measure stress concentration areas in VAWT blades. These tests are consistent with the methods described in BS EN ISO 3452 and EN 4179, but IEC 61400-23 provides more stringent requirements for wind power applications.

IEC 61400-23 (2014) summarizes static and fatigue testing methods for full-scale structures. VAWT blades, especially those with complex curvature and layered reinforcement, need to simulate extreme load events such as gusts and grid outages, and withstand cyclic fatigue loads exceeding millions of cycles, as well as combined bending and torsional loads. Full-scale test rigs allow blades to be subjected to realistic wind loads, usually exaggerated, to determine the failure margin. Standards typically do not include severe delamination, cracking, or energy absorption below safety thresholds. Strain gauges and DIC measurements can verify the tests; these measurements can map surface strain variations and identify potential failure areas.

Modal analysis verifies the dynamic behavior of the blade, preventing resonance with the tower or wind excitation. Accelerometers, impact hammers, and electromechanical shakers can be used to extract the first to third natural frequencies, which are then compared to the modal simulation results of finite element analysis (FEA). Deviations between theoretical and experimental natural frequencies may indicate material inhomogeneity, layup defects, or stiffness variations due to curvature. VAWT blades need to demonstrate resilience under environmental stresses, such as UV exposure, humidity cycling, salt spray resistance, corrosion resistance, and freeze-thaw cycles. These tests are governed by BS EN 61400-2 Appendix D, simulating 20 years of operational exposure under similar climatic conditions in the UK. For example, accelerated aging chambers (such as QUV) can replicate UV degradation in a few months, equivalent to several years of exposure in real-world conditions.

Durability verification also focuses on the integrity of the blade's bond lines, surface roughness limits (Ra < 5μm), coating adhesion, and water resistance. If PVC or PU foam cores are used, delamination due to water immersion and frost cracking is of particular concern. These tests are typically conducted through hot liquid aging tests or edge seal durability tests.

A key regulatory requirement is verification of the turbine's actual power output under realistic wind conditions. According to IEC 61400-12-1, small wind turbines must undergo a verified power curve at wind speeds between 5 and 25 m/s, measured at hub height using an anemometer and data logger, and energy production estimated in a reference wind zone. The turbines are typically installed at a dedicated test site equipped with a standardized meteorological tower. Test results must demonstrate that the turbines meet their claimed capacity and efficiency specifications.

To be legally and efficiently connected to the UK grid, vertical wind turbine (VAWT) systems must comply with the following standards:

- *The Electricity Safety, Quality and Continuity Regulations 2002 (as amended),*
- *G98/G99 grid connection regulations (per the Energy Networks Association),*
- *The Microgeneration Certification Scheme (MCS) standards.*

MCS 006 and MCS 010 documents specify the structural requirements and installation safety of small wind power systems. Only products certified by the MCS are eligible for certain government subsidies, the traditional Feed-in-Tariff (FiT) scheme, or the Smart Export Guarantee (SEG).

The blade manufacturing process is directly impacted by these schemes: for example, material traceability, quality assurance documentation, and batch tracking are often part of the MCS technical review. Furthermore, under post-market surveillance obligations, manufacturers must retain design documents, test records, and simulation models for at least 10 years.

Certification must be performed by an ISO/IEC 17065-accredited organization, such as Lloyd's Register, TÜV SÜD, or the British Board for Accreditation (BBA).

Appendix E: Location of Nodes and Design Variables

In SU2-based adjoint shape optimization, it is crucial to clearly distinguish the roles of discrete surface nodes and design variables (DVs) on the airfoil surface. Airfoil nodes are densely packed at the leading and trailing edges, resulting in a large number of nodes connected by linear boundary elements. Therefore, the surface geometry is a piecewise linear curve in a discrete sense. In contrast, DVs are not equivalent to all geometric nodes. Instead, they describe controllable shape degrees of freedom in a lower dimension (typically 10–20), such as a small number of control points, Hicks–Henne perturbation function parameters, or FFD control grid points. This setup aims to achieve smooth, manufacturable deformation of the overall geometry with limited design degrees of freedom, while avoiding the high-dimensional ill-posedness and numerical instability that result from treating each surface node directly as an independent design variable.

At the geometric update level, the effect of DVs on the displacement of airfoil surface nodes is not specified independently point-by-point. Instead, it is interpolated across the entire surface by the parametric model through an influence function (shape basis/weighting function). The actual displacement direction of the nodes is usually dominated by the local surface normal. Therefore, in Cartesian coordinates, the coordinate changes of a node are reflected simultaneously in both the x and y directions: when the normal is not aligned with the global coordinate axis, the geometric perturbation caused by the design variables naturally decomposes into x and y components.

The core idea of Hicks–Henne parameterization is not to treat each surface node as an independent degree of freedom, but rather to "spread out" shape changes in the chord direction using a small number of local perturbation functions; each design variable controls the geometric bulge or depression of a local region, and its influence on nodes far from that region gradually diminishes. The superposition of multiple perturbation functions allows for controllable adjustment of airfoil thickness distribution, camber distribution, and local geometric features while maintaining geometric smoothness. However, it is worth noting that in unsteady motion problems such as oscillating airfoils or VAWT rotating blades, the rigid body motion of the airfoil (pitch, heave, or rotation with azimuth) causes its "chord direction" in the global coordinate system to change over time. Therefore, the chord parameters in Hicks–Henne are defined based on a fixed reference configuration.

The reason is that tangential slip is undesirable for turbulent wall models/near-wall resolution. In RANS/URANS, near-wall meshes typically have high aspect ratios and a well-defined normal layer structure (y+ controlled). If the near-wall connection direction is skewed, a non-physical jump will occur between the local y+ and the wall tangential mesh distribution, and wall functions or near-wall models are very sensitive to this distortion. Normal displacement, on the other hand, is more of a "stretching/compression in the overall thickness direction," causing less damage to the near-wall layer structure and making it easier to maintain the y+ target.

When defining the airfoil node parameters, a Python-based resampling procedure is used to scale the airfoil geometry to the required number of nodes. The implementation uses NumPy and SciPy, particularly parametric interpolation methods such as `scipy.interpolate.interp1d` or `splprep/splev`, to reconstruct the airfoil contour and redistribute the nodes along the curve.

The basic principle is to first parameterize the original airfoil coordinates using cumulative arc length. The airfoil surface is treated as a continuous parametric curve, where each point is represented as a function of its normalized curve length. New node locations are then generated along this parameter and interpolated from the original geometry. In this way, the total number of airfoil nodes can be increased or reduced while preserving the original geometric distribution characteristics.

This method allows the airfoil data, typically containing around 100–200 nodes, to be smoothly resampled to a higher or lower resolution. Regions with strong geometric variation, such as the leading edge and trailing edge, can retain any user-defined node density, while flatter middle sections remain more sparsely distributed.

Appendix F: Angle of Attack Offset and Reasonable Range

Under natural rotation (passive pitch) conditions, the instantaneous angle of attack of an airfoil cannot be reliably given solely by geometric relationships because the local incoming flow direction exhibits significant spatial and temporal inhomogeneities due to the influence of induced velocity, wake disturbances, and dynamic stall vortex structures. To obtain an engineering-usable and repeatable "actual angle of attack" characterization, the equivalent angle of attack is typically defined using aerodynamic inversion: First, an aerodynamic database of the airfoil under two-dimensional steady conditions is established (e.g., steady CFD or wind tunnel testing), obtaining the characteristic curve of the lift coefficient as a function of angle of attack; then, the instantaneous or phase-averaged lift coefficient history is extracted from the unsteady calculations of free rotation and mapped to the corresponding angle of attack position on the steady curve, thereby inverting to obtain an angle-of-attack time series "equivalent" to the current unsteady aerodynamic response.

Therefore, the Darrieus function can only be considered a "lowest complexity kinematic baseline" for constructing a unified research framework. When the research objective shifts to natural rotation, strong wake interference, or overall power prediction, it is necessary to introduce effective angle-of-attack correction, induced velocity models, or directly adopt unsteady CFD for the entire rotor to avoid phase shifts and load differences that cannot be explained by Darrieus geometric angles of attack alone.

In the Darrieus-based kinematics optimization framework, introducing a constant initial pitch angle is equivalent to shifting the entire angle-of-attack time history, thereby changing the "primary operating angle-of-attack range" of the airfoil within one cycle. As shown in Eq. F1:

$$\alpha(\theta) = \alpha_0(\theta) + \alpha_p \qquad [Eq. F1]$$

When the pitch offset is positive, the blade is at a higher positive angle of attack, even close to the dynamic stall range, for a longer period in the windward section. Optimization will tend to enhance adhesion and lift retention capabilities at positive angles of attack, typically manifested as an increased leading-edge radius, smoother upper surface pressure recovery, and a shape more biased towards anti-stall and high-lift design. Simultaneously, the negative angle-of-attack performance in the leeward section is often sacrificed, potentially leading to stronger negative torque or drag loss. Conversely, when the pitch bias is negative, the angle-of-attack history shifts negatively overall, reducing the effective positive angle of attack in the windward section and expanding the negative angle of attack range in the leeward section. Optimization tends to favor reducing leeward losses and load fluctuations (e.g., through drag reduction or lowering unfavorable pressure gradients), but this usually comes at the cost of reduced peak lift and positive torque in the windward section.

This study did not use the constant initial pitch angle in the VAWT model, primarily because the maximum angle of attack varies significantly with the speed ratio and azimuth. During the attachment and weak separation phases, the aerodynamic response to geometric disturbances is relatively smooth, and the accompanying gradient has good usability and interpretability. However, when the angle of attack is high enough to cause abrupt changes in separation/reattachment and the LEV detachment phase becomes highly sensitive to geometric perturbations, the gradient becomes significantly noisy and may lead to directional misdirection, making optimization prone to instability or convergence to non-generalizable local patterns. For NACA0015 and NACA0018, 15° typically marks the beginning or near static stall, with significant flow separation/bubble expansion, accompanied by increasing gradient noise and sensitivity to grid/time step. Separation occurs even earlier at lower Reynolds numbers. Therefore, any time interval exceeding this value in the modified Darrieus function should not be included in the window.

Appendix G: Analysis of Natural Tip Speed Ratio

In actual vertical axis wind turbine (VAWT) operation, the speed ratio is not pre-set but naturally formed as a result of the system's dynamic response. This process is essentially a rotational dynamic equilibrium problem, determined by the interaction of aerodynamic torque, rotor inertia, and external load torque.

From a dynamic perspective, the rotor's instantaneous angular velocity $\Omega(t)$ is controlled by the rotational equation, whose basic form can be written as:

$$I\frac{d\Omega}{dt} = T_a(\Omega, t) - T_L(\Omega) \qquad [Eq. G1]$$

Where I is the rotor's moment of inertia, $T_a(\Omega, t)$ is the aerodynamic torque, and $T_L(\Omega)$ is the external load torque (which may include generator electromagnetic torque, mechanical damping, or equivalent damping introduced by the control strategy). This equation shows that the rotor's angular acceleration, which is entirely determined by the difference between the aerodynamic torque and the load torque.

Under uniform flow conditions, when the blade rotates around its axis, the aerodynamic torque $T_a(\Omega, t)$ exhibits strong periodic variation with the azimuth angle. This is caused by unsteady effects such as relative flow velocity, effective angle of attack, and dynamic stall. In engineering, the time-averaged aerodynamic torque over one rotational cycle is of greater interest, and its expression is as follows:

$$\overline{T_a} = \frac{1}{T}\int_0^T T_a(\Omega, t)dt \qquad [Eq. G2]$$

This average value directly determines the rotor's energy balance in a statistical sense. When T_a is greater than T_L, the rotor gains net energy and continues to accelerate. When T_a is less than T_L, the rotor decelerates. As the angular velocity changes, the magnitude and direction of the relative incoming flow velocity experienced by the blades change, thereby altering the angle-of-attack history, stall behavior, and the aerodynamic torque distribution per unit period. This feedback mechanism between velocity, aerodynamics, and torque makes T_a a function of the angular velocity Ω.

When the system evolves to a steady-state operating point, i.e., $T_a = T_L$, the angular acceleration is 0 in a periodically average sense, and the rotor no longer undergoes continuous acceleration or deceleration, retaining only small periodic velocity fluctuations. The corresponding speed ratio is the natural tip speed ratio (natural TSR). Under light load or weak damping conditions, the rotor can accelerate to higher speeds, making the natural TSR approach or even exceed the TSR corresponding to the peak aerodynamic efficiency. Under heavy load or strong damping conditions, the equilibrium point will appear in the lower speed range.

In CFD research, the assumption of a constant speed ratio (TSR) is widely adopted. The fundamental reason for this is not that real wind turbines always operate at a constant TSR, but rather to obtain a closed, controllable, and repeatable problem description at both the numerical and physical levels. If the rotational speed were allowed to vary freely over time, the rotor rotational dynamics equations would have to be solved simultaneously, introducing inertia, generator characteristics, and control strategies, thus extending the problem to a strongly coupled aerodynamic-structural-control system. This not only significantly increases computational costs and uncertainties but also makes aerodynamic mechanisms difficult to analyze in isolation. Conversely, under constant TSR conditions, rotor kinematics are predetermined, the blade's angle-of-attack history and relative velocity distribution are deterministic, and aerodynamic forces become "response variables" rather than "feedback variables." Therefore, this assumption allows CFD to focus on core physical processes such as unsteady aerodynamics, dynamic stall, and wake interactions, and is the standard practice in current research for analyzing aerodynamic mechanisms and comparing different airfoils or parameter settings.

Natural TSR is not necessarily equivalent to the TSR corresponding to the maximum power coefficient. The peak power coefficient (TSR) is the "optimal aerodynamic point" obtained under a given speed ratio with the goal of maximizing aerodynamic performance. It assumes that the rotor can operate stably at that speed ratio without being limited by load or inertia. The natural TSR, on the other hand, is determined by the balance between aerodynamic torque and load torque, and its position depends on the specific system's load characteristics: under light load or weak damping conditions, the natural TSR may be close to or even higher than the aerodynamically optimal TSR; while under heavy load or strong damping conditions, the natural TSR is often lower than the TSR corresponding to the peak power coefficient.

Based on this understanding, this study does not assume that a single speed ratio can represent all the operating characteristics of a VAWT. Instead, it consciously repeats numerical experiments under multiple different TSR conditions. The purpose of this is twofold: firstly, by using a constant TSR CFD setting, the aerodynamic response of the airfoil and flow structure under different kinematic conditions can be systematically evaluated, avoiding binding the results to a specific operating point; secondly, these different TSR conditions can be regarded as a parameter scan of the possible natural TSR range, thus providing a basis for understanding the performance changes of real wind turbines under different loads and operating states.

Appendix H: Analysis of Failure Cases Accompanied by Gradient

The adjoint method essentially eliminates the most expensive path mathematically (tracking how the entire flow field changes with the design), transforming the calculation from "recalculating the flow field for each design variable" to "only needing one adjoint solution," followed by a rapid evaluation of each design variable." While the adjoint method offers significant computational efficiency advantages in high-dimensional design spaces, it suffers from four fundamental limitations compared to the direct method.

The adjoint gradient can provide local improvement directions, but it struggles to predict new flow phenomena that may arise after large deformations, such as new separation structures, stall mode changes, or abrupt load phase shifts. Furthermore, the adjoint method implicitly assumes that the flow response caused by small deformations is smooth and continuous. However, in CFD, for example, flow separation can occur suddenly, reattachment can disappear abruptly, vortex structures can suddenly detach, or impact structures can suddenly move.

In the periodic motion of VAWT, the flow state constantly switches with the azimuth angle, making the adjoint gradient inherently more unstable in certain phases. The following four potential failure regions make the gradient more likely to be dominated by noise or lead to misleading optimization directions:

1. High Angle of Attack Region: This region typically corresponds to high relative velocities and large effective angles of attack. Airfoils easily approach or enter pre- or post-stall states, and the generation and enhancement of leading-edge vortices are highly sensitive to minute geometric changes. The flow may exhibit bifurcation behavior here, either generating strong vortices or not generating them at all, leading to completely different load responses due to minute geometric changes. Near such bifurcation points, the first-order gradient is difficult

to represent the true trend, so optimization may jump to a different flow regime with slightly larger step sizes.

2. Dynamic Stall and Reattachment Region: When the flow switches between "attachment-separation-reattachment," the timing and location of key events (e.g., separation points or vortex shedding phases) are often highly sensitive to shape perturbations. Even if the objective function is continuous in a periodically average sense, the local spikes caused by these events will cause the gradient to oscillate at high frequencies. The accompanying gradient is likely to be "numerically strong but directionally unstable," thus causing optimization oscillations or non-convergence.

3. Leeward Wake Crossing Region: The leeward section of the blades frequently crosses the wakes formed by themselves or upstream blades, resulting in a highly uneven distribution of incoming flow direction and velocity, and significant "historical memory" (vortex structures generated upstream continue to influence downstream). This non-local, time-delayed effect is difficult to describe as a "small instantaneous disturbance – small instantaneous response," making the gradient more susceptible to mesh and time discretization errors, manifesting as noise or sensitivity to different time step settings.

4. Regions with Minimal or Negative Tangential Force: At certain azimuth angles, the tangential force may approach zero, but this does not necessarily mean that pressure and shear are small; rather, it often means that positive and negative contributions strongly cancel each other out in that phase. For numerical calculations, "subtracting two large numbers results in a small one," amplifying the relative impact of noise and making the gradient direction more unstable. This situation is very common in engineering; many snapshot-based optimization cases improve power coefficients in this region. Near the zero-crossing tangential force, the sensitivity distribution appears scattered, with frequent sign switching, and uncontrolled optimization can easily produce non-physical local deformations.

Appendix I:
First-Order Smooth Inflow Velocity Distribution

The sudden variation of inlet velocity or relative velocity with time (or azimuthal angle) significantly impacts numerical stability. It may appear in the abrupt changes or discontinuous derivatives of the velocity profile (e.g., continuous velocity values but discontinuous rates of change). This situation will directly introduce non-physical instantaneous accelerations, and inducing high-frequency numerical oscillations in the flow field and affecting the reliability of load predictions and associated sensitivity. The velocity time history can be continuous at the first order can deal with this issue, meaning the velocity itself and its first-order time derivative must maintain C1 continuity.

For example, consider a piecewise velocity function. Assume the velocity is constant in the 0°-180° range and varies sinusoidally in the 180°-360° range. If a strict piecewise definition is directly applied, a jump in the rate of change of velocity occurs at 180°. To achieve at least first-order smoothness, a smooth transition can be introduced near the piecewise points, matching the constant segment with the sinusoidal segment in function values and first-order derivatives. For example, the velocity can be written as:

$$U_\theta = U_0 - AS(\theta - \pi)\sin(\theta - \pi) \qquad [Eq.I1]$$

Where $S(\theta - \pi)$ is a smooth transition function that smoothly transitions from 0 to 1 within the range of 0°-180°, and has a continuous first derivative within the transition interval (e.g., constructed based on a sine or polynomial). This treatment ensures that the velocity and its rate of change remain continuous throughout the entire period, thus avoiding the introduction of non-physical excitations into numerical calculations.